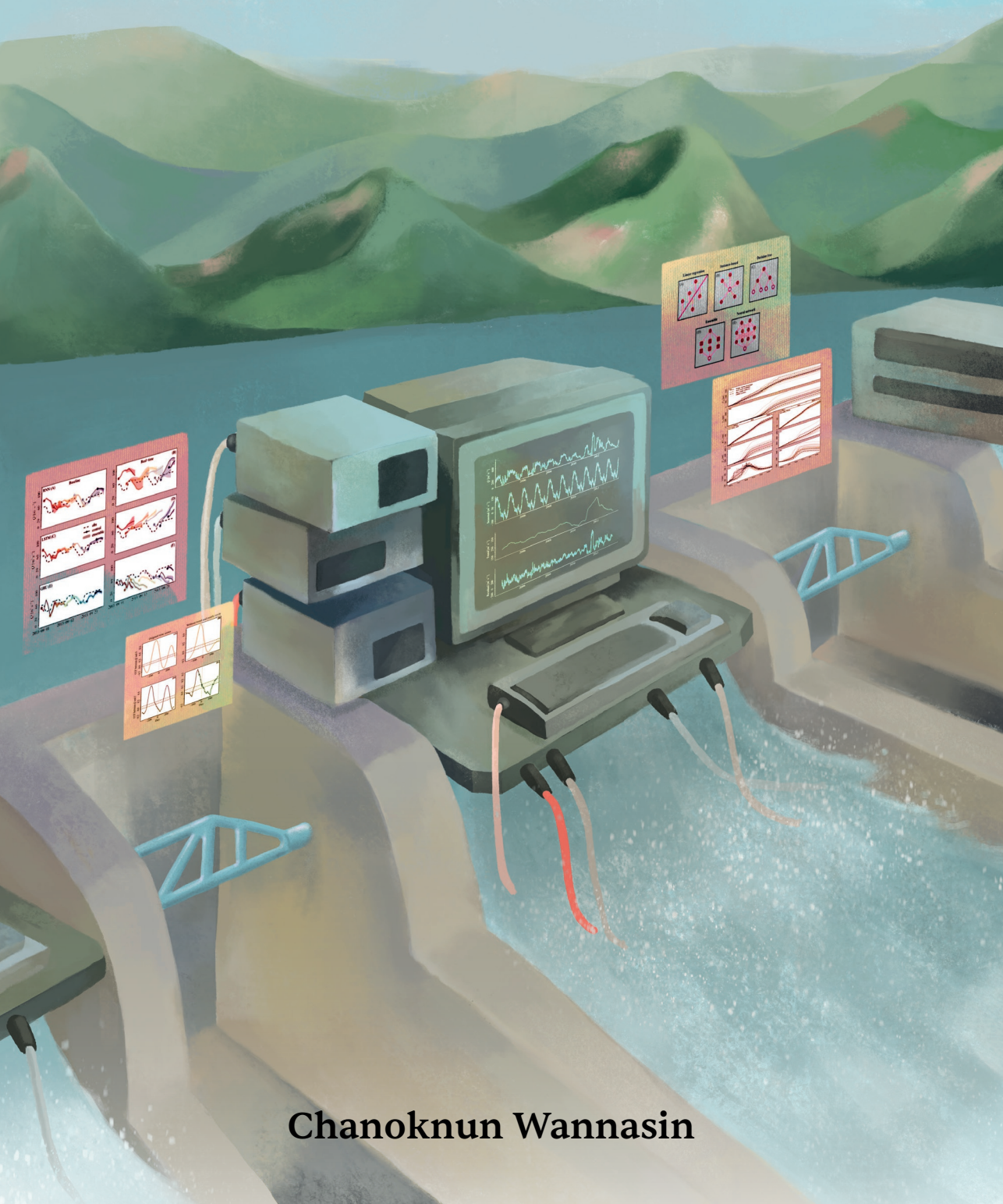


# Modelling and forecasting daily streamflow with reservoir operation in the upper Chao Phraya River basin, Thailand



**Chanoknun Wannasin**

## Propositions

1. Effective real-time reservoir operation simulation requires combining process-based and data-driven modelling.  
(this thesis)
2. Water-related disasters are more likely to occur in reservoir-dominated river basins than in free-flowing river basins.  
(this thesis)
3. Scientists should share their research findings with non-scientists through visual storytelling.
4. 'Bridging science and society' is a hollow phrase without a concrete outcome.
5. Living a balanced life is more challenging than operating multi-purpose reservoirs.
6. Hydropower energy is renewable but not sustainable.

Propositions belonging to the thesis, entitled:

Modelling and forecasting daily streamflow with reservoir operation  
in the upper Chao Phraya River basin, Thailand

Chanoknun Wannasin

Wageningen, 21 February 2023

# **Modelling and forecasting daily streamflow with reservoir operation in the upper Chao Phraya River basin, Thailand**

Chanoknun Wannasin

## **Thesis committee**

### **Promotors**

Prof. Dr A.H. Weerts  
Special professor, Hydrological Predictability  
Wageningen University & Research

Prof. Dr R. Uijlenhoet  
Professor of Hydrology and Water Resources  
Delft University of Technology

### **Co-promotor**

Dr C. C. Brauer  
Lecturer and researcher, Hydrology and Quantitative Water Management Group  
Wageningen University & Research

### **Other members**

Prof. Dr K.M. de Beurs, Wageningen University & Research  
Prof. Dr A. van Griensven, Vrije Universiteit Brussel, Belgium  
Dr M.H. Ramos, INRAE, Antony, France  
Dr M.G.F. Werner, IHE Delft Institute for Water Education, The Netherlands

This research was conducted under the auspices of the Graduate School for Socio-Economic and Natural Sciences of the Environment (SENSE).



# **Modelling and forecasting daily streamflow with reservoir operation in the upper Chao Phraya River basin, Thailand**

Chanoknun Wannasin

## **Thesis**

submitted in fulfilment of the requirements for the degree of doctor  
at Wageningen University  
by the authority of the Rector Magnificus  
Prof. Dr A.P.J. Mol,  
in the presence of the  
Thesis Committee appointed by the Academic Board  
to be defended in public  
on Tuesday 21 February, 2023  
at 4 p.m. in the Omnia Auditorium.

Chanoknun Wannasin

Modelling and forecasting daily streamflow with reservoir operation  
in the upper Chao Phraya River basin, Thailand  
xx+228 pages.

PhD thesis, Wageningen University, Wageningen, The Netherlands (2023)  
With references, with summaries in English, Dutch and Thai

ISBN: 978-94-6447-550-0

DOI: 10.18174/584572

© 2023 C. Wannasin

What distinguishes a mathematical model from, say,  
a poem, a song, a portrait or any other kind of “model,”  
is that the mathematical model is an image or picture of reality  
painted with logical symbols instead of with words, sounds or watercolors.  
—John L. Casti



# Contents

	Page
Contents	vii
Summary	ix
Summary (Dutch)	xiii
Summary (Thai)	xvii
Chapter 1 General introduction	1
Chapter 2 Upper Chao Phraya River Basin and reservoirs	19
Chapter 3 Data, models and performance criteria	29
Chapter 4 Distributed hydrological modelling with global datasets	55
Chapter 5 Hydrological effects of reservoir operation	77
Chapter 6 Machine learning for reservoir operation modelling	105
Chapter 7 Reforecasting real-time reservoir operation and outflow	135
Chapter 8 Synthesis	163
Appendices	179
References	197
Statement of authorship contribution	220
Acknowledgements	221
About the author	224
Graduate school certificate	226





# Summary

Reservoirs and dams are key infrastructures in major river basins worldwide. Despite the global expansion in their construction, reservoirs are controversial regarding their benefits and negative impacts. Reservoir operation modelling is, therefore, essential for the efficient planning and management of water resources. However, it has been a long-standing challenge in hydrological modelling. This PhD thesis contributes to an improved understanding of reservoir operation, its hydrological effects and its modelling and forecasting. The main aim is to develop, examine and apply reservoir operation models with available data and modelling techniques to simulate and forecast daily streamflow. It covers four topics: (i) process-based hydrological modelling with global datasets, (ii) hydrological effects of reservoir operation, (iii) data-driven modelling for reservoir operation simulation and (iv) forecasting real-time reservoir operation and outflow.

In this thesis, we first give an overview of global reservoir development and explain the principle of multi-purpose reservoir operation, including challenges in theory, in practice and in modelling (Chapter 1). We focus on the major reservoirs, Sirikit and Bhumibol, in the upper region of the Greater Chao Phraya River (GCPR) basin in Thailand as a case study (Chapter 2). In order to develop, examine and apply reservoir operation models for simulating and forecasting daily streamflow, several (in-situ and global) datasets and (process-based and data-driven) models are used (Chapter 3).

In Chapter 4, we propose a process-based hydrological model, namely the distributed `wflow_sbm` model, with global meteorological data and most parameters estimated from global data sources using (pedo)transfer functions. A target storage-and-release-based reservoir operation module (ROM) is applied to simulate the Sirikit and Bhumibol reservoir operations. The considered global datasets can reasonably compensate for the lack of in-situ data. The model can simulate daily streamflow for natural catchments (i.e., without reservoirs) well, in terms of magnitude, timing and duration. The ROM, however, can only capture the seasonal variability of reservoir outflow, but cannot simulate daily outflow very accurately since the actual operation of the two major reservoirs is too complex to be reconstructed by the module.

In Chapter 5, we unravel the hydrological effects of the Sirikit and Bhumibol reservoir operations by examining the water balance, daily streamflow regime and extreme

flows. The two reservoirs affect the various terms of the water balance, especially for cumulative daily water balance components during the course of a year. The reservoirs invert the natural seasonality of the daily streamflow regime, with higher flows in the dry season and lower flows in the rainy season. They smooth flow variability, with greater baseflow contribution and lower flashiness. They have mitigated many extreme flows although the operation has been adjusted in time. Nonetheless, the magnitude and timing of extreme flows become more variable and difficult to predict when reservoir operation is involved. These effects highlight the importance of effective reservoir operation modelling, including reservoir inflow and outflow forecasting, particularly in real-time.

In Chapter 6, we present data-driven models, machine learning (ML) in particular, for simulating the operation and outflow of the Sirikit reservoir, with a focus on gaining insights into the characteristics and relationships of available reservoir-related data as input variables. Widely-used ML algorithms in reservoir operation modelling, namely Multiple Linear Regression, Support Vector Machine, K-Nearest Neighbor, Classification and Regression Tree, Random Forest, Multi-Layer Perceptron and Recurrent Neural Network, are selected for performance comparison. From the 17 input combination scenarios taken into account, the most suitable input dataset for the considered ML models consists of (i) observed reservoir storage from the previous day, (ii) simulated inflow (by `wflow_sbm`) from two days ago to two days ahead and (iii) month of the year. All ML models perform significantly better than the ROM. The Recurrent Neural Network is found to offer the highest potential for further improvement.

In Chapter 7, we explore the capability of the most promising ML model, the Recurrent Neural Network and its advanced algorithms, Long Short-Term Memory and Gated Recurring Unit, in simulating and forecasting real-time operation and outflow of the Sirikit reservoir. The `wflow_sbm` model is used for probabilistic inflow reforecasting. The ML models are trained and tested with a 10-fold cross-validation. They can reconstruct the real-time operation of the Sirikit reservoir and provide accurate daily outflow, especially when training data cover both normal and extreme outflow conditions. They can reforecast outflow up to two days ahead for low outflows and up to one week for high outflows, and perform better for high outflows (during the dry season) than for low outflows (during the wet season). Gated Recurring Unit is found to be the most accurate, robust and convenient model given the current training setup. It is suggested to further improve the model setup and combine it with data assimilation for applications in practice.

Chapter 8 synthesizes the findings of the four core chapters from a broader perspective. The main conclusions are: (i) global data can reinforce hydrological modelling, but better availability and accessibility of in-situ data are needed for effective reservoir operation modelling and forecasting. (ii) Reservoir operation, its hydrological impacts and its modelling will continue to be a challenging topic in hydrology. However, advancements in data, modelling techniques and computational technologies provide model

development and application opportunities. The future development of reservoir operation modelling lies in the integration of process-based and data-driven models. (iii) Reservoir construction and operation should be based on experience with previously built reservoirs, considering the balance of their lifetime benefit and negative impacts. This thesis is beneficial for sustainable planning and management of reservoir operation in the upper GCPR basin in light of the 20-year National Water Resource Management Master Plan for the 2018–2037 period. It is also applicable at the national level and for neighboring countries in Southeast Asia, which are hot spots for new reservoir construction.



# Summary (Dutch)

Reservoirs en stuwdammen zijn belangrijke infrastructuur in stroomgebieden wereldwijd. Ondanks de wereldwijde toename zijn reservoirs controversieel vanwege hun positieve en negatieve effecten. Het modelleren van het beheer van reservoirs is daarom essentieel voor het efficiënt plannen en beheren van het water als hulpbron. Aan de andere kant is het een lang bestaande uitdaging in het hydrologisch modelleren. Dit proefschrift draagt bij aan een verbeterd begrip van het beheer van reservoirs, hun hydrologische effect en het modelleren en voorspellen ervan. Het hoofddoel is het ontwikkelen, toetsen en toepassen van reservoirbeheermodellen met beschikbare data en modelleertechnieken voor het simuleren en voorspellen van rivierafvoeren. Het bevat vier onderwerpen: (i) proces-gebaseerd hydrologisch modelleren met mondiale datasets, (ii) de hydrologische effecten van reservoirbeheer, (iii) data-gedreven hydrologisch modelleren voor het simuleren van reservoirbeheer en (iv) het real-time voorspellen van reservoirbeheer en -uitstroom.

In dit proefschrift geven we eerst een overzicht van de ontwikkeling van reservoirs wereldwijd en leggen we de principes uit van reservoirbeheer voor meerdere doelen, inclusief uitdagingen in de theorie, in de praktijk en in het modelleren (hoofdstuk 1). We focussen op de belangrijkste reservoirs, Sirikit en Bhumibol, in het bovenstroomse deel van de Grote Chao Phraya Rivier (GCPR) in Thailand (hoofdstuk 2). Voor het ontwikkelen, toetsen en toepassen van reservoirbeheersmodellen voor het simuleren en voorspellen van rivierafvoeren op dagbasis zijn verschillende (in-situ en mondiale) datasets en (proces-gebaseerde en data-gedreven) gebruikt (hoofdstuk 3).

In hoofdstuk 4 presenteren we een proces-gebaseerd model, namelijk het gedistribueerde `sflow_sbm`-model, met wereldwijd beschikbare meteorologische data en waarbij de meeste parameters zijn geschat met werelddekkende databronnen, gebruikmakend van (pedo)transferfuncties. Een module met een doelfunctie voor het beheer van berging en uitstroom van reservoirs (reservoir operation module; ROM) is toegepast om het operationeel beheer van de reservoirs Sirikit en Bhumibol te simuleren. De gebruikte mondiale datasets kunnen redelijk goed compenseren voor het gebrek aan in-situ-data. Het model kan afvoer op dagelijkse resolutie goed simuleren voor natuurlijke stroomgebieden (t.w. zonder reservoirs) qua grootte, timing en duur. De ROM vangt

daarentegen alleen de seizoensvariatie van de reservoiruitstroom, maar kan de dagelijkse uitstroom niet nauwkeurig simuleren doordat het werkelijke beheer van de twee reservoirs te complex is om te worden gereconstrueerd door de module.

In hoofdstuk 5 pluizen we de effecten van de reservoirs Sirikit en Bhumibol uit door in detail te kijken naar de waterbalans, het regime van de dagelijkse afvoer en extreme afvoeren. De twee reservoirs beïnvloeden de verschillende termen van de waterbalans, met name voor de cumulatieve dagelijkse waterbalanscomponenten gedurende het jaar. De reservoirs keren de natuurlijke seizoensvariatie in dagelijkse afvoer om, met hogere afvoeren in het droge seizoen en lagere afvoeren in het regenseizoen. Ze dempen de variatie in afvoer, met een grotere bijdrage van basisafvoer en minder pieken. Ze hebben veel extreme afvoeren gemitigeerd, hoewel het beheer is aangepast in de loop der tijd. De grootte en timing van extreme afvoeren is daarentegen meer variabel geworden en moeilijker te voorspellen wanneer reservoirbeheer een rol speelt. Deze effecten onderstrepen het belang van het effectief modelleren van reservoirbeheer, inclusief het voorspellen van reservoirinstroom en -uitstroom, vooral in real-time.

In hoofdstuk 6 presenteren we data-gedreven modellen, met name machine learning (ML), voor het simuleren van het beheer en de uitstroom van het Sirikit reservoir, met een focus op het verwerven van inzichten in de karakteristieken van en relaties tussen beschikbare reservoir-gerelateerde data als invoervariabelen. We vergeleken de prestaties van ML-algoritmes die veel gebruikt worden voor reservoirbeheer, namelijk Multilineaire Regressie, Support Vector Machines, K-Nearest Neighbor, Classificatie en Regression Tree, Random Forest, Multi-Layer Perceptron en Recurrent Neural Network. Van de 17 gebruikte invoercombinatiescenario's bestaat de meest geschikte dataset voor ML-modellen uit (i) gemeten reservoirberging van de vorige dag, (ii) gesimuleerde instroom (door `wflow_sbm`) van twee dagen geleden tot twee dagen vooruit en (iii) maand van het jaar. Alle ML-modellen presteren significant beter dan de ROM. De Recurrent Neural Network bleek de grootste potentie te bieden voor verbetering.

In hoofdstuk 7 verkennen we het vermogen van het meest veelbelovende ML-model, de Recurrent Neural Network, en zijn geavanceerde algoritmes Long Short-Term Memory en Gated Recurring Unit, in het simuleren en voorspellen van real-time beheer en uitstroom van het Sirikit reservoir. Het `wflow_sbm`-model is gebruikt voor probabilistisch hervoorspellen van de instroom. De ML-modellen zijn getraind en getest met een 10-voudige kruisvalidatie. Ze kunnen het real-time beheer van het Sirikit reservoir reconstrueren en leveren nauwkeurige dagelijkse afvoeren, vooral wanneer de trainingsdata zowel normale als extreme uitstroomcondities bevatten. Ze kunnen de uitstroom hervoorspellen tot twee dagen vooruit voor lage afvoeren en een week vooruit voor hoge afvoeren, en presteren beter voor hoge uitstromen (gedurende het droge seizoen) dan voor lage uitstromen (gedurende het natte seizoen). Gated Recurring Unit bleek het meest nauwkeurig, robuust en gemakkelijk gegeven de huidige opzet voor de training van het model. We stellen voor om de modelopzet verder te verbeteren en te combineren met data-assimilatie voor toepassingen in de praktijk.



Hoofdstuk 8 synthetiseert de bevindingen van de vier kernhoofdstukken vanuit een breder perspectief. De belangrijkste conclusies zijn: (i) mondiale datasets kunnen hydrologisch modelleren versterken, maar een betere beschikbaarheid en toegankelijkheid van in-situ-data is nodig voor effectief modelleren en voorspellen van reservoirbeheer. (ii) Reservoirbeheer en de hydrologische impacts en modellering ervan zal een uitdagend onderwerp in hydrologie blijven. Vooruitgang in data, modelleertechnieken en computerkracht bieden mogelijkheden voor modelontwikkeling en -toepassing. De toekomstige ontwikkeling van reservoirbeheersmodellen ligt in het integreren van proces-gebaseerde en data-gedreven modellen. (iii) Keuzes voor de bouw en het beheer van reservoirs zouden gebaseerd moeten worden op ervaringen met reeds gebouwde reservoirs, gegeven de balans van hun baten gedurende de levensduur van de dam enerzijds en negatieve impacts anderzijds. Dit proefschrift kan bijdragen aan het duurzaam plannen en beheren van reservoirs in het bovenstroomse deel van het GCPR stroomgebied in het zicht van het 20-jaar durende nationale masterplan voor waterbronnen (National Water Resource Management Master Plan) voor de periode 2018-2037. Het is ook toepasbaar op nationaal niveau en voor naburige landen in Zuidoost-Azië, die hotspots zijn voor de bouw van nieuwe reservoirs.



# Summary (Thai)

อ่างเก็บน้ำและเขื่อนเป็นสิ่งปลูกสร้างพื้นฐานที่สำคัญในลุ่มน้ำหลักๆทั่วโลก อนึ่ง แม้ว่าจะมีการก่อสร้างอ่างเก็บน้ำและเขื่อนเพิ่มขึ้นเรื่อยๆในลุ่มน้ำหลายๆแห่ง แต่ประโยชน์และผลกระทบเชิงลบของอ่างเก็บน้ำและเขื่อนยังคงเป็นที่ถกเถียงในวงกว้าง ด้วยเหตุนี้ แบบจำลองการปฏิบัติการอ่างเก็บน้ำ (reservoir operation modelling) จึงมีความจำเป็นต่อการวางแผนและการจัดการทรัพยากรน้ำอย่างมีประสิทธิภาพ อย่างไรก็ตาม การปฏิบัติการอ่างเก็บน้ำถือเป็นส่วนที่ท้าทายในการสร้างแบบจำลองอุทกวิทยา (hydrological modelling) วิทยานิพนธ์ปริญญาเอกเล่มนี้จึงช่วยสร้างความรู้ความเข้าใจเกี่ยวกับการปฏิบัติการ ผลกระทบทางอุทกวิทยา และการจำลองและพยากรณ์การปฏิบัติการอ่างเก็บน้ำ โดยมีวัตถุประสงค์หลักคือเพื่อพัฒนา วิเคราะห์ตรวจสอบ และประยุกต์ใช้แบบจำลองการปฏิบัติการอ่างเก็บน้ำ ด้วยข้อมูลและเทคนิคการสร้างแบบจำลองที่มีอยู่ในปัจจุบัน ทั้งนี้ เพื่อจำลองและคาดการณ์การปล่อยน้ำจากเขื่อนรายวัน ขอบเขตของวิทยานิพนธ์ครอบคลุม ๔ หัวข้อ ได้แก่ (๑) การสร้างแบบจำลองอุทกวิทยาเชิงกระบวนการ (process-based) โดยใช้ข้อมูลสารสนเทศจากฐานข้อมูลนานาชาติ (๒) ผลกระทบทางอุทกวิทยาของการปฏิบัติการอ่างเก็บน้ำ (๓) การสร้างแบบจำลองอุทกวิทยาที่ขับเคลื่อนด้วยข้อมูล (data-driven) เพื่อการจำลองการปฏิบัติการอ่างเก็บน้ำ และ (๔) การพยากรณ์ (forecasting) การปฏิบัติการอ่างเก็บน้ำและการปล่อยน้ำจากเขื่อนแบบเรียลไทม์ (real-time)

ในวิทยานิพนธ์เล่มนี้ ผู้เขียนได้อธิบายถึงภาพรวมของการพัฒนาอ่างเก็บน้ำทั่วโลก และหลักการพื้นฐานของการปฏิบัติการอ่างเก็บน้ำประเภทเนกประสงค์ (multi-purpose) ซึ่งรวมถึงความท้าทายของการปฏิบัติการในทางทฤษฎี ในทางปฏิบัติ และในกระบวนการสร้างแบบจำลอง (ดูบทที่ ๑) เนื่องจากวิทยานิพนธ์มุ่งเน้นไปที่การศึกษาอ่างเก็บน้ำและเขื่อนขนาดใหญ่ ผู้เขียนจึงใช้อ่างเก็บน้ำและเขื่อนที่สำคัญทางตอนบนของลุ่มแม่น้ำเจ้าพระยาในประเทศไทย ได้แก่ เขื่อนสิริกิติ์และเขื่อนภูมิพล เป็นกรณีศึกษา (ดูบทที่ ๒) ทั้งนี้ ผู้เขียนได้ประยุกต์ใช้ข้อมูลจากหลายแหล่ง (ข้อมูลภาคสนามในลุ่มน้ำที่ศึกษา และข้อมูลสารสนเทศจากฐานข้อมูลนานาชาติ) และแบบจำลองอุทกวิทยาหลายประเภท (แบบจำลองเชิงกระบวนการ และแบบจำลองที่ขับเคลื่อนด้วยข้อมูล) ในการพัฒนา วิเคราะห์ตรวจสอบ และประยุกต์ใช้แบบจำลองการปฏิบัติการอ่างเก็บน้ำเพื่อจำลองและพยากรณ์การปล่อยน้ำจากเขื่อนและน้ำท่ารายวัน (ดูบทที่ ๓)

ในบทที่ ๔ ผู้เขียนได้นำเสนอแบบจำลองอุทกวิทยาเชิงกระบวนการ ชื่อ wflow\_sbm โดยประยุกต์ใช้ข้อมูลอุทุนิยมวิทยาจากฐานข้อมูลนานาชาติ และใช้ค่าพารามิเตอร์ (parameters) ส่วนใหญ่ที่คำนวณมาจากแหล่งข้อมูลทั่วโลกโดยใช้ฟังก์ชันถ่ายโอน ((pedo)transfer functions) ทั้ง-

นี้ ในการจำลองระบบปฏิบัติการอ่างเก็บน้ำของเขื่อนสิริกิติ์และเขื่อนภูมิพล ผู้เขียนได้พัฒนาโมดูลการปฏิบัติการอ่างเก็บน้ำในแบบจำลอง wflow\_sbm ด้วยหลักการรักษาสมวลและเป้าหมายของปริมาณเก็บกักน้ำและการปล่อยน้ำจากระบบอ่างเก็บน้ำ (target storage-and-release-based reservoir operation module; ROM) โดยในการศึกษานี้พบว่า การประยุกต์ใช้ข้อมูลสารสนเทศจากฐานข้อมูลนานาชาติสามารถใช้แทนข้อมูลภาคสนามที่ขาดแคลนได้อย่างสมเหตุสมผล ดังนั้น แบบจำลอง wflow\_sbm นี้จึงสามารถจำลองน้ำท่ารายวันสำหรับลุ่มน้ำธรรมชาติ (ลุ่มน้ำย่อยที่ไม่มีอ่างเก็บน้ำและเขื่อน) ได้เป็นอย่างดี ทั้งในด้านปริมาณ (magnitude) เวลา (timing) และระยะเวลา (duration) อย่างไรก็ตาม พบว่า ROM สามารถบันทึกความผันแปรทางฤดูกาลของการปล่อยน้ำจากเขื่อนได้แต่ไม่สามารถจำลองการปล่อยน้ำรายวันจากเขื่อนได้อย่างแม่นยำเนื่องจากในความเป็นจริงนั้น ระบบการปฏิบัติการของอ่างเก็บน้ำทั้งสองแห่งมีความซับซ้อนเกินกว่าที่จะสามารถถ่ายทอดออกมาได้อย่างชัดเจนด้วยโมดูลทางคณิตศาสตร์

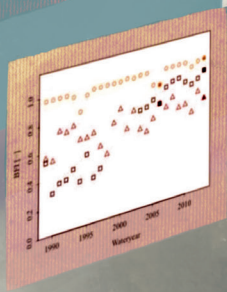
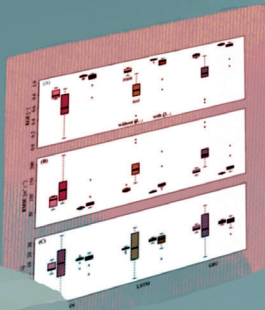
ในบทที่ ๕ ผู้เขียนได้ศึกษาถึงผลกระทบทางอุทกวิทยาของการปฏิบัติการอ่างเก็บน้ำ ของเขื่อนสิริกิติ์และเขื่อนภูมิพล โดยการวิเคราะห์วัฏจักรความสมดุลของน้ำ (water balance) ระบบน้ำท่ารายวัน (streamflow regime) และน้ำท่าที่ผิดปกติ (extreme flows) โดยในการศึกษานี้พบว่า อ่างเก็บน้ำทั้งสองแห่งส่งผลกระทบต่อความสมดุลของน้ำในหลายด้าน โดยเฉพาะอย่างยิ่งในด้านปริมาณสะสมของน้ำไหลเข้าและน้ำไหลออกรายวัน (cumulative daily water balance components) ในแต่ละปี ทั้งนี้ การปฏิบัติการอ่างเก็บน้ำได้ปรับเปลี่ยนลักษณะของระบบน้ำท่ารายวันไปจากฤดูกาลตามธรรมชาติโดยสิ้นเชิง โดยทำให้ปริมาณน้ำท่าสูงขึ้นในฤดูแล้งและน้อยลงในฤดูฝน และลดความผันแปรของน้ำท่า (flow variability) ลงโดยการเพิ่มปริมาณน้ำพื้นฐาน (baseflow) และลดการแปรปรวนโดยเฉียบพลัน (flashiness) นอกจากนี้ การปฏิบัติการอ่างเก็บน้ำยังช่วยบรรเทาเหตุการณ์น้ำท่าที่ผิดปกติหลายครั้งในอดีต อย่างไรก็ตาม พบว่าการปฏิบัติการอ่างเก็บน้ำได้ทำให้ปริมาณและช่วงเวลาของการเกิดน้ำท่าที่ผิดปกติมีความแปรปรวนมากขึ้น ซึ่งทำให้ยากต่อการคาดการณ์ ผลกระทบเหล่านี้ได้เน้นย้ำถึงความสำคัญของการสร้างแบบจำลองการปฏิบัติการอ่างเก็บน้ำที่มีประสิทธิภาพ ซึ่งรวมไปถึงการพยากรณ์การไหลเข้าและออกของน้ำในอ่างเก็บน้ำ โดยเฉพาะในแบบเรียลไทม์

ในบทที่ ๖ ผู้เขียนได้นำเสนอแบบจำลองที่ขับเคลื่อนด้วยข้อมูล ซึ่งเป็นปัญญาประดิษฐ์ด้วยการเรียนรู้ของเครื่อง (machine learning; ML) เพื่อการจำลองการปฏิบัติการอ่างเก็บน้ำและการปล่อยน้ำของเขื่อนสิริกิติ์ โดยมุ่งเน้นไปที่การวิเคราะห์ลักษณะและความสัมพันธ์ของข้อมูลที่เกี่ยวข้องกับอ่างเก็บน้ำที่มีอยู่ในปัจจุบัน เพื่อใช้เป็นตัวแปรต้น (input variables) ของอัลกอริทึม ML ทั้งนี้ ได้เลือกศึกษาอัลกอริทึมที่มีการใช้กันอย่างแพร่หลายในการสร้างแบบจำลองการปฏิบัติการอ่างเก็บน้ำ ได้แก่ Multiple Linear Regression, Support Vector Machine, K-Nearest Neighbor, Classification and Regression Tree, Random Forest, Multi-Layer Perceptron และ Recurrent Neural Network จากการพิจารณาเปรียบเทียบชุดข้อมูลตัวแปรต้นที่แตกต่างกัน ๑๗ ชุด พบว่า ชุดข้อมูลตัวแปรต้นที่เหมาะสมที่สุดสำหรับแบบจำลอง ML ข้างต้นประกอบด้วย (๑) ปริมาณน้ำในอ่างเก็บน้ำที่สังเกตการณ์ (observed reservoir storage) จากวันก่อนหน้า (๒) ปริมาณน้ำที่ไหลเข้าอ่างเก็บน้ำที่ได้จากการจำลอง (simulated inflow) โดยแบบจำลอง wflow\_sbm จากสองวันที่แล้วถึงสองวันวันข้างหน้า และ (๓) เดือนนั้นๆ ของปี โดยแบบจำลองทุกอัล-

กอร์ธิมแสดงถึงประสิทธิภาพในการทำนายที่สูงกว่าการทำนายด้วย ROM อย่างเห็นได้ชัด โดยพบว่า Recurrent Neural Network มีศักยภาพสูงสุดสำหรับการปรับปรุงประสิทธิภาพเพิ่มเติมต่อไป

ในบทที่ ๗ ผู้เขียนได้วิเคราะห์ความสามารถของแบบจำลอง ML ที่มีศักยภาพสูงสุดมากที่สุด ได้แก่ Recurrent Neural Network และอัลกอริทึมขั้นสูงของมัน คือ Long Short-Term Memory และ Gated Recurring Unit โดยมีวัตถุประสงค์เพื่อจำลองและคาดการณ์การปฏิบัติการอ่างเก็บน้ำแบบเรียลไทม์และการปล่อยน้ำของเขื่อนสิริกิติ์ ทั้งนี้ ได้ใช้แบบจำลอง wflow\_sbm ในการคาดการณ์ความน่าจะเป็นของปริมาณน้ำที่ไหลเข้าอ่างเก็บน้ำ (probabilistic inflow reforecasting) แบบจำลอง ML ได้รับการฝึกฝน (train) และทดสอบ (test) ประสิทธิภาพแบบ 10-fold Cross Validation โดยพบว่าแบบจำลองจากทั้งสามอัลกอริทึมสามารถจำลองการปฏิบัติการอ่างเก็บน้ำและการปล่อยน้ำของเขื่อนสิริกิติ์ได้อย่างแม่นยำ โดยเฉพาะอย่างยิ่งเมื่อข้อมูลชุดเรียนรู้ (training data) ครอบคลุมทั้งสภาวะการปล่อยน้ำแบบปกติและแบบที่ผิดปกติ แบบจำลองทั้งสามสามารถคาดการณ์การปล่อยน้ำล่วงหน้าได้สูงสุดสองวันสำหรับการปล่อยน้ำน้อย (low outflows) และสูงสุดหนึ่งสัปดาห์สำหรับการปล่อยน้ำมาก (high outflows) และมีประสิทธิภาพในการคาดการณ์สำหรับการปล่อยน้ำมาก (ในช่วงฤดูแล้ง) ได้การปล่อยน้ำน้อย (ในช่วงฤดูฝน) ทั้งนี้ Gated Recurring Unit ถือเป็นแบบจำลองที่แม่นยำ มีประสิทธิภาพ และสะดวกมากที่สุดเมื่อพิจารณาจากการฝึกและทดสอบนี้ อย่างไรก็ตาม แบบจำลองควรได้รับการปรับปรุงและพัฒนาเพิ่มเติม รวมถึงการประยุกต์ใช้ร่วมกับการผนวกข้อมูลเชิงตัวเลข (การผนวกข้อมูลจริงจากการตรวจวัด) เพื่อใช้ในการคาดการณ์จริงในทางปฏิบัติ

ในบทที่ ๘ ผู้เขียนสังเคราะห์ผลการศึกษาของ ๔ บทหลักข้างต้นในมุมมองที่กว้างขึ้น โดยมีข้อสรุปหลักดังนี้ (๑) ข้อมูลสารสนเทศจากฐานข้อมูลนานาชาติสามารถส่งเสริมการสร้างแบบจำลองอุทกวิทยาได้ แต่จำเป็นต้องมีความพร้อมใช้งานและการเข้าถึงข้อมูลในแหล่งต่างๆ ที่ดีกว่านี้ เพื่อส่งเสริมการสร้างแบบจำลองและคาดการณ์การปฏิบัติการอ่างเก็บน้ำได้อย่างมีประสิทธิภาพ (๒) การปฏิบัติการอ่างเก็บน้ำ ผลกระทบทางอุทกวิทยา และการสร้างแบบจำลองจะยังคงเป็นหัวข้อที่ท้าทายในการศึกษาวิจัยด้านอุทกวิทยา อย่างไรก็ตาม ความก้าวหน้าของข้อมูล เทคนิคการสร้างแบบจำลอง และเทคโนโลยีการคำนวณ ได้เพิ่มโอกาสในการพัฒนาและใช้งานแบบจำลองมากขึ้น ทั้งนี้ การพัฒนาแบบจำลองการปฏิบัติการอ่างเก็บน้ำในอนาคตขึ้นอยู่กับกระบวนการระหว่างแบบจำลองเชิงกระบวนการและแบบจำลองที่ขับเคลื่อนด้วยข้อมูล (๓) การก่อสร้างเขื่อนและการปฏิบัติการอ่างเก็บน้ำ ควรอยู่บนพื้นฐานของประสบการณ์ที่มีจากอ่างเก็บน้ำที่มีมาก่อนหน้านี้ โดยคำนึงถึงคุณสมบัติของผลประโยชน์ตลอดอายุการใช้งานและผลกระทบเชิงลบ อนึ่ง ผู้เขียนหวังเป็นอย่างยิ่งว่าวิทยานิพนธ์เล่มนี้จะเป็นประโยชน์ต่อการวางแผน และจัดการทรัพยากรอ่างเก็บน้ำและเขื่อนอย่างยั่งยืนในลุ่มน้ำเจ้าพระยาตอนบน ตามแผนแม่บทการบริหารจัดการทรัพยากรน้ำแห่งชาติ 20 ปี ในช่วงปี พ.ศ. 2561-2580 ของประเทศไทย นอกจากนี้ผลการศึกษาในวิทยานิพนธ์เล่มนี้ยังสามารถเป็นประโยชน์ต่อการศึกษาและจัดการลุ่มน้ำอื่นๆ ทั้งในประเทศไทยและประเทศเพื่อนบ้านในเอเชียตะวันออกเฉียงใต้ ซึ่งเป็นภูมิภาคที่มีการก่อสร้างอ่างเก็บน้ำและเขื่อนใหม่ๆ เพิ่มขึ้นเป็นจำนวนมาก





# **Chapter 1**

## **General introduction**

## 1.1 Anthropogenic rivers

### 1.1.1 Most of the world's rivers are no longer flowing naturally

Rivers are the vital bloodstreams of the Earth that support environmental health, economic wealth and human welfare. Big rivers and their basins around the globe are the cradle of human culture and civilization (Bianchi, 2016) and are home to diverse ecosystems and biodiversity (Abell et al., 2017). Since the ancestral settlement of humankind some 10,000 years ago, rivers have continuously provided essential resources for human well-being and society, including domestic water supply, agriculture and food production, transportation and, more recently, industrial production and hydropower generation (Ripl, 2003; Vuorinen et al., 2007). As these societal functions require the right amount of water with the right quality in the right places at the right times, river flows have long been controlled and regulated by humans in efforts to maximize water resource utilization.

To control and regulate river flows for water diversion, extraction and collection, humans have altered the natural dynamics and connectivity of rivers in four dimensions: longitudinally (upstream and downstream of the river channel), laterally (from the river to the floodplain), vertically (between the river and groundwater) and temporally (flow seasonality) (Ward, 1989). Most rivers have been altered directly by placing hydraulic structures, such as dams, barrages, weirs, sluice gates, levees, dikes and groynes, and by taking hydraulic measures, such as channelization and dredging (Ylla Arbós et al., 2021). Other rivers have been altered indirectly by modifying the hydrological, thermal and sediment regimes (Nilsson & Berggren, 2000).

Since the beginning of the 20<sup>th</sup> century, rapid global population growth, economic development and climate change have generated rising demands for water, food, energy, the industry as well as water-related disaster management. These demands increase stresses on rivers and their limited water resources, calling for even more river alteration to sustain river services globally (De Stefano et al., 2017). Subsequently, at least two-thirds of the world's rivers longer than 1000 km (representing 41% of the world's rivers' discharge volume) are no longer flowing naturally and more than 500,000 km of the world's rivers are actively regulated (Figure 1.1; Revenga et al., 2000; Grill et al., 2015, 2019).

### 1.1.2 There is a global expansion in reservoirs and damming

Amongst several engineering solutions, the construction of reservoirs and dams, and their flow regulations, have been the main contributors to major river alteration worldwide (Grill et al., 2019). It is believed that the first dam was built in Mesopotamia (Jain & Singh, 2003). Since then, several types of reservoirs and dams have been designed and increasingly applied for several purposes. Nowadays, dammed reservoirs, referred to as *reservoirs* in this PhD thesis, play a key role in the planning, management

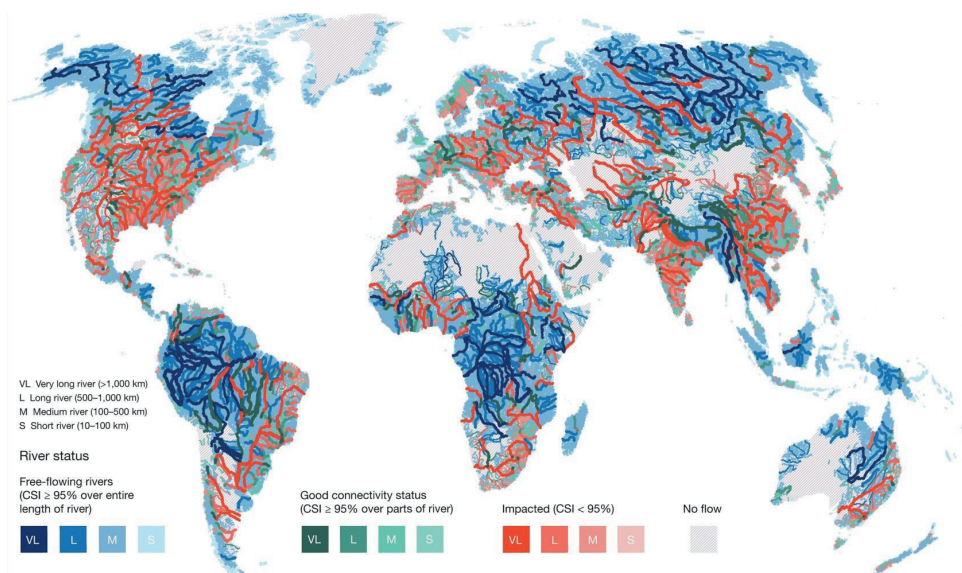


**Figure 1.1:** Map of the world's river connectivity: free-flowing and non-free-flowing. Free-flowing rivers are indicated with the entire lengths (shown in blue shades). Non-free-flowing rivers are divided into stretches according to the connectivity status index (CSI): stretches with CSI above the threshold (green) and below the threshold (red) (Grill et al., 2019).

and control of water resources from the local to regional scale. The main purpose of most reservoirs is serving irrigation (48%), followed by generating hydropower (20%), securing domestic and industrial water supply (15%), mitigating floods (8%), and aiding inland navigation, aquaculture, recreation and environmental considerations (9%) (Altinbilek, 2002).

Rapid population growth and economic development since the beginning of the 20<sup>th</sup> century have led to the global expansion in reservoir construction. The global irrigated agricultural area increased by 385% from 1900 to 2010 (Siebert et al., 2013), and the global electricity generation increased by 72% from 2000 to 2015 (Hennig & Magee, 2017). To accommodate these rising demands, the construction of reservoirs was intensified. It started in developed countries and was soon followed by developing countries (Hogeboom et al., 2018). As of 2011, around 2.8 million reservoirs (with reservoir areas > 0.001 km<sup>2</sup>) had been built, giving a total storage volume of over 8,000 km<sup>3</sup> and a combined area of over 305,700 km<sup>2</sup> (Lehner et al., 2011). From this total number, 37,600 reservoirs are considered major (with dams higher than 15 m), of which over 8,600 are primarily designed for hydropower generation (Zarfl et al., 2015). In 2014, only 22% of the world's technically feasible hydropower was harnessed (Zarfl et al., 2015). The World Commission on Dams (2000) estimated that toward the end of the

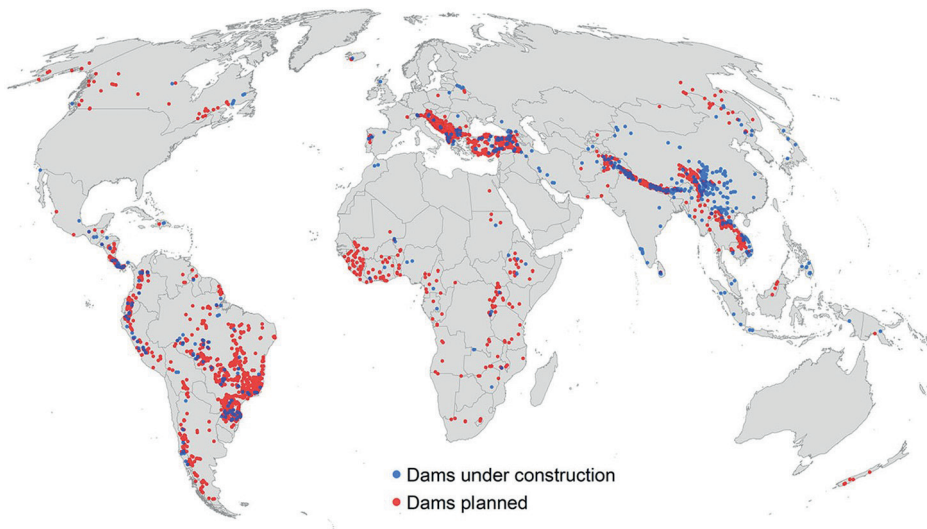


**Figure 1.2:** Map of the world's major reservoirs with the main purpose of hydropower generation that were either under construction (17%; blue dots) or planned (83%; red dots) in 2014 (Zarfl et al., 2015).

20<sup>th</sup> century, major reservoirs contributed directly to 16% of the global food production and 19% of the global electricity generation. The annual use of the world's reservoirs for all purposes is valued at USD 265 billion per year (Hogeboom et al., 2018).

As the world's development rapidly continues, recent projections suggest that the global crop production will be more than double the current value by 2100 (Beltran-Peña et al., 2020) and the global electricity is expected to rise by an additional 56% by 2040 (Zarfl et al., 2015). With the urgent need to meet these ongoing demands, a resurgence in the plans for and construction of new reservoirs has been witnessed in the past decade (Best, 2019). In 2014, at least 3,700 new major reservoirs were officially being planned (83%) or under construction (17%) (Zarfl et al., 2015). The expansion in reservoir construction mainly takes place in tropical and subtropical countries with emerging economies, including Southeast Asia, South America and Africa (Figure 1.2; Zarfl et al., 2015; International Hydropower Association, 2022). Very large reservoirs will primarily be located in Asia and South America (Zarfl et al., 2015). Within the next decades, these new reservoirs are expected to foster the expanding irrigated agricultural areas and increase the desired hydropower supply worldwide by 73%, accounting for 39% of the technically feasible hydropower (Zarfl et al., 2015). Considering their remaining potential, reservoirs have been—and continue to be—a crucial measure to cope with the world's increasing water demand resulting from population growth, economic development and the urge for renewable energy in response to climate change.

### 1.1.3 Controversial impacts of reservoirs call for local-scale research

Although reservoirs are undoubtedly a necessity in water resources management and the world's development, they have become more controversial due to their negative impacts. Most major reservoirs are located in the world's big rivers (Figure 1.1), disturbing the rivers' natural dynamic and connectivity, as previously explained. New major reservoirs, which are being planned or under construction in 25 of the 120 major free-flowing rivers (Figure 1.2), will further decrease the number of remaining free-flowing rivers by 21% (Nilsson et al., 2005; Zarfl et al., 2015). When rivers cease to be free-flowing and become highly regulated, their hydrological characteristics change, which consequently poses considerable risks to the environment and society (Baxter, 1977; Wang et al., 2012).

Since reservoirs impound, divert and control river flows, they are bound to alter the hydrological cycle, water balance and flow variability (Lehner et al., 2011). Although most reservoirs present the same objective of flow regulation to eliminate peak flows and stabilize low flows, their impacts on the hydrological characteristics vary in terms of flow rate, magnitude, duration, timing and frequency, depending on the reservoir purposes, operation scheme, location and hydrological and climatic conditions. In addition, while reservoirs are known to avert excessive downstream floods and droughts, recent research shows that some reservoirs may reduce the flood buffering capacity or increase water shortages due to conflicts and mismanagement of reservoir water (Ogilvie et al., 2019). Apart from mismanagement, some reservoirs induce downstream riverbank erosion, causing more severe flood peaks (Mei et al., 2018). In many cases, over-reliance on reservoirs also reduces communities' incentive for adaptive actions, increasing their vulnerability and potential damages caused by socioeconomic droughts (Di Baldassarre et al., 2018).

Several impacts of reservoirs on the environment and society are well-known. These include, for example, habitat changes and extinctions of species for riverine and terrestrial ecosystems (Bunn & Arthington, 2002; Benchimol & Peres, 2015), downstream sediment and nutrient starvation (Vörösmarty et al., 2003), downstream changes in water and food security (Veldkamp et al., 2017) and resettling of human populations (Scudder, 2012). Some other impacts are more indirect, for example, the release of greenhouse gases from decaying vegetation (Räsänen et al., 2018), the blue water footprint from additional water loss through evaporation (Hogeboom et al., 2018) and the increasing incidence of communicable diseases (Scudder, 2012). Like the hydrological impacts, the environmental and societal impacts are also different per reservoir and river basin.

While the massive plans and construction of reservoirs significantly affect rivers, the environment and society, the projected climate change is also expected to alter the precipitation and temperature, and thus the water availability and distribution (Lauri et al., 2012). To sustain the world's development against climate change, there is an

urgent yet challenging need to comprehensively understand reservoirs, their operation and their effects in order to assist the sustainable planning and management of water resources. Hence, as the vigorous debate on reservoir construction continues, research focused on their impacts on hydrological regimes (and thus on environment and society) and their operation modelling, particularly in real-time, remains indispensable.

Previous studies have investigated the quantitative and qualitative impacts of reservoirs from the local scale (e.g., Camargo & de Jalon, 1990; Wu et al., 2018) to the regional scale (e.g., Li et al., 2012; Hecht et al., 2019; Yun et al., 2020) and the global scale (e.g., Chao et al., 2008; Döll et al., 2009). The regional- and global-scale studies have provided a comprehensive overview of reservoir impacts that are valuable and should be considered for new reservoir construction. However, as previously emphasized, each reservoir is unique and is managed and controlled independently to some extent. Therefore, its hydrological, environmental and societal impacts should also be evaluated and understood locally. This calls for more research at the reservoir scale, the multi-reservoir system scale and the basin scale.

## 1.2 Reservoir operation

### 1.2.1 In theory: balance, zones and rule curves

Reservoirs are used for two main tasks: storing and releasing water with the right amount and at the right time. The regulation and control of reservoir storage and release are called *reservoir operation*. Before diving into the theoretical concept of reservoir operation, it is important to note that there are different classes of reservoirs, which are thus operated under different operation schemes. Reservoirs can be categorized based on various characteristics. In general, they are categorized based on purpose: single-purpose reservoirs, which are usually small, and multi-purpose reservoirs, which are usually large and account for around 30% of the total number of reservoirs (Altinbilek, 2002). Other classifications include size (minor, medium and major), and storage (over-year and seasonal) (Jain & Singh, 2003). This thesis focuses on *major* (dams higher than 15 m), *multi-purpose* and *over-year storage* (designed to serve for the entire year and, in some cases, more than a year) reservoirs, as they have a large impact on the economy, society and environment. Therefore, the following detail on reservoir operation is mainly specified for this class of reservoirs.

A major multi-purpose reservoir normally contains four main structural features: reservoir, dam, outlet and spillway (Figure 1.3; Jain & Singh, 2003). The outlet, located almost at the bottom of the dam, is used to release water on a routine basis for irrigation, hydropower generation, water supply and downstream environmental flow. The spillway, located almost at the top of the dam and either gated or ungated, is used to spill any excess water, mostly occurring during high inflow and flood periods. Based on these releasing structures and their releasing magnitudes, the operation of a ma-



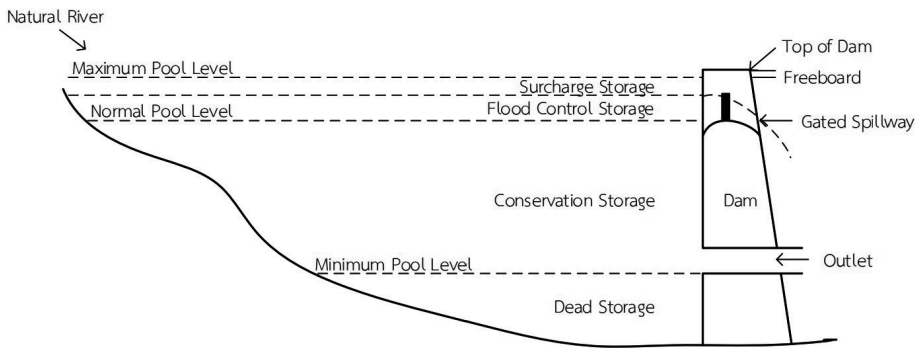


**Figure 1.3:** Schematic diagram of a reservoir, including the main structural features and the reservoir storage zones (Rittima, 2018).

For multi-purpose reservoir is designed with respect to three approaches: the reservoir water balance, reservoir storage zoning and reservoir operating rule curves.

#### *Reservoir water balance*

In the same manner as the water balance in any water system, the reservoir water balance is the mass balance or continuity equation. It states that the sum of fluxes into and out of the reservoir and the change in water storage is equal to zero over a given period. According to Jain & Singh (2003), the complete reservoir water balance can be expressed as

$$I_S + I_G + P - E - Q - L - \Delta S \pm \delta = 0, \quad (1.1)$$

where  $I_S$  is the surface water inflow into the reservoir,  $I_G$  is the groundwater inflow,  $P$  is the precipitation over the reservoir surface,  $E$  is the evaporation over the reservoir surface,  $Q$  is the reservoir outflow,  $L$  is the storage loss (such as groundwater seepage and dam leakage),  $\Delta S$  is the change in reservoir storage during the given period and  $\delta$  is the error term. All components in the equation are expressed either in volume or depth units.

In reservoir operation, it is, therefore, necessary to be acquainted with the net inflow and net outflow to determine the storage change. It is also important to keep track of the actual reservoir storage capacity and its change over time, which could be caused by sediment trapping or sediment flushing.

#### *Reservoir storage zoning*

When a reservoir is designed to serve multiple purposes with the over-year storage scheme, it is difficult to define a simple operating policy. Dividing the reservoir stor-

age capacity into *zones* provides a means to address and determine water availability and allocation for different purposes (Beard, 1967). Therefore, on top of the reservoir water balance, a reservoir is usually operated upon the principle of storage zoning. In most cases, the reservoir storage is divided into four zones from the bottom to the top: *inactive* storage, *conservation* storage, *flood control* storage and *surcharge* storage (Figure 1.3; Jain & Singh, 2003). The inactive storage zone, so-called dead storage, stores upstream sediment and provides minimum needs for the reservoir ecosystem. The conservation storage zone supports various requirements on a routine basis through the reservoir outlet, including irrigation, hydropower generation, water supply and downstream environmental flow. This zone, therefore, generally accounts for most of the reservoir storage capacity. The flood control storage zone is used to prevent and control downstream floods by storing excess water to attenuate flood peaks. After the flood has passed, water stored in this zone is gradually emptied through the spillway to prepare for subsequent flood events. The surcharge storage zone is used during extreme floods. The storage level in this zone is dangerously high and only used in cases of emergency. After a threatening flood peak has been mitigated, the surcharge storage is spilled as soon as possible to prevent dam failure. Some reservoirs also identify a buffer storage zone between the inactive and conservation storage zones, which becomes operational for sustaining water to meet essential needs under extreme drought situations.

Computing and zoning reservoir storage capacity is imperative and individually attributed to each reservoir. The focus is typically on the conservation storage zone as its volume varies the most (Rippl, 1883). The reservoir storage zoning involves complicated procedures, which are beyond the scope of this thesis, and thus the detail is omitted here. For a major, multi-purpose and over-year storage reservoir, the boundary between the conservation storage and flood control storage zones usually changes during the course of a year to maximize the useful water storage capacity and its usage. For example, a larger conservation storage and a smaller flood control storage are needed in seasons that are likely to encounter low inflow. This more advanced aspect of the reservoir operation is further explained in the following section.

#### *Reservoir operating rule curves*

Operational policies with the zone-based operation approach are usually implemented based on dynamic rules established for the storage zones (Sigvaldson, 1976). The operating rules consist of *release rules* that are applicable for each storage zone and overall *storage rules*. In general, these rules vary on a long-term monthly basis, depending on the seasonality of inflow and the variability of water demands. The rules represent the monthly optimum, maximum and minimum values for the storage and/or release. These target monthly values throughout the year are known as the *operating rule curves* (see Figure 1.4). In most cases, the release rule curves represent high releases in the dry season (to support irrigated agriculture and domestic and industrial water demands) and low releases in the wet season (to sustain hydropower generation while preventing

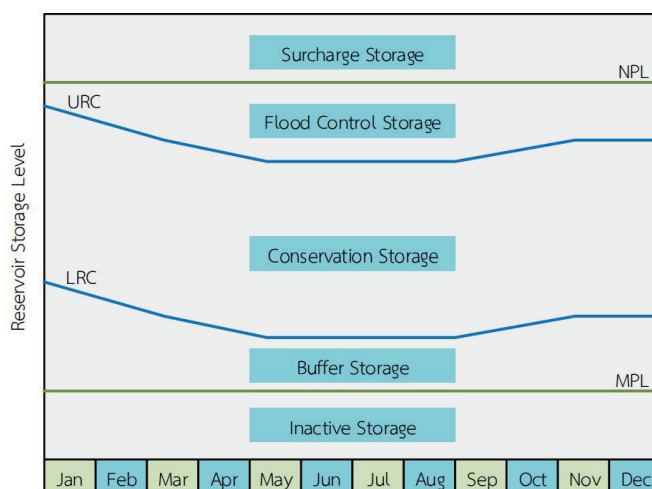


**Figure 1.4:** Example of variation of reservoir storage zoning and operating rule curves that are set on a monthly basis. The rule curves include the upper (maximum) rule curve (URC) and the lower (minimum) rule curve (LRC), which remain within the minimum pool level (MPL) and the normal pool level (NPL) of the conservation storage zone (Rittima, 2018).

or moderating downstream floods). The storage rule curves aim to remain below the maximum storage level in the wet season and above the minimum storage level in the dry season. Therefore, the storage is aimed to reach a higher level with a larger flood control storage zone in the wet season (to fill the reservoir and store excess water) than in the dry season. The operating rule curves are strongly tailored to individual reservoirs and their purposes.

The inclusion of operating rule curves permits operational flexibility at certain times of the year to satisfy different purposes. Therefore, optimizing and updating the rule curves are crucial tasks to maintain high reservoir system performance. The rule curves are traditionally derived through intensive simulation techniques. A detailed description of rule curve optimization is not included here since this thesis does not intend to modify existing operating rule curves.

### 1.2.2 In practice: real-time decisions

Based on the theoretical concept, the ideal reservoir operation is releasing water to satisfy multiple purposes, while maintaining the reservoir storage as close as possible to the target levels assigned by the predefined operating rule curves and storage zoning. This 'storing and releasing water with the right amount and at the right time' concept is, however, easier said than done. In practice, a reservoir is operated on a daily or hourly basis, so-called *real-time reservoir operation*. In real-time, reservoir operation is continuously affected by variable and uncertain reservoir inflows and water and/or en-

ergy demands from various stakeholders. As a consequence, the zone-based operation approach with the operating rule curves alone tends to be inadequate, especially during extreme or urgent situations (Oliveira & Loucks, 1997). Therefore, the operating rule curves are commonly used as guidelines by reservoir operators. When either the target release or the target storage is not satisfied, the reservoir operators make decisions that deviate from the predefined rule curves, considering all relevant factors, including available real-time and forecast data, and their knowledge and historical experience (Sigvaldson, 1976). This procedure is so-called *real-time decision-making*, which plays an essential role in real-time reservoir operation, especially for a major, multi-purpose and over-year storage reservoir.

Adapting from Lund & Guzman (1999), Jain & Singh (2003) and Yang et al. (2019), the real-time reservoir operation function can be simplified to

$$Q = f(W, Z, R, D, J), \quad (1.2)$$

where  $Q$  is the reservoir outflow,  $f$  represents the real-time reservoir operation function,  $W$  represents the reservoir water balance (Equation (1.1)),  $Z$  represents the reservoir storage zoning,  $R$  represents the reservoir operating rule curves commonly used as guidelines,  $D$  is the total downstream water demand based on the different purposes and circumstances (which include the requirements of irrigation, hydropower generation, flood and drought control, water supply and environmental flow), and  $J$  accounts for the operators' judgments and decisions made in real-time.

### 1.2.3 In modelling: model capability and data availability

Since reservoirs alter the natural hydrological cycle, water balance and flow variability, the representation of reservoir operation in hydrological modelling and land-surface modelling frameworks is necessary for studying and managing reservoir-dominated river basins. Two types of reservoir operation models exist: (i) *simulation-based models*, which simulate the historical storage and release and (ii) *optimization-based models*, which aim to find the optimal releases to comply with competing water demands (Coerver et al., 2018). An adequate representation of actual reservoir operation mechanisms in both model types is an outstanding challenge and the current capability of hydrological models is rather limited, especially for real-time operation modelling.

Reservoir operation modelling has been progressing from local to global scales over the past decades (e.g., Pokhrel et al., 2016; Wada et al., 2017). Existing methods in both simulation-based and optimization-based reservoir operation models can be categorized into two groups based on their structure: (i) *process-based models* and (ii) *data-driven models*. Process-based models can be further classified based on their method and complexity in representing the reservoir operation: (i) natural lake methods, (ii) inflow- and demand-based methods and (iii) target storage-and-release-based methods. A compre-

hensive overview of the development in reservoir operation modelling from the primitive methods in the 20<sup>th</sup> century to the more advanced methods available nowadays can be found in Yassin et al. (2019). The main challenges in the integration of reservoir operation in modelling systems are (i) the requirement of a large amount of detailed reservoir-related data, which are often not available, and (ii) the complex model capability and high computational demands for the inclusion of real-time decision-making into the models.

## 1.3 Hydrological models with reservoir operation

This thesis concentrates on simulation-based reservoir operation modelling, including (i) process-based modelling with target storage-and-release-based methods and (ii) data-driven modelling, which can represent the reservoir operation for major, multi-purpose and over-year storage reservoirs. It focuses on modelling near real-time (daily) reservoir operation, which is important for reservoir operation in practice, especially for flood and drought control. Optimization-based reservoir operation models are beyond the scope of this thesis, and therefore, they are not elaborated on here.

### 1.3.1 Process-based models

*In general*

Process-based hydrological models have been widely used in hydrological modelling, both in research and in practice. Their major strong point is the transparent representation and parameterization of hydrological processes that are interpretable and straightforward in terms of mathematical descriptions. Therefore, they are easy to understand and apply. It has been claimed regularly over the past decades that the development of process-based models is hindered by limitations in data availability and model complexity and flexibility (Klemeš, 1986; Beven, 2000; Kirchner, 2006; McDonnell et al., 2007; Wagener et al., 2007). Nearing et al. (2021) recently pointed out that process-based models with a more realistic hydrological process representation could have been obtained from currently available data, but hydrologists have not yet figured out how to do so. They claimed that the main issue is not in data availability nor model limits, but in the human ability to attain more complete hydrological theories and subsequently build more accurate models. Therefore, the pressing question for hydrologists is: how can process-based models be improved by utilizing data that are currently available?

In parallel with the concept of model complexity and flexibility, it has been claimed that calibrating several model parameters often leads to overparameterization and equinality (Schoups et al., 2008). Calibrated process-based models often perform well for a certain area at a specific spatial and temporal resolution, but perform poorly elsewhere. This concept suggests that process-based models should rely on physical laws governing the hydrological processes as much as possible, so that models perform more robustly

and reliably when conditions change (Kirchner, 2006). It is hypothesized that when a process-based model is minimally calibrated, it becomes more obvious where significant errors and uncertainties originate. With such realizations, one can tackle the remaining errors and uncertainties at their origin and accordingly improve the model's realism. However, it should be noted that this strategy is not straightforward. As Beven (2000) claimed, the uniqueness of basins results in varying importance of different hydrological processes at different places and times, and thus increased physical model realism requires both more data and more parameters. The challenge, therefore, lies in balancing the need for more model parameters (and thus model complexity and flexibility) and less calibration.

#### *For reservoir operation modelling*

Process-based hydrological models with target storage-and-release-based reservoir operation methods attempt to mimic the reservoir water balance, reservoir storage zoning and reservoir operating rule curves (Yates et al., 2005). This type of method seems to originate from the Soil & Water Assessment Tool (SWAT), where a reservoir operation module was added to the model, with four storage zones indicated, namely sediment, principal supply, flood control and emergency flood control. Each zone is identified either manually by users or as a function of soil wetness (Arnold et al., 1998; Neitsch et al., 2005). This module was later modified with the adjusted reservoir storage zoning and the addition of a reservoir-release simulation strategy with a decision-based parameterization (Wu & Chen, 2012). This modification aimed to better fit both the storage and release functions of multi-purpose reservoirs.

Afterward, process-based reservoir operation modules have been added to several other hydrological models and land-surface models. In the Distributed Hydrology Soil-Vegetation Model (DHSVM), predefined complex operating rules have been implemented, which divide the reservoir storage into inactive, conservation and flood control zones (Zhao et al., 2016b). DHSVM determines reservoir release from the conservation zone using water demands for multiple purposes, while the release from the flood storage zone is determined as a function of inflow (flood inflow or non-flood inflow) and downstream flow. It also provides the possibility for a multi-reservoir operation system. A similar approach has been developed within the LISFLOOD model, where the reservoir storage is divided into conservative, normal and flood zones, and the release is defined according to these zones using multiple linear regression (Zajac et al., 2017). The capability of LISFLOOD in capturing impacts of lakes and reservoirs at the global scale was found to be improved using a parameterization that depends on naturalized inflow and maximum storage. Further progress was conducted with the Environment and Climate Change Canada's land-surface-hydrology (MESH) modelling system, where a parametric reservoir operation module based on piecewise-linear relationships between reservoir storage, inflow and release has been included (Yassin et al., 2019). The reservoir-related model parameters in MESH can be defined with two strategies:

(i) generalized parameterization that requires a relatively limited amount of data and (ii) direct calibration using multi-objective optimization when historical storage and release data are available. This addition increased the simulation accuracy of MESH in many reservoirs. Several other process-based reservoir operation models have been continuously proposed and improved. More examples of well-known simulation-based reservoir operation models are the CalSim model (Draper et al., 2004), WEAP21 (Yates et al., 2005) and HEC-ResSim (Klipsch & Evans, 2006).

Overall, the primary advantages of process-based models in reservoir operation modelling are that they allow approximation of reservoir-storage-and-release policies, have the potential of utilizing detailed reservoir-related data if available and provide transparent representations and interpretable calculations of reservoir operation. Therefore, they are easily understood, trusted and applied by reservoir operators and water managers in practice (Lund & Guzman, 1999; Yang et al., 2016). Their performance, however, is restricted to the limitations in data availability and model complexity, which pose a challenge when modelling reservoir operation in real-time.

### 1.3.2 Data-driven models

#### *In general*

The developments in data sciences and computer technologies have led to the accelerating application of advanced data-driven models in hydrological modelling. Machine learning (ML), in particular, is complementing traditional knowledge, theories and models that hydrologists have been using as research foundations. The fact that ML models can estimate streamflow (and many other hydrological variables) based on the same amount of data, which is claimed to be the main limitation of process-based models, has raised suspicions about our understanding of hydrological processes and our ability to interpret them (Nearing et al., 2021). Currently, questions regarding ML modelling in hydrology range from (i) whether ML models can outperform process-based models to (ii) why they perform better, (iii) how we can maximize the capability of ML models and (iv) if they can ever match or replace the need for process-based models.

While the performance of process-based models tends to deteriorate when transferring to other basins or using regional calibration, recent studies suggested that advanced ML models, especially neural networks, can learn and translate relationships of hydrological variability from a large data sample into a better estimate for any basin (Nearing et al., 2021). They also found that advanced ML models can estimate streamflow in ungauged basins based on data of other basins (Kratzert et al., 2019a) and work better when they are trained on multiple basins than when trained on an individual basin (Gauch et al., 2021). These recent findings suggested the existence of inter-basin characteristics and consistency, which are somewhat opposed to Beven's theory on basin uniqueness (as stated in Section 1.3.1). Moreover, Nearing et al. (2021) oppose the long-established concept of a minimized number of parameters and calibration. They argued that ML

models generally have several hyper-parameters and more degrees of freedom than calibrated process-based models, which are exactly what allows ML models to learn the transferable and scalable hydrological relationships. This, again, links back to the unfortunate fact that the bigger modelling problem beyond the basin uniqueness, lack of data and overparameterization is the limited human ability to learn and interpret very complex and high-dimensional hydrological relationships like ML models do.

#### *For reservoir operation modelling*

Data-driven models have been increasingly applied in both simulation-based and optimization-based modelling of reservoir operation. Originally, data-driven schemes were proposed to assist simulations of reservoir operation in process-based models, such as by empirically determining parametric relationships using observed data (Wisser et al., 2010; Wu & Chen, 2012). ML algorithms, in particular, have gained more attention in the past decade due to their potential to learn and reconstruct the complex processes of reservoir operation.

Unlike process-based models, ML models are black-box by nature, which means they are not straightforwardly interpretable in the form of explicit processes and equations. The lack of interpretability of ML models can make it difficult for reservoir operators to understand the operation processes, which undermines trust in using these models in practice. However, ML models tend to fit complex and high-dimensional relationships better than process-based models based on the same data limitation. Therefore, they are better able to extract the actual operating rules from available historical data of reservoir storage, inflow and outflow, which is very beneficial, especially for real-time applications. Several well-known classes of ML algorithms have been widely applied in simulation-based reservoir operation modelling, including instance-based learning, decision tree, ensemble learning and neural network algorithms (more details in Chapter 3; Section 3.4). Since each ML algorithm comes with different benefits and drawbacks (e.g., in computation time and ability to handle data with noise), the suitability of algorithms based on the study aims, available data and computational support should also be taken into account when selecting an appropriate algorithm.

## 1.4 Research framework

### 1.4.1 Background

As noted before, the expansion of reservoir construction mainly takes place in countries with emerging economies, including in Southeast Asia (SEA). There is a vigorous debate on reservoir existence and operation, leading to an urgent need for more research focusing on their hydrological impacts (and thus environmental and societal impacts). This requires operation modelling, particularly in real-time, at the reservoir scale and the basin scale. Also, there are several challenges in representing reservoir operation



in hydrological modelling systems due to current limitations in model capability and data availability. These challenges hold particularly for real-time operation of major, multi-purpose and over-year storage reservoirs.

Hydrologists still have a long way to go in order to achieve appropriate reservoir operation modelling, and thus the desired model fidelity, especially for real-time modelling and applications. As indicated by Nazemi & Wheeler (2015a,b), better integration of reservoir operation requires available models and in-situ data in conjunction with advancements in global data, remote sensing and computation and modelling techniques. These requirements contribute to a more realistic representation and parameterization of reservoir operational processes and to improved model performance for estimating reservoir outflow. However, the pressing question is: is it possible to attain a real-time reservoir operation model that sufficiently represents operation with explicit processes and equations and also accurately calculates reservoir outflow? And perhaps equally important: is it necessary to accomplish such a model?

#### 1.4.2 Objectives and research questions

The main goal of this PhD thesis is to improve understanding of reservoir operation, its hydrological effects and its modelling. The title of this thesis, *Modelling and forecasting daily streamflow with reservoir operation in the upper Chao Phraya River basin, Thailand*, reflects the research scope. It focuses on the daily (near real-time) streamflow simulation and forecasting of major, multi-purpose and over-year storage reservoirs. In an attempt to overcome the modelling challenges previously mentioned, it contains the development, examination and application of reservoir operation models on the basis of maximizing the use of available data (from in-situ to global) and available modelling techniques (process-based and data-driven). The upper region of the Greater Chao Phraya River (GCPR) basin with its two major reservoirs, Sirikit and Bhumibol, represents the SEA region, which is experiencing an expansion of reservoir construction and is vulnerable to climate change. To achieve the main goal, the following research objectives and questions were formulated:

Research objective 1: To gain insight into the physical representation and parameterization of hydrological processes with reservoir operation in a process-based model (Chapter 4).

- To what extent can a process-based model that is minimally calibrated with maximum utilization of globally available data represent hydrological processes and simulate daily streamflow in natural catchments (i.e., without reservoirs)?
- To what extent can such a model represent hydrological processes with reservoir operation and simulate daily streamflow in reservoir-dominated catchments?

Research objective 2: To gain insight into hydrological effects of reservoir operation (Chapter 5).

- *How does reservoir operation affect the water balance and daily streamflow regime?*
- *What are the roles of reservoir operation in mitigating or amplifying extreme flow events?*

Research objective 3: To gain insight into the capability of data-driven models in reconstructing actual reservoir operation and outflow (Chapter 6).

- *Which data-driven models can be used to simulate daily reservoir operation and outflow?*
- *Which reservoir-related data variables can serve as input for such data-driven models?*

Research objective 4: To improve multi-day forecasting of daily reservoir operation and outflow by combining a process-based model and data-driven models (Chapter 7).

- *How well can a process-based model forecast daily reservoir inflow?*
- *How well can data-driven models forecast daily reservoir operation and outflow several days ahead using the modelled inflows as one of the inputs?*

The connection between the research topics is illustrated within the research framework in Figure 1.5. It should be noted that the scope of the thesis covers hydrological modelling of individual reservoirs at the basin scale. The importance of multi-reservoir systems, which have become an increasing concern for the planning and management of both existing and planned reservoirs, is acknowledged here. However, their investigation requires a different research scheme that is not within the scope of this thesis. It should also be noted that this thesis focuses on simulation-based reservoir operation modelling, which simulates and forecasts outflow. Optimization-based reservoir operation modelling, which calculates optimal outflow for decision-making, is beyond the scope of this thesis. Ultimately, this thesis aims to contribute to a better understanding of reservoir operation modelling, forecasting and in the end operation in practice.

### 1.4.3 Thesis outline

This thesis is organized as followed. After this introductory chapter, the reader is introduced to the study area, the upper GCPR basin, and its reservoirs in Chapter 2. It gives an overview of the basin characteristics, climatology, hydrology, reservoirs and study catchments, water management with flood and drought history, socio-economics and the importance of the case study. Chapter 3 describes the (in-situ and global) data, (process-based and data-driven) models and goodness-of-fit criteria (for model simulation and reforecasting) that were used to conduct the studies presented in this thesis, according to the research framework shown in Figure 1.5. Chapters 4–7 constitute the core chapters of this thesis, which are linked to the four research objectives. Chapter 4 (research objective 1) presents a ( $\sim 1$  km) distributed hydrological model, wflow\_sbm, with a target storage-and-release-based reservoir operation module (ROM). The model

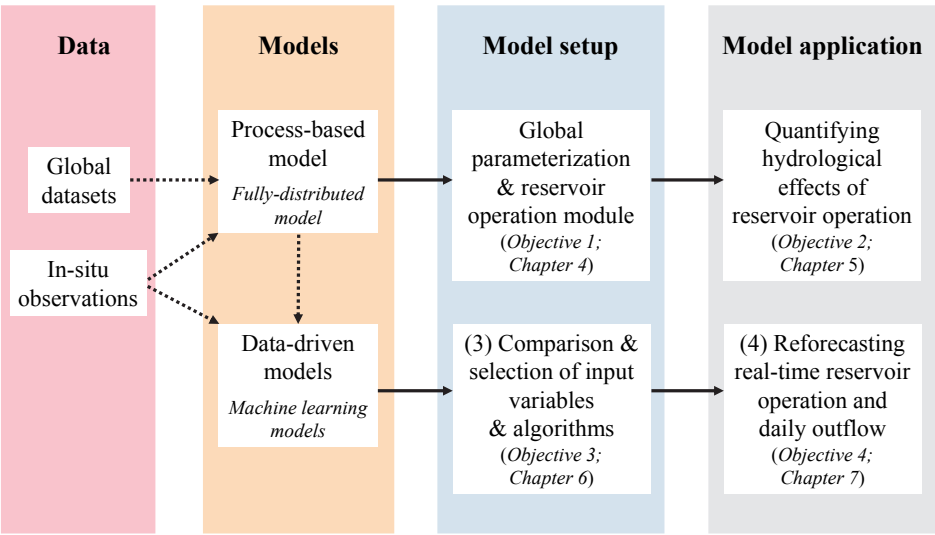
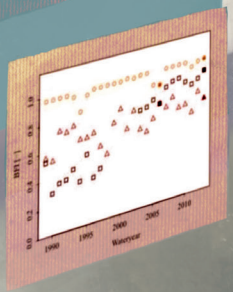
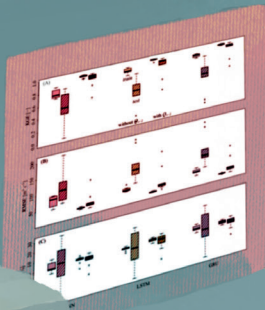


**Figure 1.5:** Research framework of this thesis, including data, models, model setups and model applications. The four core chapters of this thesis, which represent research objectives 1–4, are linked to model setups (Chapters 4 and 6) and applications (Chapters 5 and 7).

was set up with global spatial datasets and parameterization for estimating daily streamflow in four study catchments that are either natural or regulated by reservoir operation in the upper GCPR basin. Chapter 5 (research objective 2) assesses how reservoir operation affects the water balance, daily streamflow regime and extreme flows in the study basin. The hydrological effects were assessed by comparing streamflow in the naturalized scenario (without reservoir), in the baseline operation scenario (with the ROM) and the real-time operation scenario (observations). Chapter 6 (research objective 3) investigates the characteristics and relationships of the available reservoir-related data and their roles as inputs for machine learning models to simulate daily reservoir operation and outflow in the study basin. Chapter 7 (research objective 4) investigates the capabilities of three advanced machine learning models in simulating and reforecasting daily reservoir operation and outflow, considering uncertainties in the input data, training-testing periods and different algorithms. Lastly, a synthesis of the research reported in this thesis is presented in Chapter 8, including the main findings to meet the research objectives and answer the research questions, implications and recommendations for future research and operational purposes.



## **Chapter 2**

### **Upper Chao Phraya River Basin and reservoirs**

This chapter introduces the study area and its reservoirs that were used to conduct the studies presented in this thesis. The overview of the basin characteristics, its climatology and hydrology, reservoirs and dams, water management with flood and drought history, socio-economics and the importance of the case study are described.

## 2.1 Physical characteristics

The Greater Chao Phraya River basin (GCPR), located in the heart of Thailand, is the country's largest and most important basin with respect to land and water resource development (see Figure 2.1). The entire basin covers an area of 158,600 km<sup>2</sup>, accounting for 30% of the country's surface area. At Nakhon Sawan, the basin can be divided into two separate regions based on its distinct geography: the upper region (66%), which ranges from the elevated northern area to the large valley, and the lower region (34%), which is the low alluvial plain and delta. Around and downstream of Nakhon Sawan are widespread floodplain areas, with a longitudinal gradient of approximately 1/12,000. The slope in the lower region is even more gentle, with a gradient of 1/50,000 (Sayama et al., 2015).

The upper GCPR region, which is the focus area in this thesis, consists of four sub-basins, namely the Ping River (34,500 km<sup>2</sup>), Wang River (10,800 km<sup>2</sup>), Yom River (24,000 km<sup>2</sup>) and Nan River (34,700 km<sup>2</sup>). The Wang River joins the Ping River and the Yom River joins the Nan River (see Figure 2.1). In Nakhon Sawan valley, the Ping and Nan Rivers merge and form the Chao Phraya River, marking the beginning of the lower region. The elevation of the upper region ranges from 2,534 to 22 m above sea level (see Figure 2.2). It is mostly covered by forest and grassland, which have been gradually converted into agricultural areas, primarily rice fields, in the past decades (Jamrussri & Toda, 2017).

The lower GCPR region also consists of four sub-basins, namely the Chao Phraya River (20,500 km<sup>2</sup>), Pa Sak River (14,300 km<sup>2</sup>), Sakae Krang River (5,000 km<sup>2</sup>) and Tha Chin River (10,900 km<sup>2</sup>) (see Figure 2.1). The Pa Sak and Sakae Krang Rivers contribute to the Chao Phraya River, while the Tha Chin River branches off from the main river. Both the Chao Phraya and Tha Chin Rivers then drain through the central floodplains, with intensive agricultural areas, such as rice, sugarcane and corn (Ligaray et al., 2015). The Chao Phraya, in particular, flows through industrial and densely populated areas, including the capital city, Bangkok. The two rivers empty into the Gulf of Thailand.

## 2.2 Climatology and hydrology

The climate of the GCPR basin is characterized by tropical monsoons and cyclones, contributing to the high seasonal variability of precipitation. A year is distinctly divided into the wet (rainy) and dry seasons. The wet season is when the southwest monsoons

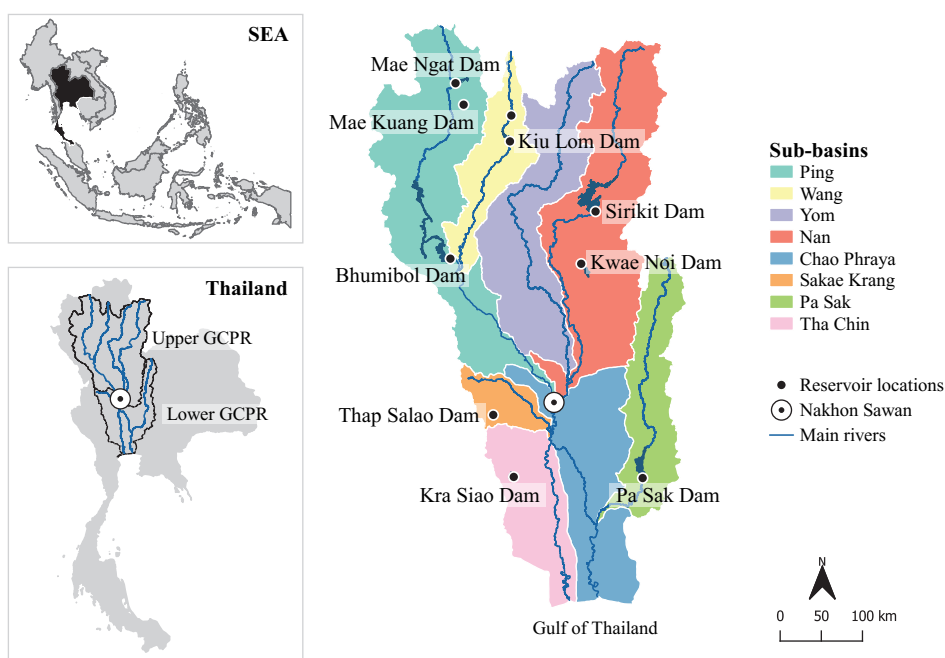


**Figure 2.1:** Overview of the GCPR basin. The top left panel shows the location of Thailand in Southeast Asia. The bottom left panel shows the location of the GCPR basin in Thailand, with the division into the upper and lower region. The right panel shows the GCPR basin with its eight main sub-basins and the locations of its 10 multi-purpose reservoirs.

from the Indian Ocean and the cyclones from the Pacific Ocean and the South China Sea bring humid air towards the basin, causing heavy rainfalls from May to October. After that, the northeast monsoons bring cool and dry air from the Siberian anticyclone, causing the dry season from November to April (Bachelet et al., 1992; Kripalani et al., 1995).

Considering the seasonality, the Thai water-year is a period from April 1<sup>st</sup> of any given year to March 31<sup>th</sup> of the following year. In Chapters 4 and 5, where the annual water balance was taken into account in the studies, the water-year is applied in the analyses, and the terms water-year and water-yearly are referred to as year and yearly/annual (i.e., the year 2011 is from April 1<sup>st</sup>, 2011 to March 31<sup>th</sup>, 2012). In Chapters 6 and 7, where the water-year does not play an important role in the studies, the terms year and yearly/annual represent the calendar year from January to December.

Focusing on the upper region of the GCPR basin, the long-term water-yearly average precipitation from 1989 to 2013 is 1,060 mm. The highest water-yearly precipitation was recorded in 2011 (1,449 mm) and the lowest in 1993 (841 mm). Most (86%) of precipitation occurs in the rainy season. Accordingly, annual maximum daily stream-

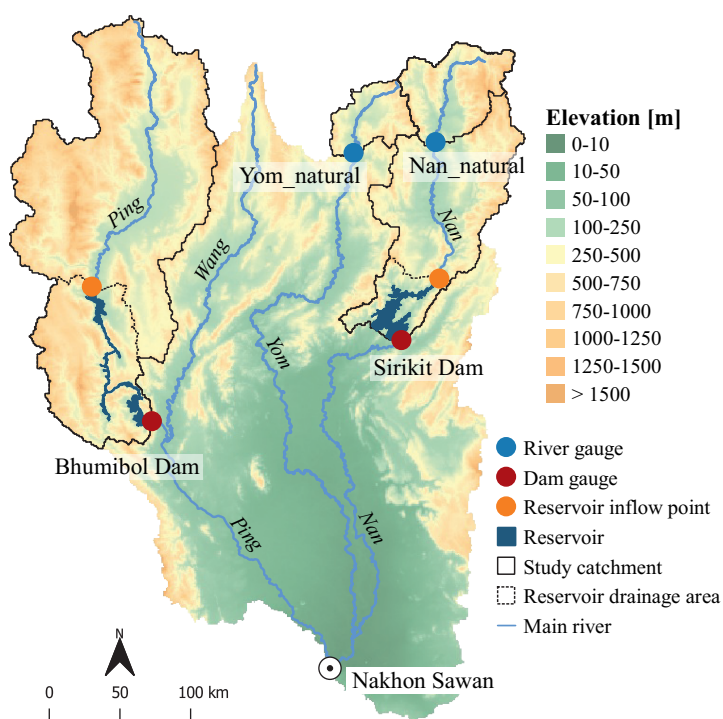


**Figure 2.2:** Overview of the upper GCPR basin with the elevation and the spatial distribution of the Sirikit and Bhumibol reservoirs and study catchments. The study catchments consist of two natural catchments (Nan\_natural and Yom\_natural) and two regulated catchments (Sirikit and Bhumibol). The solid black lines indicate the drainage areas from the headwater until the gauge location (study catchments used in Chapter 4), while the dotted black lines indicate the drainage areas from the inflow point of each reservoir to the dam location (study catchments used in Chapter 5).

flows often occur in September and October, while annual minimum daily streamflows mostly occur in January. The highest daily streamflow ever recorded at Nakhon Sawan was  $5,450 \text{ m}^3 \text{ s}^{-1}$  (October 2006) and the lowest was  $52 \text{ m}^3 \text{ s}^{-1}$  (April 1994). It should be noted that the annual maximum and minimum daily streamflows in the GCPR basin are not only influenced by the seasonal precipitation, but also by the water regulations with the reservoirs and dams.

## 2.3 Reservoirs and dams

Over the past 60 years, 10 main dammed reservoirs have been constructed and operated in the GCPR basin for multiple purposes. These reservoirs are currently managed by the Royal Irrigation Department (RID) and the Electricity Generating Authority of



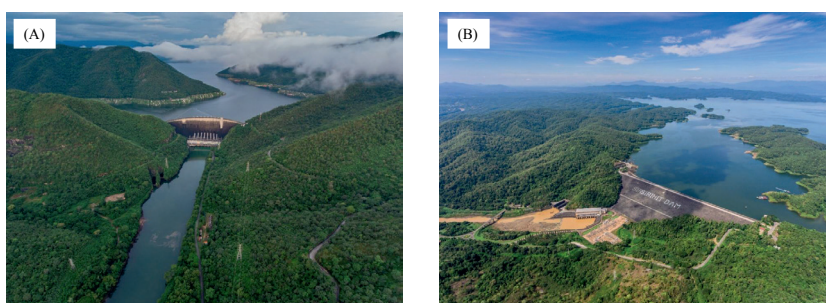


**Figure 2.3:** Bhumibol (A) and Sirikit (B) reservoirs behind the dams (from EGAT, 2013).

Thailand (EGAT). Seven reservoirs are located in the upper GCPR region, while three other reservoirs are located in the lower region (locations shown in Figures 2.1).

The seven reservoirs in the upper GCPR region are responsible for irrigation, hydroelectricity generation, water supply, and flood and drought controls of the entire basin. The Bhumibol and Sirikit reservoirs (Figure 2.3) are the two largest ones in terms of storage capacity. The Bhumibol reservoir (storage capacity 13.46 billion  $\text{m}^3$ ) has been operated on the Ping River since 1964 and the Sirikit reservoir (storage capacity 9.51 billion  $\text{m}^3$ ) has been operated on the Nan River since 1977. Subsequently, the other five reservoirs (total storage capacity 1.73 billion  $\text{m}^3$ ) were constructed on the Ping River (two), Wang River (two) and Nan River (one). The Bhumibol and Sirikit reservoirs together account for 93% of the total reservoir capacity (24.7 billion  $\text{m}^3$ ) in the upper region, of which their total inflow volumes for 2.3 years and 1.5 years can be stored, respectively (Komori et al., 2013). A plan to build the first reservoir on the Yom River has been postponed since 1980 due to an ongoing controversial discussion about the myriad of negative environmental and social impacts (Apichitchat & Jung, 2015).

The other three reservoirs in the lower region were operated since 1980. Their total storage capacities (1.37 billion  $\text{m}^3$ ) are considerably smaller compared to the upstream reservoirs. Since they were mainly designed for hydropower generation and irrigation, they hardly contribute to flood and drought mitigation at the basin scale. In addition to the dammed reservoirs, the Chao Phraya Dam, a main barrage dam across the Chao Phraya River, was constructed around 100 km downstream of Nakhon Sawan in 1957. It further controls the upstream reservoir outflows and irrigates water to the surrounding floodplains, and thus can support the downstream flood and drought controls.

## 2.4 Study reservoirs and catchments

This thesis focuses on the upper GCPR region (Figure 2.2), where the most important reservoirs are located. The two major upstream reservoirs, Sirikit and Bhumibol (Figure 2.3), were selected for the studies. Since the other five upstream reservoirs only account

**Table 2.1:** Characteristics of the Bhumibol and Sirikit reservoirs.

Characteristic	Bhumibol	Sirikit
River	Ping	Nan
Dam type	Gravity arch	Earthfill
Operation since	1964	1977
Dam height [m]	154	114
Crest elevation [m above sea level]	261	169
Crest length [m]	486	810
Crest width [m]	6	12
Maximum width at base [m]	52.2	630
Number of hydroelectric turbines	8	4
Generating hydroelectric capacity [MW]	779	500
Mean daily inflow [ $\text{m}^3 \text{s}^{-1}$ ]	178	184
Mean daily outflow [ $\text{m}^3 \text{s}^{-1}$ ]	170	179
Minimum daily outflow recorded [ $\text{m}^3 \text{s}^{-1}$ ]	0	0
Maximum daily outflow recorded ( <i>ResMaxQ</i> ) [ $\text{m}^3 \text{s}^{-1}$ ]	746	809
Reservoir capacity ( <i>ResMaxVol</i> ) [billion $\text{m}^3$ ]	13.46	9.51
Reservoir surface area ( <i>ResArea</i> ) [ $\text{km}^2$ ]	297	315

for 7% of the total reservoir capacity in the upper region, and two of them are located above the Bhumibol reservoir, their influences were assumed insignificant at the basin scale, and thus they were excluded. The principle characteristics of the Sirikit and Bhumibol reservoirs obtained from RID and EGAT are presented in Table 2.1. While both reservoirs were examined in the process-based modelling studies (Chapters 4–5), only the Sirikit reservoir was further examined in the data-driven modelling studies (Chapters 6–7).

To investigate the process-based model performance (Chapter 4), two types of study catchments were selected: natural catchments and regulated catchments. The natural catchments from the Nan and Yom headwaters were selected based on available data and will be called the Nan\_natural ( $3,546 \text{ km}^2$ ) and Yom\_natural ( $2,018 \text{ km}^2$ ). The regulated catchments represent the drainage areas from the headwater until the dam location and will be called the Sirikit catchment ( $13,155 \text{ km}^2$ ) and Bhumibol catchment ( $25,988 \text{ km}^2$ ). Locations and boundaries of the four study catchments are shown in Figure 2.2 (solid black lines).

To investigate the hydrological effects of reservoirs (Chapter 5), both the natural catchments and regulated catchments were used. However, in this chapter, the Sirikit and Bhumibol catchments were defined as the drainage areas from the inflow point of each reservoir, instead of from the headwater, to the dam location. Therefore, the Sirikit catchment covers  $2,020 \text{ km}^2$  and the Bhumibol catchment covers  $6,863 \text{ km}^2$ , as shown in Figure 2.2 (dashed black lines). Using the drainage areas from the reservoir inflow point instead of from the headwater allows for a more comprehensive investigation of reservoir effects on water balance components.

## 2.5 Water management with floods and droughts

The climatology and geographical characteristics make the GCPR basin highly prone to water-related disasters. The basin has been enduring flood and drought occurrences regularly. The distinct rainy and dry seasons cause the streamflows to keep rising or declining for several months. The gentle slope of the downstream part of the upper region and most of the lower region slows down the streamflows. Generally, the downstream river capacity increases where rivers come together. However, this is not the case for the Chao Phraya River, which receives water from four upstream rivers at once as the streamflows from the upper region has to flow slowly through the narrow section at Nakhon Sawan (Komori et al., 2012). These factors pose a real challenge in water resources planning and management in the GCPR basin throughout the year. The most catastrophic floods occurred in 1995, 2006 and 2011, followed by serious droughts in 2013–2016 (Takeda et al., 2016; Kinouchi et al., 2018).

In rainy seasons, flooding often occurs in the GCPR basin. High and low streamflow volumes from the upper region are likely to increase downstream water levels, disperse excess water onto the floodplain and inundate the lower region. On many occasions, upstream floodwater cannot flow down at once due to the elevated water level in the Chao Phraya River itself. Consequently, the upper floodplain around the narrow section at Nakhon Sawan can also be flooded for several weeks (Sayama et al., 2015). The lower region starts to be threatened when the streamflow at Nakhon Sawan exceeds  $2,000 \text{ m}^3 \text{ s}^{-1}$ , and the flood risk dramatically increases when exceeding  $3,500 \text{ m}^3 \text{ s}^{-1}$  (Jamrussri & Toda, 2017). Historically, Thailand has controlled flooding in the lower region by giving priority to protecting Bangkok and the surrounding industrial areas, which are densely populated and economically crucial. Flooding is, therefore, controlled by storing water in the Sirikit and Bhumibol reservoirs and by expanding the inundation areas, using the Chao Phraya barrage dam, to prevent the excess floodwater from entering the important areas (Komori et al., 2012). Since the floodwater flows slowly, it seldom causes real damage to human life, but damage to properties can be large. However, in 2011, five storms hit the upper region, filling the Sirikit and Bhumibol reservoirs to their 95% capacities (Komori et al., 2013). The over-topped reservoir outflows and continuous rainwater (as high as  $4,686 \text{ m}^3 \text{ s}^{-1}$  at Nakhon Sawan) inundated a downstream area of over  $30,000 \text{ km}^2$ , including Bangkok. The event caused devastating damages, with 13 million people affected, more than 800 fatalities and USD 46.5 billion of economic loss, making it one of the most devastating hazards recorded in Southeast Asia (SEA) (Komori et al., 2012; Sayama et al., 2015).

In dry seasons, droughts tend to occur in the GCPR basin when the water storage in the two major reservoirs fails to meet the irrigation and consumption demands, e.g., the Bhumibol water shortage in 2016 (Zenkoji et al., 2019). Water shortages in the past have led to large losses in agricultural and industrial production (Kinouchi et al., 2018). In addition, they have caused serious issues, such as saltwater intrusion and groundwa-

ter over-pumping. Streamflows from the upper region usually push away saltwater from the Gulf of Thailand, but the saltwater creeps upstream during drought periods and turns the rivers brackish, affecting fishery and agriculture. Over-pumping of the groundwater for industrial use has resulted in land subsidence, especially in Bangkok, which has been sinking by 2–12 cm annually (Aobpaet et al., 2013). Therefore, even though droughts in the GCPR basin may not receive attention and concerns as much as floods, they should not be overlooked.

## 2.6 Socio-economics

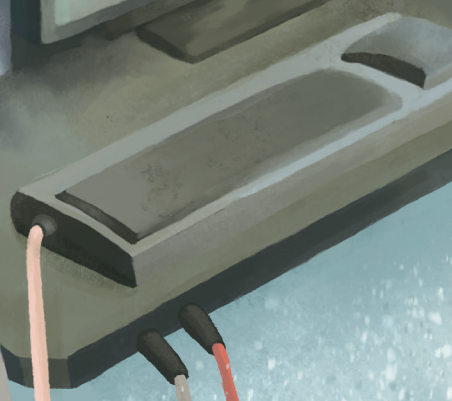
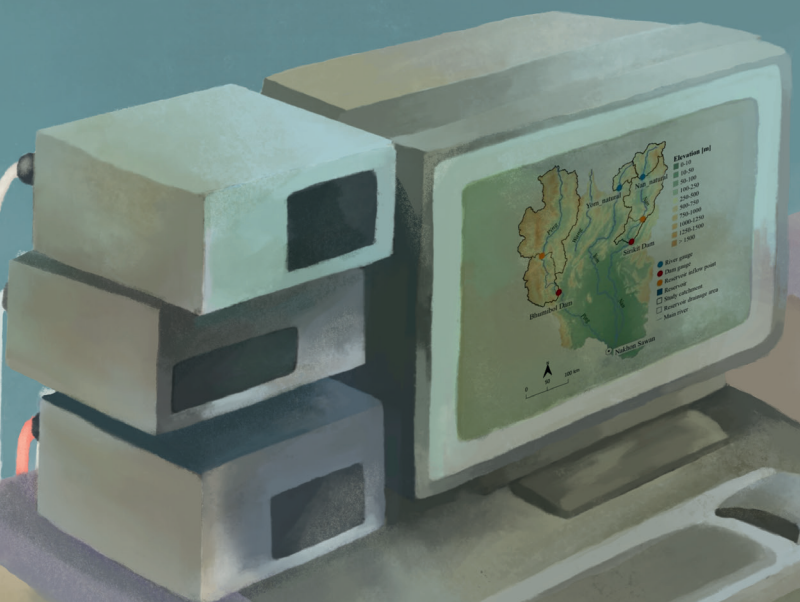
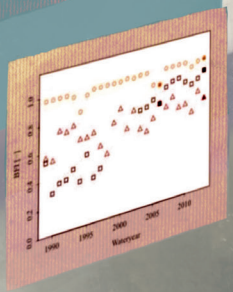
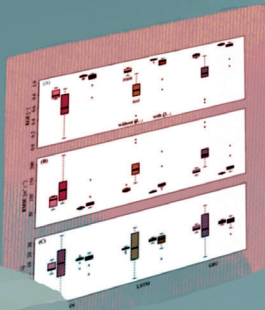
The GCPR basin serves as the blood vessel of Thailand's development and well-being. It contains the main agricultural, industrial and residential areas, which drive the economic growth of the country. It is also home to about 23 million people (40% of the country's population), 8 million of whom live in Bangkok (Mateo et al., 2014). Accordingly, 66% of the Gross Domestic Product (GDP) is generated inside the basin.

The socio-economics of the GCPR basin, and thus Thailand, relies on water resources management of the basin, which almost solely depends on the planning and operations of the Sirikit and Bhumibol reservoirs. The economic development of Thailand would decline if these two reservoirs could not fulfill their roles, as evident from the 2011 historical flood year (Tebakari et al., 2012). While both reservoirs have been operated to increase low streamflows in the dry season and reduce floodwater in the rainy season (Komori et al., 2013), climate change and changes in the socio-economic structure have had a considerable influence on the hydrometeorological regime and water circulation of the basin. The increasing development, rapid urbanization and intensification of agricultural practices have resulted in a higher overall risk of floods and droughts. Therefore, sustainable planning and management of water resources with the reservoir operation to balance water surplus and scarcity remain crucial challenges for this basin and country.

## 2.7 Importance of the case study

The GCPR basin is one of the most highly regulated river basins by dammed reservoirs in SEA. The delta area in the basin is also among the most vulnerable areas in the region (Yusuf & Francisco, 2009). It can, therefore, be representative of the other similar river basins in SEA, considering its agriculture and water resources management. Despite the support of several multipurpose reservoirs, the GCPR basin still suffers from floods and droughts regularly, which devastate the agricultural and environmental resources, and subsequently the economic development of the country and SEA (Takeda et al., 2016; Kinouchi et al., 2018). Similar extreme events have occurred in neighboring countries, such as Vietnam and Myanmar (Luu et al., 2018; Myo Lin et al., 2018). While most reservoirs in neighboring basins, such as in the Mekong River, have been constructed

in recent years (Urban et al., 2018), the main reservoirs in the GCPR basin have been operated for over half a century, and data on daily reservoir storage and outflows are available for the last 25 years. The longer period of observational records in the GCPR basin allows for a comprehensive analysis. Therefore, knowledge of hydrological modelling and reservoir operation obtained from the GCPR basin can also contribute to the understanding and improvement of water resources planning and management in other basins in SEA.



## **Chapter 3**

### **Data, models and performance criteria**

This chapter describes data, models and goodness-of-fit criteria that were used to conduct the studies presented in this thesis, according to the research framework demonstrated in Figure 1.5 in Chapter 1. The description includes theories and information on the selected data, models and criteria. The data implementations, model setups, model performance evaluations and model applications, on the other hand, are explained separately for each study in Chapters 4–7.

## 3.1 Data

The modelling work in this thesis required geospatial data, meteorological data and hydrological data for the hydrological model setups, parameterization and validations. The geospatial data were used to represent the physical characteristics of the GCPR basin in the process-based model. The meteorological data were used as the driving forces of the process-based model. The hydrological data were used in both process-based and data-driven models, regarding parameter optimization, data-driven inputs, model performance evaluation and result analyses. In an attempt to overcome data scarcity in the study area, which is a common challenge in SEA, the geospatial and meteorological data were obtained from global databases. The hydrological data were obtained from national observations, as they are less available from open sources and also required at high accuracy to evaluate the models' performance and improve the models' results. An overview of the data used is shown in Figure 3.1.

### 3.1.1 Geospatial data

The geospatial data comprised the Digital Elevation Model (DEM), land cover types, soil types and river network. The DEM was obtained from the Shuttle Radar Topography Mission (SRTM; Jarvis et al., 2008), the land cover from GLOBCOVER (Bontemps et al., 2011), the soil from SoilGrids (Hengl et al., 2017) and the river network from HydroRIVERS (HydroSHEDS; Lehner & Grill, 2013). The DEM and river network data were employed to create the distributed maps of basin boundary, local drainage direction, Strahler stream orders and river length per grid cell in the process-based hydrological model. These maps indicate the flow directions and control hydrological processes in a distributed way. In this thesis, the land cover and soil data were not directly used as model inputs, but were used in the estimation of seamless distributed parameter maps (see Chapter 4).

### 3.1.2 Meteorological data

The meteorological data for forcing the process-based hydrological model were precipitation ( $P$ ) and potential evapotranspiration ( $PET$ ). For the simulation models (Chapters 4–7), the historical  $P$  data were obtained from the Multi-Source Weighted-Ensemble Precipitation Version 2 (MSWEP V2; Beck et al., 2019). The dataset was constructed using gauges, satellites and reanalyses, with corrections for distributional biases and



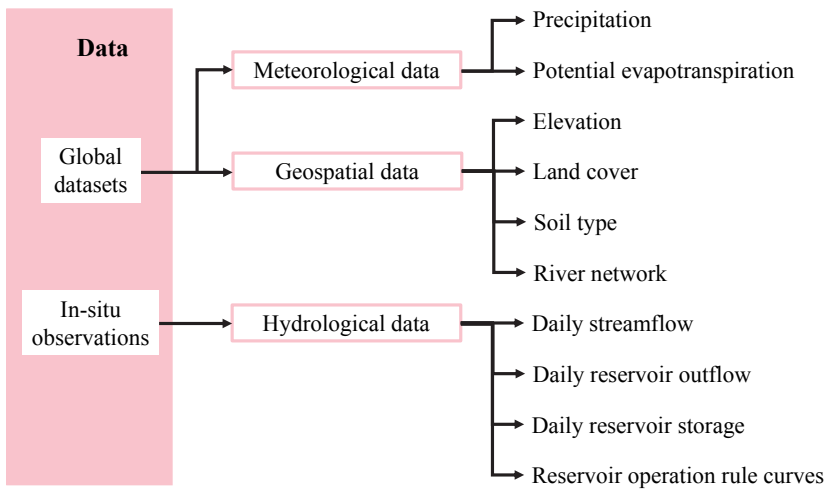


**Figure 3.1:** Overview of the data used in this thesis, including geospatial and meteorological data obtained from global databases and hydrological data obtained from in-situ observations.

systematic terrestrial  $P$  biases. It is available at high spatial ( $\sim 10$  km) and temporal (3-hourly) resolutions for the 1979–2017 period. The historical  $PET$  data were obtained from the earthH2Observe database (Schellekens et al., 2017) as the successor of the WATCH-Forcing-Data-ERA-Interim (WFDEI) data (Weedon et al., 2014). They are offered with many calculation methods, of which we selected the FAO Penman-Monteith  $PET$  dataset (Allen et al., 1998). It is also available at high spatial ( $\sim 10$  km) and temporal (daily) resolutions for the 1979–2014 period (Sperna Weiland et al., 2015). Both the MSWEP V2  $P$  and the earthH2Observe  $PET$  datasets have been shown to produce promising model results in many hydrological and meteorological studies (e.g., Tarnavsky et al., 2018; Liu et al., 2019a; Xu et al., 2019; Beck et al., 2017, 2020), and therefore were chosen to force the process-based hydrological model in this thesis. Since we did not have to compute the  $PET$  nor account for snow processes within the model, other forcing data, such as temperature and solar radiation, were unnecessary.

For the reforecasting models, which is referred to as forecasting of historical streamflow using archived forecast input data (Chapter 7), the forecast  $P$  data for the period of 2004–2013 were obtained from the European Centre for Medium-Range Weather Forecasts (ECMWF, 2022). Two  $P$  forecast types were included: a deterministic (control) forecast and ensemble (perturbed) forecasts that contain 10 probabilistic forecasts. The forecasts are available on a daily basis at high spatial ( $\sim 3$  km) and temporal (6-hourly) resolutions. Both the ECMWF deterministic and ensemble  $P$  forecasts have been applied in many hydrological and meteorological studies with promising performance (e.g., Aminyavari & Saghafian, 2019; Nanda et al., 2019; Liu et al., 2021), and thus were used in this thesis.

### 3.1.3 Hydrological data

The required hydrological data included observed daily streamflow at the outlets of the study catchments, observed daily reservoir outflow, observed daily reservoir storage, dynamic operating rule curves of each reservoir and downstream water demand. The streamflow, reservoir outflow and reservoir storage were employed in both the process-based hydrological model and data-driven models. The dynamic operating rule curves and downstream water demand were only employed in the process-based model.

The data were provided by the Royal Irrigation Department (RID) and the Electricity Generating Authority of Thailand (EGAT). The observed daily streamflow and reservoir outflow is the average of the observed hourly streamflow/outflow from 6.00 p.m. on the previous day to 6.00 p.m. on the defined day. Their availability varies among gauges. The observed daily reservoir storage is instantaneous, pertaining to the end of each day. The reservoir operating rule curves consist of the long-term monthly target maximum and minimum storage of each reservoir derived from the RID report. The long-term monthly target downstream water demand was manually extracted from the observed daily streamflow data of each reservoir (more detail in Section 3.3.2). In reality, these reservoir operating rule curves and water demand information serve as guidelines for reservoir operators.

## 3.2 Model overview

To model and analyze the daily streamflows that are highly regulated by reservoir operation in the upper GCPR basin, two types of hydrological models were employed; a *process-based* hydrological model and *data-driven* models. Among widely used process-based models, the fully-distributed wflow\_sbm model was selected and implemented in Chapter 4 (model setup with global data and parameterization) and Chapter 5 (model application on quantifying effects of reservoir operation on streamflows). Several data-driven models, which are machine learning algorithms, were applied in Chapter 6 (input and algorithm investigation) and Chapter 7 (model application on simulating and reforecasting real-time reservoir operation and outflows). Some of the output from the wflow\_sbm model was also used as input for the data-driven models. An overview of models that were employed in this thesis is illustrated in Figure 3.2.

## 3.3 Process-based model

### 3.3.1 The wflow\_sbm model

wflow is a spatially distributed hydrological modelling platform developed by Deltares (Van Verseveld et al., 2022b). It allows for flexible and transparent implementation of hydrological model concepts, which can be easily applied and modified by model developers and users. Several models have been included in wflow, such as the wflow\_hbv

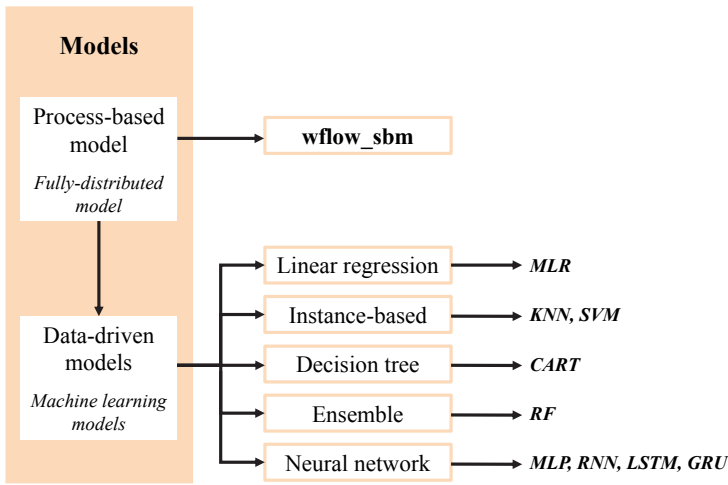


**Figure 3.2:** Overview of the models employed in this thesis, including the process-based (fully-distributed) hydrological model and data-driven (machine learning) models. Several machine learning algorithms were applied, including Multiple Linear Regression (MLR), K-Nearest Neighbor (KNN), Support Vector Machine (SVM), Classification and Regression Tree (CART), Random Forest (RF), Multi-Layer Perceptron (MLP), Recurrent Neural Network (RNN), Long Short-Term Memory (LSTM) and Gated Recurring Unit (GRU).

model (derived from the HBV96 model; Bergström, 1992), the `wflow_flextopo` model (derived from the FLEXTopo model; Savenije, 2010) and the `wflow_sbm` model (derived from the Topog\_SBM model; Vertessy & Elsenbeer, 1999). The different `wflow` models share the same structure, including the geospatial settings and the spatially hydrological routing via the kinematic wave function, but are fairly different with respect to conceptualizations.

The `wflow` simple bucket model, called `wflow_sbm` (Van Verseveld et al., 2022b), was chosen in this thesis. The `wflow_sbm` model is a conceptual rainfall-runoff model, with the soil water processes based on the Topog\_SBM model. The flow processes for the subsurface, overland and river flows are based on the kinematic wave approach that is comparable to the TOPKAPI (Todini & Ciarapica, 2002) and G2G (Bell et al., 2007) models. While Topog\_SBM is suitable for fast runoff processes in small areas, `wflow_sbm` is more widely applicable (Vertessy & Elsenbeer, 1999; Van Verseveld et al., 2022b). In contrast to many conceptual models, `wflow_sbm` calculates the lateral subsurface flow explicitly and uses parameters that represent simplified physical characteristics of a basin (Vertessy & Elsenbeer, 1999).

The scheme of `wflow_sbm` is illustrated in Figure 3.3. The one-dimensional model is constructed on a grid cell network of eight flow directions (D8) for surface and subsurface flow routing, with the presence of both vertical and lateral flows. It has four main

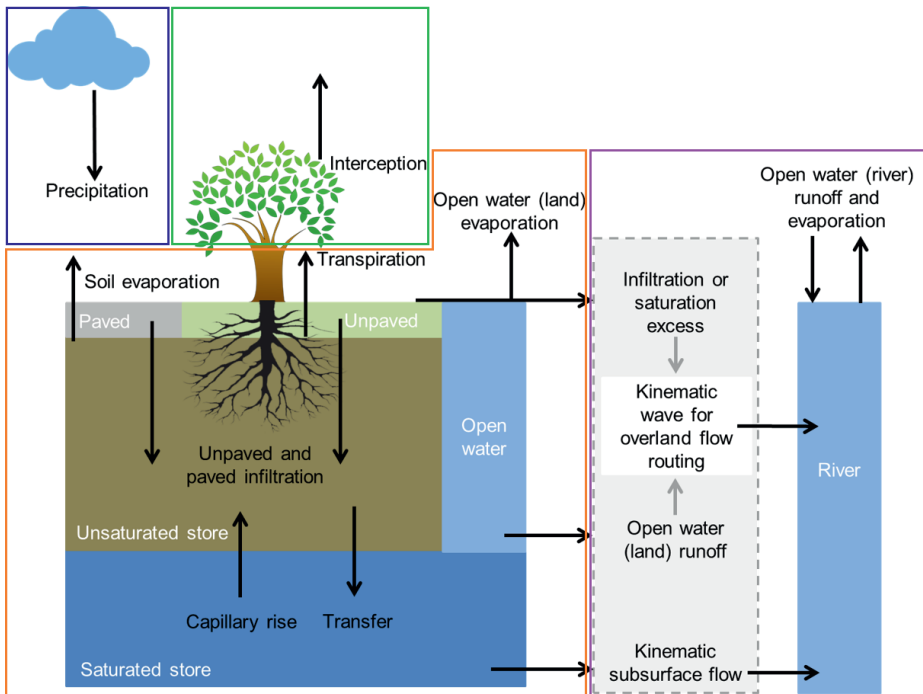


**Figure 3.3:** Schematic structure of water processes and fluxes in the wflow\_sbm model. The model includes four routines: precipitation-snow routine (blue box), rainfall interception routine (green box), soil water routine (orange box) and runoff generation routine (purple box) (adapted from Schellekens et al., 2019; Van Verseveld et al., 2022b).

routines: (i) a precipitation routine based on the HBV model (Lindström et al., 1997), (ii) a rainfall interception routine based on the modified Rutter model (Rutter et al., 1971, 1975) or Gash model (Gash, 1979), (iii) a soil water routine based on topog\_sbm and (iv) a flow generation routine with the kinematic wave function. Water enters each grid cell through the precipitation-snow routine and is transferred to the rainfall interception routine. Throughfall and stemflow infiltrate into the soil and flows between the stacked unsaturated zone and saturated zone. The soil column can also be divided into different layers to allow for the transfer of water within the unsaturated zone (Brooks & Corey, 1964). Part of the water evaporates depending on soil water content and vegetation cover. The soil water routine assumes an exponential decay of the saturated hydraulic conductivity with soil depth (Beven & Kirkby, 1979). In the flow generation routine, the subsurface, overland and river flows are then routed according to the D8 direction.

The continuous development of the wflow\_sbm model maximizes the use of available spatial data (Schellekens et al., 2019; Imhoff et al., 2020b; Van Verseveld et al., 2022b),

which demonstrates its potential to improve the realism of the hydrological process and parameter representation. It has also shown good performance in a broad range of applications (e.g., López López et al., 2016; Hassaballah et al., 2017; Giardino et al., 2018; López López, 2018; Gebremicael et al., 2019; Rusli et al., 2021; Aerts et al., 2022). Therefore, it was selected for this thesis.

### 3.3.2 The reservoir operation module

To model the regulated outflows of the Sirikit and Bhumibol reservoirs, a reservoir operation module (ROM) was included within the kinematic wave routing of `wflow_sbm`. To do so, grid cells of the dam locations and reservoir surface areas were indicated. The ROM is a reservoir water balance algorithm with a target storage-and-release-based operation method. The reservoir storage in the ROM is divided into four zones: inactive storage, conservation storage, flood control storage and surcharge storage, as illustrated in Figure 3.4(A). The storage-and-release calculation is based on the target downstream water demand and the operating rule curves, including the target maximum and minimum storage. The monthly values of the target downstream water demand and operating rule curves for the Sirikit and Bhumibol reservoirs are shown in Figure 3.4(B) and 3.4(C). As part of the distributed model, the ROM also requires parameters representing reservoirs' physical characteristics. See details on ROM parameterization in Chapter 4; Section 4.2.2.

Although the ROM was developed as part of `wflow_sbm` (Schellekens et al., 2019; Van Verseveld et al., 2022a), its complete description has not been published before. Therefore, we explain step-wise calculations of the ROM in brief here. It should be noted that the equations in this section belong to the calculation of the ROM and that all equations take place within one time step. Each equation, therefore, does not represent the complete reservoir water balance. Overall, at a given time step, the ROM updates the reservoir water storage state and computes a volume of water to be released with algorithms to meet a required demand, while also maintaining the storage at an optimal level, considering the target maximum and minimum storage (operating rule curves). To initially calculate the change in the reservoir storage, the storage at the previous time step, upstream inflow, and precipitation and evaporation over the reservoir surface at the current time step are taken into account:

$$ResVol_t = ResVol_{t-1} + (ResInflow_t + ResP_t - ResET_t) \times \Delta t, \quad (3.1)$$

where  $ResVol$  is reservoir storage [ $m^3$ ],  $ResInflow$  is upstream inflow [ $m^3$  time step $^{-1}$ ],  $ResP$  is precipitation over the reservoir surface [ $m^3$  time step $^{-1}$ ],  $ResET$  is evaporation over the reservoir surface [ $m^3$  time step $^{-1}$ ],  $\Delta t$  is the computing time step (e.g., daily),  $t$  is the current time step and  $t-1$  is the previous time step. Then, the current  $ResVol$  as a fraction of the reservoir maximum storage is computed:

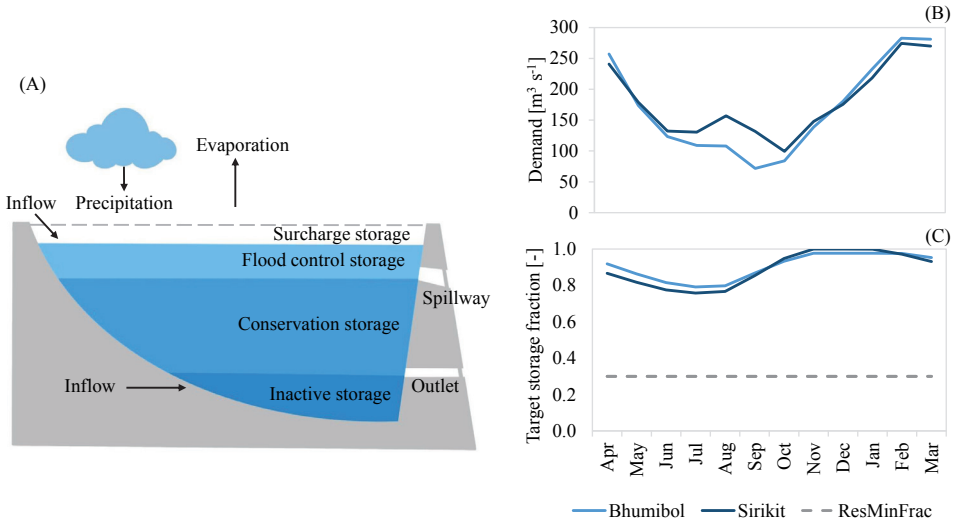


**Figure 3.4:** Conceptual representation of the reservoir operation module (ROM), including reservoir storage zones (A) and operating rule curves for the Bhumibol and Sirikit reservoirs (B and C). Figure (B) represents the target downstream water demand of each reservoir, which is defined by the long-term monthly averages of reservoir outflow observations. Figure (C) represents the target storage as a fraction of the maximum storage (flood control storage level). Colored lines indicate the fraction of the long-term monthly target maximum storage (conservation storage level; *ResMaxFrac*) from the RID guideline. The dashed line indicates the fraction of the target minimum storage (inactive storage level; *ResMinFrac*), which was set to 0.3 for both reservoirs.

$$ResVolFrac_t = \frac{(ResVol_t + ResVol_{t-1})}{2 \times ResMaxVol}, \quad (3.2)$$

where *ResVolFrac* is the storage fraction [-], *ResMaxVol* is the reservoir maximum storage known as the flood control storage level [m³]. The environmental outflow of a given reservoir, here called the demanded release, is determined using a sigmoid curve to scale for the target storage and downstream water demand of the reservoir:

$$ResQdemand_t = \min(SF_t \times (DD_t \times \Delta t), ResVol_t), \quad (3.3)$$

where *ResQdemand* is the demanded release [m³], *SF* is the sigmoid curve factor [-] and *DD* is the downstream water demand [m³ time step⁻¹], which is associated with the seasonality and often set on a long-term monthly basis (see Figure 3.4(B)). *SF* influences the extent to which *ResQdemand* increases or decreases, and is calculated by:

$$SF_t = \frac{1}{1 + \exp(-c \times (ResVolFrac_t - ResMinFrac))}, \quad (3.4)$$

where  $c$  is the steepness of the sigmoid curve [-] and  $ResMinFrac$  is the target fraction of minimum storage, known as the inactive storage level [-] (see Figure 3.4(C)). When the current  $ResVolFrac$  equals  $ResMinFrac$ , the argument of the exponential function is zero and the denominator becomes two. This implies that when the reservoir storage reaches the inactive storage level, which can occur in dry seasons, the reservoir only releases a  $ResQdemand$  equal to half of  $DD$ .  $ResQdemand$  decreases further as  $ResVolFrac$  drops below  $ResMinFrac$ .  $ResVol$  is updated after taking out  $ResQdemand$ . Subsequently,  $ResVolFrac$  is re-determined with Equation (3.2).

The target fraction of maximum storage, known as the conservation storage level, is used as a guideline to maintain the active storage and prevent the flood storage. It is conditional on water supply and demand throughout the year and often set on a long-term monthly basis (see Figure 3.4(C)). The amount of water to be released from the reservoir to let  $ResVol$  continuously meet the conservation storage level is computed as:

$$ResQtarget_t = \max(0, ResVol_t - (ResMaxVol \times ResMaxFrac_t)), \quad (3.5)$$

where  $ResMaxFrac$  is the target fraction of maximum storage [-] and  $ResQtarget$  [ $m^3$ ] is the target amount of water to be released to meet  $ResMaxFrac$ . If  $ResVol$  is higher than  $ResMaxVol$ , the surcharge storage,  $ResQspill$  [ $m^3$ ], is spilled to prevent dam failure:

$$ResQspill_t = \max(0, ResVol_t - ResMaxVol) \quad (3.6)$$

Equations (3.5) and (3.6) indicate that the reservoir release does not exceed  $DD$  unless  $ResVol$  is projected to surpass  $ResMaxFrac$  or  $ResMaxVol$ . In case of water excess, the amount of water to be released apart from the demanded release is:

$$ResQextra_t = \min(ResQtarget_t, ResQspill_t, (ResMaxQ \times \Delta t) - ResQdemand_t), \quad (3.7)$$

where  $ResQextra$  [ $m^3$ ] is the extra amount of water to be released and  $ResMaxQ$  [ $m^3$  time step $^{-1}$ ] is the maximum release capacity of a reservoir (see Table 2.1). Since the environmental outflow ( $ResQdemand$ ) is already calculated before updating  $ResVol$  (Equation (3.3)), it is subtracted from the  $ResMaxQ$  amount in this step. Finally, the total release,  $ResQtotal$  [ $m^3$  time step $^{-1}$ ], of the current time step is calculated according to:

$$ResQtotal_t = \frac{ResQdemand_t + ResQextra_t}{\Delta t} \quad (3.8)$$

### 3.3.3 wflow\_sbm packages

In the first phase of development (2008–2021), the wflow platform was programmed in the PCRaster-python framework (Karssen et al., 2010; Schellekens et al., 2019). This wflow version was used in this thesis and can be downloaded from <https://github.com/openstreams/wflow> (Schellekens et al., 2020). In the current development phase (from 2021 onward), the platform has been switched to the programming language Julia, which offers high performance for large-scale and high-resolution applications of hydrological models (Bezanson et al., 2012; Van Verseveld et al., 2022b). Note that there is no further development of wflow in the PCRaster-python framework. The model development in the Julia framework is available at <https://github.com/Deltares/Wflow.jl> (Van Verseveld et al., 2022a).

## 3.4 Data-driven models

Machine learning (ML) models are a type of data-driven models that generally look at the independent variables (*inputs*) and dependent variable (*output*) in order to explain their behaviors and relationships, and calculate the output values. Generally, an ML model is set up and learns these behaviors and relationships on a training dataset to derive the mathematical expression that best fits the data and produces the output with the least error. This learning process is called *training*. The mathematical expression is then used to predict the output from the unseen dataset to evaluate the model performance, which is called *testing*. The training and testing procedures of ML models are similar to the calibration and validation procedures of process-based models. ML models can solve both classification and regression problems.

In the attempt to improve the reservoir operation and outflow modelling, five classes of regression ML models were used in this thesis, including the linear regression model, instance-based learning models, decision tree model, ensemble learning model and neural network models. The generalized characterization of each ML class is represented in Figure 3.5. The selected linear regression model was Multiple Linear Regression (MLR), the instance-based learning models were K-Nearest Neighbor (KNN) and Support Vector Machine (SVM), the decision tree model was Classification and Regression Tree (CART), the ensemble learning model was Random Forest (RF) and the neural network models contained Feed-Forward Neural Network/Multi-Layer Perceptron (MLP), Recurrent Neural Network (RNN), Long Short-Term Memory (LSTM) and Gated Recurring Unit (GRU). These nine algorithms have been proven to have large potential in hydrological modelling and reservoir modelling (e.g., Xu & Liang, 2021; Ibrahim et al., 2022). A brief description of each algorithm is provided here. Since this thesis focuses



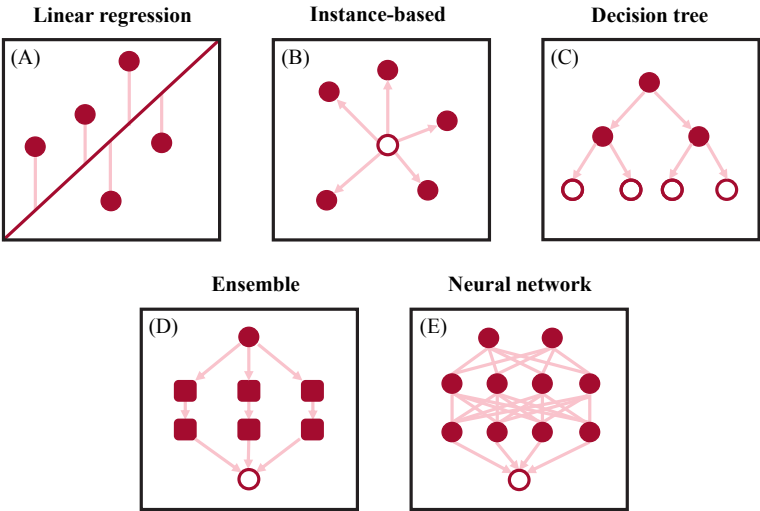


**Figure 3.5:** The generalized characterization of the selected machine learning classes, including the linear regression algorithm (MLR), instance-based learning algorithms (KNN and SVM), decision tree algorithm (CART), ensemble learning algorithm (RF) and neural network algorithms (MLP, RNN, LSTM and GRU).

on implementing the existing algorithms and not modifying them, the algorithms are not mathematically described in detail, but references for further understanding are provided.

### 3.4.1 Linear regression

Linear regressions are the most well-understood and conventional class of algorithms in data-driven modelling. They are simple linear and parametric models, i.e., models that assume a linear relationship between the input variables and output variable (see Figure 3.5(A)). More specifically, the output variable can be explicitly calculated from a linear combination of the input variables.

#### *Multiple Linear Regression (MLR)*

Multiple Linear Regression (MLR) is an extension of the simple linear regression algorithm, where two or more input variables are used for fitting a linear equation to predict the output variable. The schematic structure of MLR is illustrated in Figure 3.6. The MLR equation can be clearly expressed, including the intercept, the regression coefficient of each input variable, and the model random error term. The best fit line of MLR is determined by minimizing the sum of the squares of the vertical deviations, so-called residuals, between the simulations and the observations. A good MLR model should be able to explain most of the variance of the output variable with a minimum number

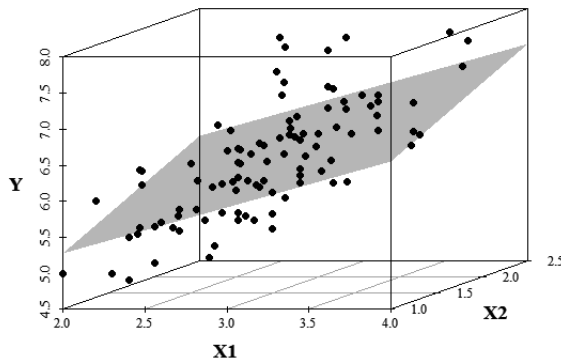


**Figure 3.6:** Schematic structure of the Multiple Linear Regression (MLR) algorithm, with an example of two input variables ( $X_1$  and  $X_2$ ) to predict an output variable ( $Y$ ). The grey plane indicates the best fit line of MLR.

of input variables (Sachindra et al., 2013). The merit of MLR is that it is a simple, explainable and rapid-to-use model. However, it may not be able to handle nonlinear hydrological processes with a limited number of input variables, and thus its performance cannot be ensured (Nourani et al., 2014). Therefore, MLR has often been used as a reference for the comparison of other ML algorithms (Zhang et al., 2018b).

### 3.4.2 Instance-based learning

Instance-based learning algorithms refer to the class of classification and regression algorithms that predict values of the output variable by learning the entire training dataset of the inputs and output (so-called instances), and then generalizing what has been learned to new instances based on some similarity measure. They are called instance-based as they simply store the training instances instead of learning an explicit description of the target function like linear regression. When a new instance is encountered, its relationship to the previously stored instances is examined to assign an output value for the new instance (see Figure 3.5(B)). Therefore, this algorithm class is also known as memory-based learning. To calculate the output value for the new instance, these algorithms construct a local approximation to a model function that applies in the neighborhood of the new instance, instead of estimating for all instances. Therefore, they can adapt to new data easily (Mitchell & Mitchell, 1997).

#### *K-Nearest Neighbor (KNN)*

K-Nearest Neighbor (KNN) is a classic instance-based learning algorithm for both classification and regression problems, which was originally developed by Fix & Hodges (1989) and further improved by many others. KNN predicts a complex nonlinear time series in a non-parametric way. Its concept posits that part of time series occurring in the past can reappear in the future with highly similar patterns, known as neighbor-

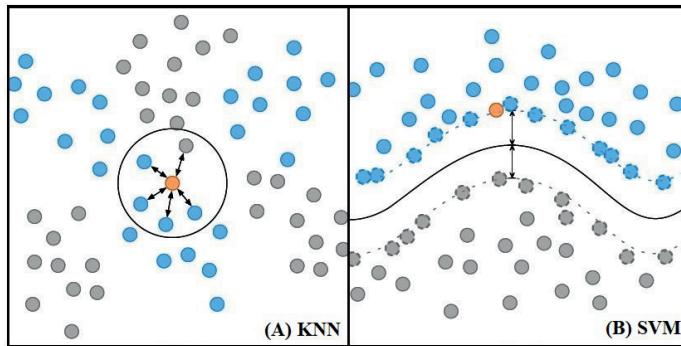


**Figure 3.7:** Schematic structure of the K-Nearest Neighbor (KNN) and Support Vector Machine (SVM) algorithms, with an example of two input variables (blue and grey dots) to predict an output variable (orange dot). The grey lines indicate the instance classification. For KNN (left panel), the dots that fall within the neighborhood (grey circle), so-called nearest neighbors, are considered in the calculation of the predicted output value. For SVM (right panel), on the other hand, only the data points outside a threshold between the hyperplane (solid grey line) and the decision boundary lines (dashed grey line) are considered (adapted from Page et al., 2014).

hood (Arroyo & Maté, 2009). The schematic structure of KNN is illustrated in Figure 3.7(A). The classification procedure of KNN recursively selects past input-output data pairs with a pattern most similar to that of the current data pair, which are referred to as the nearest neighbors (NNs) at a total number of  $K$  pairs. After that, a regression is carried out by assigning values to those NNs. These values are referred to as weights, which are inversely proportional to the distances. The weighted NNs are then summed up to predict the target output value (Atkeson et al., 1997; Imandoust et al., 2013). Therefore, the performance of KNN is strongly affected by the search range based on the data size, which determines the number of NNs (Ponomarenko et al., 2014).

The main advantage of KNN is that it is easy to implement and understand with a relatively straightforward calculation, with no predetermined parametric relation required, unlike many other ML algorithms (Kim et al., 2016). However, since KNN makes predictions based on the current time period using past data, its capability can be limited for events that did not occur in the past, especially extreme events (Tongal, 2013). Furthermore, it can become very slow as the data size grows. KNN has been used in previous reservoir modelling studies, especially for reservoir operation optimization (e.g., Ahmadi et al., 2010; Malekmohammadi et al., 2010; Yang et al., 2021).

#### *Support Vector Machine (SVM)*

Support Vector Machine (SVM) is a very specific instance-based learning algorithm developed by Vapnik (2000), which has gained popularity due to its promising empirical

performance for both classification and regression problems. The fundamental of SVM is based on the Vapnik-Chervonenkis dimension theory and structural risk minimization principle. It employs the feature space, which is a set of all possible features (inputs) in the multi-dimensional linear function (Han et al., 2007). The schematic structure of SVM is illustrated in Figure 3.7(B), in comparison to KNN. In a regression problem, the line that is required to fit the features is referred to as a hyperplane. Unlike other regression algorithms that try to minimize the error between the observed and predicted values, SVM tries to find a hyperplane in the multi-dimensional space that best fits the data points, with decision boundary lines. The distance between the hyperplane and decision boundary lines is called a threshold. Only the data points outside the threshold, so-called Support Vectors, are used for the calculation to minimize the grouping error from noise in the dataset. These Support Vectors affect the position and orientation of the hyperplane, which build SVM (Yu & Kim, 2012). The algorithm is mainly characterized by the utilization of kernels (mathematical functions that transform input data into a linear representation in the feature space) and capacity control obtained by acting on the decision boundaries or a number of Support Vectors (Karamouz et al., 2009).

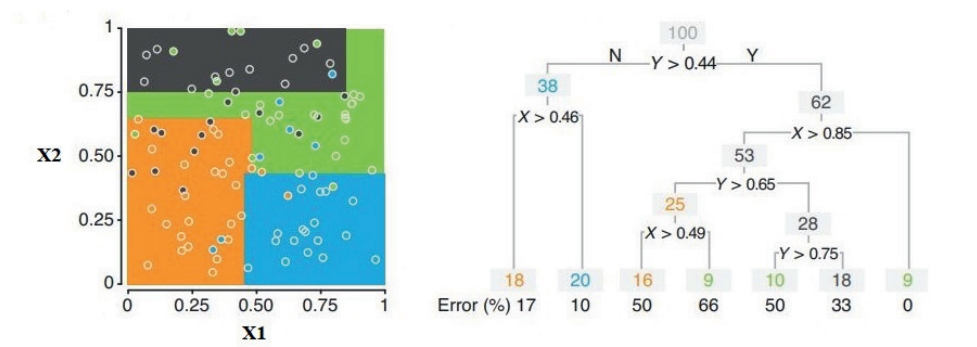
The main benefits of SVM are that it can acknowledge the presence of non-linearity in the dataset, which can provide a proficient prediction model, especially for noisy data. However, the fitting time of SVM is more than quadratic with the feature numbers, which can make it unsuitable for large datasets. Nonetheless, SVM is known as a robust and promising algorithm and has been explored in previous reservoir modelling studies (e.g., Karamouz et al., 2009; Bozorg-Haddad et al., 2018; Niu et al., 2019).

### 3.4.3 Decision tree

Decision trees are a class of non-parametric classification and regression algorithms that are based on a multistage or hierarchical decision scheme, which can be displayed as a tree-like structure (see Figure 3.5(C)). A decision tree is composed of a root node (the entire training dataset), a set of internal nodes (branches) and a set of terminal nodes or outputs (leaves). Each node of the tree makes a binary decision that splits the data. It is a top-down approach that is generally carried out by moving down the tree until the leaf node is reached (Xu et al., 2005). To learn from the training dataset, the decision tree starts with a simple structure, in terms of branches and leaves, and recursively splits the input data into subsets (more branches), according to decision rules and weights inferred from the input data. This re-branching process, so-called recursive partitioning, stops when further splitting no longer improves the prediction result.

#### *Classification and Regression Tree (CART)*

Classification and Regression Tree (CART) was proposed by Breiman et al. (1984) as a binary decision tree algorithm that can produce either classification or regression trees, depending on the output variable. The schematic structure of CART is illustrated in



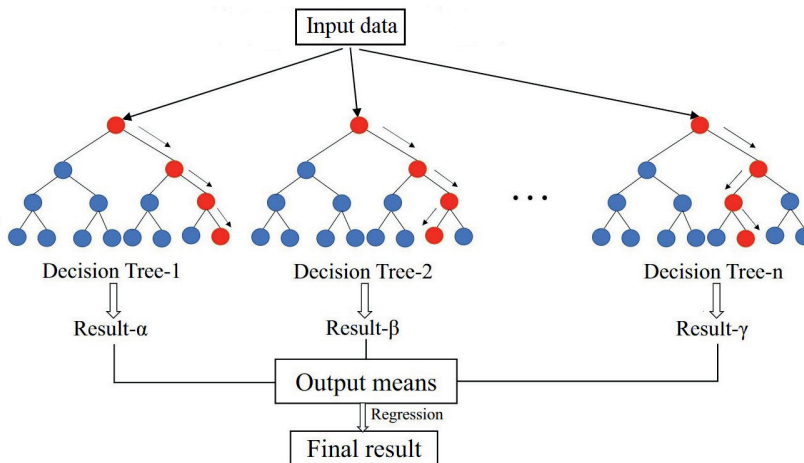
**Figure 3.8:** Schematic structure of the Classification and Regression Tree (CART) algorithm, with an example of 100 data samples with two input variables (X1 and X2). The left panel shows the classification boundaries (in different colors) of the data samples. The right panel shows a decision tree built according to the decision rules of each class (adapted from Krzywinski & Altman, 2017).

Figure 3.8. It uses the Gini index (a function that determines how well a decision tree is split) as an impurity measure for selecting the tree branches, of which the branches with the largest reduction in impurity are used for splitting the data (Brijain et al., 2014). Due to its mechanism, CART can handle both numerical and categorical input data with missing values. The classification tree divides the whole training dataset space into multiple classes (leaves), in which each class contains a set of decision rules. The regression tree, on the other hand, takes the average of the target output values in each class and stores the corresponding decision rules. When a new set of input variables is fed to the regression tree, a target output value is estimated, following the stored decision rules (Yang et al., 2016).

On the one hand, CART can be prone to noise, and can produce high output variance and over-fitting due to a large number of branches (Hastie et al., 2009). On the other hand, it has many advantages which can be suitable for hydrological prediction, including algorithm transparency and low computational demand (Bessler et al., 2003). It is one of the few algorithms that allow for the physical interpretation of the model and data. For this reason, it has been implemented in reservoir modelling studies to understand reservoir operation (e.g., Bessler et al., 2003; Yang et al., 2016; Chen et al., 2022).

### 3.4.4 Ensemble learning

Ensemble learning algorithms are a class of non-parametric classification and regression algorithms that seek better predictive performance by combining two or multiple models (see Figure 3.5(D)). The three methods of ensemble learning are bagging, stacking and boosting. Bootstrap-aggregating, so-called bagging models (e.g., bagged CART and Random Forest), fit many decision trees on different samples of the same dataset



**Figure 3.9:** Schematic structure of the Random Forest (RF) algorithm for a regression problem with an example of the  $n$  number of decision trees. Each tree is trained on a different and random subset of data, leading to different prediction values. The predictions from all tree are averaged to obtain the final value of the target output (adapted from Sun et al., 2022).

and average the predictions. Stacking models (e.g., Super Learner) fit different model classes on the same dataset and use another model to learn how to best combine the predictions. Boosting models (e.g., the Stochastic Gradient Boosting) sequentially add ensemble members that correct the predictions made by prior models and calculate a weighted average of the predictions. Many ensemble algorithms have been shown to effectively decrease the prediction variance and improve the over-fitting problem, which is generally found in other ML algorithms (Murphree et al., 2018; Mosavi et al., 2021).

#### *Random Forest (RF)*

Random Forest (RF) is the most representative algorithm in ensemble learning, which was further developed from decision trees by Breiman (2001). RF consists of an ensemble of decision trees to yield prediction for both classification and regression problems. It intends to overcome the limitations of high output variance and over-fitting in CART by generating multiple trees. The schematic structure of RF is illustrated in Figure 3.9. Each tree in RF is individually built on bagging samples of the training data. In each binary split, a subset of input data is randomly created, of which the best one is chosen to derive the decision rules at the splitting, considering the minimized sum variance of the output variable in the two resulting branches. The randomization of the input subsets avoids repeatedly chosen inputs at each split, leading to highly correlated trees (Breiman, 2001; Pham et al., 2021). Predictions on a new data point are made by running all the trees through the new input data. In the end, all the trees are combined into

the so-called forest as it averages all predictions to produce a final output value. Considering its strengths, RF has been increasingly applied in reservoir modelling studies (e.g., Yang et al., 2016; Li et al., 2020; Qie et al., 2022).

### 3.4.5 Neural network

Artificial neural networks (ANNs), simply called neural networks, are a class of ML algorithms that use a network of implicit mathematical functions to understand and reproduce the complex and non-linear relationship between the inputs and output in the dataset (see Figure 3.5(E)). They are inspired by the biological learning process with highly interconnected neurons in the human brain, which has become more computationally feasible due to the advances in data mining and increasing computer power (Kubat, 1999). ANNs can be described as a data processing system with artificial neurons that mimics two characteristics of the brain: the ability to (i) learn and (ii) generalize from limited information. The schematic structure of ANNs is illustrated in Figure 3.10. An artificial neuron, also known as a node or perceptron, has a similar function to MLR, but is not explicitly expressed in mathematical formulas. The perceptron transmits a signal to other perceptrons like the biological neurons: it receives input signals, learns and processes them, and produces an output signal to perceptrons connected to it. A value is associated with each connected signal, referred to as weight, corresponding to the synaptic strength of biological neuron connections (Ye et al., 2016). The behavior and learning progress of an ANN depends on both the weights and the input-output signal learning function, referred to as the activation or transfer function. Each perceptron calculates the output signals in two steps based on the weights and the activation function: first, it sums the input signal values multiplied by the weight associated with each interconnection, and then it passes the sum through the activation function to generate the output signal.

ANNs typically consist of an input layer where data patterns are introduced to the network, one or more hidden (processing) layers where the learning and processing are done, and one output layer that provides the final prediction for the given input pattern. Each layer contains perceptrons that are connected to those of the adjacent layer by the weighted signals. There is no connection between perceptrons in the same layer. During the learning process, so-called training, an ANN model learns and processes the dataset, starting with randomly assigned initial weights, and adjusting them to achieve a set of weights that minimizes the overall errors between the computed output and the observed one. This learning process is repeated until the error is minimized or until a specified number of training iterations is accomplished.

There are two main types of ANNs; Feed-Forward Networks and Feedback (Recurrent) Networks. A neural network model with several hidden layers is known as a deep network or deep learning model. Several ANN models have shown outstanding abilities to process complex and non-linear problems that might otherwise not be easily solved with explicit mathematical formulas (Yang et al., 2017). Compared to other classes

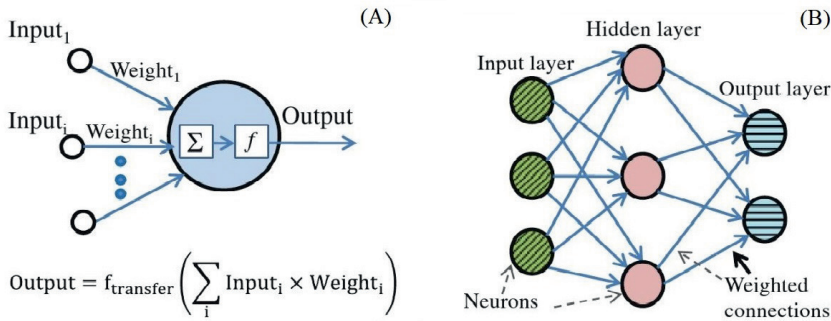


**Figure 3.10:** Schematic structure of the simple artificial neural network (ANN) algorithm, with an example of the Feed-Forward Neural Network with multi-layers, so called Multi-Layer Perceptron (MLP). The left panel shows an artificial neuron, so-called perceptron, and its components, including the weights from the inputs and the activation/transfer function ( $f$ ). The weighted input signals are summed ( $\Sigma$ ) and transferred to the next perceptron as the output signal. The right panel demonstrates the structure of a neural network, with an example of three perceptrons in the input layer, three in the processing (hidden) layer and two in the output layer. Perceptrons between the layers are connected in the forward direction (adapted from Ye et al., 2016).

of ML algorithms, ANNs can be quite slow on a large dataset. They are also ‘black-boxes’, with nontransparent architecture, limiting the opportunity to understand the mathematical relations between the inputs and output. However, known to be versatile and efficient with high fault tolerance when using sufficient training data, ANNs have become the most popular ML algorithms in hydrological modelling (Lohani et al., 2012; Tanty et al., 2015).

#### *Multi-Layer Perceptron (MLP)*

One of the most common ANN algorithms is the Feed-Forward Neural Network, which can be presented either as a Single-Layer Perceptron or a Multi-Layer Perceptron. The Single-Layer Perceptron is the simplest kind of ANN, which only contains a single layer of perceptrons, in which the inputs are fed directly to the outputs via a series of weights. The Multi-Layer Perceptron (MLP), on the other hand, represents the complete yet basic network with one input layer, one or more hidden layers and one output layer. These algorithms are called feed-forward because all of the data flows in one direction—forward—from the input perceptrons, through the hidden perceptrons, and to the output perceptrons, without any data cycles within the network (see Figure 3.10).

MLP typically applies the sigmoid or the rectified linear unit as the activation function and uses a variety of learning techniques to adjust the weights of the signal between the perceptrons, with the most popular being back-propagation (Tanty et al., 2015). With this technique, the predicted output values in the output layer are compared with



their observed values to compute the prediction error, which is then fed backwards through the network to the hidden and input layers. Using this error information, MLP adjusts the weighted signals to reduce the error. This learning process should be repeated for a sufficiently large number of training iterations to reach some state where the prediction error reaches an acceptable level. To adjust the weights properly through back-propagation, a non-linear optimization method called stochastic gradient descent is generally applied. For this, the network calculates the derivative of the error function with respect to the weights and changes the weights such that the error is minimized. Note that typical limitations of back-propagation with stochastic gradient descent are the convergence speed and the possibility of gradient disappearance and ending up in a local optimal solution of the error function (Zhang et al., 2019). Despite that, several studies have shown the good performance of MLP models for reservoir modelling, especially for reservoir inflow prediction (e.g., Jain et al., 1999; Chaves & Chang, 2008; Zarei et al., 2021).

#### *Recurrent Neural Network (RNN)*

Similar to MLP, the Feedback Neural Network, known as the Recurrent Neural Network (RNN), consists of an input layer, one or more hidden layers and an output layer. The addition in RNN is the design to specially deal with sequential data with the ability to use previous information in the sequence to produce the current output as a feedback (recurrent) loop, as shown in Figure 3.11. RNN can send inputs in either direction from and to all the layers. Especially in the hidden layer(s), it takes the predicted output from the previous step(s) together with the current inputs, and recurrently and continuously trains the network according to the input time sequence. As a result, the prediction of the network not only depends on the external inputs it receives, but also on the state of the network in the previous time step(s) (Nagesh Kumar et al., 2004). The weights in RNN are the same for all perceptrons in the same layer. With time-delayed feedback, RNN can preserve and remember the short-past and long-past information during the learning process. Therefore, it is beneficial when predicting complex dynamic timing and sequential data, like hydrological time series (Zhang et al., 2019).

Although RNN can effectively deal with complex and non-linear time series data, it has some shortcomings. During the network training with back-propagation, at each step the gradient of a loss function to minimize the prediction error is calculated, which is used to update weights in the network. If the effect of the previous layer on the current layer is small, the gradient value is also small and vice-versa, which makes the gradients exponentially shrink down as the back-propagation continues. Smaller gradients lead to no weight update and the network cannot learn the effect of earlier inputs. Therefore, as the RNN processes more steps while learning long-range dependencies, it suffers gradient vanishing and exploding problems from vanishing gradients more than other neural network architectures (Bengio et al., 1994). The RNN has been used in several reservoir modelling studies (e.g., Zhang et al., 2019; Apaydin et al., 2020), but has

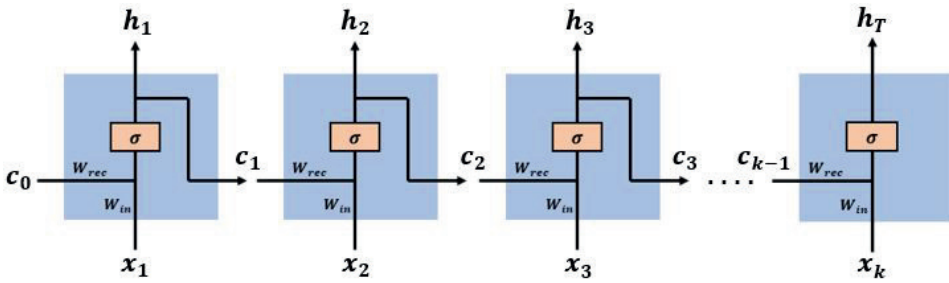


**Figure 3.11:** Diagram for an unfolded Recurrent Neural Network (RNN). From bottom to top: input state ( $X$ ), hidden state (blue box) and output state ( $h$ ).  $C$  is the recurrent input (from the previous time step),  $W_{in}$  is the weight of the current input,  $W_{rec}$  is the weight of the recurrent input and  $\Sigma$  is the sigmoid activation/transfer function (Jaiswal, 2022).

been recently replaced by LSTM and GRU networks, which are known to be successful to remedy the aforementioned problems.

#### *Long Short-Term Memory (LSTM)*

Long Short-Term Memory (LSTM) is a more complex RNN algorithm, introduced by Hochreiter & Schmidhuber (1997), to address the deficiencies of the RNN. In contrast to the hidden layer(s) in RNN, LSTM applies specially designed memory block(s) that are recurrently connected to each other, lying between an input layer and an output layer. The memory block, obtained from Gers et al. (2000), is composed of an input gate, a memory gate, a forget gate and an output gate to control the flow of information and cells to hold information, as shown in Figure 3.12(A). The cell states carry information from initial to later time steps without getting vanished in the block. The memory block replaces the hidden layer to filter out nonessential information while preserving useful information from the long past (Shen, 2018). When new data enters the memory block, LSTM determines which new information to remove from the cell state by the forget gate. The forget gate is essentially a sigmoid function that generates a value (between 0 and 1) based on the output at the previous time step and the current input to decide whether to let information that is produced in the previous moment (partially) pass. In the next step, LSTM indicates which new information to be stored in the cell state. This step is divided into two parts: first, the input gate determines which values to be updated, and then the memory cell generates a vector of new candidate values, which can be added to the cell state. In the last step, LSTM assigns which information will be output. First, it decides which parts of the cell state to output by running a sigmoid layer. Then, it resizes the candidate values (between  $-1$  and  $1$ ) through the tanh function and multiplies it by the output of the sigmoid gate, so that it outputs only the target information. LSTM has become the most popular ML algorithm in previous reservoir modelling studies (e.g., Zhang et al., 2018a; Yang et al., 2019; Guo et al., 2021; Zarei et al., 2021).

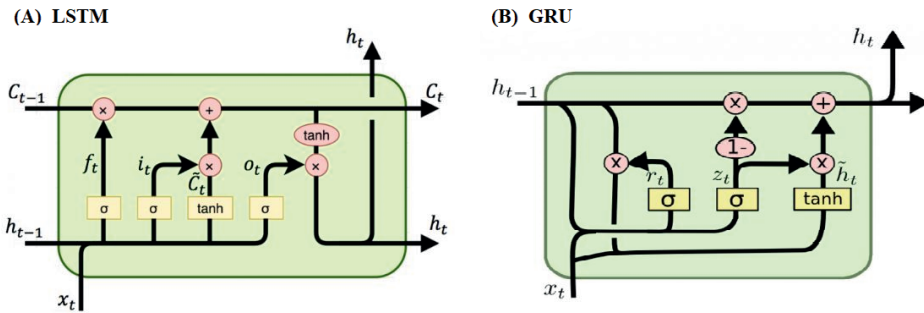


**Figure 3.12:** Diagrams for the memory blocks of the Long Short-Term Memory (LSTM; left panel) and Gated Recurring Units (GRU; right panel). The memory block contains the input state ( $X$ ), memory state (green box) and output state ( $h$ ).  $C$  is the recurrent input (from the previous time step),  $\Sigma$  and  $\tanh$  are the activation/transfer functions. For LSTM, from left to right: the forget gate (with  $\Sigma$  function), the input gate (with  $\Sigma$  function), the memory gate (with  $\tanh$  function) and the output gate (with  $\Sigma$  and  $\tanh$  functions). For GRU, from left to right: the update gate (with  $\Sigma$  function), the reset gate (with  $\Sigma$  function) and the output generation (with  $\tanh$  function) (adapted from Rathor, 2018).

### Gated Recurring Units (GRU)

Gated Recurring Units (GRU) is a simplified algorithm of LSTM suggested by Cho et al. (2014). The principle of GRU is similar to LSTM, which controls inputs, memory, output and recurrent information through a gating mechanism. The main difference from LSTM is that GRU only has two types of gates in the memory block; the update gate and the reset gate, and does not contain a cell state, as shown in Figure 3.12(B). The update gate is a combination of the forget Gate and the input Gate, which indicates how much and which information to ignore or to keep in the memory cell. If the update gate is 1, the previous memory is fully preserved, and if it is 0, the previous memory is completely forgotten. Note that while the forget gate in LSTM determines how much of the previous memory is maintained, GRU decides that either all previous memories are maintained or completely forgotten. The reset gate determines how the new input can be combined with earlier memory, which resets the past information in order to get rid of gradient explosion. The learning process of GRU is done in three steps, similar to LSTM. Firstly, the status of the memory block is updated by the update gate and the reset gate. Then, the memory cell generates a vector of new candidate values. Finally, the output of the memory block for the current time step is calculated. Since GRU has fewer parameters than LSTM, its training is easier and faster with a lower memory requirement, while providing performance comparable with LSTM (Witten & Frank, 2002).

**Table 3.1:** Machine learning models and their implemented frameworks and modules

Algorithm	Abbreviation	Framework	Module
Multiple Linear Regression	MLR		sklearn.linear_model.LinearRegression
K-Nearest Neighbor	KNN	Scikit-learn	sklearn.neighbors.KNeighborsRegressor
Support Vector Machine	SVM		sklearn.svm.LinearSVR
Classification and Regression Tree	CART		sklearn.tree.DecisionTreeRegressor
Random Forest	RF		sklearn.ensemble.RandomForestRegressor
Multi-Layer Perceptron	MLP		tf.keras.layers.Dense
Recurrent Neural Network	RNN	Keras and	tf.keras.layers.SimpleRNN
Long Short-Term Memory	LSTM	TensorFlow	tf.keras.layers.LSTM
Gated Recurring Unit	GRU		tf.keras.layers.GRU

### 3.4.6 Machine learning packages

The ML models were built and deployed in user-friendly and open-source machine learning frameworks in python, including Scikit-learn (Pedregosa et al., 2011), TensorFlow (Abadi et al., 2016) and Keras (Ketkar, 2017). Scikit-learn is a general machine learning framework built on top of Python's NumPy library. It features a wide range of traditional machine learning algorithms as well as a great variety of useful tools for data pre- and post-processing and model evaluation. TensorFlow is an end-to-end machine learning framework developed by Google and written in several languages, such as Python, Java and Swift. It is comprehensive and flexible, offering resources, libraries and tools that facilitate building and applying machine learning algorithms, primarily neural networks. Keras is an effective high-level neural network Application Programming Interface (API) written in Python, running on top of TensorFlow. It is designed to provide fast experimentation and allows for quickly building and training neural networks with minimal lines of code. All ML models with their frameworks and modules implemented in this thesis are indicated in Table 3.1.

## 3.5 Goodness-of-fit criteria

### 3.5.1 Criteria for model simulations

To examine the wflow\_sbm model parameter optimization, ML model training and performance evaluation of all models in the simulation phase, the simulated results were compared with the observed data. Amongst several suggested criteria (Moriassi et al., 2015; Houshmand Kouchi et al., 2017), four well-known criteria were applied in this thesis, including the Kling Gupta efficiency (KGE), mean square error (MSE), root mean square error (RMSE) and percent bias (PBIAS).

*Kling Gupta efficiency (KGE)*

The Kling Gupta efficiency (KGE) was proposed by Gupta et al. (2009) to better diagnose the relative importance of the three components that assess different hydrological dynamics: correlation, variability error and bias error, which were decomposed and modified from the Nash-Sutcliffe model efficiency coefficient (NSE; Nash & Sutcliffe, 1970). Gupta et al. (2009) suggested that due to the quadratic nature of NSE, the model calibration by maximizing NSE may lead to the underestimation of peak flows and overestimation of low flows, as the maximum NSE tends to be achieved when the variability error is equal to the correlation error. Since KGE equally weighs the three components and circumvents the connections between them, it is an alternative criterion that has been widely used in the past decade. KGE is given by

$$\text{KGE} = 1 - \sqrt{(r - 1)^2 + (\alpha - 1)^2 + (\beta - 1)^2}, \quad (3.9)$$

where  $r$  is the Pearson correlation coefficient between simulated streamflow and observed streamflow (giving the error in the dynamics),  $\alpha$  is the ratio of the standard deviation of simulated streamflow over the standard deviation of observed streamflow (giving the error in the variability) and  $\beta$  is the ratio between the mean simulated streamflow and the mean observed streamflow (giving the bias).

Similar to NSE, KGE ranges from  $-\infty$  to 1, with an ideal value at unity when all three components are equal to 1. However, their values should not be treated as approximately equivalent or interpreted in the same way, because, for instance, using the observed mean as prediction results in  $\text{NSE} = 0$  but  $\text{KGE} = -0.41$  (Knoben et al., 2019). Several performance benchmarks have been proposed (Althoff & Rodrigues, 2021), which is informative, but should be used carefully.

In this thesis, KGE was used as the objective function to optimize the *KsatHorFrac* parameter in the *wflow\_sbm* model (in Chapter 4) and as the performance index to evaluate the result accuracy of the *wflow\_sbm* model and ML models (in Chapters 4–7).

*Mean square error (MSE) and root mean square error (RMSE)*

While the KGE is bounded and dimensionless, the error in the model results can also be measured in terms of the units of the modelled variable. In this thesis, the mean square error (MSE) and its rooted form (RMSE) were applied. They are calculated as

$$\text{MSE} = \frac{1}{N} \sum_{i=1}^N (S_i - O_i)^2, \quad (3.10)$$

$$\text{RMSE} = \sqrt{\text{MSE}}, \quad (3.11)$$

where  $S$  represents the simulated value,  $O$  represents the observed value,  $i$  is the given time step and  $N$  is the total number of time steps.

Both MSE and RMSE range from 0 to  $\infty$ , of which smaller values refer to better model performance. As can be seen, MSE is measured in units that are the square of the target variable, while RMSE is measured in the same units as the target variable. Due to its formulation, MSE effectively penalizes larger errors. On the other hand, the advantage of RMSE is that it is more easy to interpret.

In this thesis, MSE was used as the loss function in the training process of the ML models, while RMSE was used to evaluate and compare the performance of the ML models on the reservoir outflow simulations (in Chapters 6 and 7).

#### *Percent bias (PBIAS)*

Next to RMSE, another popular error criterion, the percentage bias (PBIAS), was applied. PBIAS measures the average tendency of the simulated values to be larger or smaller than the observed counterparts and expresses it as a percentage:

$$\text{PBIAS} = \frac{\sum_{i=1}^N (S_i - O_i)}{\sum_{i=1}^N (O_i)} \times 100. \quad (3.12)$$

The optimal value of PBIAS is zero, with lower-magnitude values indicating a more accurate model simulation. Positive values indicate model overestimation bias, whereas negative values indicate model underestimation bias (Gupta et al., 1999).

In this thesis, PBIAS was used to evaluate and compare the ML model performance on the reservoir outflow simulations, together with KGE and RMSE (in Chapter 7).

### **3.5.2 Criteria for model reforecasting**

To evaluate the performance of the models in the reforecasting phase, three criteria were applied. The error index, mean absolute error (MAE) was applied for the deterministic reforecasts, while the continuous ranked probability score (CRPS) was applied for the probabilistic reforecasts.

#### *Mean absolute error (MAE)*

The mean absolute error (MAE) represents the magnitude of the average error of the reforecast in the absolute units, serving a similar purpose to RMSE. MAE is calculated per lead time as

$$\text{MAE} = \frac{\sum_{i=1}^{N_f} |F_i - O_i|}{N_f}, \quad (3.13)$$

where  $F$  represents the reforecast value and  $N_f$  corresponds to the number of reforecasts at a given lead time. MAE is expressed in the same units as the modelled variable with a perfect reforecast indicated with an MAE value of 0. By definition, MAE is never larger than RMSE.

In this thesis, MAE was used to evaluate the deterministic reforecast results of the reservoir inflows by the wflow\_sbm model and the reservoir outflows by the ML models (in Chapter 7).

#### *Continuous ranked probability score (CRPS)*

Unlike the deterministic reforecasts, an individual probabilistic reforecast can never be right or wrong, except when 0% or 100% is stated. Therefore, the predictive ability of the probabilistic or ensemble reforecasts can only be verified from large reforecast samples, using the probability scoring rules. The continuous ranked probability score (CRPS) generalizes MAE for the ensemble reforecasts. It measures the discrepancy between the reforecast cumulative distribution function (CDF) and the empirical CDF of the scalar observations. CRPS does not focus on any specific point of the probability distribution, but considers the distribution of the forecasts as a whole. CRPS is formulated as

$$\text{CRPS} = \frac{1}{N_f} \sum_{i=1}^{N_f} \int_{-\infty}^{+\infty} [P_{Fi}(x) - P_{Oi}(x)]^2 dx, \quad (3.14)$$

where  $P_{Fi}$  and  $P_{Oi}$  are the reforecast and observed cumulative distributions for the  $i$ th reforecast with a given lead time.  $x$  is the reforecast/observed sum, which is approximated numerically as an interval with a step  $dx$  that is variable and dependent on the sum per ensemble member (Hersbach, 2000; Imhoff et al., 2020a).

Similar to MAE, CRPS is expressed in the same units as the modelled variable, with smaller values indicating better model performance. CRPS reduces to MAE for single-valued (deterministic) forecasts (Gneiting & Raftery, 2007). For this reason, using CRPS enables the comparison between MAE of the single-valued reforecasts and CRPS of the ensemble reforecasts.

In this thesis, CRPS was used to evaluate the ensemble reforecast results of the reservoir inflows by the wflow\_sbm model and the reservoir outflows by the ML models (in Chapter 7).





## Chapter 4

# Distributed hydrological modelling with global datasets

This chapter is based on:

Wannasin, C., Brauer, C. C., Uijlenhoet, R., Van Verseveld, W. J., & Weerts, A. H. (2021b). Daily flow simulation in Thailand Part I: Daily flow simulation in Thailand Part I: Testing a distributed hydrological model with seamless parameter maps based on global data. *Journal of Hydrology: Regional Studies*, 34, 100794, doi:10.1016/j.ejrh.2021.100794

## Abstract

This chapter presents a ( $\sim 1$  km) distributed hydrological model, *wflow\_sbm*, with global spatial data and parameterization for estimating daily streamflow in the upper region of the Greater Chao Phraya River (GCPR) basin, with the aim to overcome in situ data scarcity often occurring in Southeast Asia (SEA). We forced the model with the MSWEP V2 precipitation and earth2Observe potential evapotranspiration datasets. Seamless distributed parameter maps based on pedotransfer functions (PTFs) and literature review were applied to bypass calibration. Only the *KsatHorFrac* parameter determining the lateral subsurface flow was calibrated. A target storage-and-release-based reservoir operation module (ROM) was implemented to simulate reservoir outflows. We compared the simulated daily streamflows obtained from different PTFs and evaluated the model performance in the period 1989–2014. The *wflow\_sbm* model with global spatial data and parameterization can reconstruct daily streamflow in the upper GCPR basin, especially for natural catchments ( $KGE = 0.78$ ). The ROM can capture the seasonal variability of reservoir outflows, but not very accurately at the daily timescale ( $KGE = 0.43$ ) since the actual reservoir operation is too complex. Different PTFs and *KsatHorFrac* values only introduce little uncertainty in the streamflow results. Therefore, the proposed model provides an opportunity for streamflow estimation in other ungauged or data-scarce basins in SEA. Nonetheless, the difficulty in the reservoir system modelling reflects the necessity of a better understanding of the quantitative effects of human intervention on daily streamflow.

## 4.1 Introduction

Floods and droughts have caused profound damage at the global scale, amplified by climate change and land use change (Chang & Franczyk, 2008; Dai, 2011; Ward et al., 2013; Bagley et al., 2014). These hydrological hazards have dramatically increased in many regions and are expected to become more frequent and severe in the future (Trenberth et al., 2014; Winsemius et al., 2016). Southeast Asia (SEA) is a region that is exceptionally prone to both floods (Hirabayashi et al., 2013; Ceola et al., 2014; Arnell & Gosling, 2016) and droughts (Cook et al., 2010; Dai, 2013; Trenberth et al., 2014). The vulnerability of SEA is partially due to the changes in monsoon dynamics and partially due to socio-economic development, such as urbanization, deforestation and cultivation, in developing countries. Mitigating these hydrological hazards in SEA requires rational water resources planning and management at the basin scale. This calls for the development of comprehensive hydrological models for the basin, particularly at the (sub)daily timescale, to assist both early warning and mitigation.

Several process-based hydrological models have been developed over the past decades for a better understanding of rainfall-runoff processes and have become important tools for scenario simulations, predictions and decision-making for river basin management (e.g., Mysiak et al., 2005; Ajami et al., 2008; Cloke & Pappenberger, 2009). Hydrological models can be classified as lumped or distributed according to the spatial representation (Singh & Woolhiser, 2002). Lumped models mathematically simplify the rainfall-runoff processes in a basin with spatially averaged parameters. Lumped model parameters have to be calibrated as they cannot be obtained from direct measurements, thus limiting model applications to gauged basins (Crawford, 1966). With improvements in computer technologies, distributed models have been developed (Singh & Woolhiser, 2002), which allow mathematically describing the rainfall-runoff processes in a spatially distributed way. This model type uses parameters directly related to the physical characteristics of the basin (e.g., topography, soil, land cover and river network) and takes into account spatial heterogeneity in both physical characteristics and meteorological inputs. Therefore, distributed models potentially provide an additional and more correct description of hydrological processes in the basin compared to lumped models (Refsgaard & Knudsen, 1996; Wicks & Bathurst, 1996). Since distributed models can fulfill various needs in spatial modelling, such as flood and drought extents, they have been widely used in water resources planning and management.

Despite their benefits, distributed models are much more complex and difficult to apply than lumped models. Firstly introduced in the 1970s, the distributed models were expected to be used without prior calibration by directly determining model parameters from field data (Abbott et al., 1986). This means the model results significantly depend on the accuracy of geospatial and spatial meteorological input data (Gourley & Vieux, 2006). In practice, however, these in situ data are not always available, especially for ungauged or sparsely gauged basins in developing countries, including in SEA (Grayson

& Blöschl, 2001). Therefore, like lumped models, some distributed parameters are still subject to calibration (Refsgaard, 1997). Calibrating a distributed model generally sets different parameter values to different grid cells, which poses a high risk of overparameterization, requires enormous computational demands at fine resolutions and obstructs model applications in large basins (Beven, 2006).

Fortunately, the advancement in remote sensing and geographic information system (GIS) data, including soils, land cover and climate, in recent decades can potentially complement some absences of field data and provide new means of spatial calibration and validation. Many remote sensing and GIS data are available in global public domains, with relatively high spatial and temporal resolutions (Fortin et al., 2001; Skidmore, 2017). With the availability of global high-resolution soil data (e.g., Hengl et al., 2017), recent attention has also been focused on pedotransfer functions (PTFs) for soil-related parameterization. Traditionally used in soil science, PTFs characterize soil hydraulic properties using predictive functions and structural soil data (Van Looy et al., 2017). Therefore, they have great potential to facilitate soil-related parameters, such as the water retention characteristic and hydraulic conductivity, in distributed models (Zhao et al., 2016a; Imhoff et al., 2020b). Together with powerful computer resources, we can attempt to maximize the use of remote sensing, GIS and PTFs data in order to minimize the number of calibrated parameters in distributed models. This offers an opportunity to develop more feasible and reliable distributed models for basins with data scarcity like in SEA.

In basins that are highly regulated by reservoirs, hydrological models also need explicit reservoir operation components. This is yet another motivation to use distributed hydrological models in this context. Failure to represent reservoir operation limits the models' performance and their applicability in scenario analyses, with climate, land use and operation changes (Yassin et al., 2019). The existing reservoir operation schemes in hydrological models are categorized into four types: natural lake, inflow- and demand-based, data-driven and target storage-and-release-based (Yassin et al., 2019). The natural lake method is limited to reservoirs without dams. The inflow- and demand-based methods determine reservoir outflows as a function of inflows and downstream water demands, but cannot account for reservoir operation in detail. The data-driven methods can simulate reservoir outflows more accurately, but cannot provide insight into the reservoir operation mechanisms due to their black-box characteristics. The target storage-and-release-based methods consider reservoir storage zoning and adjust reservoir outflows as a function of dynamic target storage, so-called operating rule curves. The main challenge for this type of method is a large amount of required data, such as the storage zone setting and actual rule curves of each reservoir, which are not always documented or easy to obtain. However, considering the growing availability of global data, the target storage-and-release-based methods are the most promising for simulating the multipurpose reservoirs at the daily timescale (e.g., Zhao et al., 2016b; Zajac et al., 2017; Yassin et al., 2019).

The Greater Chao Phraya River (GCPR) basin in Thailand represents the vulnerable and highly regulated river basins in SEA, considering its agriculture and water resources management. It contains several multipurpose reservoirs, of which the Sirikit and Bhumibol reservoirs are the largest in terms of storage capacity. Previous studies have investigated the performance of various distributed models on the monthly and daily streamflow simulations in the GCPR basin and other highly regulated basins in SEA (e.g., Kite, 2000; Kure & Tebakari, 2012; Sayama et al., 2015). Many of them have utilized global geospatial data (e.g., Thanapakpawin et al., 2007; Vo & Gourbesville, 2016; Bhagabati & Kawasaki, 2017; Livneh et al., 2017). Some studies have further implemented daily meteorological data from global databases to force the models instead of using gauged data, and they have shown promising performance. (e.g., Wang et al., 2016; Liu et al., 2017; Li et al., 2019; Yuan et al., 2019). Few studies have implemented the target storage-and-release-based methods (e.g., Kite, 2001; Mateo et al., 2014). However, all mentioned studies still needed to calibrate a few to several distributed parameters that are related to soil, land cover or reservoir operation. To date, no study has applied distributed models with global parameterization to simulate daily streamflow in the GCPR and other SEA basins.

This chapter aims to develop a ( $\sim 1$  km) distributed hydrological model with global spatial data and parameterization for estimating daily streamflow in the upper region of the GCPR basin, to overcome in situ data scarcity often occurring in SEA and to minimize the model calibration. We used the `wflow_sbm` model (Chapter 3; Section 3.3.1), which has shown good performance in basins across a large range of elevations and drainage areas (e.g., López López et al., 2016; Hassaballah et al., 2017; Giardino et al., 2018; López López, 2018; Gebremicael et al., 2019; Imhoff et al., 2020b). The utilized global remote sensing and GIS data included (i) static geospatial data from global databases; (ii) meteorological forcing data from the global reanalysis; (iii) seamless distributed maps for soil-related parameters obtained with PTFs and (iv) seamless distributed maps for land cover-related parameters obtained from literature review and global databases. Model results from different PTFs were investigated. A reservoir operation module (ROM) with a target storage-and-release-based method (Chapter 3; Section 3.3.2) was implemented with a minimum number of parameters and accessible operating rule curve data without calibration. The performance of the `wflow_sbm` model with global spatial data and parameterization, and the ROM were evaluated in both natural and regulated catchments.

## 4.2 Methodology

This chapter had a step-wise approach of (i) setting up the `wflow_sbm` model with global data and parameterization for the upper GCPR basin, (ii) including the reservoir operation module and (iii) evaluating the model performance. The modelling framework of the study is illustrated in Figure 4.1.

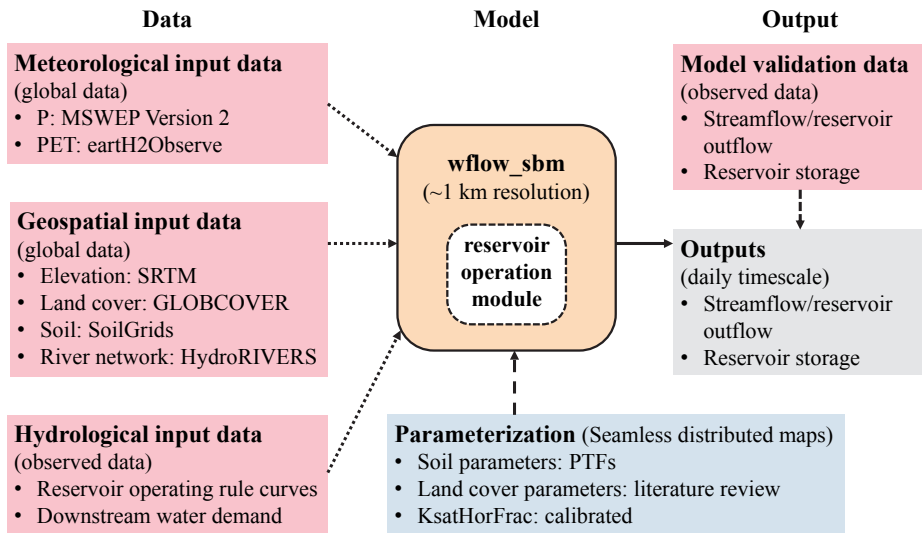


**Figure 4.1:** Modelling framework of the study, including the wflow\_sbm model setup with global data and parameterization, the reservoir operation module and the model performance evaluation.  $P$  and  $PET$  refer to precipitation and potential evapotranspiration. The dotted arrows represent inputs, the dashed arrow represents calibration and validation, and the solid arrows represent outputs.

#### 4.2.1 wflow\_sbm setup and parameterization

The wflow\_sbm model requires spatial meteorological data (precipitation and potential evapotranspiration) and geospatial data (elevation, land cover and soil). All these data were obtained from global databases, as previously described in Chapter 3; Sections 3.1.1 and 3.1.2. Aiming to tackle the issues of data scarcity and overparameterization for the upper GCPR basin, we also set up the wflow\_sbm model with global parameterization. Recently, seamless distributed parameter maps at the global scale have been available for wflow\_sbm (Schellekens et al., 2019; Imhoff et al., 2020b). The main parameters and their sources for global parameterization used in this study are indicated in Table 4.1.

##### *Global parameterization of soil-related parameters*

The seamless distributed maps of soil-related parameters for wflow\_sbm were estimated with pedotransfer functions (PTFs) based on soil types from the SoilGrids database (Imhoff et al., 2020b). They were initially applied to the Rhine basin and then regionalized to the global scale at the highest resolution of 250 m using the multi-parameter regionalization technique (MPR; Samaniego et al., 2010). Among five soil-related parameters (as indicated in Table 4.1), users can choose different PTFs, such as Braken-

**Table 4.1:** Main wflow\_sbm parameters and their sources for global parameterization (Imhoff et al., 2020b). The full list of wflow\_sbm parameters can be found in Schellekens et al. (2019).

Model parameter	Parameter interpretation	Source of value determination
<b>Soil-related parameters (pedotransfer functions; PTFs)</b>		
<i>c</i> (at different depths)	Power coefficient based on the pore size distribution index used for computing vertical unsaturated flow [-]	Rawls & Brakensiek (1989)
<i>KsatVer</i>	Vertical saturated conductivity [mm day <sup>-1</sup> ]	Brakensiek et al. (1984); Cosby et al. (1984)
<i>M</i>	Decay rate of KsatVer with depth [mm]	Fitting exponential function between KsatVer and depths of SoilGrids soil layers
<i>thetaR</i>	Residual water content [-]	Tóth et al. (2015)
<i>thetaS</i>	Saturated water content [-]	Tóth et al. (2015)
<b>Land cover-related parameters (literature review)</b>		
<i>Kext</i>	Extinction coefficient in the canopy gap fraction equation [-]	Assigned value per land cover type from Van Dijk & Bruijnzeel (2001)
<i>LAI</i>	Long-term monthly average leaf-area index [-]	Derived directly from Myneni et al. (2015)
<i>N</i>	Manning's roughness coefficient for the kinematic wave function for overland flow [m <sup>-1/3</sup> s]	Assigned value per land cover type from Engman (1986); Kilgore (1997)
<i>Nriver</i>	Manning's roughness coefficient for the kinematic wave function for river flow [m <sup>-1/3</sup> s]	Assigned value per Strahler order from Liu et al. (2005)
<i>RootingDepth</i>	Maximum length of vegetation roots	Assigned value per land cover type from Zeng (2001)
<i>Sl</i>	Specific leaf storage for the interception module [mm]	Assigned value per land cover type from Pitman (1989); Liu (1998)
<i>SoilThickness</i>	Depth of the upper aquifer [mm]	Derived directly from Hengl et al. (2017)
<i>Swood</i>	Fraction of wood in the vegetation [-]	Assigned value per land cover type from Pitman (1989); Liu (1998)
<i>WaterFrac</i>	Fraction of surface water area per gridded cell [-]	Extracted from Bontemps et al. (2011)
<b>Parameter subject to calibration</b>		
<i>KsatHorFrac</i>	Multiplication factor applied to KsatVer for the horizontal saturated conductivity used for computing the lateral subsurface flow [-]. This parameter compensates for anisotropy, small-scale KsatVer measurement (small soilcore) that do not represent larger-scale hydraulic conductivity, and model resolution (in reality smaller (hillslope) flow length scales).	Manual calibration

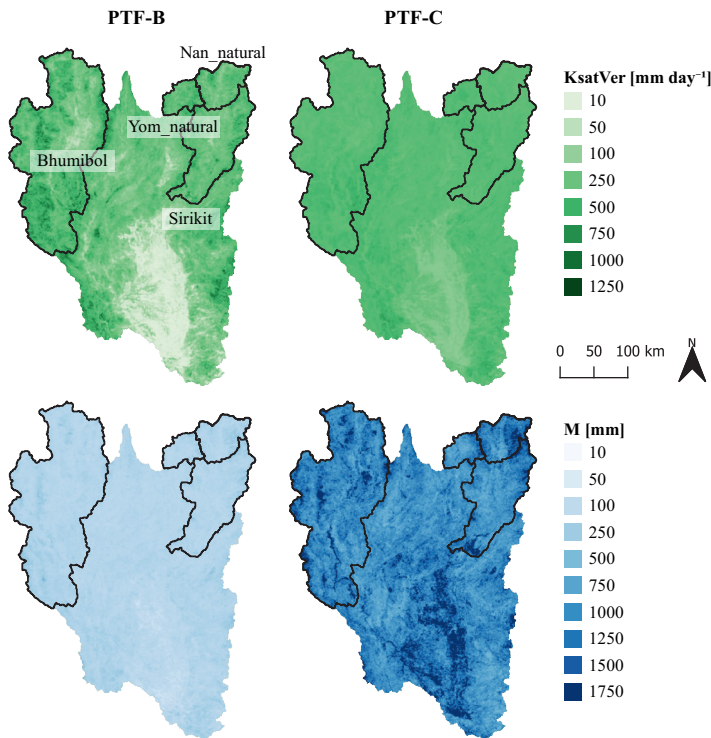


**Figure 4.2:** Spatial distribution of soil-related parameters,  $K_{satVer}$  (upper panels) and  $M$  (lower panels), for the upper GCPR basin in comparison between the PTF-B (right) and PTF-C (left) methods at the  $\sim 1$  km resolution. For parameter definitions, see Table 4.1. Boundaries of the four selected catchments are indicated in black color.

siek (Brakensiek et al., 1984) and Cosby (Cosby et al., 1984) functions, to estimate two highly sensitive parameters,  $K_{satVer}$  (vertical saturated conductivity) and  $M$  (decay rate of  $K_{satVer}$ ). We ran the `wflow_sbm` model with the Brakensiek (PTF-B) and Cosby (PTF-C) parameter sets to investigate the effect of different PTFs on the model performance. The spatial comparison of both parameter sets for the upper GCPR basin is shown in Figure 4.2.

#### *Global parameterization of land cover-related parameters*

The seamless distributed maps of land cover-related parameters for `wflow_sbm` were either estimated from a literature review or taken directly from global databases (as indicated in Table 4.1). The parameter maps from the literature review were collected as look-up tables and assigned to the land cover types of the GLOBCOVER database at its original resolution of 300 m. The parameter maps from global databases had different resolutions depending on their sources. This application assumed that the uncertainty



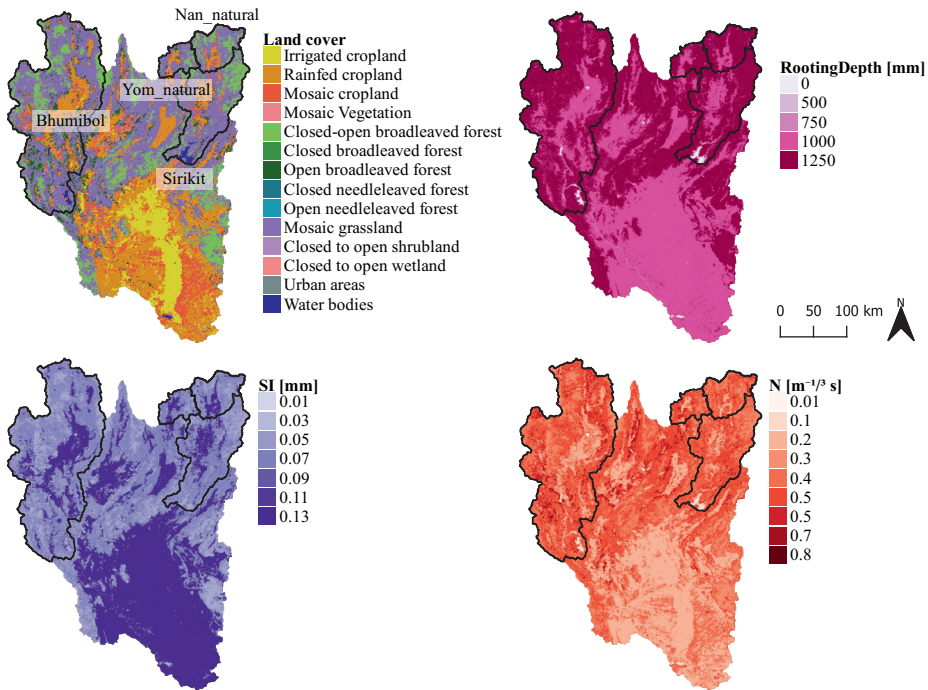


**Figure 4.3:** Spatial distribution of land cover and its related parameters, *RootingDepth*, *SI* and *N*, for the upper GCPR basin at the  $\sim 1$  km resolution. For parameter definitions, see Table 4.1. Boundaries of the four selected catchments are indicated in black color.

in land cover changes over the study period is negligible at the basin scale. Examples of the spatial distribution of land cover-related parameters for the upper GCPR basin are shown in Figure 4.3.

#### Other parameters

Other insensitive parameters of *wflow\_sbm* were set at their default values (Schellekens et al., 2019), leaving only one soil-related parameter, *KsatHorFrac* [-], to be calibrated. *KsatHorFrac* is the multiplication factor applied to *KsatVer* (vertical saturated conductivity) to calculate horizontal saturated conductivity for computing the lateral subsurface flow. This parameter compensates for anisotropy, small-scale (soil core) saturated hydraulic conductivity measurements that do not represent larger-scale hydraulic conductivity and smaller flow length scales (hillslope) in reality, which cannot be represented with the model resolution. The ratio of horizontal saturated conductivity to vertical saturated conductivity has been reported for catchments in temperate climates with typical values of 20–100 (Calver & Cammeraat, 1993; Refsgaard, 1997; Brooks et al., 2004; Weiler & McDonnell, 2007; Gauthier et al., 2009).

*Model setup, calibration and runs*

We applied the `wflow_sbm` model to the entire upper GCPR basin at a spatial resolution of approximately 1 km and temporal resolution of 3 hours over the study period of 25 years from the year 1989 to 2013. The  $\sim 1$  km grid cells could account for the areas of the two major reservoirs. The meteorological maps and seamless distributed parameter maps were upscaled or downscaled to the target resolution with parameter-specific upscaling procedures (Imhoff et al., 2020b). Although our study focused on the daily timescale, we ran the model at the 3-hourly time step to be able to calculate the model results at the daily timescale using the same aggregation period as applied in the daily observations (6.00 p.m.–6.00 p.m.; more detail in Chapter 3; Section 3.1.3). The daily *PET* data were divided into 3-hourly data using hourly fractions.

We manually calibrated *KsatHorFrac* for the years 2010–2011, which contain extremely wet and dry periods. The parameter was calibrated separately for the PTF-B and PTF-C soil-related parameter sets, with the parameter value ranging from 100 to 800. We then validated the optimized *KsatHorFrac* values for the period of 1989–2013, excluding 2010–2011. We used 2006 and 2013 as the representative years for wet and dry conditions in the upper GCPR basin. The hydro-meteorological details of the extreme years and the entire study period for the selected four catchments in the upper GCPR basin are shown in Table 4.2. The Kling Gupta efficiency (KGE; Gupta et al., 2009) was used as the objective function to optimize the *KsatHorFrac* parameter (more detail on the criteria shown in Chapter 3; Section 3.5.1).

#### 4.2.2 Reservoir operation module

The reservoir operation module (ROM) within the kinematic wave routing of the `wflow_sbm` model requires parameters representing (i) reservoir operation and (ii) the physical characteristics of each reservoir. As defined in Table 4.3, both operational and physical parameters are simplified and can be obtained directly from local data sources (RID and EGAT) or calculated from observed streamflow data without calibration. This allows for exploring the competence of available data. Amongst the five multi-purpose reservoirs in the upper GCPR region (see Chapter 2; Section 2.3), this study focused on the most important and largest reservoirs, Sirikit and Bhumibol, which accounted for 93% of the total reservoir capacity in the upper region. The values of the operating rule curve parameters for the Sirikit and Bhumibol reservoirs were previously shown in Figure 3.4(B) and 3.4(C). The physical parameter values for each reservoir were previously indicated as the last three components in Table 2.1.

#### 4.2.3 Model performance evaluation

We investigated the model performance on two natural catchments (Nan\_natural and Yom\_natural) and two regulated catchments (Sirikit and Bhumibol) in the upper GCPR basin, as shown in Figure 2.2. More explanation of the selected catchments and their

**Table 4.2:** Annual sums of water fluxes for catchments and years of interest. The fluxes comprise the MSWEP V2 Precipitation ( $P$ ), earth2Observe potential evapotranspiration ( $PET$ ) and observed streamflow ( $Q$ ). Nan.natural and Yom.natural are headwater catchments, whereas Sirikit and Bhumibol are midstream catchments. Therefore, the latter catchments also receive inflow from upstream, which is not shown here. Note that the  $P$ ,  $PET$  and  $Q$  data were obtained from independent measurements or calculations.

Catchment	Component [mm year <sup>-1</sup> ]	Wet (2006)	Dry (2013)	Long-term average (1989–2013)
Nan.natural	$P$	1225	1116	1230
	$PET$	1069	1079	1032
	$Q$	856	572	766 (1994–2013)
Yom.natural	$P$	1121	1048	1099
	$PET$	1123	1132	1086
	$Q$	513	261	386 (1996–2013)
Sirikit	$P$	1377	1030	1111
	$PET$	1223	1216	1181
	$Q$	3160	1905	2814 (1989–1997, 2003–2013)
Bhumibol	$P$	1179	858	942
	$PET$	1099	1107	1092
	$Q$	1075	569	780
Upper Chao Phraya	$P$	1248	1044	1060
	$PET$	1220	1221	1189
	$Q$	373	146	211

areas and boundaries are provided in Chapter 2; Section 2.4. The KGE was used to evaluate the accuracy of the wflow\_sbm model and the ROM at the daily timescale.

## 4.3 Results

### 4.3.1 Parameter optimization and uncertainty

During the calibration of the *KsatHorFrac* parameter, we found that higher *KsatHorFrac* values generally attenuate the magnitude of streamflow, especially for peak flows, and flatten their recession limbs. With the same *KsatHorFrac* value, the PTF-B parameter set produces daily streamflow with steeper peaks and more rapid recessions than the PTF-C parameter set. This is because PTF-B presents more varying *KsatVer* values, with lower *M* values, over the study area (Figure 4.2), resulting in less daily baseflow contribution. The optimized *KsatHorFrac* value for the upper GCPR basin is 550 for PTF-B and 120 for PTF-C. The range of the simulated daily streamflows with the *KsatHorFrac* values between 100 and 800 is more narrow for PTF-B than for PTF-C (light colored bands in Figure 4.4), indicating that PTF-B introduces a smaller uncertainty in the streamflow result compared to PTF-C.

With their optimized *KsatHorFrac* values, PTF-B and PTF-C deliver similar estimates of daily streamflow for both natural and regulated catchments, as demonstrated by the

**Table 4.3:** Reservoir parameters and their sources for parameterization. The values of the operating rule curve parameters for the Bhumibol and Sirikit reservoirs are illustrated in Figure 3.4. The values of the physical parameters are presented in Table 2.1.

Reservoir parameter	Parameter interpretation	Source of value determination
<b>Operational (rule curve) parameters</b>		
<i>DD</i>	Target of downstream water demand [ $\text{m}^3 \text{ time step}^{-1}$ ]	Long-term monthly average streamflow at a dam location (RID)
<i>ResMaxFrac</i>	Target of maximum storage (conservation storage level) as a fraction of <i>ResMaxVol</i> , ranging between 0 and 1 [-]	Long-term monthly target maximum storage (RID)
<i>ResMinFrac</i>	Target of minimum storage (inactive storage level) as a fraction of <i>ResMaxVol</i> , ranging between 0 and 1 [-]	Default setting
<b>Physical parameters</b>		
<i>ResArea</i>	Reservoir surface area used for estimating precipitation and evaporation [ $\text{m}^2$ ]	RID
<i>ResMaxQ</i>	Maximum release capacity of a reservoir [ $\text{m}^3 \text{ time step}^{-1}$ ]	As the actual value is unknown, it was set as the maximum outflow in the historical record (RID)
<i>ResMaxVol</i>	Reservoir maximum storage (flood control storage level) [ $\text{m}^3$ ]	RID

colored lines in Figure 4.4 and the goodness-of-fit indicators in Table 4.4. PTF-B outperforms PTF-C in the natural catchments, while PTF-C performs better in the regulated catchments. PTF-B tends to result in higher  $\alpha$ , but smaller  $\beta$  compared to PTF-C, indicating a lower error in the variability (less overestimating or underestimating the variability in daily streamflow), but a larger bias (more overestimating or underestimating the mean streamflow). This is because PTF-B captures the daily streamflow fluctuation and magnitudes of daily peak flows more accurately whereas PTF-C is better at simulating daily baseflow, as also visible in Figure 4.4.

#### 4.3.2 Model performance in natural catchments

Overall, the wflow\_sbm model with the global data and seamless distributed parameter maps can reconstruct the observed daily streamflow for the natural catchments. The daily hydrographs of the Nan\_natural catchment (Figure 4.5(A) and (B)) and Yom\_natural catchment (Figure 4.5(C) and (D)) show good fits in the peak timing and seasonal variability between the observed and simulated streamflows in both wet year (2006) and dry year (2013). Table 4.4 indicates satisfactory model performance, with the KGE value in the validation period ranging between 0.63 and 0.65 for the Nan\_natural catchment and 0.78 for the Yom\_natural catchment. Apart from the spatial uncertainty in model parameters, the varying model performance between the two

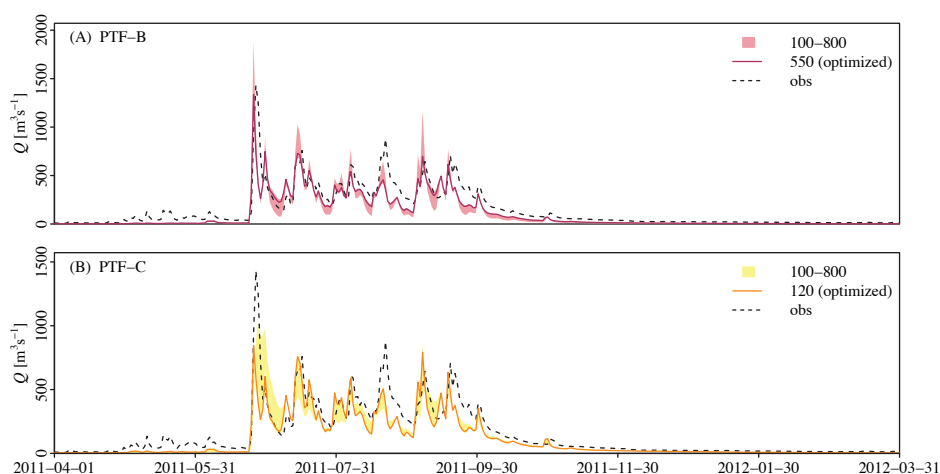


**Figure 4.4:** Simulated and observed daily streamflows for the Nan\_natural catchment in 2011, which is part of the calibration period. The simulated streamflows obtained with different  $K_{satHorFrac}$  values from 100 to 800 for the PTF-B parameter set (panel (A)) and PTF-C parameter set (panel (B)) are presented as ranges in colored bands. The simulated streamflow obtained with the optimized  $K_{satHorFrac}$  is shown in solid colored lines, compared to the observations (obs) in dashed black lines.

catchments can be attributed to the difference in the catchment characteristics, particularly the elevation and land cover. A large part of the Nan\_natural catchment is mountainous with forest areas, as shown in Figure 2.2 and 4.3. Therefore, its hydrological processes are more difficult to simulate compared to the Yom\_natural catchment that is less steep with more grasslands. The difficulty is caused by the higher amount and variability in precipitation, which result in the higher and more fluctuating streamflow, as also evident in Table 4.2. As a result, the magnitude of peak flow in the Nan\_natural catchment was five times higher than in the Yom\_natural catchment in the wet year (Figure 4.5(A) and (C)) and nine times higher in the dry year (Figure 4.5(B) and (D)). For both catchments, the model tends to underestimate flood peaks in the rainy season, especially at the beginning of the monsoon period, and miss peak flows generated by local storm events in the dry season.

### 4.3.3 Model performance in regulated catchments

The wflow\_sbm model with the ROM shows the varying performance when simulating the regulated streamflow for the Sirikit and Bhumibol catchments (Table 4.4). On the one hand, the daily streamflow estimate for the Sirikit catchment is passable, with the highest KGE of 0.43 (PTF-C) in the validation period. On the other hand, the model failed to estimate the daily streamflow for the Bhumibol catchment, resulting in negative KGE values in both calibration and validation periods. The major sources of error

**Table 4.4:** wflow\_sbm performance in simulating daily streamflow for the four study catchments and daily storage for the two reservoirs, with the PTF-B and PTF-C parameter sets. KGE and its components were obtained during the calibration (first row) and validation (second row) against observations. The model was calibrated for the years 2010–2011 and validated for the years 1989–2013, excluding 2010–2011.

		Period	PTF-B				PTF-C			
			KGE	$r$	$\alpha$	$\beta$	KGE	$r$	$\alpha$	$\beta$
Catchment (streamflow)	Nan_natural	Cal	<b>0.68</b>	0.89	0.85	0.73	<b>0.66</b>	0.89	0.80	0.74
		Val	<b>0.65</b>	0.85	0.88	0.70	<b>0.63</b>	0.83	0.83	0.71
	Yom_natural	Cal	<b>0.67</b>	0.80	0.78	0.86	<b>0.65</b>	0.79	0.75	0.87
		Val	<b>0.78</b>	0.79	1.07	0.97	<b>0.78</b>	0.78	0.96	0.97
	Sirikit	Cal	<b>0.24</b>	0.42	1.36	1.34	<b>0.25</b>	0.43	1.35	1.35
		Val	<b>0.41</b>	0.42	0.87	0.94	<b>0.43</b>	0.45	0.84	0.96
	Bhumibol	Cal	<b>-0.68</b>	0.04	2.06	1.88	<b>-0.63</b>	0.03	1.96	1.89
		Val	<b>-0.26</b>	0.04	1.73	1.37	<b>-0.21</b>	0.06	1.65	1.38
Reservoir (storage)	Sirikit	Cal	<b>0.45</b>	0.77	0.54	1.20	<b>0.41</b>	0.79	0.49	1.22
		Val	<b>0.80</b>	0.87	1.03	0.85	<b>0.81</b>	0.86	1.05	0.88
	Bhumibol	Cal	<b>0.13</b>	0.69	0.35	1.50	<b>0.12</b>	0.71	0.33	1.50
		Val	<b>0.59</b>	0.69	1.09	1.24	<b>0.59</b>	0.71	1.04	1.28

for both catchments are the inflexibility of the daily reservoir releases and the prompt releases of surcharge water by the ROM in the very wet periods, as evidenced in Figure 4.5(E), (G) and (H). Therefore, the resulting accuracy for both reservoirs tends to be higher in the dry season than in the rainy season and higher in dry years than in wet years.

To elaborate on the ROM performance, the daily water storage computed by the ROM for the Sirikit and Bhumibol reservoirs are compared to observations in Figure 4.6. Overall, the simulated reservoir storage reasonably captures the inter- and intra-annual variability, although the magnitude is not accurate. The storage tends to be underestimated for the Sirikit reservoir and overestimated for the Bhumibol reservoir. In very wet periods, the storage is overestimated and exceeds the monthly target maximum (top of the grey band in Figure 4.6). This occurred more often for the Bhumibol reservoir than for the Sirikit reservoir, especially after the year 2003. As a result, the goodness-of-fit of the simulated storage (Table 4.4) is significantly better for the Sirikit reservoir (highest KGE = 0.81 with PTF-C) than the Bhumibol reservoir (KGE = 0.59 for both PTF-B and PTF-C). Due to the storage overestimation, the ROM released surcharge storage promptly (according to Equation (3.7) in Chapter 3), producing the unrealistic streamflow, as appeared in 2006 (Figure 4.5(E) and (G)). Although the observed daily storage of both reservoirs also exceeded the monthly target maximum in some wet years, e.g., 1995, 2006 and 2011 (Figure 4.6), most of the observed surcharged water was allowed to stay in the reservoirs instead of being spilled at once. Therefore, the observed peak outflow due to surcharge storage was not as huge as the outflow simulated by the ROM (Figure 4.5(E)–(H)). Due to the limited flexibility of the ROM, it cannot cap-

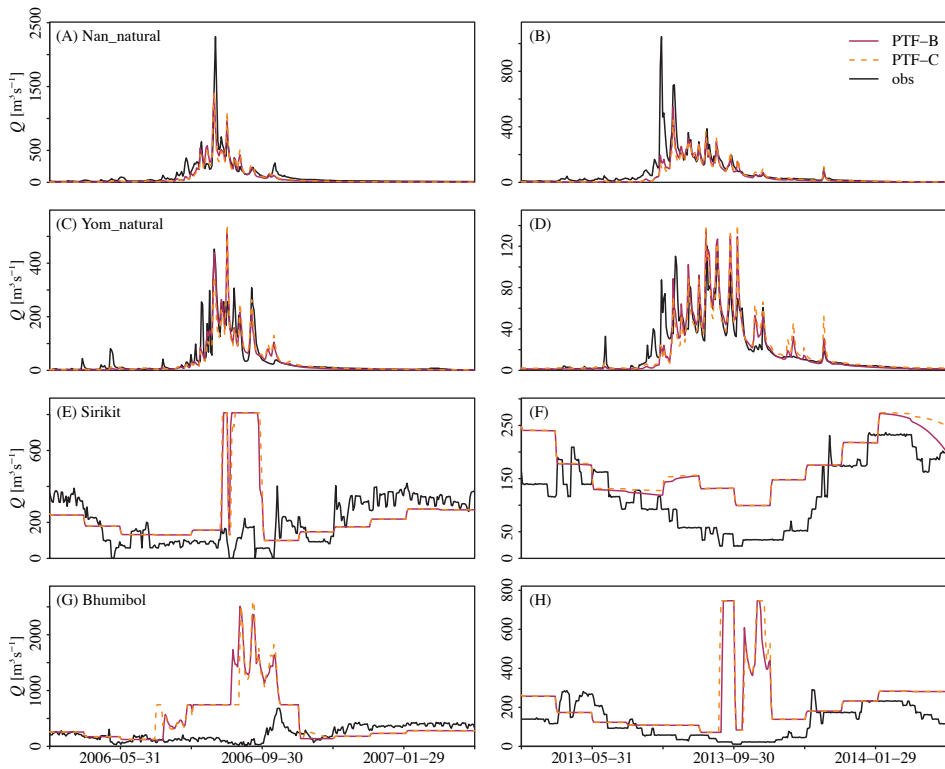


**Figure 4.5:** Simulated and observed daily streamflows in the wet year (2006; left panels) and the dry year (2013; right panels) for the Nan\_natural (first row), Yom\_natural (second row), Sirikit (third row) and Bhumibol (bottom row) catchments. The simulated streamflow with the optimized PTF-B parameter set is shown in solid red lines, the simulated streamflow with the optimized PTF-C parameter set in dashed orange lines and the observations (obs) in solid black lines.

ture the dynamics of the observed reservoir outflows at the daily timescale. However, it does show satisfactory performance for simulating reservoir outflows at the monthly timescale. The monthly hydrographs and the KGE results of all catchments are supplied in Appendix A.

## 4.4 Discussion

### 4.4.1 wflow\_sbm with global data and parameterization

To our knowledge, this is the first study that applied the wflow\_sbm model to simulate the daily streamflow in the upper GCPR basin. By setting up the model with global geospatial datasets (e.g., SRTM elevation), forcing the model with global meteorologi-

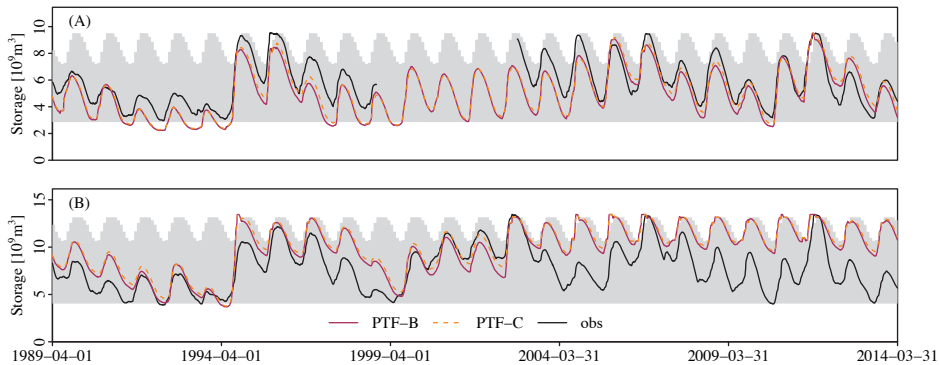


**Figure 4.6:** Simulated and observed daily storages of the Sirikit reservoir (A) and the Bhumbol reservoir (B) during the years 1989–2013. The grey bands represent the ranges between the monthly target maximum storage and the target minimum storage, which was fixed as 30 percent of the reservoir capacity. The simulated storage with the optimized PTF-B parameter set is shown in solid red lines, the simulated storage with the optimized PTF-C parameter set in dashed orange lines and the observations (obs) in solid black lines.

cal datasets (MSWEP V2  $P$  and earth2Observe  $PET$ ) and applying the seamless parameter maps based on SoilGrids, GLOBCOVER and other global databases (e.g., MODIS LAI), we can circumvent the poor availability of in-situ observations often occurring in SEA. The seamless distributed parameter maps were applied to all but one sensitive soil-related parameter,  $K_{satHorFrac}$ , for which PTFs were not available (Imhoff et al., 2020b). Although a full calibration procedure may improve the model performance, calibrating only one parameter prevented overparameterization and equinuality as well as reduced the computation time when simulating such a large basin at high spatial and temporal resolutions.

The model sensitivity to the soil-related parameter maps with different pedotransfer functions, PTF-B and PTF-C, became apparent due to the difference in the optimized  $K_{satHorFrac}$  values (550 for PTF-B and 120 for PTF-C).  $K_{satHorFrac}$  controls horizontal saturated conductivity, which influences the magnitude of the lateral subsurface flow, and thus streamflow dynamics and recession after a peak (Figure 4.4). The parameter is, consequently, sensitive to the other soil-related parameters, particularly  $K_{satVer}$  (vertical saturated conductivity) and  $M$  (decay rate of  $K_{satVer}$ ) (see full description in Table 4.1). PTF-B and PTF-C produced very different spatial values of  $K_{satVer}$  and  $M$ , as visible in Figure 4.2. Therefore, we suggest calibrating  $K_{satHorFrac}$  with respect to the selected PTF parameter set and study area. Furthermore, calibrating the  $K_{satHorFrac}$  based on soil types or evaluation instead of calibrating it as a constant value may improve the model performance, which can benefit the model application for the real-time forecasting purpose, although more computational efforts are demanded. Nevertheless, the range of streamflows simulated with the  $K_{satHorFrac}$  values of 100–800 is not very



large, especially for PTF-B (Figure 4.4). Therefore, running the model without any calibration only introduces a little uncertainty, which enhances the possibility of its applications in ungauged basins.

Other sources of model uncertainty, such as the meteorological, geospatial and hydrological input data, were not investigated in this study but could play a role in the model errors. Firstly, the synthetic meteorological data from global databases are subject to their own spatial ( $\sim 10$  km) and temporal (3 hourly–daily) resolutions, which were coarser than the target resolutions of the model ( $\sim 1$  km and 3 hourly). As a result, the  $P$  data failed to present local storm events, leading to the absence of local peak flows in dry seasons and at the beginning of rainy seasons for natural catchments (Figure 4.5(A)–(D)). Similarly, the quality of the  $PET$  data directly affects the actual evapotranspiration ( $AET$ ) estimates, but their accuracy was difficult to evaluate. Secondly, the seamless distributed maps for the land cover-related parameters were created based on the land cover database from the year 2009 (Figure 4.3). In fact, the land cover in the upper GCPR basin has gradually changed over time, with decreasing forest areas and increasing agricultural areas (Jamrussri & Toda, 2017). Therefore, assigning the land cover-related parameters based on yearly land cover maps may improve the model results. Lastly, the quality of the observed streamflow data was unverified and could also affect the model performance evaluation to some extent.

Considering the study purpose, we conclude that the `wflow_sbm` model with global data and parameterization is capable of simulating the daily streamflow for the natural catchments (Figure 4.5(A)–(D) and Table 4.4), but less effective for the regulated catchments due to mathematical limitations in the ROM (see Section 4.4.2 for more detail). In most study catchments, the goodness-of-fit results were higher during the validation than during the calibration potentially because the short calibration period (years 2010–2011) was both extremely wet and dry, while the validation period (years 1989–2013, excluding 2010–2011) also contained more regular hydrological conditions. Nonetheless, the `wflow_sbm` model outperforms the SWAT model that was run with observed daily meteorological data and fully calibrated for the same study area (Jamrussri & Toda, 2017). Therefore, it has the potential to serve as a tool for the upper GCPR basin and other ungauged or data-scarce catchments in SEA.

#### 4.4.2 Reservoir operation module

Reservoir operation modules with the target storage-and-release-based methods usually require a large amount of data for an individual reservoir that may be undocumented or difficult to obtain, particularly for data-scarce areas like SEA. Yassin et al. (2019) found that even when the required data are available, they usually contain considerable uncertainties so that optimizing operational parameters is still insufficient to represent the absolute storage-release relationship for many reservoirs, especially the multipurpose ones. Considering limited data available for the upper GCPR basin, the ROM was, therefore, designed to minimize the number of operational parameters and utilize ac-

cessible data without calibration (Figure 3.4 and Table 4.3), which also allowed for investigating the data competence.

The main error in the ROM results was the daily storage that exceeded the monthly target maximum in the rainy seasons (Figure 4.6). In response, the surcharge water was promptly released by the ROM, causing unrealistic flood peaks (Figure 4.5(E), (G) and (H)), especially for the Bhumibol reservoir. Meanwhile, the observations showed that the daily storage also exceeded the monthly target maximum in some wet years. However, the surcharge was not released at once, but was held and gradually released to prevent downstream floods. On some occasions, the daily outflows were paused for a few days to control downstream floods. This indicates the high flexibility of the actual reservoir operation on a day-to-day basis, which could not be captured by the ROM that is based on the monthly operating rule curves and piece-wise linear regression algorithm. This flexibility reflects real-time decision-making by reservoir operators to meet occasional targets, such as mitigating floods, satisfying downstream irrigation demands and increasing the hydropower generation (Yassin et al., 2019). Therefore, the ROM simulations in this study can be seen as the baseline operation scenario, which reflects the generalized operation without further impacts of human intervention. This baseline simulation is useful for analyzing effects of reservoir operation on downstream flows, which is presented in Chapter 5. Although real-time decision-making is beyond the capability of the ROM and other process-based operation modules, we suggest that the ROM performance can still be upgraded in the future with (i) a more accurate storage calculation and (ii) a more complex release algorithm.

The storage calculation may be improved with the higher accuracy of daily reservoir inflows and direct *AET* losses computed by the *wflow\_sbm* model. In this study, the upstream inflows of the Sirikit and Bhumibol reservoirs were simulated as naturalized flows and indirectly validated with upstream flows since reliable reservoir inflow data are not available. However, there are four reservoirs located upstream of the Bhumibol reservoir, which have been operated since 2003. Therefore, the simulated inflows could be inaccurate, although this was impossible to evaluate without observed data. This explains the storage overestimation for the Bhumibol reservoir after 2003 (Figure 4.6(B)). Meanwhile, the inaccuracy of the daily *AET* could be partly due to the simplification of the ROM itself. Since the water surface area of each reservoir was set as a fixed value (Table 2.1), despite the daily storage change, the amount of daily evaporating water could be under- or overestimated. Therefore, the reservoir area-elevation-storage relationship (e.g., Zhao et al., 2016b) may increase the accuracy of the daily *AET* losses, and thus the daily storage estimated by the ROM.

The main factor determining the release algorithm in the ROM is the monthly target downstream water demand (*DD*). Without existing data, the *DD* of each reservoir was estimated as the long-term-monthly average of the reservoir outflow (Figure 3.4(B)), which could be a source of significant uncertainty for the daily outflow simulation. Another limitation of this algorithm is that it intends to meet the target *DD* without consid-

ering the daily inflows (e.g., thresholds for flooding, normal and low inflows) or maximum acceptable streamflow at downstream control points (e.g., at Nakhon Sawan). Adding these factors into the outflow determination process (e.g., Zhao et al., 2016b; Yassin et al., 2019) may rectify the unrealistic surcharge releases. In addition, a release coefficient (e.g., annual coefficients as a function of mean total annual inflow) could introduce the inter-annual release variability into the module (Hanasaki et al., 2006). However, more parameters also mean more uncertainty sources, and thus their competence should be carefully assessed.

#### 4.4.3 Human impacts on hydrological modelling and streamflow

Our findings are in substantial agreement with previous studies, concluding that simulating the outflows of the Sirikit and Bhumibol reservoirs is challenging due to the complex patterns of real-time decision-making by reservoir operators. Neither target storage-and-release-based methods nor inflow-and-demand-based methods applied in the past could satisfactorily reconstruct the actual operations of these two reservoirs at the daily timescale (e.g., Hanasaki et al., 2006; Mateo et al., 2014; Yassin et al., 2019). The recent study of Yassin et al. (2019) suggested that it was mainly due to the high ratio of the maximum reservoir storage and the mean total annual inflow of both reservoirs ( $>0.5$ ), indicating more radical regulations compared to many other reservoirs worldwide. Moreover, since the outflows of the Sirikit and Bhumibol reservoirs conjugate at Nakhon Sawan, it is likely that both reservoirs are jointly operated in real-time to manage floods and droughts in the downstream floodplain, as also reported during the 2011 GCPR flooding (Komori et al., 2012).

Recently, Yang et al. (2019) found that the data-driven method, artificial neural networks (ANNs), could learn the complex pattern of the observed reservoir outflow records and reproduce the daily outflow more accurately for both Sirikit (NSE = 0.93) and Bhumibol reservoirs (NSE = 0.86). Therefore, they can be useful tools for real-time reservoir outflow simulation and forecasting. However, since ANNs are black boxes, they cannot reveal the insights of real-time decision-making for the actual operation, which remain imperative for better and more sustainable reservoir water management in the future.

Above all, the unsatisfactory simulations of the reservoir outflows by the ROM reflect the strong and prompt human intervention on daily streamflow. In the areas that are at risk of floods and droughts like the upper GCPR basin and other basins in SEA, understanding of quantitative impacts of reservoir operation, especially with real-time decision-making, on downstream flows is essential. Therefore, we further applied the developed model and results from this study to assess the effects of reservoir operation on the daily streamflow in the upper GCPR basin in Chapter 5. With deeper knowledge of both reservoir system modelling and reservoir effects, we expect to be more capable of improving hydrological modelling and water resources management simultaneously.

## 4.5 Conclusion and outlook

This chapter concerned the development of a ( $\sim 1$  km) distributed hydrological model, `wflow_sbm`, with global spatial data and parameterization and the exploration of its performance in estimating daily streamflow in the upper Greater Chao Phraya River basin. The main findings are as follows:

1. The `wflow_sbm` model with global spatial data and parameterization can satisfactorily estimate daily streamflow in the natural catchments (highest KGE = 0.78 in the validation period).
2. The `wflow_sbm` model was not able to estimate daily streamflow in regulated catchments very well due to the simplified algorithm of the reservoir operation module (ROM) (highest KGE = 0.43 in the validation period).
3. The ROM with the (monthly) operating rules can capture the seasonal variability of the reservoir storage and outflows, but cannot take into account real-time decision-making by reservoir operators. The ROM results, therefore, reflect the baseline operation without further impacts of human intervention.
4. The difference between daily reservoir outflows from the baseline operation (simulations) and the real-time operation (observations) highlights the strong effect and importance of real-time decision-making to optimize the reservoir outflows promptly, especially during extreme events. At the same time, it also addresses the source of difficulties in modelling large-scale multipurpose reservoirs. A more complex module with optimized parameters may improve the results, but uncertainties remain high.
5. With room for improvements, the proposed model can reasonably serve as a tool for analyzing catchment-scale hydrological variations in the GCPR basin and provide an opportunity for streamflow estimation in other ungauged or data-scarce basins in Southeast Asia.

Based on the findings, more studies on the use of seamless parameter maps based on global data for distributed hydrological modelling in other data-scarce basins are encouraged. Effects of using different global meteorological datasets on the model performance should also be explored. Future challenges in reservoir system modelling include gaining a better understanding of the complexity of real-time operation and improving the model performance for multipurpose reservoirs. Chapter 5 describes the application of the `wflow_sbm` model with the ROM in investigating the reservoir operation and its effects on the daily flow regime in the same basin.

“We only know what we perceive.  
Everything we experience is ultimately just our perception of it.  
It’s not what you look at that matters, it’s what you see.”  
—Matt Haig, *The Midnight Library* (2020)



## Chapter 5

# Hydrological effects of reservoir operation

This chapter is based on:

Wannasin, C., Brauer, C.C., Uijlenhoet, R., Van Verseveld, W.J., & Weerts, A.H. (2021a). Daily flow simulation in Thailand Part II: Unraveling effects of reservoir operation. *Journal of Hydrology: Regional Studies*, 34, 100792, doi:10.1016/j.ejrh.2021.100792

## Abstract

The upper region of the Greater Chao Phraya River basin is highly regulated by multipurpose reservoirs, which have altered the natural streamflow. Understanding the quantitative effects of such alteration is crucial for effective water resource management. Therefore, this chapter aims to assess how reservoir operation affects the water balance, daily flow regime and extreme flows in this basin. For this purpose, we reconstructed streamflow in the naturalized (no reservoir) and baseline operation scenarios using the distributed ( $\sim 1$  km) wflow\_sbm model. To overcome data scarcity, we ran the model with global data and parameterization. A target storage-and-release-based reservoir operation module was applied in the baseline operation scenario. The model results were analyzed in comparison to observations in a wet year, a dry year and the period 1989–2014. The reservoir operation resulted in more evaporation. It inverted the natural flow seasonality and smoothed the daily flow regime with decreasing high flows, increasing mean flows and low flows, greater baseflow contribution and lower flashiness. It prevented or mitigated many historical extreme flow incidents. The annual flood peaks and minimum flows were markedly mitigated in terms of both magnitudes and frequencies, but their timing became more variable and difficult to predict. Altogether, the results highlighted the importance of effective reservoir operation modelling and decision-making in real-time, which remain challenging in practice.



## 5.1 Introduction

The majority of rivers around the world are fragmented by dammed reservoirs (Zhou et al., 2016). Although several dams have been removed at the end of their useful lives, they are outnumbered by those in operation and under construction (O'Connor et al., 2015). The current expansion in dammed reservoir construction takes place, particularly in regions with emerging economies like Southeast Asia (SEA), where it serves not only for irrigation and hydrological hazard control, but also for hydropower generation (Zarfl et al., 2015). In fact, SEA has recently become the region with the highest investment for large multipurpose reservoirs (Siciliano et al., 2015). Currently, there are more than 130 new projects of large reservoirs planned in Laos, Malaysia, Cambodia, Myanmar and at the border of Myanmar-Thailand (Siciliano et al., 2015). Therefore, it is undeniable that dammed reservoirs are a necessity for water resources management and play an important role in flood and drought mitigation in SEA.

Despite their benefits, dammed reservoirs remain controversial due to their potentially negative impacts on streamflow, the environment and society. Reservoir operation alters the natural flow regime, i.e., flow rate, flow magnitude and fluctuation, in particular the duration, timing and frequency of wet and dry extremes, from the daily to the long-term scale (Graf, 2006; Mittal et al., 2016; Li et al., 2017). On the one hand, reservoir operation can attenuate flood and drought events by smoothing streamflow, with lower flood peaks and higher baseflows (e.g., Lee et al., 2017; Wu et al., 2018; Gai et al., 2019). On the other hand, hydrological extremes can be intensified by ineffective management of reservoir water, which in some cases had greater influence than climate change (e.g., Graf, 2006; Mittal et al., 2016; He et al., 2017; Di Baldassarre et al., 2018). Since SEA has an increasing number of dammed reservoirs while being highly exposed to hydrological hazards (Trenberth et al., 2014; Arnell & Gosling, 2016), there is an urgent need to evaluate effects of reservoir operation on streamflow in specific contexts of this region.

Considering data availability, the Greater Chao Phraya River (GCPR) basin in Thailand can provide a decent case study, as its main reservoirs have been operated with observational data records available for the last 25 years. Previous studies mentioned conflicting causes of hydrological hazards in the GCPR basin. Komori et al. (2012) suggested that the 2011 GCPR flood, one the most catastrophic floods ever recorded in SEA, was driven by intense precipitation, in line with the finding of Sayama et al. (2015) that a 1% increase in precipitation caused a 4.2% increase in flood inundation in the basin. Meanwhile, Van Oldenborgh et al. (2012) concluded that the 2011 flood volumes were magnified by non-meteorological factors, particularly reservoir water management. Gale & Saunders (2013) supported this statement as they found that the precipitation anomaly was higher in 1995 than in 2011, but the 1995 flood was not nearly as severe as the 2011 flood. However, considering the limited number of studies, the respective roles of reservoir operation and extreme weather on hydrological hazards

in the GCPR basin remain unclear.

The attention to reservoir operation and its effects on streamflow in the GCPR basin was drawn after the 2011 flood. Komori et al. (2012) provided an overview of reservoir water management in 2011. The spectrum analysis by Tebakari et al. (2012) indicated that the observed streamflow downstream of the reservoirs had a periodicity of seven days due to the irrigation purpose. Since daily streamflow data for this basin have been available only after the reservoir constructions, it is impossible to identify changes and trends of observed streamflow from natural to regulated conditions. Therefore, several studies took the approach of comparing observed streamflow to naturalized (without reservoir) streamflow obtained from hydrological models (Komori et al., 2013; Wichakul et al., 2013; Hanasaki et al., 2014; Mateo et al., 2014; Sayama et al., 2015). All these studies highlighted the effects of reservoir operation on downstream flows in the GCPR basin by analyzing hydrographs. However, they mainly focused on reservoir effects on high flows, particularly during the 2011 flood events, and excluded reservoir effects on low flows. Most studies investigated reservoir effects on hydrographs in the downstream floodplain, which may be influenced by the effects of intensive irrigation. In addition, reservoir effects on the water balance and daily flow regime in the GCPR basin have not been investigated.

Understanding the naturalized water balance and daily flow regime, and how they have been modified by reservoir operation is essential not only from a hydrological viewpoint, but also from socio-economic and environmental perspectives. The knowledge assists reservoir operators and water managers in planning and developing strategies to optimize both human consumption and ecosystem maintenance. It also supports adaptive management strategies to predict and deal with such probable changes for other existing or planned reservoirs in the same or a neighboring basin. Moreover, it helps to prepare for expected changes in streamflow after dam removals in the future. However, the main challenge in investigating the naturalized water balance and daily flow regime in many river basins, including the GCPR basin, is the lack of observed streamflow data prior to reservoir constructions.

One of the approaches to overcome the lack of observed streamflow data in reservoir operation studies is hydrological modelling. Many hydrological models can represent reservoir operation schemes and hydrological responses as part of rainfall-runoff processes (e.g., Zajac et al., 2017; Canuto et al., 2019; Gai et al., 2019). Distributed hydrological models are often used for reservoir system modelling because they allow the calculation of water interactions between a reservoir and its surrounding area in a spatially distributed manner. However, distributed models usually require an enormous amount of data, which is a drawback for data-scarce areas like in SEA. In addition, distributed models usually require area-specific and scenario-specific calibration, which poses a high risk of overparameterization and long computation times.

To tackle these issues, we used the ( $\sim 1$  km) distributed wflow\_sbm model with global

data and parameterization (Schellekens et al., 2019; Imhoff et al., 2020b). The model has been set up and evaluated for the upper region of the GCPR basin, as elaborated in Chapter 4. With a target storage-and-release-based reservoir operation module (ROM), the model was applied to simulate daily streamflow in the baseline operation scenario, when reservoir outflows were determined solely based on generalized operating rules without real-time control. In this chapter, we apply the model to simulate daily streamflow in the naturalized scenario. By comparing the simulation results in the naturalized and baseline operation scenarios to the observations, which represent real-time operation, we can comprehensively analyze effects of reservoir operation, in terms of generalized operating rules and real-time control, on daily streamflow.

The main aims of this chapter are to (i) quantify effects of reservoir operation on the water balance and daily flow regime and (ii) distinguish effects of reservoir operation and extreme weather on extreme flows in the upper GCPR basin. We analyzed the simulated and observed streamflows over a 25-year period of 1989–2013. By focusing on streamflow at the dam locations instead of floodplain gauges, we excluded probable influences of downstream irrigation and highlighted the effects of reservoir operation alone.

## 5.2 Methodology

To investigate effects of reservoir operation in the upper GCPR basin, this chapter applied the `wflow_sbm` model, which was set up with seamless distributed parameter maps and global data in Chapter 4. It contains two parts: (i) the streamflow simulations in the naturalized scenario and the baseline operation scenario and (ii) the analyses of reservoir effects on the water balance, daily flow regime and extreme flows. The study framework is illustrated in Figure 5.1.

### 5.2.1 Model simulations

For the upper GCPR basin, the `wflow_sbm` model was set up at the  $\sim 1$  km spatial resolution and the 3-hourly timescale (see Chapter 4). In this study, the simulation of the `wflow_sbm` model with the ROM for the Sirikit and Bhumibol reservoirs (see Section 4.2.2) is referred to as the baseline operation scenario, while the simulation without the reservoir existence is referred to as the naturalized scenario. To overcome data scarcity in the upper GCPR basin, which is a common challenge in SEA, most required geospatial and meteorological data for `wflow_sbm` were obtained from global databases (see Chapter 3; Sections 3.1.1 and 3.1.2). Only observed hydrological data for model evaluation were derived from local sources (see Section 3.1.3).

As for the `wflow_sbm` model parameterization, seamless distributed parameter maps were implemented instead of full calibration, which prevented overparameterization and reduced computation times (see Chapter 4; Section 4.2.1). The soil-related pa-

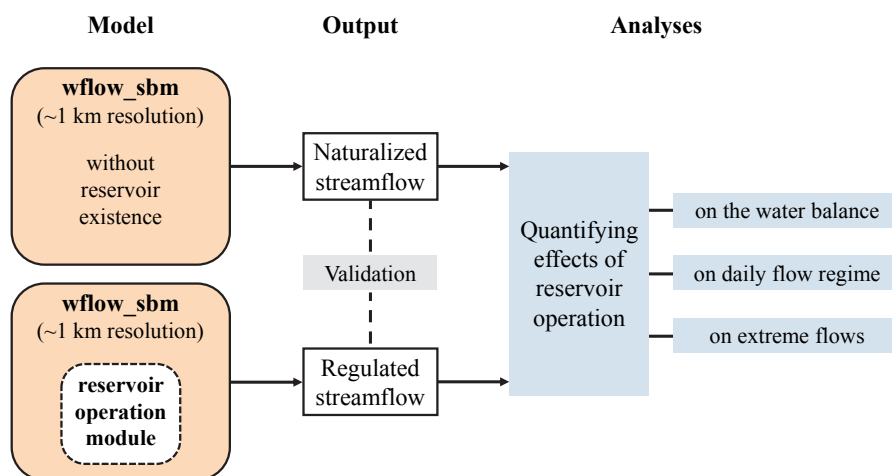


**Figure 5.1:** Study framework, including the streamflow simulations in the naturalized and baseline operation scenarios, and the analyses of reservoir effects on the water balance, daily flow regime and extreme flows.

parameter maps (e.g., hydraulic conductivity) in the previous study were calculated with two pedotransfer functions (PTFs): the Brakensiek function (Brakensiek et al., 1984) and Cosby (Cosby et al., 1984) function. In this study, the Brakensiek parameter maps were selected because the model performance was better (see Chapter 4; Section 4.3.1). They are not subject to change from the naturalized scenario to the regulated scenario. Only one soil-related parameter, *KsatHorFrac*, which is the factor for calculating horizontal saturated conductivity, and thus greatly affects the lateral subsurface flow, was manually calibrated.

The land cover-related parameter maps were obtained from global databases (e.g., leaf-area index) or by assigning parameter values from the literature review (e.g., Manning's roughness coefficient) to the GLOBCOVER land cover types. To create the land cover-related parameter maps for the naturalized scenarios, we first converted GLOBCOVER grid cells marked as reservoir water to naturalized land cover types using the nearest-neighbor-upscaled interpolation method. Then, we assigned parameter values for the new land cover types. We assumed that impacts of gradual land use changes, such as agricultural expansion and urbanization, were much smaller at the basin scale compared to impacts of reservoirs. Therefore, the uncertainty of naturalized land cover, and thus the uncertainty of naturalized parameters, was assumed negligible.

In the baseline operation scenario, the number of operational and physical parameters of the ROM were minimized to overcome data scarcity. The parameter values were determined based on the operating rule curves and databases provided by RID and EGAT and were applied without calibration, as elaborated in Chapter 4; Section 4.2.2.

In this study, we analyzed water balance and streamflow in two regulated catchments, the Sirikit catchment (2,020 km<sup>2</sup>) and the Bhumibol catchment (6,863 km<sup>2</sup>). Note that unlike in Chapter 4, in which the drainage areas of the two catchments were defined from the headwater, their drainage areas here were defined from the inflow point of each reservoir in the hydrological model to the dam location to be able to analyze their upstream inflows in the water balance. Two natural catchments located upstream of the reservoirs, the Nan\_natural and Yom\_natural, were also investigated. They were used to point out the resemblance of the upstream natural streamflow to the naturalized flow simulation of the Sirikit and Bhumibol catchments since the observations before the reservoir construction are not available for the model result validation. Locations and boundaries of the four catchments are shown in Figure 2.2. By focusing on the reservoir catchments instead of floodplain catchments downstream, we avoided the effects of intensive irrigation.

We carried out the 25-year simulation from 1989 to 2013 according to the naturalized scenario (wflow\_sbm without reservoir; sim\_nat) and baseline operation scenario (wflow\_sbm with the ROM; sim\_base). The daily simulation results were then analyzed in comparison to the daily observations, which reflect real-time operation. We used 2006 and 2013 as the representative years for wet and dry conditions. Although these two years were not the most extreme years recorded, they were carefully chosen to distinguish effects of reservoir operation and extreme weather on extreme flows.

By focusing on the selected catchments, we conduct the analyses in four parts. Firstly, we validated the simulated streamflows in the naturalized scenario. Secondly, we used the data from the naturalized scenario, baseline operation scenario and observations to quantify effects of reservoir operation on the long-term water balance components. Next, we assessed reservoir effects on key signatures of the daily flow regime. Lastly, we examined effects of reservoir operation and extreme weather on the frequency and recurrence of extreme flows.

### 5.2.2 Simulated streamflow evaluation

Since daily streamflow observations before the construction of the Sirikit and Bhumibol reservoirs are not available, it was impossible to directly evaluate the accuracy of the naturalized flow simulation for the Sirikit and Bhumibol catchments. Therefore, we validated their naturalized flows by visually comparing the resemblance of their daily hydrographs to those of the natural catchments upstream. Note that the model performance in the baseline operation scenario has been evaluated in Chapter 4.

### 5.2.3 Analyses of reservoir effects on the water balance

To evaluate effects of reservoir operation on the catchment water balance, the water balance of the upstream natural catchments was deliberated as baselines. We then compared the water balance components of the regulated catchments among the nat-

uralized scenario, baseline operation scenario and observations. Precipitation ( $P$ ) and upstream inflow ( $I$ ) are partitioned into actual evapotranspiration ( $AET$ ), streamflow ( $Q$ ) and storage change ( $\Delta S$ , which includes both subsurface storage and reservoir storage) during a given period. Since some water balance components (e.g., ground-water storage change and seepage) are difficult to estimate, they are often assumed to be in the residuals of the water balance equation (Kampf & Burges, 2010). Therefore, the water balance is expressed as

$$P + I - AET - Q = \Delta S, \quad (5.1)$$

where  $I$  and  $Q$  refer to streamflow in this context. Subsurface and overland flows across the catchment boundary were excluded as they were negligible in the simulations and not available from the observations. In the naturalized and baseline operation scenarios, the water balance components on the left-hand side of Equation (5.1) were extracted from the wflow\_sbm simulations. Then,  $\Delta S$  was calculated as the residual of the water balance. For the water balance based on observations, we calculated  $\Delta S$  with observed  $Q$  and made use of MSWEP V2  $P$ , and  $I$  and  $AET$  data from the simulations because the observed data were not available.

#### 5.2.4 Analyses of reservoir effects on the daily flow regime

To understand effects of reservoir operation on the daily flow regime, we focus on the Sirikit reservoir and analyzed three streamflow signatures: the Flow-Duration Curve (FDC), Base Flow Index (BFI) and Flashiness Index (FI). The signatures were compared among the naturalized scenario, baseline operation scenario and observations. Considering the missing data in the observed streamflow record, we quantified the signatures for each year available and for the long periods of 1989–1997 and 2003–2013.

##### *Flow-Duration Curve*

The daily flow regime can be summarized in the comprehensive form of the FDC, which is the empirical cumulative frequency of daily streamflow as a function of the percentage of time that the streamflow is exceeded. The slope of the FDC represents the streamflow variability, including both high and low flows. A steeper slope refers to a higher flow variability. To quantify reservoir effects on the daily FDC, we calculated and compared the slopes of the FDCs, median flows ( $Q_{50}$ ), high flows and low flows among the simulations and observations. We defined high flows as the flows that are exceeded 10% of the time ( $Q_{10}$ ), and low flows as being exceeded 90% of the time ( $Q_{90}$ ). As generally, the FDC between the 33<sup>rd</sup> and 66<sup>th</sup> flow percentiles is nearly linear on a semi-log scale (Sawicz et al., 2011), the FDC slope ( $Slope_{FDC}$ ) is defined as

$$Slope_{FDC} = \frac{\ln(Q_{33}) - \ln(Q_{66})}{(0.66 - 0.33)}, \quad (5.2)$$

where  $Q_{33}$  and  $Q_{66}$  are the daily streamflow values at the 33<sup>rd</sup> and 66<sup>th</sup> percentile.

### Base Flow Index

Baseflow is part of streamflow that comes from persistent, delayed sources and is thus highly correlated to the water storage in a catchment (Hisdal et al., 2004). In natural catchments, baseflow mainly comes from groundwater, whereas in catchments with highly regulated dammed reservoirs, baseflow mainly comes from reservoir water. In this study, we separated baseflow from the daily streamflow time series using the separation procedure of Gustard et al. (1992). We calculated the minima of 5-day non-overlapping consecutive periods and identified turning points of the minima sequence. A minimum became a turning point if 0.9 times its value was less than or equal to the neighboring minimum. Connecting the turning points formed the baseflow separation line in the hydrograph. Daily baseflow values were then assigned with linear interpolation between the turning points. The baseflow was set equal to the total streamflow on any day that the estimated baseflow exceeded the total streamflow.

The Base Flow Index, BFI [-], is the ratio of baseflow to total flow in a given period,

$$BFI = \frac{\sum_{i=1}^n Q_{base}}{\sum_{i=1}^n Q_{total}}, \quad (5.3)$$

where  $Q_{base}$  refers to the daily baseflow,  $Q_{total}$  refers to the daily streamflow,  $i$  is the given time step (day) and  $n$  is the number of days in the given period. BFI values range between 0 and 1. A higher index value means a higher contribution of baseflow to total streamflow. To quantify reservoir effects on the daily baseflow, we calculated and compared the BFI values among the simulated and observed streamflow time series.

### Flashiness Index

While the  $Slope_{FDC}$  indicates the overall variability of daily streamflow regardless of the chronological order, flashiness reflects the absolute day-to-day fluctuations in the streamflow magnitude. Flashy streams have rapid rates of daily change, while stable streams have slow rates of daily change (Poff et al., 1997). We used the Richards-Baker Flashiness Index (FI [-]; Baker et al., 2004), which is quantified by the ratio of daily streamflow fluctuations relative to the total streamflow in a given period,

$$FI = \frac{\sum_{i=1}^n |Q_i - Q_{i-1}|}{\sum_{i=1}^n Q_i}, \quad (5.4)$$

where  $Q$  is daily streamflow,  $i$  is the given time step (day) and  $n$  is the number of days in the given period. FI values range between 0 and 2, of which zero represents an absolutely constant flow; higher index values mean larger fluctuations of daily streamflow. Streamflow time series with a steep  $Slope_{FDC}$  tend to give a high FI value. However, streamflow time series with similar  $Slope_{FDC}$  values can result in very different FI values because FI excludes the seasonal and inter-annual variability within the given period. Therefore, to quantify reservoir effects on the daily flashiness, we calculated and compared the FI values among the simulated and observed streamflow time series.

### 5.2.5 Analyses of reservoir effects and extreme weather effects on extreme flows

To understand effects of reservoir operation on extreme flows, we focus on the Sirikit reservoir and assessed the frequency and recurrence of extreme flows in relation to magnitude and timing among the simulations and observations. In this study, extreme flows refer to annual maximum daily flows (*AMAX*) and annual minimum daily flows (*AMIN*). For the upper GCPR basin, very high flows in the dry season are usually employed for irrigation and do not cause flooding. Likewise, very low flows in the rainy season are meant to prevent downstream inundation and do not lead to drought. Therefore, we computed *AMAX* in the period of May–October (rainy season) and *AMIN* in the rest of the year. Although Durrans (1988) suggested that total probability methods are suitable for estimating flood frequency in regulated catchments, the capability of the Gumbel extreme value distribution to represent flood frequency in reservoir-dominated catchments has been demonstrated (e.g., Batalla et al., 2004; Lee et al., 2017). In addition, the Gumbel distribution was suggested as one of the best-fit functions to analyze yearly low flows (Matalas, 1963; Langat et al., 2019). Hence, it was selected for the frequency analysis of *AMAX* and *AMIN* based on the 25-year period of daily streamflow data.

To distinguish effects of extreme weather on daily extreme flows, we assessed the relationship between the *AMAX* or *AMIN* and the associated weather. We used the sum of precipitation and upstream inflow minus actual evapotranspiration ( $P + I - AET$ ), here called effective inflow, on the day that the *AMAX* or *AMIN* occurred and over the 30 days preceding the extreme flow event to represent the weather condition.

## 5.3 Results

### 5.3.1 Naturalized flow

The visual comparison of the simulated daily streamflow in the naturalized scenario (sim.nat),  $Q_{sim.nat}$ , for the Sirikit and Bhumibol catchments to the daily streamflow observations (obs),  $Q_{obs}$ , for the upstream natural catchments implies satisfactory results produced by the wflow\_sbm model. The daily hydrographs of  $Q_{sim.nat}$  for both regulated



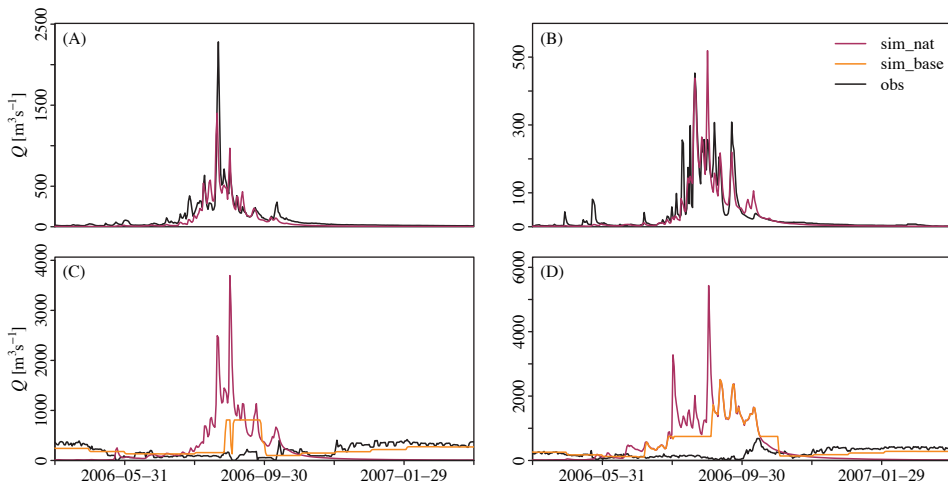


**Figure 5.2:** Simulated and observed daily streamflows for the Nan\_natural (A), Yom\_natural (B), Sirikit (C) and Bhumibol (D) catchments in the wet year (2006). The streamflow in the naturalized scenario (sim\_nat) is shown in red lines, the baseline operation scenario (sim\_base) in orange lines and the observations (obs) in black lines. Since the hydrographs in the dry year (2013) show similar flow patterns, they are not included here.

catchments, shown as red lines in Figures 5.2(C) and (D), present trends comparable to the hydrographs for the upstream natural catchments in Figures 5.2(A) and (B). The strong seasonal variation, with very low flows in the dry season as well as steep rising limbs and high flood peaks in the rainy season, suggests that the model can reconstruct the naturalized flows regardless of the uncertainty in the naturalized land cover setting.

### 5.3.2 Effects of reservoir operation on the water balance

The simulated water balances of the Nan\_natural and Yom\_natural catchments are similar to each other in terms of water budget distribution based on the yearly average data (Table 5.1). Note that these natural catchments are located at the headwaters, and thus do not have upstream inflows (see their locations in Figure 2.2). The annual  $AET/PET$  ratios for the two catchments ranged between 0.68 and 0.70. Approximately two-thirds of the annual  $P$  evaporated and one-third flowed downstream. The annual  $Q_{sim\_nat}$  tends to underestimate the annual  $Q_{obs}$ , especially for the Nan\_natural catchment. Consequently, the disparity between the simulated and observed storage changes ( $\Delta S_{sim\_nat}$  and  $\Delta S_{obs}$ ) is also considerable. However, it should be noted that the  $\Delta S_{obs}$  values were calculated using the MSWEP V2  $P$  data and the simulated  $AET$  data from the naturalized scenario since the observed  $AET$  data are not available. These data sources could also be a source of bias, affecting the simulated storage.

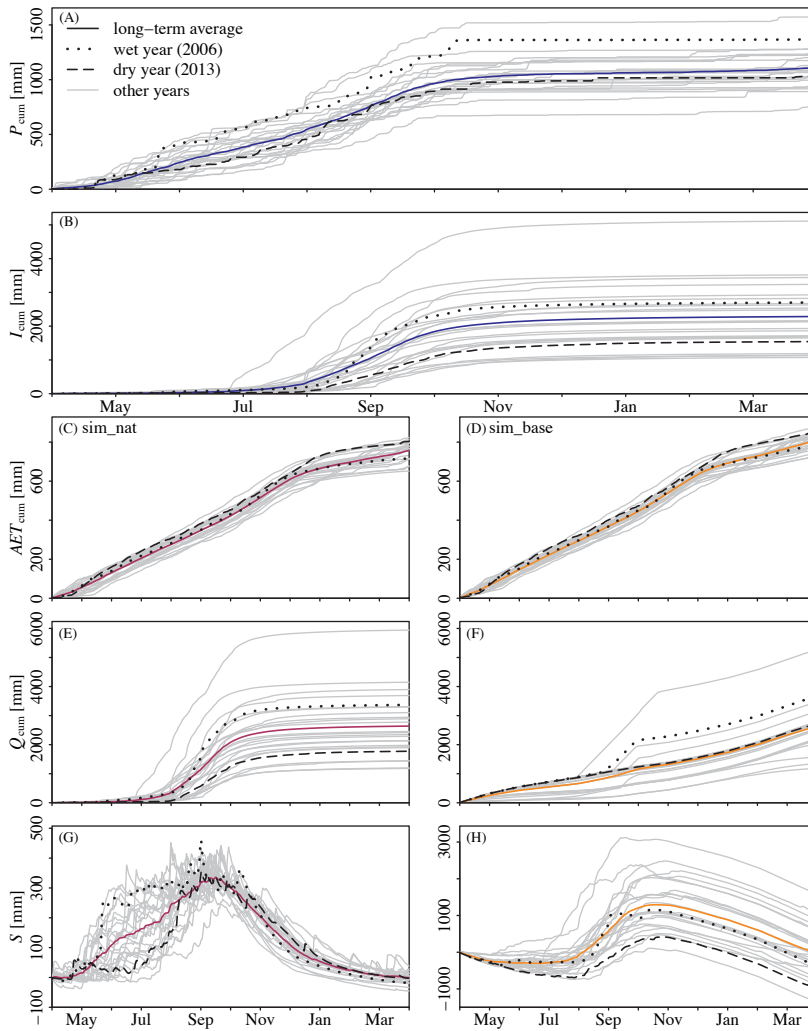


**Figure 5.3:** Cumulative daily water balance components for the Sirikit catchment in the naturalized and baseline operation scenarios. The components comprise daily precipitation ( $P_{\text{cum}}$ ; panel (A)), inflow ( $I_{\text{cum}}$ ; panel (B)), actual evapotranspiration ( $AET_{\text{cum}}$ ; panel (C) and (D)), streamflow ( $Q_{\text{cum}}$ ; panel (E) and (F)) and storage with respect to the start of the year ( $S$ ; panel (G) and (H)). Yearly data from 1989 to 2013 are shown in grey lines. The long-term averages of  $P_{\text{cum}}$  and  $I_{\text{cum}}$  remain the same between the naturalized and baseline operation scenarios and are shown in blue lines. The long-term average values of the other three components are shown in red lines for the naturalized scenario (sim\_nat; left panels) and orange lines for the baseline operation scenario (sim\_base; right panels). The dotted black lines represent the selected wet year (2006), while the dashed black lines represent the selected dry (2013) year.

**Table 5.1:** Yearly averages of water balance components [ $\text{mm year}^{-1}$ ] obtained from the naturalized scenario (sim\_nat), baseline operation scenario (sim\_base) and observations (obs) for the study catchments and individual reservoirs. The components comprise MSWEP V2 precipitation ( $P$ ), earth2Observe potential evapotranspiration ( $PET$ ), simulated actual evapotranspiration ( $AET$ ), simulated inflow ( $I$ ), simulated and observed streamflows ( $Q$ ), and simulated and observed changes in water storage ( $\Delta S$ ). For the observations, the  $\Delta S$  values of the four catchments were calculated based on the MSWEP V2  $P$  and the simulated  $AET$  as residual of the water balance. For the water balance at the reservoir scale (the last two rows),  $\Delta S$  represents the reservoir storage change. The simulated  $\Delta S$  data of the reservoirs were obtained from the ROM and the observed  $\Delta S$  data were available from RID observations. Note that the  $P$  and  $PET$  values in this table were calculated in the period of available observed  $Q$  for each catchment.

Catchment/reservoir	$P$	$I$	$PET$	sim_nat			sim_base			obs			Year
				$AET$	$Q$	$\Delta S$	$AET$	$Q$	$\Delta S$	$Q$	$\Delta S$		
Nan_natural	1261	0	1031	725	540	-5				766	-230		1994-2013
Yom_natural	1114	0	1082	741	364	10				386	-13		1996-2013
Sirikit catchment	1114	2279	1190	750	2645	-2	810	2685	-102	2814	-231		1989-1997, 2003-2013
Bhumibol catchment	942	835	1093	654	1123	-1	669	1102	6	780	328		1989-2013
Sirikit reservoir	1202	16703	1205				1203	17193	-488	18019	-610		1989-1997, 2003-2013
Bhumibol reservoir	889	25964	1126				1122	25503	229	18050	-337		1989-2013

The simulated water balance in the baseline operation scenario (sim\_base) of the Sirikit catchment is different from its naturalized scenario (Table 5.1). Note that the Sirikit catchment is located midstream, and thus receives inflows from upstream (see its location in Figure 2.2). The annual  $AET/PET$  ratio increased from 0.63 in the naturalized scenario to 0.68 in the baseline operation scenario, with an 8% increase in evaporation loss. Concurrently, the annual streamflow from the baseline operation scenario ( $Q_{sim\_base}$ ) increased with respect to the annual  $Q_{sim\_nat}$ , leading to a greater  $\Delta S_{sim\_base}$  than  $\Delta S_{sim\_nat}$ . Table 5.1 (the last two rows) also shows the water balance components in the baseline operation scenario at the reservoir scale compared to the measurements of reservoir outflow and storage change. For the Sirikit reservoir, the annual  $Q_{sim\_base}$  tends to be smaller than the annual  $Q_{obs}$ . The difference between the  $\Delta S_{sim\_base}$  and  $\Delta S_{obs}$  is also large since they were both computed by closing the water balance.

The simulated water balance in the baseline operation scenario of the Bhumibol catchment, on the other hand, is similar to its water balance in the naturalized scenario (Table 5.1). This catchment is also located midstream and receives inflows from upstream (see its location in Figure 2.2). Due to the prompt surcharge releases by the ROM, the  $Q_{sim\_base}$  behaved like the  $Q_{sim\_nat}$  in very wet periods, as also evident in Figure 5.2(D). As a result,  $AET/PET$  ratios in the naturalized scenario (0.60) and baseline operation scenario (0.61) were almost the same, with only a 2% increase in evaporation loss by reservoir operation. The annual  $Q_{sim\_base}$  for the Bhumibol reservoir was much higher than its annual  $Q_{obs}$ , leading to the large gap between the  $\Delta S_{sim\_base}$  and  $\Delta S_{obs}$ .

Focusing on the Sirikit catchment, the dissimilarity in magnitude and timing of its cumulative  $Q$  time series between the naturalized and baseline operation scenarios further clarifies the reservoir effects on the catchment water balance (Figure 5.3). In the naturalized scenario, the long-term mean cumulative  $Q_{sim\_nat}$  (red line in Figure 5.3(E)) increased dramatically from July to October, consistently with the long-term mean cumulative  $P$  and  $I$  (blue lines in Figure 5.3(A) and (B)). The cumulative  $Q_{sim\_nat}$  was significantly higher in the wet year (2006; dotted line) than in the dry year (2013; dashed line). On the contrary, the long-term mean cumulative  $Q_{sim\_base}$  (orange line in Figure 5.3(F)) increased more gradually over the period of one year. Exceptions are found for 2006 and other wet years, when the cumulative  $Q_{sim\_base}$  surged in the rainy season due to the ROM surcharge releases, as also evident in Figure 5.2(C). Notably, the cumulative  $Q_{sim\_base}$  in 2013 is comparable to the long-term average, despite the lower  $P$  and  $I$ .

Figure 5.3 also illustrates the different patterns of the Sirikit catchment storage in the naturalized and baseline operation scenarios, here called  $S_{sim\_nat}$  and  $S_{sim\_base}$  (because the cumulative value of the catchment storage changes is a catchment storage with respect to the initial condition). The long-term mean  $S_{sim\_nat}$  (red line in Figure 5.3(G)) increased during the first half of the year, peaking in mid-September (330 mm) before dropping to around zero by the end of the year. In 2006, the  $S_{sim\_nat}$  rose strikingly since the beginning of the rainy season in response to stormwater. In 2013, on the other

hand, it remained small until July as monsoons arrived later than usual. In contrast, the long-term mean  $S_{\text{sim\_base}}$  (orange line in Figure 5.3(H)) slightly decreased from the start of the year and remained negative until August. After that, it rose to a peak in mid-October (1,285 mm). In the latter half of the year, the  $S_{\text{sim\_base}}$  volume steadily declined. A smaller negative  $S_{\text{sim\_base}}$  value was found at the end of 2013 compared to at the end of 2006.

### 5.3.3 Effects of reservoir operation on the daily flow regime

The daily  $Q_{\text{sim\_nat}}$  time series of the Sirikit catchment deviated significantly from the  $Q_{\text{sim\_base}}$  and  $Q_{\text{obs}}$  time series, as visible in Figure 5.2(C). The  $Q_{\text{sim\_nat}}$  time series presented a strong seasonal variation, with very low flows in the dry season and steep rising limbs and high peak flows in the rainy season. Meanwhile, the  $Q_{\text{sim\_base}}$  and  $Q_{\text{obs}}$  time series were smoother, with higher flows in the dry season and diminished peak flows in the rainy season. The  $Q_{\text{sim\_base}}$  time series, however, had a short period with high peak flows from the reservoir surcharge releases by the ROM. The poor fits between the  $Q_{\text{sim\_nat}}$  and  $Q_{\text{obs}}$  for the Sirikit catchment reflect the effect of reservoir operation on daily streamflow. In addition, the difference between the  $Q_{\text{sim\_base}}$  and  $Q_{\text{obs}}$  indicates the effect of real-time operation with decision-making on top of the generalized operating rules.

The daily FDCs and flow signatures of the Sirikit catchment are different among the naturalized scenario ( $\text{FDC}_{\text{sim\_nat}}$ ), baseline operation scenario ( $\text{FDC}_{\text{sim\_base}}$ ) and observations ( $\text{FDC}_{\text{obs}}$ ), as demonstrated in Figure 5.4 and Table 5.2. Overall, the  $\text{FDC}_{\text{sim\_nat}}$  is steeper than the  $\text{FDC}_{\text{sim\_base}}$  and  $\text{FDC}_{\text{obs}}$ , as indicated by the greater  $\text{Slope}_{\text{FDC}}$  values. The flattening of the  $\text{FDC}_{\text{sim\_base}}$  and  $\text{FDC}_{\text{obs}}$  is the result of increasing mean flow and low flow, and reducing high flow. The  $\text{FDC}_{\text{sim\_base}}$  shows less variability, with lower  $\text{Slope}_{\text{FDC}}$ , compared to the  $\text{FDC}_{\text{obs}}$  due to lower high flows and higher low flows. In addition, the  $\text{FDC}_{\text{sim\_base}}$  differed more from the  $\text{FDC}_{\text{obs}}$  in the dry year (2013) than in the wet year (2006) as the  $Q_{\text{sim\_base}}$  maintained low flows at a higher level. Notably, the  $Q_{\text{sim\_nat}}$  and  $Q_{\text{sim\_base}}$  were perennial throughout the study period, whereas the  $Q_{\text{obs}}$  ceased for 4% of the time during the years 1989–1997. The flow signatures also differ between the years 1989–1997 and the years 2003–2013, with increased median, high and low flows in the latter period in all scenarios.

In accordance with the steep slope of the  $\text{FDC}_{\text{sim\_nat}}$ , the  $Q_{\text{sim\_nat}}$  for the Sirikit catchment received only a small contribution from baseflow (low BFI) and was very flashy (high FI), as illustrated in Table 5.2 and Figure 5.5. The  $\text{BFI}_{\text{sim\_nat}} = 0.62$  and  $\text{FI}_{\text{sim\_nat}} = 0.22$  in the years 1989–1997 express that the  $Q_{\text{sim\_nat}}$  had a baseflow contribution of 62% and an average day-to-day fluctuation of 22%. Similar index values are found for the years 2003–2013. The  $Q_{\text{sim\_base}}$ , on the contrary, presented significantly higher BFI and lower FI values, in line with the flatter FDC curves in both the 1989–1997 and 2003–2013 periods. Note that in the baseline operation scenario and observations, the BFI is no longer representing slowly emptying aquifers but emptying the reservoirs.

**Table 5.2:** Signatures of daily streamflow from the simulations and observations for the Sirikit catchment. High flows are defined as the flows that are exceeded 10% of the time, and low flows as being exceeded 90% of the time.

Signature	Years 1989–1997			Years 2003–2013			Year 2006 (wet)			Year 2013 (dry)		
	sim.nat	sim.base	obs	sim.nat	sim.base	obs	sim.nat	sim.base	obs	sim.nat	sim.base	obs
Median flow [mm day <sup>-1</sup> ]	1.17	5.82	5.86	1.68	7.44	8.82	2.00	7.65	8.23	0.94	7.5	5.00
High flow [mm day <sup>-1</sup> ]	18.46	11.20	13.38	29.88	11.74	15.40	29.97	13.29	15.43	17.73	10.82	9.91
Low flow [mm day <sup>-1</sup> ]	0.35	1.81	0.89	0.40	4.27	2.98	0.43	5.59	2.51	0.35	5.15	1.51
<i>Slope<sub>FDC</sub></i> [-]	5.22	1.46	2.43	5.46	1.18	2.02	5.64	1.30	3.17	5.64	1.09	1.73
BFI [-]	0.62	0.95	0.40	0.64	0.95	0.81	0.73	0.87	0.73	0.68	0.98	0.89
FI [-]	0.22	0.02	0.28	0.18	0.02	0.08	0.20	0.04	0.10	0.18	0.01	0.04

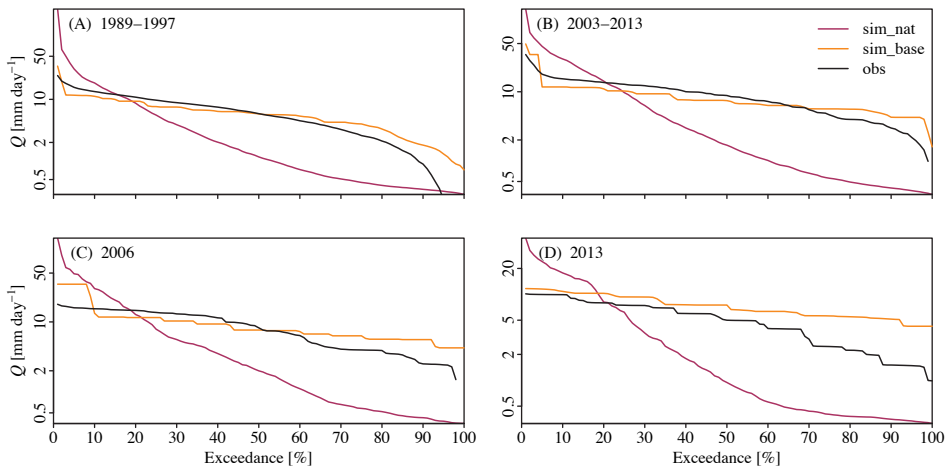


**Figure 5.4:** Simulated and observed daily flow-duration curves of the Sirikit catchment during 1989–1997 (A), 2003–2013 (B), the wet year 2006 (C) and the dry year 2013 (D). The streamflows are shown on a logarithmic scale. The streamflow in the naturalized scenario (sim\_nat) is shown in red lines, the baseline operation scenario (sim\_base) in orange lines and observations (obs) in black lines.

Although the  $FDC_{sim\_base}$  and  $FDC_{obs}$  show relatively similar shapes (Figure 5.4), the  $Q_{obs}$  was more flashy and had a lower baseflow contribution than the  $Q_{sim\_base}$  (Figure 5.5). Especially in the years 1989–1997, the  $Q_{obs}$  was even more flashy, with a lower baseflow contribution than the  $Q_{sim\_nat}$  (Table 5.2). The  $BFI_{obs}$  increased and the  $FI_{obs}$  reduced in the years 2003–2013. All scenarios indicate that the streamflow was slightly more flashy in the wet years than in the dry years.

#### 5.3.4 Effects of reservoir operation on extreme flows

The annual maximum daily flows ( $AMAX$ ) for the Sirikit catchment were significantly higher in the naturalized scenario ( $AMAX_{sim\_nat}$ ) than in the baseline operation scenario ( $AMAX_{sim\_base}$ ) and observations ( $AMAX_{obs}$ ), as illustrated in Figure 5.6(A). The  $AMAX_{sim\_nat}$  showed notable inter-annual variability, whereas the  $AMAX_{sim\_base}$  and  $AMAX_{obs}$  were more stable throughout the 25-year period. The long-term mean of  $AMAX$  decreased from the naturalized scenario ( $92 \text{ mm day}^{-1}$ ) by 84% to the baseline operation scenario and the observations ( $15 \text{ mm day}^{-1}$ ). The highest  $AMAX$  volume in the naturalized scenario ( $292 \text{ mm day}^{-1}$  in 1989) was significantly greater than in the baseline operation scenario ( $49 \text{ mm day}^{-1}$  in 2011) and the observations ( $35 \text{ mm day}^{-1}$  in 2011). The differences in  $AMAX$  among the two simulation scenarios and the observations were larger in the wet years than in the dry years.

The annual daily minimum flows ( $AMIN$ ) for the Sirikit catchment were significantly lower in the naturalized scenario ( $AMIN_{sim\_nat}$ ) than in the baseline operation sce-

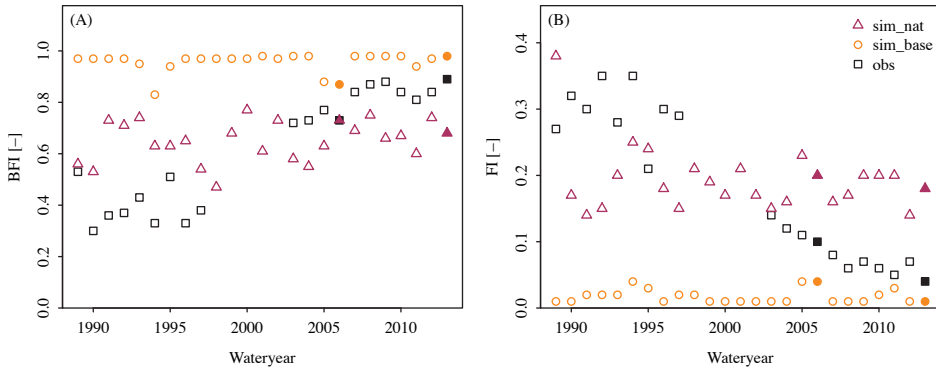


**Figure 5.5:** Yearly Base Flow Index (A) and Flashiness Index (B) of the simulated and observed daily streamflows for the Sirikit catchment. The index values in the naturalized scenario (sim\_nat) are shown in red triangles, the baseline operation scenario (sim\_base) in orange circles and the observations (obs) in black squares. The filled symbols represent the index values in the wet year (2006) and dry year (2013).

nario ( $AMIN_{sim\_base}$ ), as demonstrated in Figure 5.6(B). The long-term mean of  $AMIN$  increased from the naturalized scenario ( $0.3 \text{ mm day}^{-1}$ ) by 1,567% to the baseline operation scenario ( $5 \text{ mm day}^{-1}$ ) and by 507% to the observations ( $2 \text{ mm day}^{-1}$ ). The  $AMIN_{sim\_nat}$  remained less than  $1 \text{ mm day}^{-1}$ , but the river was not ephemeral. The  $AMIN_{sim\_base}$  remained lower than  $7 \text{ mm day}^{-1}$ . Interestingly, the observations ( $AMIN_{obs}$ ) showed more variability, with an evident increasing trend from the years 1989–1997 (less than  $1 \text{ mm day}^{-1}$ ) to the years 2003–2013 ( $1\text{--}5 \text{ mm day}^{-1}$ ), in line with the BFI in Figure 5.5(A). Note that the  $AMIN_{obs}$  reached zero six times during the 1989–1997 period.

The return periods of  $AMAX$  for the Sirikit catchment indicate that annual flood peaks occurred most frequently and with the highest magnitudes in the naturalized scenario (Figure 5.7(A)). The 5-year-return-period flood was significantly reduced from the naturalized scenario ( $135 \text{ mm day}^{-1}$ ) by approximately 84% to the baseline operation scenario ( $22 \text{ mm day}^{-1}$ ) and observations ( $20 \text{ mm day}^{-1}$ ). The  $AMAX_{sim\_nat}$  with the up-to-5-year return periods tend to take place in August and September (Figure 5.7(B)). On the other hand, the  $AMAX_{sim\_base}$  and  $AMAX_{obs}$  with the up-to-5-year return periods tend to take place in May, which is the transition period from the dry season to the rainy season, and thus may not cause as severe flooding as those occurred in August–October.

The return periods of  $AMIN$  for the Sirikit catchment indicate that annual minimum flows occurred most frequently and severely in the naturalized scenario (Figure 5.7(C)). The 5-year-return-period minimum flow increased from the naturalized scenario ( $0.3 \text{ mm day}^{-1}$ ) by 1,233% to the baseline operation scenario ( $4 \text{ mm day}^{-1}$ ) and



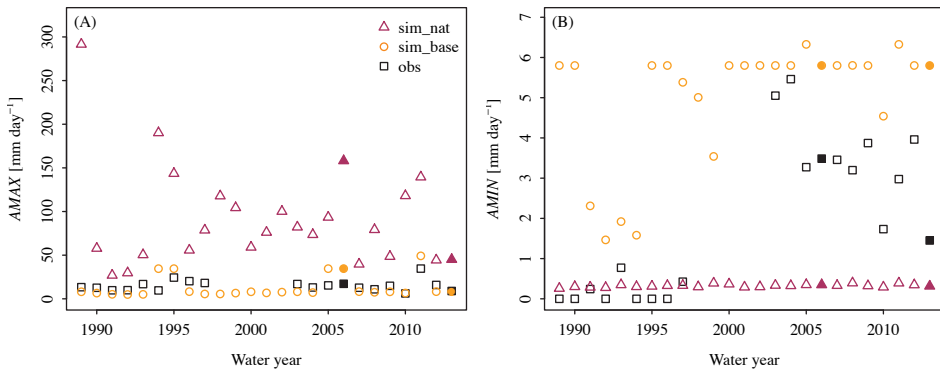


**Figure 5.6:** Annual maximum daily flows (A) and annual minimum daily flows (B) from the simulations and observations for the Sirikit catchment. The values in the naturalized scenario ( $sim\_nat$ ) are shown in red triangles, the baseline operation scenario ( $sim\_base$ ) in orange circles and the observations ( $obs$ ) in black squares. The filled symbols represent the values in the wet year (2006) and dry year (2013). Note that the annual maximum flows were computed in the rainy season, while the annual minimum flows were computed in the dry season to exclude the flows that did not cause flood or drought issues.

by 100% to the observations ( $0.6 \text{ mm day}^{-1}$ ). Figure 5.7(D) shows that the  $AMIN_{sim\_nat}$  with the up-to-5-year return periods tend to occur at the end of the dry season (March–April). The  $AMIN_{sim\_base}$  and  $AMIN_{obs}$  with the up-to-5-year return periods, on the other hand, tend to occur at the beginning of the dry season (November).

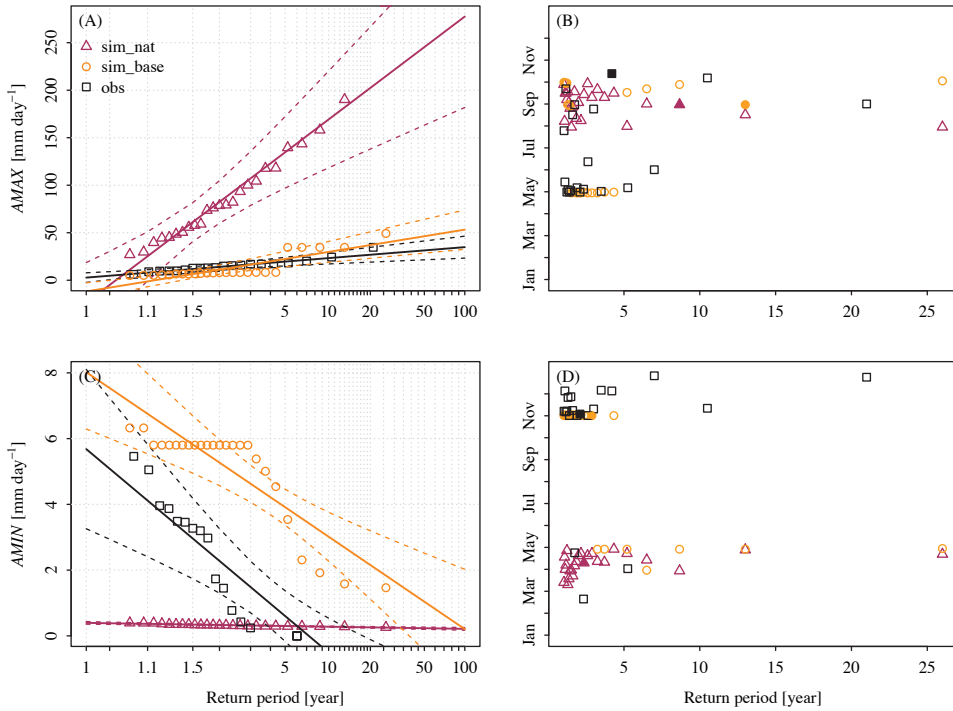
### 5.3.5 Effects of extreme weather on extreme flows

Figure 5.8 illustrates the relationship between extreme flows, including  $AMAX$  and  $AMIN$ , and cumulative amounts of effective inflow ( $P+I-AET$ ) in one day and 30 days prior to the extreme flow incidents. The cumulative effective inflows had an influence on the  $AMAX$ , especially in the naturalized scenario (Figure 5.8(A) and (C)). The  $AMAX_{sim\_nat}$  has the highest correlation to the one-day effective inflow ( $R^2 = 0.92$ ), the  $AMAX_{sim\_base}$  to the 30-day effective inflow ( $R^2 = 0.45$ ), and the  $AMAX_{obs}$  to the 30-day effective inflow ( $R^2 = 0.21$ ). On the other hand, there is no clear relation between  $AMIN$  and effective inflow in any scenario (Figure 5.8(B) and (D)).

## 5.4 Discussion

### 5.4.1 Effects of reservoir operation on the water balance

The water balance of the Sirikit and Bhumibol catchments changed significantly from the naturalized scenario to the baseline operation scenario in terms of magnitude and timing. The higher annual  $AET$  in the baseline operation scenario resulted from the



**Figure 5.7:** Return periods of the simulated and observed extreme flows, including the annual maximum daily flows (AMAX; panels A,B) and annual minimum daily flows (AMIN; panels C,D) for the Sirikit catchment based on the Gumbel distribution. Figures A and C show the relation between the magnitude and frequency of the extreme flows. The symbols represent actual values of extreme flows, solid lines represent the probability distribution and dashed lines represent the 95% confidence interval. The values in the naturalized scenario (*sim\_nat*) are shown in red color, the baseline operation scenario (*sim\_base*) in orange and the observations (*obs*) in black. Figures B and D show the relation between the frequency and timing of the extreme flows. The filled symbols represent the values in the wet year (2006) and dry year (2013). Note that the annual maximum flows were computed from the rainy season, while the annual minimum flows were computed from the dry season in order to exclude the flows that did not cause flood or drought issues.

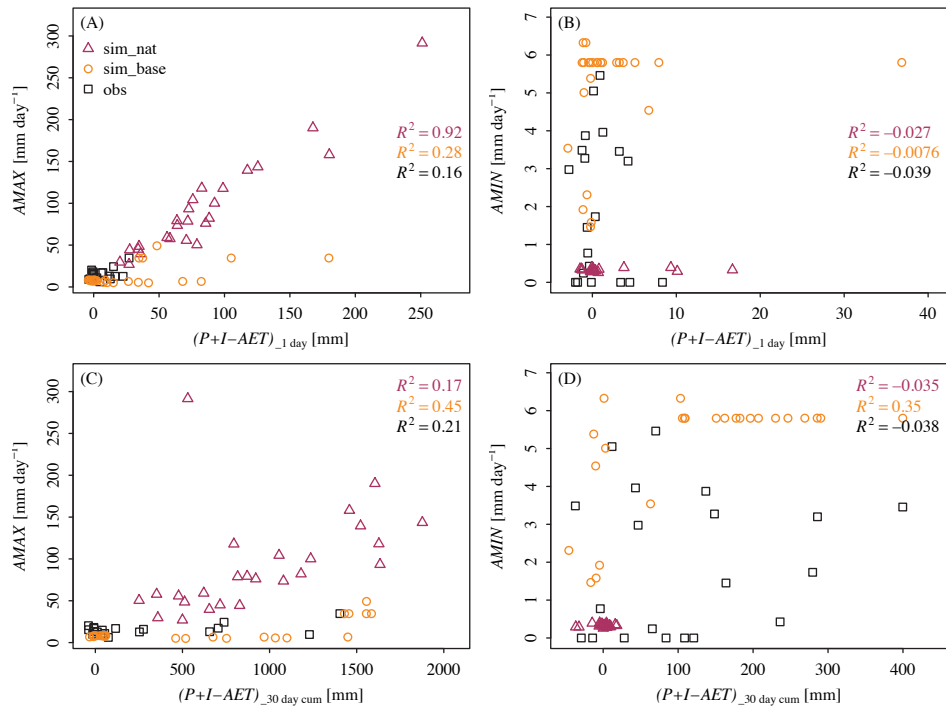


**Figure 5.8:** Relationship between cumulative effective inflows and daily extreme flows, including annual maximum daily flows (left panels) and annual minimum daily flows (right panels) from the simulations and observations for the Sirikit catchment. The values in the naturalized scenario (sim\_nat) are shown in red triangles, the baseline operation scenario (sim\_base) in orange circles and the observations (obs) in black squares. The effective inflows (x-axis) is the sum of precipitation ( $P$ ) and inflow ( $I$ ) minus the actual evapotranspiration ( $AET$ ) on the day that an extreme flow occurred (first row) and the cumulative amount 30 days prior to the extreme flow date (second row).

direct evaporation from the reservoir water surface and streamflow (Table 5.1). The corresponding trends between  $P$  and  $I$ , and the rapid  $Q_{\text{sim,nat}}$  (visible as a sharp increase of its cumulative) indicate the natural rainfall-runoff process with a quick catchment response (Figure 5.3). On the other hand, the steady  $Q_{\text{sim,base}}$  (visible as a gradual increase of its cumulative) and the large annual  $\Delta S_{\text{sim,base}}$  values imply that the reservoir operation markedly altered the natural rainfall-runoff process with a longer residence time of water. The effects of the reservoir operation on the water balance were apparent in dry years as the reservoirs tried to fulfill the target downstream water demand with stored water from the previous rainy season, although this led to very low reservoir storage at the end of the year.

It should be kept in mind that the aforementioned effects refer to the baseline reservoir operation with the generalized operating rules (by the ROM), which are different from the real-time reservoir operation (observations). Since only the observed reservoir storage and outflow are available, we could not thoroughly analyze the effects of the real-time operation on the water balance. However, it is obvious that the real-time operation is unique and much more flexible for each reservoir due to the circumstance-specific judgments by reservoir operators, affecting the water balance to another extent. This was reflected in the higher annual streamflow for the Sirikit catchment but lower annual streamflow for the Bhumibol catchment compared to their naturalized flows (Table 5.1).

#### 5.4.2 Effects of reservoir operation on the daily flow regime

Major alterations by the reservoir operation were the flatter FDC and more smooth flow regime due to increasing daily median flows ( $Q_{50}$ ) and daily low flows ( $Q_{90}$ ), and decreasing daily high flows ( $Q_{10}$ ) compared to the naturalized flow (Figure 5.4 and Table 5.2). The reservoir operation completely inverted the seasonality of the naturalized flow regime, with significantly higher daily streamflow in the dry season and lower daily streamflow in the rainy season (Figures 5.2(C) and (D)). Hanasaki et al. (2006) and Yassin et al. (2019) also reported similar results for the Sirikit and Bhumibol reservoirs. The high reservoir outflows in the dry season were mainly to compensate for environmental flows, including downstream irrigation supply and hydropower generation. At the same time, the draw-down of reservoir storage provided space to restore water in the next rainy season. Meanwhile, the low reservoir outflows in the rainy season were to prevent overflows in the downstream floodplains. Changes in the daily flow regime were more complicated with the real-time operation than with the baseline operation. A good example is when the real-time operation slowly released the surcharge water or paused the daily release to prevent or moderate flooding downstream (Figures 5.2(C) and (D)).

Since water in the upper GCPR basin comes from seasonal precipitation, the naturalized flow was very variable (low BFI and high FI; Figures 5.5), causing the basin to be at risk of both flash floods and intensive dry periods. On the other hand, the regu-

lated flow with the baseline operation had a high and stable baseflow contribution from the reservoir storage (high BFI and low FI). This indicates that the daily streamflow was not flashy and was enabled to sustain the minimum water demands in the period of low or absent precipitation. The real-time operation, however, failed to overcome these problems during 1989–1997, but significantly improved with more daily baseflow contribution and less daily flashiness in 2003–2013. More experiences of reservoir operators gained over time may have been relevant for this improvement.

#### 5.4.3 Effects of reservoir operation on extreme flows

Both baseline and real-time reservoir operations substantially reduced the magnitude and frequency of the annual flood peaks (annual maximum daily flows), although the extent of the effects varied between years. Most of the naturalized flood peaks in the rainy season were absorbed by the reservoirs, as visible in Figures 5.2(C) and 2(D). The magnitudes of annual flood peaks (Figure 5.6(A)) and the 5-year-return-period flood (Figure 5.7(A)) were significantly diminished by both baseline and real-time operations, especially in wet years. This included the 2011 catastrophic flooding that affected the entire GCPR basin. Interestingly, the timing of the annual flood peak incidents shifted and became more variable with the real-time operation (Figure 5.7(B)). It should be noted that the annual flood peaks that occurred in May are unlikely to cause flooding as it is the beginning of the rainy season after a prolonged dry period. The naturalized annual flood peaks and the annual flood peaks with the baseline operation usually occurred in August and September. Meanwhile, the real-time operation disrupted this pattern, causing the annual flood peaks to take place from June to October. For this reason, the real-time operation alleviated many historical flood incidents, but at the same time, their variable timing can pose a challenge in reservoir system modelling.

The severity and frequency of the annual minimum flows also markedly declined with the baseline operation (Figures 5.6(B) and 5.7(C)). However, the real-time operation worsened the annual minimum flows in the years 1989–1997. During this period, the observed annual minimum flows were lower than those in the naturalized scenario and even ceased in some dry seasons, indicating that the real-time operation might trigger some drought events. These drastic minimum flows were eliminated in the years 2003–2013, correspondingly to the BFI improvement. The timing of the annual minimum flows also shifted (Figure 5.7(D)). Note that the annual minimum flows occurring in November–December usually do not lead to water shortage as the extensive monsoon period just passed. The naturalized annual minimum flows occurred in March and April, which is the driest period of the year, thus putting the basin at risk of droughts. The real-time operation apparently solved this issue better than the baseline operation, with only three years of the annual minimum flows occurring in the drought-risk period.

#### 5.4.4 Effects of extreme weather on extreme flows

The reservoir operation was the main cause of the inconsistency in the relationship between the effective inflows ( $P+I-AET$ ) and annual flood peaks in the baseline and real-time operation scenarios (Figure 5.8). Therefore, based on our results, it is likely that the reservoir operation played a more important role than extreme weather in mitigating or magnifying the extreme flow events in the upper GCPR basin. However, the slightly positive correlation between the effective inflows and annual flood peaks indicates that extreme precipitation events magnified historical flood incidents to some extent, although they were not as severe as those in the naturalized scenario. Similar results were reported by Komori et al. (2012) and Sayama et al. (2015). Unfortunately, it is difficult to completely separate the roles of extreme weather and reservoir operation.

This study did not explicitly account for the effects of climate variability on extreme flows and the Gumbel extreme value analyses (Figure 5.7) assumed that there was no trend in annual precipitation. However, we acknowledge the probable changes in monsoon patterns in terms of magnitudes, timing and direction over the past decades in SEA and Thailand (e.g., Singhrattana et al., 2005; Loo et al., 2015). The shift in monsoon direction, for example, can result in a smaller amount of reservoir inflows, and concurrently more direct floodwater in the downstream region. These climate factors influence extreme weather events and real-time reservoir operation, which will affect extreme flows.

#### 5.4.5 Effects of real-time control on extreme flows

According to our findings, we deduce that the generalized operating rules (as represented by the baseline operation scenario) alone could not effectively manage the reservoir water resources throughout a year and that decision-making and real-time control (as represented by the observations) are necessary for preventing and mitigating extreme flow incidents. There was apparently a change in the real-time operation from the 1989–1997 period to the 2003–2013 period, resulting in notable improvements in the streamflow signatures (Table 5.2 and Figure 5.5). It highlights the importance of experience in the decision-making of reservoir operators gained over time. As a result, we acknowledge that the Gumbel extreme value analyses of the observations should be interpreted with care. With real-time control, the reservoir could, for instance, release more water in drier years and close the spillway for a while in wetter years to prevent overtopping the downstream floodwater during storm events. For some events in the past, however, the real-time operation was problematic, such as when the reservoir stored too much stormwater and had to release surcharge water to prevent dam failures, thus intensifying downstream inundations (Komori et al., 2012). This underlines the need for more effective real-time forecasting and decision-supporting tools in order to provide more sustainable reservoir operation in the future.

## 5.5 Conclusion and outlook

The upper GCPR basin has been highly regulated by multipurpose reservoirs for over half a century. While the reservoirs support agriculture and hydropower generation, their regulations have modified the natural flows, posing a challenge to water resources management. This chapter explored the quantitative effects of the major reservoirs, Sirikit and Bhumibol, on the water balance, daily flow regime and extreme flows during the 1989–2013 period. We used the wflow\_sbm model with global spatial data and parameterization to simulate streamflows in the naturalized scenario (without reservoir) and the baseline operation scenario (with generalized operating rules) as thoroughly described in Chapter 4. We analyzed key hydrological signatures in both scenarios and compared these to the observational data, which represent the real-time operation. The main findings are as follows:

1. The reservoir operation disrupted the natural water balance and rainfall-runoff processes in terms of both magnitude and timing, especially with higher evaporation loss.
2. The reservoir operation inverted the natural seasonality of the daily flow regime, with higher flows in the dry season and lower flows in the rainy season. In the long-term, the daily median flows ( $Q_{50}$ ) and low flows ( $Q_{90}$ ) markedly increased, while daily high flows ( $Q_{10}$ ) markedly reduced. The daily baseflow contribution was greater, indicating that streamflow came mostly from the delayed source (reservoirs), and thus that the daily flows became less flashy and more constant throughout a year.
3. The reservoir operation prevented or mitigated many extreme flow incidents in the past. It reduced the magnitude of annual flood peaks and increased the annual minimum flows. Most of the annual minimum flows were also maintained above the naturalized environmental flows, except in some dry seasons during the 1990s. Both annual flood peaks and minimum flows occurred less frequently, but their timing became more variable, and thus difficult to predict.
4. Annual flood peaks and minimum flows were more influenced by the real-time reservoir operation than by extreme weather. However, extreme weather does tend to amplify the severity of flooding.
5. The difference between reservoir outflows from the baseline operation (simulation) and from the real-time operation (observations) highlights the importance of decision-making and real-time control to optimize reservoir outflows on the daily basis.

The findings on the effects of reservoir operation in the upper GCPR basin can benefit Thailand in the light of sustainable reservoir management under the recent National Water Resource Management Master Plan for the 2018–2037 period. At a larger scale,

the insights into the reservoir effects from this basin can be of assistance to reservoir operators and water managers for both existing and planned reservoirs in SEA and other tropical regions. In the future, the river basins in Thailand and SEA will probably be more intensively regulated by more reservoirs. Such management needs to be carefully planned in all aspects of hydrology, ecology and economic development to optimize water resources and prevent hydrological hazards. More studies on the effects of other reservoirs, considering their different purposes, sizes and locations are encouraged. The future challenge lies in predicting and optimizing real-time operation for more effective and sustainable operational and strategic water management, especially for floods and droughts under changing climate and rapid economic development.



“It’s easy to lie with statistics,  
but it’s hard to tell the truth without them.”

—Charles Wheelan, *Naked Statistics: Stripping the Dread from the Data*, (2012)



## **Chapter 6**

### **Machine learning for reservoir operation modelling**

## Abstract

Real-time reservoir operations are highly dependent on decisions made by reservoir operators, which are difficult to simulate accurately with process-based models. Data-driven models, particularly those based on machine learning (ML), have been shown to be able to overcome the limitations of process-based models. Despite a large number of ML studies in reservoir operation modelling, little is known about the roles of reservoir-related input data on ML model performance. This chapter aims to investigate the characteristics and relationships of the available reservoir-related data as the inputs of ML models for simulating real-time reservoir operation and outflow. The Sirikit reservoir in the Greater Chao Phraya River basin in Thailand was used as the case study. With time series decomposition and correlation analyses, we considered the Sirikit reservoir storage ( $S$ ), the Sirikit reservoir inflow ( $I$ ), the Bhumibol reservoir outflow ( $Q_B$ ; another important reservoir in the basin), the downstream river discharge ( $Q_D$ ), the month of the year ( $M$ ) and the day of the week ( $D$ ). ML models with 17 scenarios of input combinations were run and compared. We chose the ML algorithms that have been widely used in reservoir operation modelling, including Multiple Linear Regression, K-Nearest Neighbor, Support Vector Machine, Classification and Regression Tree, Random Forest, Multi-Layer Perceptron and Recurrent Neural Network. We took  $S_{t-1}$ ,  $I_{t-2}$  to  $I_{t+2}$  and  $M$  as input variables for the Sirikit reservoir. Ultimately, we acknowledge that the most suitable input variables vary per ML algorithm, reservoir and study area, and thus should be considered individually.

## 6.1 Introduction

Reservoirs and dams are key infrastructures for water resource utilization and management in major river basins around the globe. They have an essential role in flood and drought control, agricultural irrigation, hydropower generation and water supply. Real-time reservoir operation is required to efficiently achieve these different purposes and to minimize adverse effects on downstream floods, droughts, environmental flow and river ecosystems (Zhang et al., 2018a). Real-time reservoir operation is usually unique for each reservoir, depending on their purpose, location, climatology, and judgments and experience of reservoir operators. Consequently, controlled reservoir outflows are significantly different from natural upstream inflows (as demonstrated in Chapter 5). Hence, real-time reservoir operation is undoubtedly an important component in hydrological models for accurate streamflow simulations. Hydrological modelling with reservoir operation, however, has been a long-standing challenge, especially for large multi-purpose reservoirs.

Reservoir operation modelling with process-based models has been widely used to simulate controlled reservoir outflows and storage. In the late 1970s, a process-based model of multi-purpose reservoir operation was developed based on a priority ranking concept (Sigvaldson, 1976). Since then, process-based reservoir operation models have been continuously proposed and improved, in parallel with the increasing development in computer technology and data availability. The examples of favored models are CalSim (Draper et al., 2004), WEAP21 (Yates et al., 2005) and HEC-ResSim (Klipsch & Evans, 2006). They provide transparent representations and interpretable calculations of reservoir operation in modelling systems, which allowed them to be understood, trusted and applied by reservoir operators and water managers (Lund & Guzman, 1999; Yang et al., 2016).

Despite their benefits in model transparency and interpretation, process-based models are only effective and accurate if the predefined reservoir operating rules and policies (so-called reservoir operating rule curves) represented in the models realistically reflect the actual real-time reservoir operation and outflow (Johnson et al., 1991; Yang et al., 2016). However, it has been commonly acknowledged that reservoir operating rule curves are generally used as long-term guidance. The actual operation processes, on the other hand, are highly dependent on real-time decisions made by reservoir operators to optimize the outflows to specific conditions and purposes, and thus often deviate from the rules (Oliveira & Loucks, 1997). Converting these real-time decisions and deviations into explicit processes or numerical inputs is beyond the limited complexity and mathematical description of process-based models (Chang & Chang, 2001; Draper et al., 2004; Wannasin et al., 2021b). Therefore, it remains difficult to accurately simulate real-time reservoir operation and controlled outflow with process-based models, especially for extreme outflows.

In the past two decades, data-driven models, particularly machine learning (ML) mod-

els, have gained increasing attention in reservoir operation modelling. This is because of their potentially higher accuracy in simulating real-time reservoir operation and outflow compared to process-based models. ML algorithms establish data-driven rules that relate input data (e.g., reservoir storage) and output data (i.e., reservoir outflow), while minimizing the need for explicit mathematical representation and information on real-time decision-making by reservoir operators (Yassin et al., 2019). Similar to the calibration-validation procedure of process-based models, ML models require training and testing for each reservoir to implicitly deduce the actual reservoir operation and compute the actual outflow. Due to their black-box nature, ML models may not be suitable for understanding the operation processes. However, their ability to fit complex, non-linear, high-dimensional relationships between input and output data can highly benefit the need for accurate reservoir outflow simulations.

Several studies have shown the good performance of ML models in simulating real-time reservoir outflows. Some studies have proposed and compared the performance amongst different ML algorithms (e.g., Hsu et al., 2015; Zhang et al., 2018a; Yang et al., 2019; Guo et al., 2021). Other studies have further explored and maximized the applications of well-known ML algorithms in reservoir studies (e.g., Chaves & Chang, 2008; Yang et al., 2016; Liu et al., 2019b; Zheng et al., 2022; He et al., 2022). Yet other studies have investigated model training, tuning and parameterization to optimize model performance in a detailed manner (e.g., Zhang et al., 2018a, 2019; Ouyang et al., 2021). However, only a few studies have focused on influences of input data selection and pre-processing on ML model performance (e.g., Chen et al., 2018). Instead, most studies have assumed that ML models required the same input data as process-based models.

While a large number of ML applications have focused on algorithms, their training and parameterization to improve the model accuracy and efficiency, the equally fundamental problem of selecting and pre-processing input data deserves to receive more attention. This is because input data are the core of data-driven models, and thus unsuitable choices of input variables can significantly affect model speed and predictive ability (Breck et al., 2019; Jain et al., 2020). Therefore, the right input data must be fed to an ML algorithm to achieve the right target output. Apart from the input data selection, pre-processing, especially input data scaling, can also determine the model accuracy (Ahsan et al., 2021). Hence, to improve real-time simulations of reservoir operation and outflow, input data and their influence on ML model performance should be carefully taken into account.

The purpose of this chapter is to gain insight into the influence of input data on the performance of different ML algorithms in order to improve the accuracy of real-time reservoir operation and outflow simulations. The step-wise approach to achieve this goal consists of (i) reservoir data analysis, (ii) input data selection and pre-processing and (iii) performance comparison of different ML algorithms with the selected input dataset. Eventually, we aim for simulating reservoir outflow on a daily timescale.

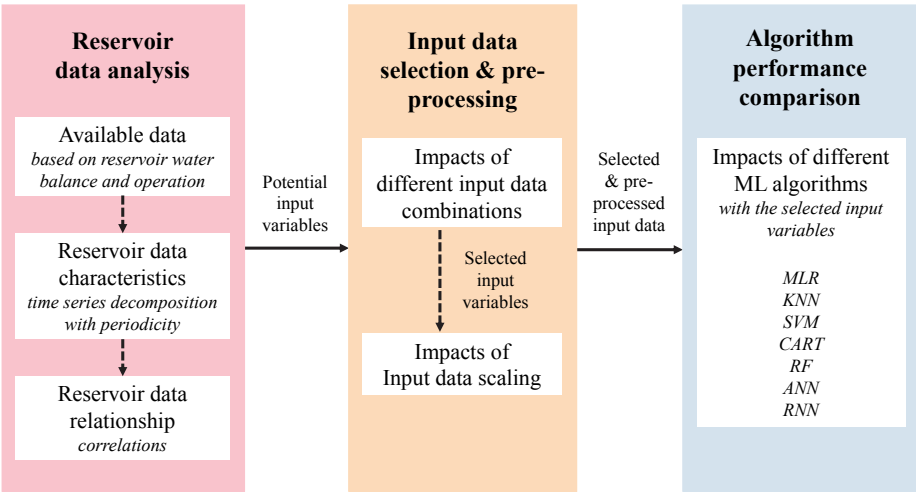


**Figure 6.1:** Study framework, including reservoir data analysis (left), input data selection and pre-processing (middle), and algorithm performance comparison with the selected input data (right).

## 6.2 Methodology

According to the study aim and aforementioned step-wise approach, the study framework is illustrated in Figure 6.1. First, we analyzed the characteristics and relationships of readily available reservoir-related time series data to identify *potential* input variables of ML models. Next, we used different combinations of potential input data to train the ML models and evaluated and compared their performance. The impact of input data scaling was also assessed. We then carefully selected the most suitable input datasets. Seven ML algorithms with the *selected* input datasets were run and the accuracy of their simulated reservoir outflows was evaluated. We focused on the Sirikit reservoir.

### 6.2.1 Reservoir data analysis

#### *Available data based on reservoir operation and reservoir water balance*

Real-time reservoir operation is a complex task, which entails determining reservoir outflow and maintaining reservoir storage to satisfy different purposes under continuously changing circumstances. In theory, the outflow determination is mostly based on the reservoir water balance, reservoir storage zoning and reservoir operating rule curves (see Chapter 1; Section 1.2.1). In practice, however, real-time decision-making by reservoir operators also plays an important role (see Chapter 1; Section 1.2.2). Therefore, the real-time reservoir operation function (Equation (1.2)) consists of several components, including the reservoir water balance, reservoir operating rule curves commonly

used as a guideline, total downstream water demand (which includes requirements of irrigation, hydropower generation, flood and drought control, water supply and environmental flow), and operators' judgments and decisions (which are based on their expert knowledge and historical experience).

The reservoir water balance (Equation (1.1)) contains the reservoir outflow, reservoir inflow from surface water and groundwater, reservoir storage, precipitation and evaporation over the reservoir surface, and storage loss (e.g., from groundwater seepage and dam leakage). According to Kumar & Reddy (2007) and Yang et al. (2019), the simplified relationship amongst the reservoir outflow, inflow and storage at the daily timescale is indicated as

$$S_i = S_{i-1} + \frac{\Delta i(I_i + I_{i-1})}{2} - \frac{\Delta i(Q_i + Q_{i-1})}{2}, \quad (6.1)$$

where  $S$  is the reservoir storage [ $\text{m}^3$ ],  $Q$  is the reservoir outflow [ $\text{m}^3 \text{s}^{-1}$ ],  $I$  is the reservoir inflow [ $\text{m}^3 \text{s}^{-1}$ ] and  $\Delta i$  is the given time interval, assuming precipitation over the reservoir, evaporation from the reservoir and storage loss to be negligible. Note that  $S$  pertains to the end of each time step, whereas  $Q$  and  $I$  pertain to the entire time step (i.e., they are averages over that time step).

Focusing on the Sirikit reservoir, the daily aggregated values of historical reservoir outflow and storage time series data are available from observations. Generalized information on the downstream water demand and the operating rule curves can be acquired as the long-term monthly reference values (as previously demonstrated in Figure 3.4). Since these reference values are subject to adjustments (e.g., they are set differently for predicted wet and dry years), using these values directly as inputs of ML models may lead to insufficient simulation accuracy in some years. However, the values of both the downstream water demand and operating rule curves can be defined as functions of the month of the year (seasonality). Tebakari et al. (2012) indicated that the Sirikit reservoir outflow had a seven-day periodicity (weekly cycle) for irrigation purposes, which contributes to a large part of the water demand. Another hint to the water demand may be obtained through the downstream river discharge at Nakhon Sawan (location shown in Figure 2.2). It is impossible to derive the operators' judgments and decisions numerically, but they are to some extent reflected in the historical reservoir outflow and storage time series data. In addition, since the Sirikit reservoir is simultaneously operated with the Bhumibol reservoir, of which outflow also markedly contributes to the downstream discharge (see Figure 2.2), the Bhumibol reservoir outflow may also be considered.

By taking into account the roles and availability of the reservoir-related data based on the reservoir operation and the reservoir water balance, we decided to take into account the following variables: the Sirikit reservoir outflow ( $Q$ ), the Sirikit reservoir storage ( $S$ ), the Sirikit reservoir inflow ( $I$ ), the Bhumibol reservoir outflow ( $Q_B$ ) and



the downstream river discharge ( $Q_D$ ). Timing information, including the month of the year ( $M$ ) and the day of the week ( $D$ ), was also investigated.  $Q$  was taken as the target output variable of the ML models, while the others were considered as potential input variables. The historical time series data of  $Q$ ,  $S$ ,  $Q_B$  and  $Q_D$  were obtained from observations (see Chapter 3; Section 3.1.3). The  $I$  data were derived from the hydrological simulation using the `wflow_sbm` model (as elaborated in Chapter 4). The observed data were available continuously for a period of 10 years from 2004 to 2013.

To specify the importance and usefulness of the potential reservoir-related data as inputs of the considered ML models for  $Q$  simulations, we analyzed their daily time series, focusing on their characteristics and changes with time. The time series analyses included univariate analysis (single time series) and bivariate analysis (two time series). We used the univariate analysis to investigate the characteristics and time dependencies in the variables, while the bivariate analysis was used to assess the relationships and effects of the potential input variables on the target output,  $Q$ .

#### *Reservoir data characteristics*

To investigate the characteristics of the daily time series of  $Q$ ,  $S$ ,  $I$ ,  $Q_B$  and  $Q_D$ , we focused on the long-term trend and periodicity, including the weekly and monthly cycles. This is because trend and periodicity are valuable signatures for data-driven models. To do so, the daily time series were decomposed. Time series decomposition is the process of deconstructing a time series into three components: *trend* (the long-term progression with a persistent increasing or decreasing direction in the data), *cycle/seasonality* (the periodic behaviors captured over a fixed and known period) and *residual* (the random or noise of the time series after the other components have been removed).

Considering the prior knowledge of the timing dependence of the data, including the annual cycle and the weekly cycle, we decomposed the time series accordingly. Firstly, we decomposed the original time series, concerning the annual cycle. After that, we decomposed the residual component of the original time series, concerning the weekly cycle. By using the residual component, from which the trend and seasonal cycle were already removed, we can better extract the remaining weekly cycle, which is often less prominent. The time series were decomposed using the Classical Seasonal Decomposition by Moving Averages function (Kendall, 1946), which is available in R. Apart from the time series decomposition, we also used the non-parametric Mann-Kendall trend test (Hamed & Rao, 1998) to statistically identify any existing long-term trends in the time series data. If the test indicates a  $p$ -value lower than a significance level (here defined as 5%), there is significant evidence that a trend is present in the data.

#### *Reservoir data relationships*

We investigated relationships of the  $Q$ ,  $S$ ,  $I$ ,  $Q_B$  and  $Q_D$  time series using both univariate and multivariate analyses. For the univariate analysis, the simple correlation

function, also called *auto-correlation*, was applied. The auto-correlation considers relationships among successive terms of a single time series based on the hypothesis that one series at the given time step may be systematically correlated with its own lagged values (Jenkins, 1968; Angelini, 1997). The auto-correlation coefficients (ACs) range between  $-1$  and  $1$ . Plotting ACs against the time lag gives the auto-correlation function (ACF), also known as the correlogram. Lag 0 has an AC of 1, and other lags with high AC values suggest a strong linear dependence or memory and, if any, periodicity within the data. Therefore, the ACF gives useful information about memory effects, i.e., the duration of the influence of the variable.

*Spectral analysis* also allows an understanding of periodicity, especially components that may not be clearly visible in the ACF. The spectral density function (SDF) is the Fourier transform of the ACF, which can be either obtained in a non-parametric way (using the Fast Fourier Transform) or in a parametric way (using an Auto-Regressive Moving Average model). Detailed explanations can be found in Jenkins (1968) and Shumway & Stoffer (2000). The SDF describes the time series in terms of frequencies with the squared correlation between the series and the sine/cosine waves, also known as the periodogram. It shows the decomposition of the total variance of a time series over its frequency components, allowing the identification of dominant periodicities. Although the ACF and SDF are two sides of the same coin, we also included SDF for clear visualization of periodicity, especially when the residual component of the time series was decomposed again.

Just as ACF measures the extent of a lagged relationship within a time series, *cross-correlation*, the bivariate analysis, indicates the degree of the lagged relationship between two time series (Box et al., 2015; Manga, 1999). One series at the given time step may be correlated with another series at a certain time lag. Plotting cross-correlation coefficients (CCs) versus the time lag gives the cross-correlation function (CCF), the so-called cross-correlogram. The lag with the highest positive or negative CC value represents the best linear correspondence between the two series, giving the duration by which one series leads or trails the other or the response time it takes an effect to propagate from one variable to the other. Nonetheless, it should be noted that correlation is not causality.

### 6.2.2 Input data selection and pre-processing

After reservoir data analysis revealed the potential of the reservoir-related variables as input variables of the considered ML models, we assessed impacts of different input data combinations and data scaling on ML model performance.

#### *Different input data combinations*

To simulate  $Q$  with the ML models, the potential input variables can be categorized into the Sirikit reservoir variables ( $S$  and  $I$ ), the timing variables ( $M$  and  $D$ ) and the other

related variables ( $Q_B$  and  $Q_D$ ). With these variables, we created 17 scenarios of input data combinations for the considered ML models, taking also into account the data availability in the real world of the reservoir operation, as shown in Table 6.1.

### Data scaling

The potential input variables have different units and ranges of values (e.g.,  $S$  ranges from 3.14 to 9.5 million  $\text{m}^3$ , while  $I$  ranges from 12 to 4136  $\text{m}^3 \text{ s}^{-1}$ ), referring to different scales and distributions in the time series data. Therefore, we investigated if scaling the input data could improve model performance. Two common data scaling techniques for ML models are standardization and normalization. Standardization is a re-scaling to make the mean of the data equal to 0 with a standard deviation of 1, and thus it is most suitable for data with a Gaussian marginal distribution. Normalization is a re-scaling of data to fit the range of 0 and 1. It requires the minimum and maximum values of the data. Since most times series data in this study are not normally distributed (see Figure B.1 in Appendix B), we selected normalization as the scaling method. A value is normalized as follows:

$$X_{norm} = \frac{X - X_{min}}{X_{max} - X_{min}}, \quad (6.2)$$

where  $X_{norm}$  is the normalized value of  $X$ ,  $X_{min}$  is the minimum value of the time series and  $X_{max}$  is the maximum value. The  $I$  time series was also logarithmically transformed to make the distribution less skewed before being normalized. The other input variables were not transformed as their distributions are not strongly skewed.

### 6.2.3 Algorithm performance evaluation and comparison

With the 17 input dataset scenarios, we evaluated and compared the  $Q$  simulation results of seven ML models. The chosen models are Multiple Linear Regression (MLR), K-Nearest Neighbor (KNN), Support Vector Machine (SVM), Classification and Regression Tree (CART), Random Forest (RF), Multi-Layer Perceptron (MLP) and Recurrent Neural Network (RNN). Details of the algorithms are described in Chapter 3; Section 3.4. For a fair comparison, we ensured that all ML models were implemented in the same manner. To do so, we built the ML models based on their simplest structures within the open-source machine learning frameworks in python (see more detail in Chapter 3; Section 3.4.6). For the MLR, KNN, SVM, CART and RF models, hyper-parameters were set at their default values. For the MLP and RNN models, the models were simplified with one input layer, one processing layer of 64 neurons and one output layer. MLP and RNN were trained with 50 iterations, using the initial learning rate of 0.001 and the Adaptive Moment Estimation (ADAM) as the optimizer. It should be noted that this study did not focus on obtaining the best model performance with their parameterization.

**Table 6.1:** Scenarios of input variable combinations for machine learning models to simulate the Sirikit reservoir outflow  $Q$ . The inputs consist of the Sirikit reservoir storage ( $S$ ), the Sirikit reservoir inflow ( $I$ ), the timing data and the other related data. The timing data include the month of the year ( $M$ ) and day of the week ( $D$ ). The other related data include the Bhumbol reservoir outflow ( $Q_B$ ) and the downstream discharge ( $Q_D$ ).  $t$  is the current model time step.

Scenarios	Input variables				Investigation
	Reservoir stor- age data	Reservoir inflow data	Timing data	Other data	
Baseline	$S_{t-1}$	$I_{t-1}$			$S$
1	$S_{t-2}, S_{t-1}$	$I_{t-1}$			$I$
2	$S_{t-1}$	$I_{t-2}, I_{t-1}$			$S$ & $I$
3	$S_{t-2}, S_{t-1}$	$I_{t-2}, I_{t-1}$			$I$ (past)
4	$S_{t-1}$	$I_{t-3}, I_{t-2}, I_{t-1}$			$I$ (past)
5	$S_{t-1}$	$I_{t-4}, I_{t-3}, I_{t-2}, I_{t-1}$			$I$ (past & present)
6	$S_{t-1}$	$I_{t-4}, I_{t-3}, I_{t-2}, I_{t-1}, I_t$			$I$ (past, present & future)
7	$S_{t-1}$	$I_{t-4}, I_{t-3}, I_{t-2}, I_{t-1}, I_t, I_{t+1}$			$I$ (past, present & future)
8	$S_{t-1}$	$I_{t-4}, I_{t-3}, I_{t-2}, I_{t-1}, I_t, I_{t+1}, I_{t+2}$			$I$ (past, present & future)
9	$S_{t-1}$	$I_{t-3}, I_{t-2}, I_{t-1}, I_t, I_{t+1}, I_{t+2}$			$I$ (past, present & future)
10	$S_{t-1}$	$I_{t-2}, I_{t-1}, I_t, I_{t+1}, I_{t+2}$	$M$		Timing
11	$S_{t-1}$	$I_{t-2}, I_{t-1}, I_t, I_{t+1}, I_{t+2}$	$D$		Timing
12	$S_{t-1}$	$I_{t-2}, I_{t-1}, I_t, I_{t+1}, I_{t+2}$	$M, D$		Timing
13	$S_{t-1}$	$I_{t-2}, I_{t-1}, I_t, I_{t+1}, I_{t+2}$		$Q_{B,t-1}$	Other factor
14	$S_{t-1}$	$I_{t-2}, I_{t-1}, I_t, I_{t+1}, I_{t+2}$		$Q_{D,t-1}$	Other factor
15	$S_{t-1}$	$I_{t-2}, I_{t-1}, I_t, I_{t+1}, I_{t+2}$			Other factor
16	$S_{t-1}$	$I_{t-2}, I_{t-1}, I_t, I_{t+1}, I_{t+2}$	$M$	$Q_{B,t-1}, Q_{D,t-1}$	Other factor

We trained and tested all ML models on the same dataset, using 80% of the data for training (the years 2004–2011) and 20% for testing (the years 2012–2013). We used the Mean Square Error (MSE) as the error estimation function during the training and testing, and used the Root Mean Square Error (RMSE) and the Kling Gupta efficiency (KGE; Gupta et al., 2009) to evaluate and compare the models' performance. More details on the MSE, RMSE and KGE criteria are provided in Chapter 3; Section 3.5.1.

## 6.3 Results

### 6.3.1 Reservoir data characteristics

The decomposed time series of the daily reservoir-related data consist of the Sirikit reservoir outflow ( $Q$ ; Figure 6.2), Sirikit reservoir storage ( $S$ ; Figure 6.3), Sirikit reservoir inflow ( $I$ ; Figure 6.4), Bhumibol reservoir outflow ( $Q_B$ ; Figure B.2 in Appendix B) and downstream discharge ( $Q_D$ ; Figure B.3 in Appendix B). Overall, the decomposition reveals trends and periodicity, with the most distinct patterns being the annual cycle (month of the year) and weekly cycle (day of the week).

#### *Annual cycle*

The seasonal components of  $Q$  (Figure 6.2(B and E)) and  $Q_B$  (Figure B.2(B and E)) show similar behavior. The outflow of both Sirikit and Bhumibol reservoirs increases from October to February when releasing water is more important than storing it. At the end of the wet season, excess water (surcharge and flood control storage previously shown in Figure 3.4) is released to prevent too full reservoir storage. In the dry season, the stored water is released to support irrigation and drought control. The outflow decreases from February to October when storing water becomes more important. Less stored water is available in the late dry season. The reservoir is in the refilling state (conservation storage shown in Figure 3.4) from the early wet season. Also, excess water is held back for downstream flood control until the late wet season.

The seasonal component of  $S$  (Figure 6.3(B and E)) varies oppositely to  $Q$  and  $Q_B$ . The storage increases from June to November, as most rainwater and inflow are stored in the wet season. It then decreases during the entire dry season as water is continuously released to meet the requirements for irrigation and other downstream water demand.

In contrast to the human-induced seasonality of  $Q$ ,  $Q_B$  and  $S$  due to the reservoir operation, the seasonality component of  $I$  (Figure 6.4(B and E)) follows a natural pattern. The inflow increases from May (the start of the wet season) to its peak in August or September, before decreasing during the rest of the year. The seasonal component of  $Q_D$  (Figure B.3(B and E)) reveals the same pattern as  $I$ , but with a delayed peak in October, implying a more natural characteristic, despite being influenced by the two major reservoirs.

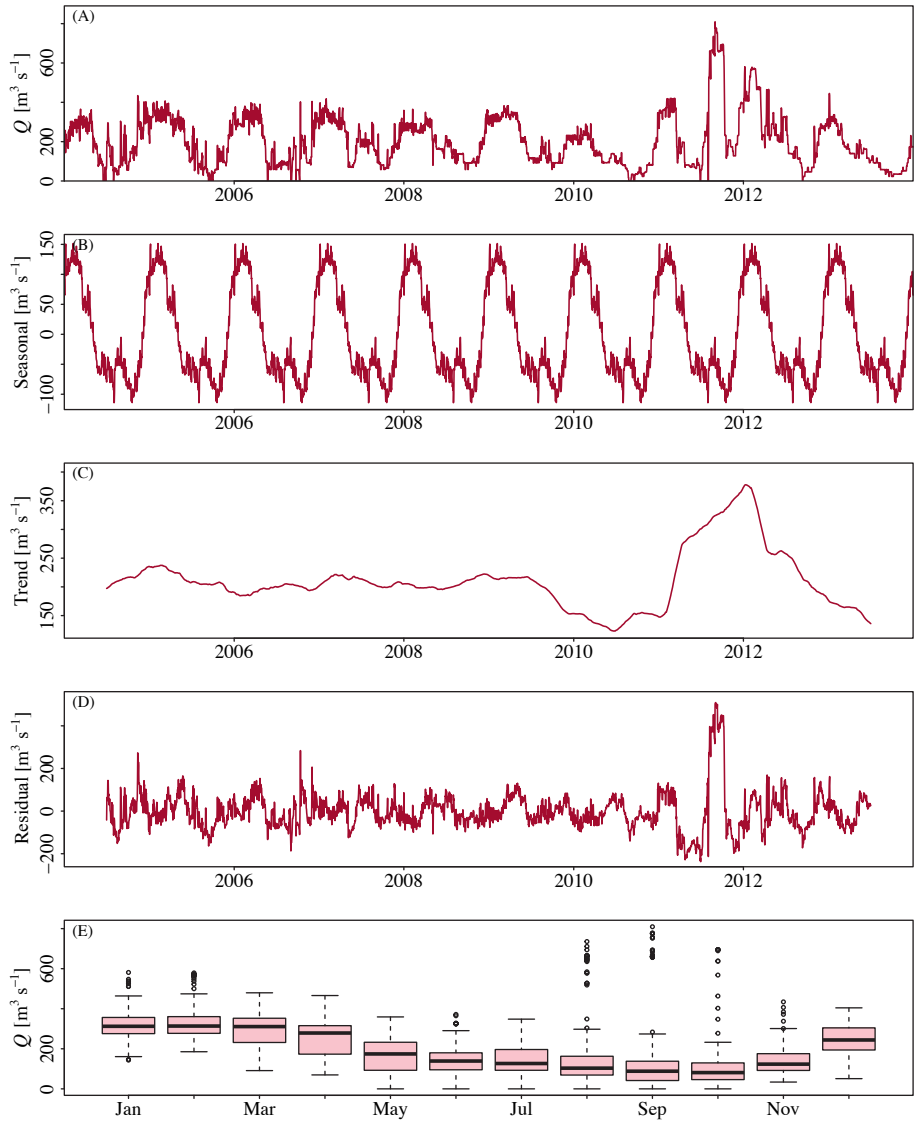


**Figure 6.2:** Decomposition of the observed daily Sirikit reservoir outflow ( $Q$ ) data. The original time series (A) is decomposed into the seasonal (B), trend (C) and residual (D) components. Panel (E) shows the distribution of the daily  $Q$  per month.

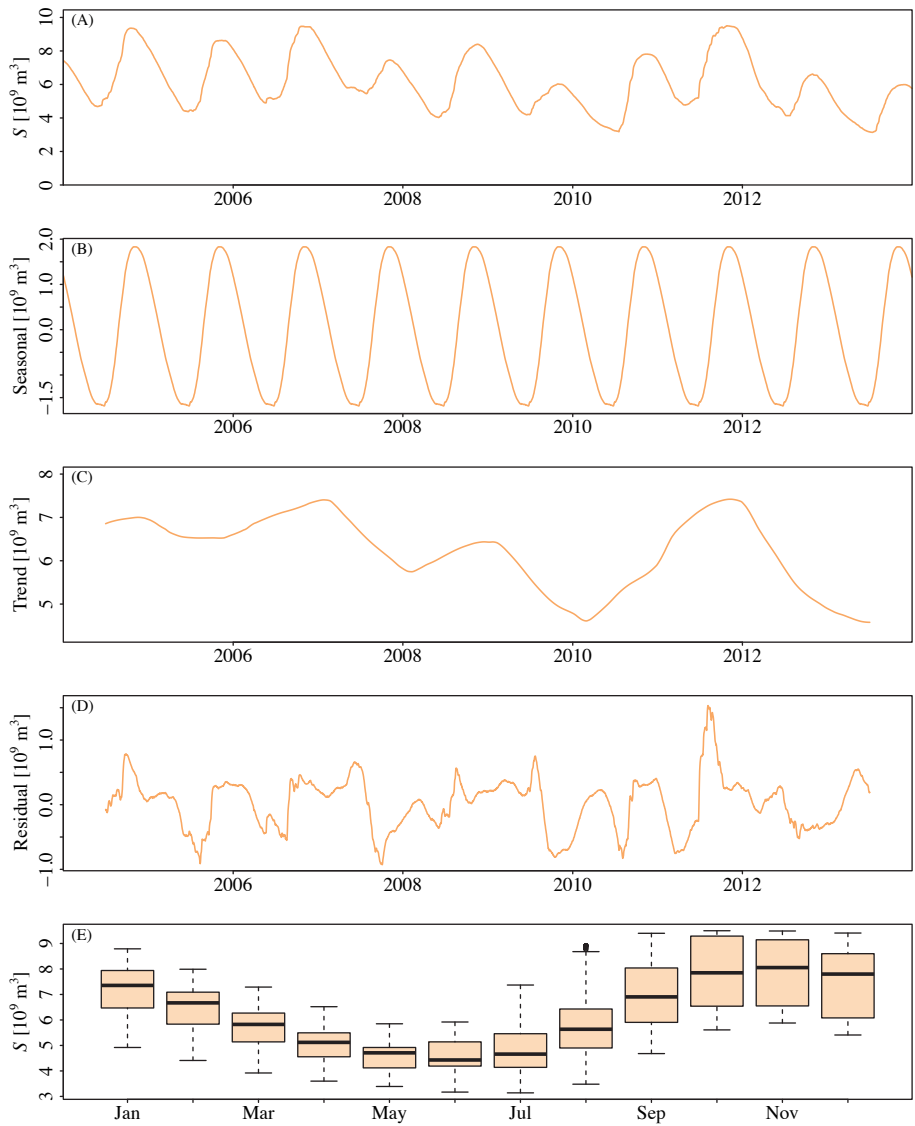


**Figure 6.3:** Decomposition of the observed daily Sirikit reservoir storage ( $S$ ) data. The original time series (A) is decomposed into the seasonal (B), trend (C) and residual (D) components. Panel (E) shows the distribution of the daily  $S$  per month.

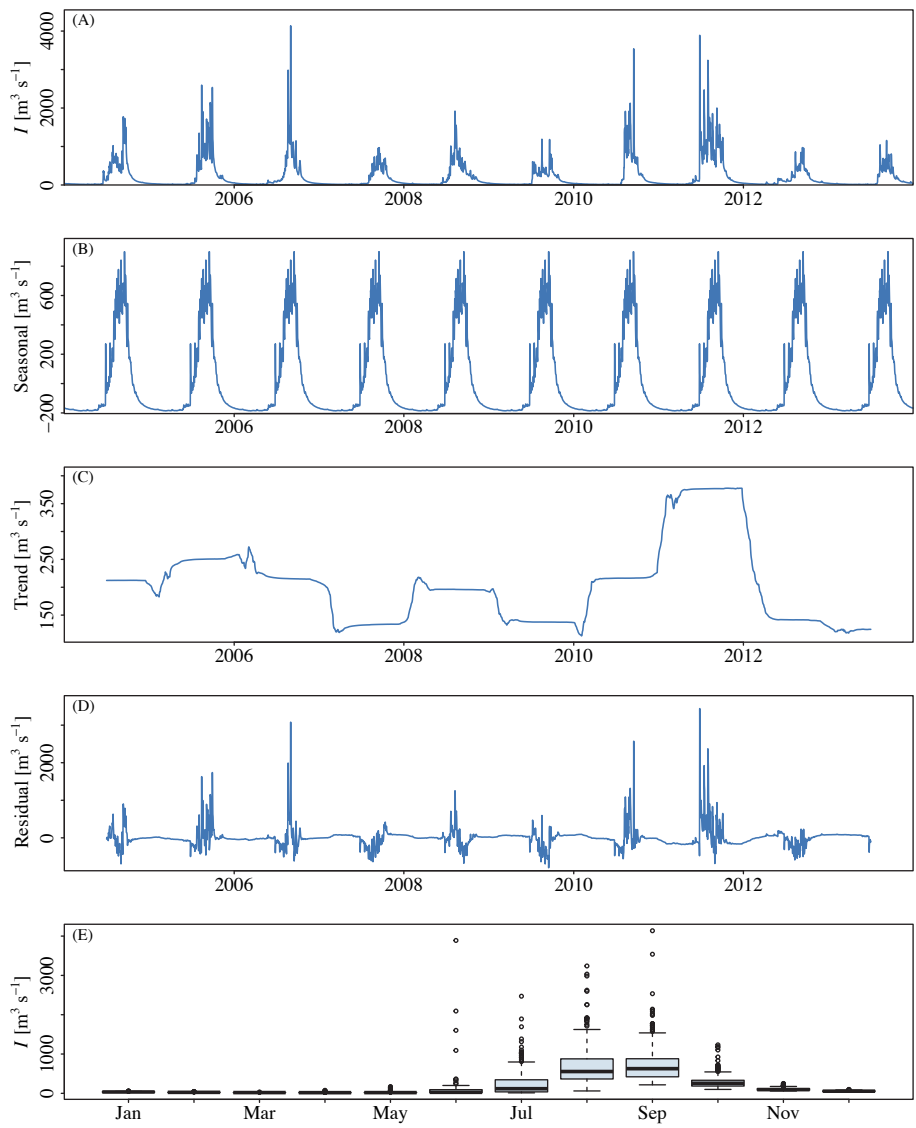


**Figure 6.4:** Decomposition of the simulated daily Sirikit reservoir inflow ( $I$ ) data. The original time series (A) is decomposed into the seasonal (B), trend (C) and residual (D) components. Panel (E) shows the distribution of the daily  $I$  per month.



### *Long-term trend*

According to the Mann-Kendall trend test, a significant long-term trend at the 5% significance level over the 10-year period of 2004–2013 was found for  $Q$  (Figure 6.2(C)),  $S$  (Figure 6.3(C)) and  $Q_D$  (Figure B.3(C), of which  $p$ -value  $\ll 0.01$ . This may indicate the effect of adjusted reservoir operation policies during the study period. There is, however, an exception for  $I$  (Figure 6.4(C);  $p$ -value = 0.43) and  $Q_B$  (Figure B.2(C);  $p$ -value = 0.21), in which no significant long-term trend was found. It should be noted that there was an apparent change in the signatures of  $Q$  between the 1989–1997 and the 2003–2013 period, as the reservoir operating rules were officially adjusted (as previously demonstrated in Table 5.2 and Figure 5.5). The trend component of  $S$  tends to increase for one year and then decrease for another year. This fluctuating pattern was interrupted in 2011 when  $S$  was supposed to decrease, but instead kept increasing according to the enormous amount of  $I$ . The trend component of  $I$  (which shows no significant trend) contains humps that reflect the wet and dry years in the basin. It is acknowledged that with different time windows and other trend-extracting methods, more or different trends may appear.

### *Weekly cycle*

The residuals of the  $Q$  and  $S$  time series (Figures 6.2(D) and 6.3(D)) were decomposed again, focusing on the weekly cycle. The weekly cycle of the residual of  $Q$  shows a prominent amplitude (Figure 6.5(C)). When looking carefully at the spectral density function (SDF; Figure 6.5(I)) there are spikes at the frequency of 0.14 and 0.29, which correspond to a periodic cycle of  $1/0.14 \approx 7$  days and  $1/0.29 \approx 3.5$  days, consistent with the decomposed weekly cycle. The 3.5-day cycle can be an artifact of the processing. This is in accordance with the finding of Tebakari et al. (2012) that  $Q$  had a seven-day periodicity due to the irrigation requirement. The weekly cycle of the residual also reveals that  $Q$  starts at a smaller amount on Monday and gradually increases to the peak on Thursday, before decreasing during the rest of the week (Figure 6.5(C)).

The weekly cycle of  $S$  is not as distinct as the weekly cycle of  $Q$ , as shown in Figure 6.5(D and J). The SDF result (Figure 6.5(J)) displays several frequency peaks in the spectrum, with periods of  $1/0.004 \approx 250$  days,  $1/0.06 \approx 17$  days,  $1/0.15 \approx 7$  days, and  $1/0.32 \approx 3$  days. This can be because  $S$  does not solely depend on reservoir operation, but also on  $I$ .

## 6.3.2 Reservoir data relationship

### *Auto-correlation*

The auto-correlation functions (ACFs) of the daily  $Q$ ,  $S$  and  $I$  time series are presented in Figure 6.6, while the ACFs of  $Q_B$  and  $Q_D$  can be found in Figure B.4 in Appendix B. The ACFs were analyzed for (i) the original time series, (ii) the residual of the first time series decomposition (Residual<sub>1</sub>; representing the data without the long-term trend and

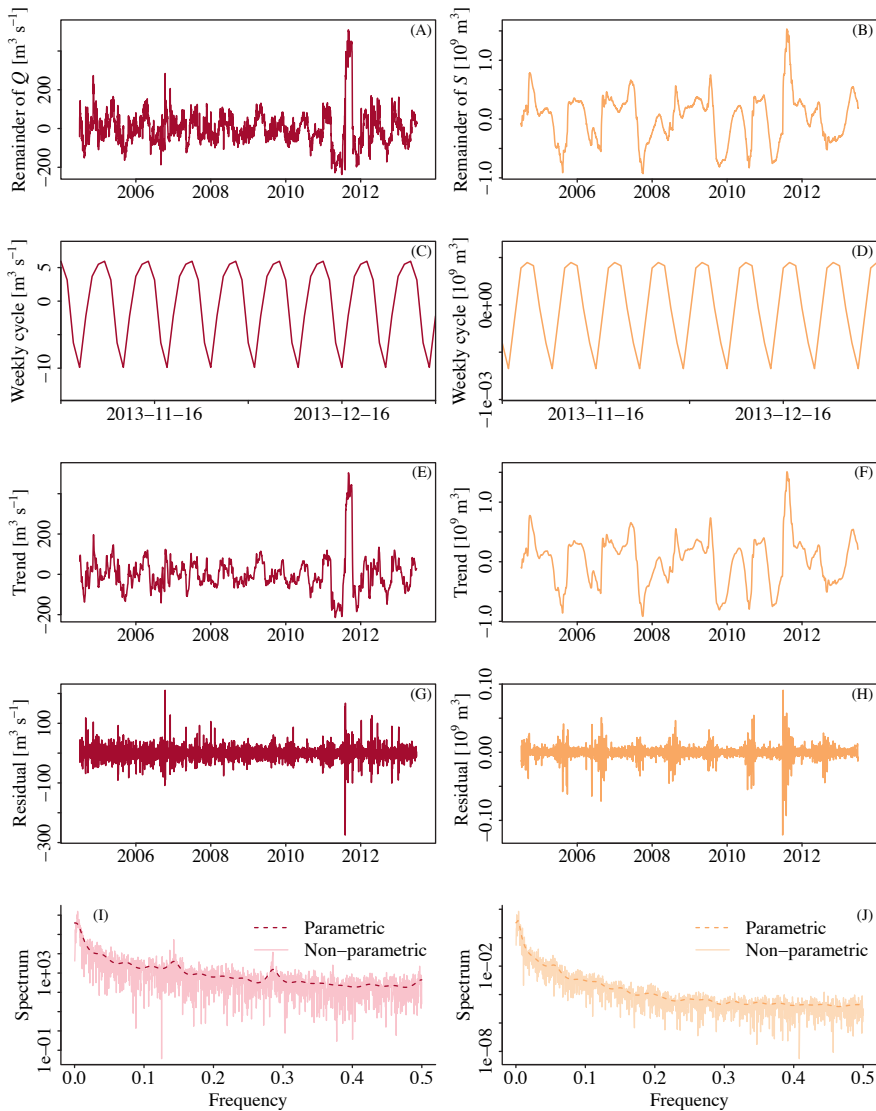


**Figure 6.5:** Decomposition of the Sirikit reservoir outflow ( $Q$ ) and storage ( $S$ ), focusing on the weekly cycle. The initial time series (panels A and B) are the residuals of the decomposed original time series (shown in Figures 6.2(D) and 6.3(D)). The weekly component (panels C and D) is a zoom-in into a two-month period so that the periodicity is visible. The residual component (panels G and H) are the residuals of the residual time series after further excluding the weekly cycle. The spectral density function (SDF; panels I and J) shows the periodicity estimated with both non-parametric and parametric methods. Note that the y-axis of the SDF is presented on a logarithmic scale.

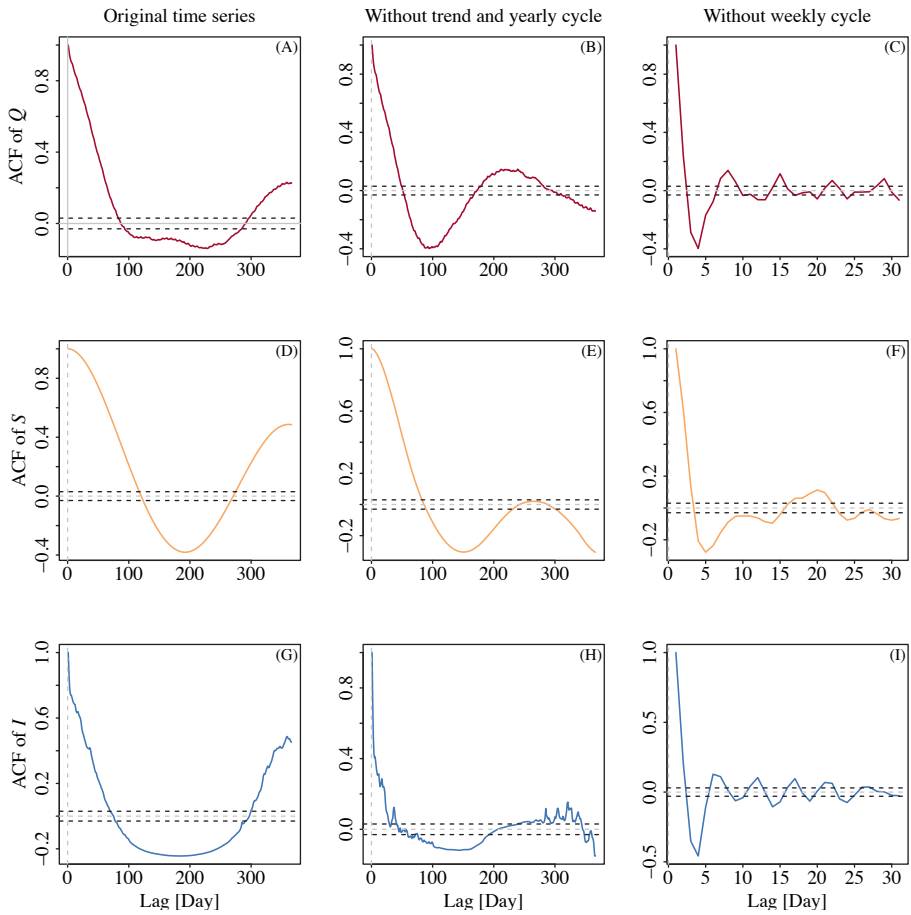


**Figure 6.6:** Auto-correlation function (ACF) of the daily Sirikit reservoir outflow ( $Q$ ), storage ( $S$ ) and inflow ( $I$ ) data. The left panels show the ACFs of the original time series. The middle panels show the ACFs of the 1<sup>st</sup> residual time series (as shown in Figures 6.2(D), 6.3(D) and 6.4(D)), representing the data without the long-term trend and annual cycle. The right panels show the ACFs of the 2<sup>nd</sup> residual time series (as shown in Figure 6.5(G and H)), representing the data without the long-term trend, annual cycle and weekly cycle. Dashed black lines indicate where the correlation is significant to the 95% level.

annual cycle) and (iii) the residual of the second decomposition ( $\text{Residual}_2$ ; representing the data without the long-term trend, annual cycle and weekly cycle). Interpreting the ACFs of time series with strong (yearly and weekly) cycles can be difficult. However, interpreting the ACFs of the residuals can reveal interesting information about the dynamics of the system.

The ACFs of the original time series (left panels in Figures 6.6 and B.4) show slow decays, implying that the variables gradually change and have long-term influences on the hydrological and operation systems. The decreasing correlation of  $Q$  reached the decorrelation threshold ( $1/e \sim 0.37$ ) after 51 lag days,  $S$  after 85 lag days,  $I$  after 39 lag days,  $Q_B$  after 64 lag days (not shown) and  $Q_D$  after 106 lag days (not shown). The shorter decorrelation times of  $I$  reflect the natural seasonality, while the longer decorrelation times of the other regulated variables also reflect the long-term memory effects of the reservoir operation. In other words, the seasonal inflow was stored and released gradually over many months.

The ACFs of the  $\text{Residual}_1$  time series (middle panels in Figures 6.6 and B.4) show considerably faster decays to reach the decorrelation threshold compared to the original time series; at 31 days for  $Q$ , 55 days for  $S$ , 7 days for  $I$ , 24 days for  $Q_B$  and 29 days for  $Q_D$ . This implies the extent of the annual cycle's influence on the reservoir operation and the hydrological system. Although it is invisible in the figures,  $Q$  and  $Q_B$  also contain a seven-day periodicity, aligning with the SDF result in Figure 6.5(I).

The ACFs of the  $\text{Residual}_2$  time series (right panels in Figures 6.6 and B.4) show a very rapid decay, reaching the decorrelation threshold only after 1–2 days.  $I$  has no correlation left after around 3 months, while the other variables keep showing small oscillations with local positive correlations as the time lag increases.

### *Cross-correlation*

Similar to the ACFs, the CCFs were also analyzed for (i) the original time series, (ii)  $\text{Residual}_1$  and (iii)  $\text{Residual}_2$ . The CCFs of the original time series (left panels in Figure 6.7 and Figure B.5 in Appendix B) show that  $S$  and  $I$  lead  $Q$  with a lag time of 83 days ( $\sim 3$  months) and 158 days ( $\sim 5$  months), respectively. Hence, one could expect the highest  $Q$  3 months after the highest  $S$  and 5 months after the highest  $I$ . This is in accordance with the seasonal cycles of the variables, where the highest  $I$  was found in September, the highest  $S$  in October–November, and the highest  $Q$  in January–February (see Figures 6.2(E), 6.3(E) and 6.4(E)).  $Q$  and  $Q_B$  are highly correlated at lag zero, indicating that both reservoirs are operated simultaneously in real-time.

The CCFs of the  $\text{Residual}_1$  time series (middle panels in Figures 6.7 and B.5) show a similar correlation pattern, but with faster response times. The high  $\text{Residual}_1$  of  $Q$  could be expected 35 days ( $\sim 1$  month) after the high  $\text{Residual}_1$  of  $S$  and 54 days ( $\sim 2$  months) after the high  $\text{Residual}_1$  of  $I$ . The  $\text{Residual}_1$  of  $Q$  and  $Q_B$  are still highly correlated at lag zero. The  $\text{Residual}_1$  of  $Q_D$  positively correlates with  $Q$ , with a lead

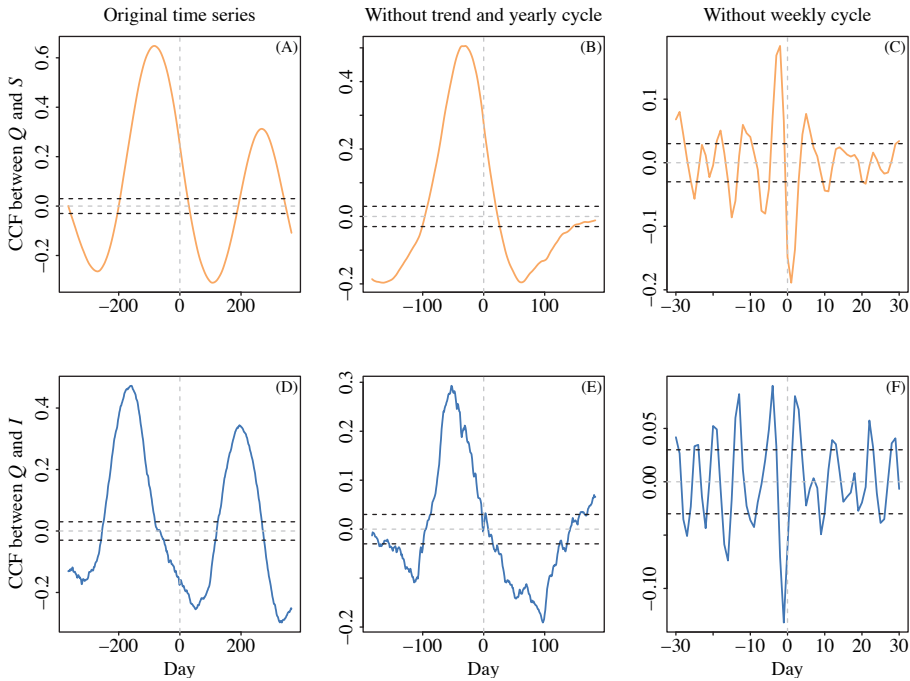


**Figure 6.7:** Cross-correlation function (CCF) between the daily Sirikit reservoir outflow ( $Q$ ) and storage ( $S$ ) (top panels), and between the outflow and inflow ( $I$ ) (bottom panels). The left panels show the CCFs of the original time series. The middle panels show the CCFs of the 1<sup>st</sup> residual time series. The right panels show the CCFs of the 2<sup>nd</sup> residual time series. Dashed black lines indicate where the correlation is significant to the 95% level.

time of 22 days, partly reflecting the travel time of  $Q$  to the downstream region.

The CCFs of the  $\text{Residual}_2$  time series (right panels in Figures 6.7 and B.5) show short response times. The high  $\text{Residual}_2$  of  $Q$  tends to occur 2 days after the high  $\text{Residual}_2$  of  $S$  and 1 day before the low  $\text{Residual}_2$  of  $S$ . On the other hand, the high  $\text{Residual}_2$  of  $Q$  was likely to occur 4 days after the low  $\text{Residual}_2$  of  $I$  and 2 days before the high  $\text{Residual}_2$  of  $I$ . The high  $\text{Residual}_2$  of  $Q_B$  took place 1 day before the high  $\text{Residual}_2$  of  $Q$ . The  $\text{Residual}_2$  of  $Q$  was also high on the day that the  $\text{Residual}_2$  of  $Q_D$  was low and 4 days before the high  $\text{Residual}_2$  of  $Q_D$ .

### 6.3.3 Selection of input data

#### *Influence of different data combinations*

The characteristics and relationships of the daily reservoir-related time series ( $S$ ,  $I$ ,  $Q_B$  and  $Q_D$ ) and timing information ( $M$  and  $D$ ) show their importance, correlation and potentials as the input variables of the ML models. According to the CCFs (Figures 6.7

and B.5), we deduced that, in order to simulate  $Q$  at the current day ( $t$ ), the most important values of  $S$  are at days  $t - 2$ ,  $t - 1$ ,  $t$  and  $t + 1$ , while the most important values of  $I$  are from days  $t - 4$  to  $t + 2$ , considering high positive or negative correlations, particularly of the Residual<sub>2</sub> time series. In reality, past data are usually available from observations and simulations. Current and future data, however, must be carefully considered. In principle, future  $I$  data can be derived from hydrological forecasts. On the other hand, future  $S$  data are not commonly available, as they depend on the other components in the reservoir water balance (See Equation (6.1)). Therefore, only the past  $S$  data at  $t - 2$ ,  $t - 1$  were considered in the input scenarios. For  $Q_B$  and  $Q_D$ , the past data at  $t - 1$  were included.

With 17 combination scenarios of the input data (see Table 6.1), performances of the seven ML models (MLR, KNN, SVM, CART, RF, MLP and RNN) during the testing period (years 2012–2013) are illustrated in Figure 6.8(A). The performance results in the training period are supplied in Figure B.6(A) in Appendix B. The baseline scenario contains  $S_{t-1}$  and  $I_{t-1}$  as the inputs. We found that adding the past Sirikit storage ( $S_{t-2}$ ; scenarios 1 and 3) in the inputs did not improve the performance of most models, except for the MLR and CART models. Likewise, although adding the past, current and future inflow ( $t - 4$  to  $t + 2$ ; scenarios 2–10) slightly improved the model performance, their effects were not remarkable. There was no clear indication whether past, current, or future inflow data play more a important role in the model performance. Therefore, we decided to use  $S_{t-1}$  and  $I_{t-2}-I_{t+2}$ , which allowed for accounting past, current and future data, but not too computationally intensive for the models. Based on this selection, we further explored the effects of timing information ( $M$  and  $D$ ; scenarios 11–13). The results show that  $D$  slightly reduced the model performance, while  $M$  improved the model performance (scenario 11). With the further addition of  $Q_{B,t-1}$  (scenario 14), the performance of many models, except for MLP and RNN, was significantly enhanced. In contrast, including  $Q_{D,t-1}$  (scenario 15) did not benefit the models and even deteriorated the performance of some models (KNN, SVM and CART). The models with both  $Q_{B,t-1}$  and  $Q_{D,t-1}$  (scenario 16), therefore, did not perform differently.

#### *Influence of data scaling*

Overall, running the ML models with the scaled (normalized) input data increased the resulting accuracy, as can be seen in Figure 6.8(B). Compared to their performance with the raw inputs in Figure 6.8(A), the MLR and KNN model results improved the most in the scenarios that focus on  $S$  and  $I$  data (scenarios 0–10). Meanwhile, the MLP and RNN model results improved the most in the scenarios that include timing information and other data ( $M$ ,  $D$ ,  $Q_B$  and  $Q_D$ ; scenarios 11–16), of which RNN improved the most in scenario 11. The SVM, CART and RF models did not show as much improvement as other models. The most distinct improvements were found in scenarios 15 and 16 (where  $Q_D$  was included) for the KNN and SVM models. The difference in the RMSE results after the data scaling during the training period is supplied in Figure B.6(B).

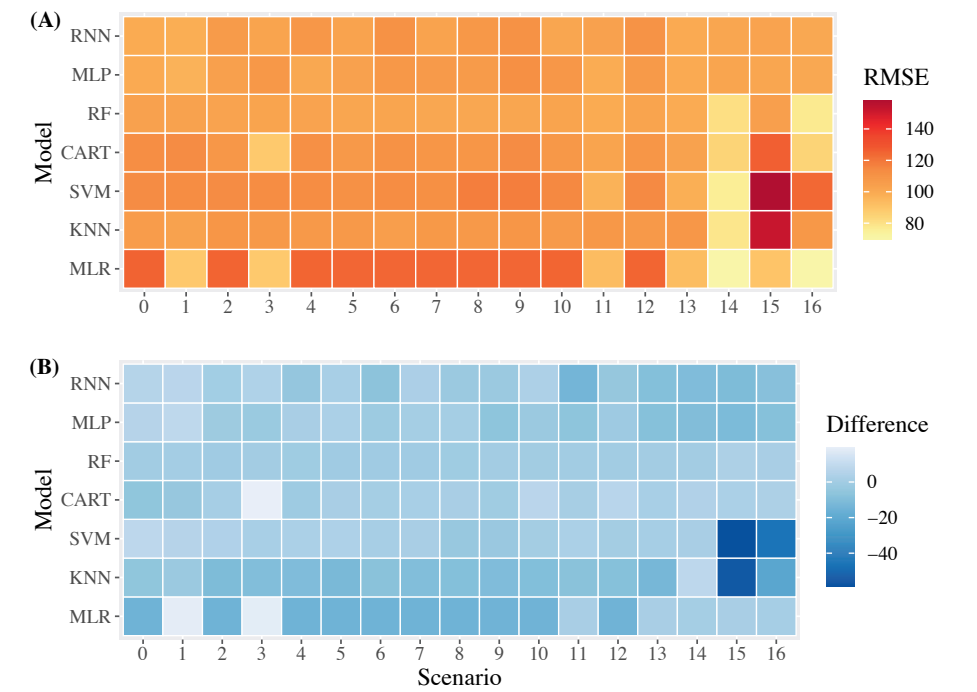


**Figure 6.8:** Performance of the seven ML models on the Sirikit reservoir outflow simulations for the 17 input combination scenarios during the testing period (years 2012–2013), using RMSE as the criterion. Panel (A) shows the RMSE of the model simulations with the raw input data, while Panel (B) shows the difference in RMSE between the model simulations with the raw input data and with the normalized input data, reflecting the effect of input data scaling on the model performance. The ML models consist of Multiple Linear Regression (MLR), K-Nearest Neighbor (KNN), Support Vector Machine (SVM), Classification and Regression Tree (CART), Random Forest (RF), Feed-Forward Neural Network/Multi-Layer Perceptron (MLP) and Recurrent Neural Network (RNN). Differences between the input combination scenarios are explained in Table 6.1. In Panel (A), a lower RMSE value presented in a lighter color indicates a better model performance. In Panel (B), a higher difference presented in a darker color indicates an improvement in the model performance with the scaled input data. Lighter to white color indicates that the model performance did not improve or even decrease. The models' performance in the training period is provided in Figures B.6 in Appendix B.

### 6.3.4 Performance comparison of different algorithms

Based on the analysis results of the input data scenarios and data scaling, we selected the two best-performing input datasets: scenario 11 ( $S_{t-1}$ ,  $I_{t-2}$  to  $I_{t+2}$  and  $M$ ) and scenario 16 ( $S_{t-1}$ ,  $I_{t-2}$  to  $I_{t+2}$ ,  $Q_{B,t-1}$ ,  $Q_{D,t-1}$ ,  $M$  and  $D$ ). The simulated  $Q$  by the seven ML models in these two scenarios during the testing period (years 2012–2013) are displayed in Figure 6.9. As can be seen, the KGE values are higher in scenario 16 for most models, except for the RNN model, which shows no improvement. Interestingly, the MLR and RNN models had the best performance in scenario 11, while MLR also outperformed other models in scenario 16. The performance comparison for the training period is supplied in Figure B.7 in Appendix B.

## 6.4 Discussion

### 6.4.1 Available data to reflect real-time reservoir operation

In this study, the potential input variables of the ML models for simulating the Sirikit reservoir outflow ( $Q$ ) were selected based on their availability, considering also multi-purpose reservoirs worldwide in general. The variables consist of the Sirikit reservoir storage ( $S$ ), the Sirikit reservoir inflow ( $I$ ), the Bhumibol reservoir outflow ( $Q_B$ ), the downstream river discharge ( $Q_D$ ) and the timing information, including month of the year ( $M$ ) and day of the week ( $D$ ). While these variables allow for a specific investigation of the Sirikit reservoir, they are also general enough to provide a basis for ML modelling of other reservoirs in the same basin, neighboring basins, and possibly other basins with similar purposes and the same climatological setting.

The aforementioned variables can represent most components in the simplified reservoir water balance (Equation (6.1)). However, it should be noted that the reservoir water balance in reality is more complex due to the contribution of precipitation and evaporation over the reservoir surface (as previously indicated in Chapter 1; Equation (1.1)). Some previous studies found that the meteorological variables played a more important role in ML model performance than timing information (e.g., Zhang et al., 2019; He et al., 2021). Other studies stated that meteorological variables had an insignificant influence on ML model performance, as they were already captured by the timing information, and thus could be neglected (e.g., Yang et al., 2016). These conflicting findings point to differences in the characteristics and relationship of the reservoir-related data, reflecting different reservoir operations. In this study, we deduced that timing information influences ML model performance more than meteorological variables as the Sirikit reservoir operation is more conditional on water demands than seasonal rainfall. In practice, the reservoir water balance also includes groundwater inflow from aquifers to the reservoir and infiltration losses from the reservoir (Fowe et al., 2015). These data are not commonly considered as input variables in ML modelling since they are usually not available. However, they may play an important role in the water budget.



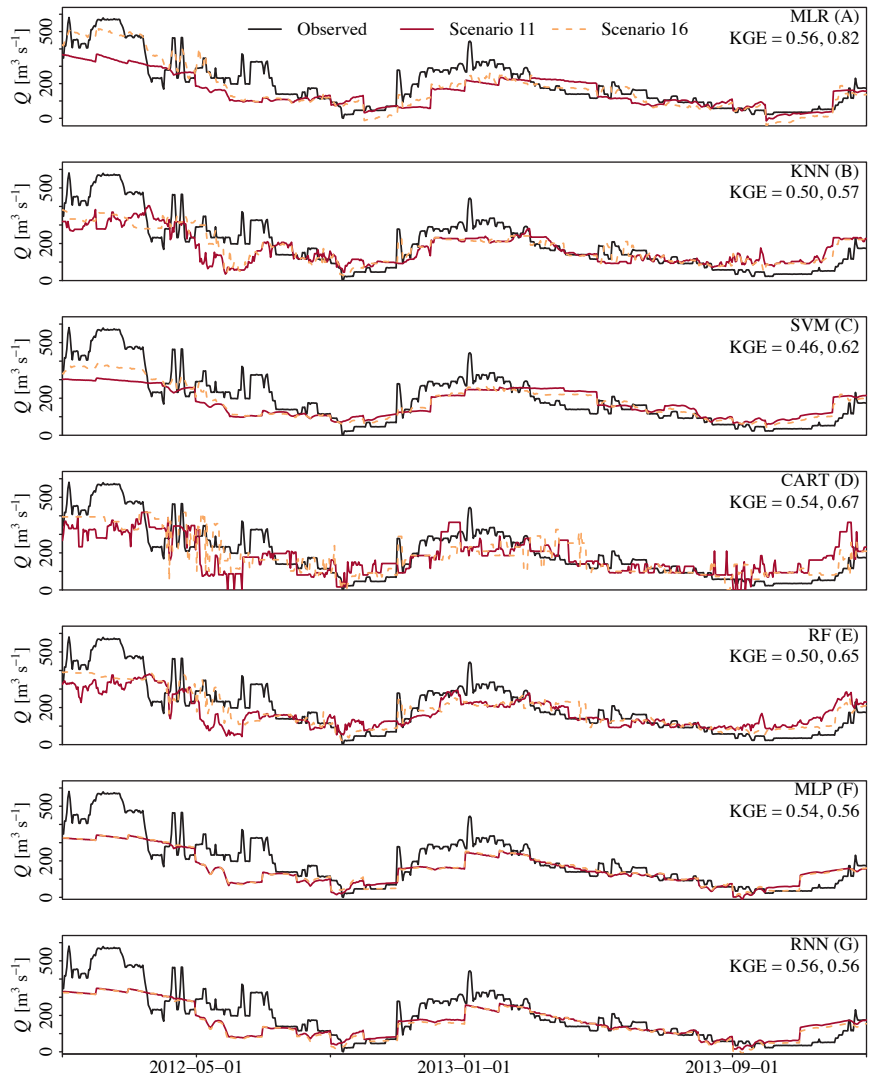


**Figure 6.9:** Simulated daily outflows of the Sirikit reservoir by the seven ML models compared to the observations in the testing period (years 2012–2013). The ML models consist of Multiple Linear Regression (MLR), K-Nearest Neighbor (KNN), Support Vector Machine (SVM), Classification and Regression Tree (CART), Random Forest (RF), Feed-Forward Neural Network/Multi-Layer Perceptron (MLP) and Recurrent Neural Network (RNN). The simulation results of two selected and scaled input scenarios are compared: scenario 11 (in solid red color) and scenario 16 (in dashed orange color), which are the best input datasets. The details of each scenario can be found in Table 6.1. The KGE values are also indicated for scenarios 11 and 16, respectively.

Although the aforementioned variables can represent the important components in the reservoir water balance, they cannot fully represent the real-time reservoir operation function (Equation (1.2)). This is due to the lack of detailed data and information required for capturing factors that influence real-time decision-making by reservoir operators. Some additional data, such as hydroelectricity generation (e.g., Zhang et al., 2019) and water allocation policies, can be obtained for specific reservoirs and have proved to notably increase ML model performance (e.g., Yang et al., 2016; Zhang et al., 2019). Unfortunately, these important data are generally difficult to record and provide in detail for most reservoirs without authority support or collaboration.

#### 6.4.2 Importance of input data selection

With the insight into the characteristics and relationships of the potential input variables obtained in this study, we concluded that the recent past and future values of the  $S$  and  $I$  data were closely correlated with the current value of the  $Q$  data, after eliminating the long-term trend, annual cycle and weekly cycle in their time series (Figure 6.7). This correlation reflects the short-term memory effect of real-time decision-making by the reservoir operators. However, including the  $S$  and  $I$  data at different time lags and lead times in the inputs did not significantly improve the performance of the ML models (Figure 6.8(A)). Similarly, while the  $Q$  data contained an obvious seasonal cycle (Figure 6.2) and weekly cycle (Figure 6.5), only the  $M$  information notably increased the resulting accuracy of the ML models. The same circumstance applied to the  $Q_B$  and  $Q_D$  data; although both variables showed the short-term memory effect on  $Q$  (Figure B.5),  $Q_B$  positively contributed to the ML model performance, while  $Q_D$  even deteriorated the performance of some ML models (Figure 6.8(A)). This can be because the shifted  $S$  and  $I$  data, the  $D$  information and the  $Q_D$  data added more complexities and noise than linearity into the ML models.

Despite insignificant or negative effects of some potential input variables, we found that including all data as inputs in scenario 16 ( $S_{t-1}$ ,  $I_{t-2}$  to  $I_{t+2}$ ,  $Q_{B,t-1}$ ,  $Q_{D,t-1}$ ,  $M$  and  $D$ ) provided the best performance in most ML models, considering the RMSE (Figure 6.8(A)) and KGE (Figure 6.9) criteria. However, we cannot conclude that this input dataset is the best choice for the Sirikit reservoir simulation with the ML models. Since the input dataset contains variables with trivial roles (e.g.,  $D$ ) and redundancy (e.g.,  $Q_{B,t-1}$ ), they can increase the complexity of the ML model unnecessarily, cause model over-fitting and require more computational demand. In addition, although  $Q_B$  had an important role in the ML model performance, this variable should be considered carefully as the input.  $Q_B$  presented a strong linear correlation with  $Q$ , in terms of both values and variations, since both reservoirs are operated simultaneously (Figure B.5). Therefore, adding the past  $Q_B$  value as the model input is similar to mimicking the past  $Q$  value. It is also noteworthy that the input dataset in scenario 16 seems reasonable for ML model simulations of historical  $Q$ , but it can be unrealistic and requires more modelling effort if one wants to apply the ML models for real-time  $Q$  prediction. This

is because the past, current and future data of  $I$ ,  $Q_B$  and  $Q_D$  would not be readily available, and thus would require real-time predictions as well. The future and real-time  $I$  data can be commonly predicted with a process-based model using meteorological forecast data, in a similar way to the historical  $I$  data simulated by the wflow\_sbm model in this study. Predicting the  $Q_B$  and  $Q_D$  data, on the other hand, is burdensome and risks adding more uncertainty (resulting from forcing and model uncertainty) in the input dataset.

After careful consideration, we suggest that scenario 11 ( $S_{t-1}$ ,  $I_{t-2}$  to  $I_{t+2}$  and  $M$ ) represents the most suitable input dataset for the ML models to simulate the Sirikit reservoir operation and its  $Q$ , considering all aspects, including data importance, data availability, ML model performance and computational demand. The  $Q$  simulation results with this input dataset were satisfactory for all ML models and were not remarkably different from the simulation results with the input dataset in scenario 16, especially for the MLP and RNN models (Figure 6.9). With this input dataset, we can capture four out of five components in the real-time reservoir operation function (Equation (1.2)). The four components include the storage, inflow, downstream water demand and operating rule curves. By using the timing information ( $M$ ) to indirectly refer to the downstream water demand and the operating rule curves, we can avoid unnecessary complexities in the input data. The remaining component is the reservoir operators' judgments and decisions in real-time.

To account for the real-time judgments and decisions of the operators, one may make use of the previous  $Q$  values as the input to simulate the current  $Q$  value. This addition has been proven very successful to achieve excellent accuracy of reservoir outflow simulations in several ML model studies (Chen et al., 2018; Zhang et al., 2018a, 2019; He et al., 2021; Hong et al., 2021). This is due to the increasing linear relationship between the inputs and output. However, we state here that using the previous  $Q$  data as the input is only logical and useful for ML model application in practice when the  $Q$  input data are obtained from prediction instead of from historical observations. A realistic example is to use an ML model to predict  $Q$  in real-time and feed the predicted  $Q$  result back into the model as an input for the next  $Q$  calculation. This presumption is further explored in Chapter 7.

We acknowledge that there are available statistical approaches to assist the input variable selection in ML modelling. A well-known approach is the Recursive Feature Elimination (RFE; Chen & Jeong, 2007). Some ML algorithms, such as MLR, CART and RF, also provide optional functions to quantify and compare the importance of potential input variables during their modelling process. However, these approaches are suitable for classification ML models or univariate ML models. To our knowledge, there is so far no exclusive input variable selection approach for regression ML models with multivariate input time series. Nevertheless, for comparison, we applied the RFE and the built-in approaches of the MLR, CART and RF models to assess the potential input data variables in this study. The results support our findings of the data characteristics and

relationships using traditional statistics, like time series decomposition, ACF, CCF and SDF. Moreover, the most suitable input variables can be subjective to different ML algorithms, meaning that one input dataset can give high accuracy for some ML models, but not for others (Figure 6.8(A)). Therefore, the statistical methods used in this study are advised, since they can also provide more insight into the data.

### 6.4.3 Importance of data scaling

Many ML algorithms are sensitive to data scales and distributions during their training. For example, MLR uses a weighted sum of the inputs, KNN uses distance measures that are calculated based on the input scales and RNN initializes the input weights to small random values during the training process. Therefore, many ML algorithms can achieve better performance if the input data have a consistent scale and distribution, which is consistent with the findings of this study (Figure 6.8(B)).

An important concern when scaling the input data for ML models is data leakage. It occurs when an ML model is already aware of some unknown or future data in the training process, causing model over-fitting with an overly optimistic training result but poor testing or validating results. To prevent data leakage, we first normalized the training dataset (years 2004–2011) and used the statistical values (minimum and maximum) to normalize the testing dataset (years 2012–2013). We strongly recommend this approach in order to obtain the realistic performance of the ML models.

It is also important to note that the training period in this study represents a comprehensive variation of the Sirikit reservoir operation, including the normal flow condition, flood events and drought events, while the testing period covers a relatively typical flow period. This may cause model over-fitting to a certain extent. The reason is that if the training dataset does not include the range of future extreme events, the scaling factors (minimum and maximum in this case) in the training period cannot provide proper scaling of the extreme values in the testing dataset, resulting in lower accuracy of the ML model result. For example, if the 2011 historical flood year would be included in the testing period instead of the training period, the model performance could be significantly reduced. This circumstance is likely to happen when applying the ML models to predict the reservoir outflow in practice. Therefore, we suggest evaluating the model performance, including the data selection and scaling, in different periods. This is further investigated with the model cross-validation in Chapter 7.

### 6.4.4 Importance of algorithm selection

Although this study did not focus on obtaining the best ML algorithms for simulating the Sirikit reservoir outflow, it reveals an interesting finding that is worth clarifying. The model performance comparison (Figure 6.9) shows that simple algorithms, like MLR, outperformed more complex algorithms. This can be explained in two ways. Firstly, the testing period does not include extreme events. In the training period of scenario

11 (Figure B.7), the KGE value of the MLR model (0.52) was significantly smaller than the KGE values of KNN (0.90) and RF (0.95), and was similar to MLP (0.54) and RNN (0.52). This implies that if the testing period contains more extreme reservoir outflow values to be simulated, the performance of MLR is likely to decrease, while the other models, particularly KNN, CART and RF, can retain the same performance (although the CART model seems to be over-fitted with a KGE of 1). Secondly, the ML models in this study were set up based on their basic structures and parameterization for fair comparison purposes (as explained in Section 6.2.3). While the MLR model already performed at its best due to its explicit linearity, the other ML models can still be improved through a more complex structure and proper hyper-parameterization. For example, the CART and RF models can identify the number of estimators in their training process. This is especially the case for the MLP and RNN models, which in this study were simplified with only one hidden layer of 64 neurons. Also, the models were trained with only 50 iterations. No recurrent input memory was applied in the RNN, despite being a beneficial function. This indicates that these ML models can still perform better, although this was not in the scope of this study.

## 6.5 Conclusion and outlook

The study provides insight into the characteristics and relationships of the available reservoir-related data and their values as the inputs of machine learning (ML) models for simulating real-time operation and outflow of the Sirikit reservoir in Thailand. The potential input variables consist of the Sirikit reservoir storage ( $S$ ), the Sirikit reservoir inflow ( $I$ ), the Bhumibol reservoir outflow ( $Q_B$ ), the downstream river discharge ( $Q_D$ ) and the timing information, including month of the year ( $M$ ) and day of the week ( $D$ ). The chosen ML algorithms consist of the Multiple Linear Regression (MLR), K-Nearest Neighbor (KNN), Support Vector Machine (SVM), Classification and Regression Tree (CART), Random Forest (RF), Multi-Layer Perceptron (MLP) and Recurrent Neural Network (RNN). The major findings are as follows:

1. The recent past and future values of the potential input data, especially  $S$  and  $I$ , were closely correlated with the current value of the  $Q$  data, after eliminating the long-term trend, annual cycle and weekly cycle in their time series, reflecting the short-term memory effect of real-time decision-making by the reservoir operators. However, including the input data at different time lags and lead times in the inputs did not always significantly improve the model performance. One reason for that may be that the data may add more complexities and noise than linearity to the ML models.
2. Although including all potential data ( $S_{t-1}$ ,  $I_{t-2}$  to  $I_{t+2}$ ,  $Q_{B,t-1}$ ,  $Q_{D,t-1}$ ,  $M$  and  $D$ ) as the inputs provided the best performance in most ML models, it may not represent the most suitable dataset in practice, considering the trivial roles and redundancy of some variables. Instead, the input dataset with fewer variables ( $S_{t-1}$ ,

$I_{t-2}$  to  $I_{t+2}$  and  $M$ ) was suggested, considering data importance, data availability, ML model performance and computational demand.

3. Many ML algorithms can achieve a better performance if the input data have a consistent scale and distribution. Therefore, data should be carefully scaled during the model training process.
4. Ultimately, the most suitable input variables depend on the choice of ML algorithms and are unique for each reservoir and study area, and thus should be considered individually.

This chapter reveals the potential of ML applications with available input data on real-time reservoir operation modelling in practice. Based on these findings, we applied advanced ML models and evaluated their performance on multi-day reforecasting of real-time operation and outflow with real-time inflow reforecasting for the Sirikit reservoir, as demonstrated in Chapter 7.

“Often people think of developments in computation as arising when we make our computers more blazingly fast, so they can compute more stuff, bigger data. It’s actually just as important to prune away big parts of the data that aren’t relevant to the problem at hand! The fastest computation is the one you don’t do.”

—Jordan Ellenberg, *Shape: The Hidden Geometry of Information, Biology, Strategy, Democracy, and Everything Else*, (2021)





## **Chapter 7**

### **Reforecasting real-time reservoir operation and outflow**

## Abstract

Machine learning (ML) models have become increasingly popular in reservoir operation modelling as they can overcome the limitations typically encountered in process-based models. This chapter aims to investigate the capabilities of the Recurrent Neural Network (RNN), Long Short-Term Memory (LSTM) and Gated Recurring Unit (GRU) in simulating and reforecasting real-time (daily) reservoir operation and outflow, considering uncertainties in input data, training-testing periods and different algorithms. The Sirikit reservoir in Thailand was used as the case study. The main inputs for the ML operation models included the daily reservoir outflow, inflow, storage and the month of the year. We applied the distributed wflow\_sbm model for inflow simulation (using MSWEP precipitation data) and inflow reforecasting (using ECMWF precipitation data). Daily reservoir storage was obtained from observations and real-time recalculation based on the reservoir water balance. The ML models were trained and tested with 10-fold cross-validation. Results show that RNN, LSTM and GRU can reconstruct real-time reservoir operation and provide accurate outflow when training data cover both regular and extreme conditions. For multi-day reforecasting, the model performances are appropriate for the current day up to 2-day lead times for low outflows and up to 6–7 days for high outflows. GRU is potentially the most accurate, robust and convenient model to be used in practice. We conclude that with some further improvements, the ML models can be effective and applicable tools to support decision-making for real-time operational water management.

## 7.1 Introduction

Real-time reservoir operation modelling, which is essential for the efficient planning and management of water resources, is a long-standing challenge in hydrological modelling. Streamflows in river basins that are highly regulated by dammed reservoirs are dependent on real-time reservoir operation, which alter the natural flow regimes both in timing and magnitude (Li et al., 2017; Wannasin et al., 2021a). Therefore, to adequately simulate and forecast streamflows in such river basins, real-time reservoir outflows must be computed accurately first, especially during extreme flow periods. To accurately compute real-time reservoir outflows, a model must comprehensively capture the actual operation processes, which require real-time reservoir-related data and information. The most difficult real-time information to be obtained and taken into account in the models concerns the rapidly changing judgments and decisions made by reservoir operators to continuously optimize the outflows under changing circumstances (Oliveira & Loucks, 1997). Since these real-time decisions are based on experiential knowledge and rarely recorded, they do not have a straightforward pattern and cannot be easily and explicitly converted into numerical inputs, especially for multi-purpose reservoirs (Draper et al., 2004; Wannasin et al., 2021b). Nonetheless, to enhance the effectiveness and applicability of reservoir operation modelling for water resources planning and management, it is crucial to develop models that comprise this important information to represent and reproduce the actual reservoir operation and outflow in real-time.

An effective and applicable reservoir operation model should be able to compute real-time operation and outflow by using typically available reservoir-related data (e.g., storage and inflow), while also incorporating the operators' decisions and operating rules without the requirement of a large amount of data and high computational demand. To date, there are two approaches for this ambitious attempt: (i) improving *physical* model representations and (ii) improving *statistical* model relations. The former concerns the improvement of physically-based and mathematical representation, parameterization and integration of the reservoir operation processes in traditionally process-based hydrological models (Yassin et al., 2019). This approach hypothesizes that a higher *model realism* will increase the model's ability to compute real-time reservoir operation and outflow. Improving statistical model relations, on the other hand, concerns directly building statistical relationships between real-time outflows (output) and other reservoir-related data (inputs) by using data-driven models (Solomatine & Ostfeld, 2008). This approach is based on the idea that higher *model accuracy* can be achieved without explicitly diving into the underlying physical processes and mathematical description of real-time reservoir operation. While the need to understand and reconstruct the real-time reservoir operation processes for long-term and sustainable model applications necessitates the former approach, limitations in the model complexity and data availability make it less practical (Zhao et al., 2016b; Yassin et al., 2019). The latter approach, on the other hand, has shown greater potential in computing real-

time reservoir operation and outflow, despite the same data limitation (Tanty et al., 2015; Coerver et al., 2018).

Although the black-box nature of most data-driven models does not encourage the understanding of the reservoir operation processes or improvement of model realism, its superior capability to fit complex and high-dimensional relationships between input and output data can satisfy the need for higher model accuracy. Therefore, data-driven models, particularly machine learning (ML) models, have been increasingly explored in simulations and forecasts of real-time reservoir operation and outflow, especially for urgent flood and drought controls. An overview of ML model classes and algorithms that have been widely applied in reservoir operation modelling is provided in Chapter 3; Section 3.4. In particular, the Recurrent Neural Network (RNN), Long short-term memory (LSTM) and Gated Recurring Unit (GRU) have gained popularity amongst all ML algorithms. Their main advantage is their ability to use prior information in the sequence to produce the current output in a feedback loop, which allows them to deal with complex and non-linear time series more effectively. As a result, RNN, LSTM and GRU have shown superior and promising performance in real-time reservoir operation modelling (e.g., Zhang et al., 2019; Apaydin et al., 2020; Guo et al., 2021).

Despite the extensive applications of RNN, LSTM and GRU in real-time reservoir operation modelling, previous studies have primarily focused on historical reservoir outflow simulations. Some studies have implemented the aforementioned algorithms to simulate real-time outflows for small or single-purpose reservoirs (e.g., Zhang et al., 2019; He et al., 2021; Hong et al., 2021; Yang et al., 2021; Gangrade et al., 2022). Some other studies have investigated the algorithms' performance in simulating real-time outflows for large or multi-purpose reservoirs (e.g., Chen et al., 2018; Zhang et al., 2018a; Zheng et al., 2022). However, very few studies have been conducted on multi-day reforecasting of real-time reservoir outflows. Here, reforecasting refers to forecasting of historical outflows using archived forecast input data. The study of Yang et al. (2019) used LSTM to reforecast daily reservoir outflows, using observed daily storage and reforecast daily inflow obtained from a distributed hydrological model as inputs. Assuming that the role of forecast meteorological data was negligible, they used the historical meteorological data to reforecast the inflow. For that reason, the influence of meteorological forecasts on the algorithm's performance and the forecast skill in practice could not be addressed. The study of Liu et al. (2022) utilized ensemble forecasts of meteorological data in an LSTM application to reforecast streamflows in a cascade reservoir system. However, they did not use LSTM to directly reforecast the streamflows, but to further correct the reforecast results computed by a distributed hydrological model. Thus far, no study has applied either RNN, LSTM or GRU with reforecast input data for real-time operation and outflow modelling of large and multi-purpose reservoirs, as far as we know. Therefore, the effectiveness and applicability of these ML algorithms to reforecast reservoir operation and outflow remain unclear.

This chapter strives to assess the effectiveness and applicability of three well-known ML

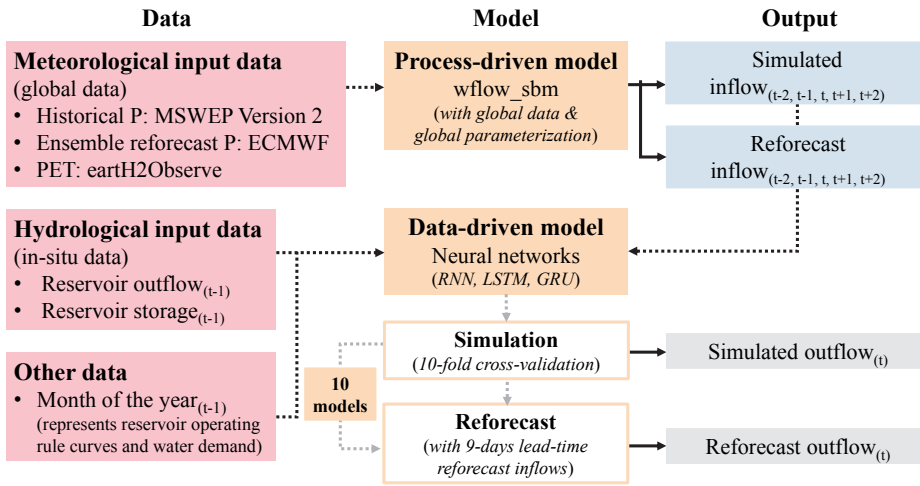


**Figure 7.1:** Modelling framework of the study, including employed data, model setups and model outputs.  $P$  and  $PET$  represent precipitation and potential evapotranspiration.  $t$  refers to the modelling time step [day]. The dotted arrows refer to inputs, while the solid arrows refer to outputs.

algorithms, RNN, LSTM and GRU, in real-time reservoir operation modelling. This includes both simulating and multi-day reforecasting reservoir operation and outflow at the daily timescale. We focus on a large-scale, multi-purpose reservoir, of which real-time operation is difficult to compute by process-based models. With the process-based wflow\_sbm model, we obtained historical and reforecast data of the reservoir inflow, which was one of the inputs for the ML models. This chapter provides a comprehensive investigation, considering uncertainties in the inflow input data, training-testing periods and different ML algorithms. The viability and convenience of the ML model applications in practice were also taken into account.

## 7.2 Methodology

This chapter contains three step-wise sections: (i) input data selection, (ii) daily reservoir inflow modelling using a process-based model and (iii) daily reservoir operation and outflow modelling using three data-driven (ML) models with the modelled inflow as one of the inputs. Accordingly, the modelling framework is illustrated in Figure 7.1. The Sirikit reservoir in the Greater Chao Phraya River basin in Thailand was used as a case study, with the location shown in Figure 2.2.

### 7.2.1 Selecting reservoir-related input data for data-driven models

Real-time reservoir operation is a complex function of several variables, including the reservoir outflow, inflow, storage, downstream water demand, operating rules and operators' decisions, established within the reservoir water balance function (Lund & Guzman, 1999; Yang et al., 2019). The real-time reservoir operation function is presented in Equation (1.2). Since real-time operation is unique for each reservoir, it is advised to individually consider input variables for ML models, taking into account also the modelling purposes, algorithms, data importance, data availability and computational demand. In this study, we carefully selected available data of the Sirikit reservoir for the ML models based on statistical analyses, including time series decomposition and correlation, as elaborated in Chapter 6.

The daily Sirikit reservoir outflow ( $Q$ ) was the target output variable of the ML models. The selected input variables were the daily reservoir storage ( $S$ ), the daily reservoir inflow ( $I$ ) and the timing information in terms of month of the year ( $M$ ). The  $Q$ ,  $S$  and  $I$  variables represent the reservoir water balance components (Equation (6.1)), while the  $M$  variable reflects the seasonal downstream water demand and operating rules in the real-time reservoir operation function (referred to as  $D$  and  $R$  in Equation (1.2)). The daily  $S$  and  $Q$  data were obtained from in-situ observations (see Chapter 3; Section 3.1.3), while the daily  $I$  data were computed by the `wflow_sbm` model (Section 7.2.2). To simulate the Sirikit outflow at the current day ( $Q_t$ ), the input dataset consisted of the outflow from the previous day ( $Q_{t-1}$ ), the storage from the previous day ( $S_{t-1}$ ) and the inflows between the time lags and lead times of two days ( $I_{t-2}$ ,  $I_{t-1}$ ,  $I_t$ ,  $I_{t+1}$  and  $I_{t+2}$ ). This is coherent with previous findings that short-term forecasts are usually utilized in real-time reservoir operation (Nayak et al., 2018).

### 7.2.2 Simulating and reforecasting daily reservoir inflows with a process-based model

To simulate and reforecast the daily  $I$  data of the Sirikit reservoir, we used the distributed `wflow_sbm` model with seamless distributed parameter maps and global data. Full detail on the model setup and evaluation is provided in Chapter 4. The required meteorological input data for `wflow_sbm`, including precipitation ( $P$ ) and potential evapotranspiration ( $PET$ ), were obtained from global databases (see Chapter 3; Section 3.1.2). The MSWEP historical  $P$  data were used in the  $I$  simulation. The ECMWF forecast  $P$  data, which contain the deterministic (control) forecast and an ensemble of 10 probabilistic forecasts, were used in the  $I$  reforecasts. The forecasts are available on a daily basis at high spatial ( $\sim 3$  km) and temporal (6-hourly) resolutions. However, downloading the forecast data at such high resolutions is a very time-consuming task. Therefore, we attained the ECMWF forecast data that were updated twice a week (every three and four days). For example, if the first forecast would be on January 4<sup>th</sup>, 2004, the next forecasts would be on January 7<sup>th</sup>, 2004 (three days apart) and January 11<sup>th</sup>, 2004 (four days apart). Each forecast contains forecasting values for 11

days, including the current day and the next 10 days. For example, the forecast on January 4<sup>th</sup>, 2004 would contain the forecasting values of January 4<sup>th</sup>–14<sup>th</sup>, 2004. The earth2Observe historical *PET* data were used in both the *I* simulation and reforecasts. We acknowledge that the forecast *PET* data should be considered when applying the model in practice (Van Osnabrugge et al., 2019), but their influence on the modelled *I* results was assumed to be negligible in this study.

Since reliable in-situ *I* data of the Sirikit reservoir were not available, we validated the simulated *I* result by visually comparing the resemblance of its daily hydrograph to those of the upstream catchments, which are not affected by the dam. The reforecast *I* results were then compared with the simulated *I* result. We applied the mean absolute error (MAE) to evaluate the control *I* reforecast and the continuous ranked probability score (CRPS) to evaluate the ensemble *I* reforecasts. Details on the forecast skill criteria are provided in Chapter 3; Section 3.5.2. The simulated and reforecast *I* results for the years 2004–2013 were then used as one of the inputs for the ML models.

### 7.2.3 Simulating and reforecasting daily reservoir operation and outflows with data-driven models

To investigate the effectiveness and applicability of ML models for computing the daily Sirikit reservoir operation and *Q*, three popular neural network algorithms, RNN, LSTM and GRU, were applied and their performance was evaluated and compared. The modelling contained two phases, simulation and reforecasting. In the simulation phase, we used the three algorithms to learn and reconstruct the real-time operation and reproduce the historical daily *Q* time series of the Sirikit reservoir, using the in-situ *Q* and *S* data, the simulated *I* data, and *M* as inputs. The derived simulation models are called operation models. In the reforecasting phase, we then applied the reforecast *I* data to run the operation models to reforecast the daily *Q* in real-time.

For a fair comparison, we set up the RNN, LSTM and GRU algorithms with their simplest structures and parameterization. With the attempt to build operation models that are viable and convenient in real-time applications, model construction and parameterization were simplified. Despite model simplification, some hyper-parameters of the algorithms needed to be determined. In this study, we built the operation models using algorithms with three layers, including an input layer, a hidden (processing) layer and an output layer. The Backpropagation Through Time algorithm (Werbos, 1990) was used to train the models, and the Adaptive Moment Estimation (ADAM) algorithm (Kingma & Ba, 2014) was used as the learning algorithm. We chose the Mean Square Error (MSE) as the loss function, and the tanh and sigmoid functions as the activation functions. For each computing time step, previous inputs and outputs of the past seven days were fed back into the models to provide the recurrent information, according to the weekly cycle of the irrigation supply and hydropower generation (as previously indicated in Figure 6.5). Details on the hyper-parameters and functions of the RNN, LSTM and GRU models are shown in Table 7.1. The ML models were built and run within

Scenario	2004	2005	2006	2007	2008	2009	2010	2011	2012	2013
1										
2										
3										
4										
5										
6										
7										
8										
9										
10										

**Figure 7.2:** Ten training-testing scenarios for cross-validation of the RNN, LSTM and GRU simulation models. The training periods are indicated in pink and the testing periods are indicated in red.

the open-source machine learning frameworks in python (see more detail in Chapter 3; Section 3.4.6).

#### *Simulations with 10-fold cross-validation*

In general, an ML model requires training and testing. An ML model is built and trained on known data (training dataset) and tested against unknown data (testing dataset). In the simulation phase, we conducted cross-validation for each algorithm with 10 scenarios of different training and testing periods (see Figure 7.2). The purpose of cross-validation is to assess the robustness of the operation models to predict  $Q$  from new data in practice. With the available input data for the 10-year period of 2004–2013, we trained and tested the ML models with 80% (8 years) and 20% (2 years) of the input data, respectively. Apart from the different training-testing scenarios, we also trained and tested the ML models for two input conditions: with and without using the  $Q_{t-1}$  variable, in order to investigate its role in the model performance. Therefore, the outcome of the simulation phase was the 10 derived operation models for each algorithm and each input condition. The model performance was evaluated and compared using the Kling Gupta efficiency (Gupta et al., 2009), root mean square error (RMSE) and percent bias (PBIAS). More details on the simulation performance criteria are described in Chapter 3; Section 3.5.1.

#### *Multi-day reforecasting*

In the reforecasting phase, we selected the best operation model out of the 10 derived models from cross-validation for each ML algorithm. The selected operation models were then tested with the reforecast  $I$  data as inputs. In correspondence with the simulations, the past seven days were required for reforecasting the  $Q$  value at any given time step. In reality, these past data are available from observations ( $Q_{t-1}$  and  $S_{t-1}$ )



Table 7.1: Hyper-parameters of the RNN, LSTM and GRU models, and their values or methods used in this study.

Hyper-parameter	Value/method	Explanation
Number of hidden layers	1	A typical neural network consists of one input layer, one or more hidden (processing) layers and one output layer.
Number of neurons	64	A neuron (so-called perceptron/node) is a computational unit with weighted input connections, activation functions that configure inputs, and a weighted output connection.
Number of recurrent steps [day]	7	A recurrent neural network contains loops to feed the previous inputs and outputs back to the network and pass the information from one step to the next. The number of recurrent time steps indicates the number of steps back in time taken into account.
Initial learning rate	0.001	To train a neural network is to update the weights. How much the weights are updated in each epoch (iteration) is called the learning rate, usually ranging between 0 and 1. Smaller learning rates give smaller changes and require more epochs. Too small learning rates can cause the weight updating to get stuck, while too large learning rates can cause the model to converge too quickly to a suboptimal solution.
Activation function	tanh and sigmoid	The activation function defines how the weighted sum of the inputs is transformed into an output from the neuron(s) in a layer. The choice of activation function largely impacts the model's capability and performance, and different activation functions may be used in different parts of the model.
Kernel initializer	Glorot Uniform	The Kernel initializer statistically generates and distributes the weights to be used as the starting weights in the model training.
Optimizer	Adaptive Moment Estimation (ADAM)	The optimizer is a method used to change the internal parameters, including weights and learning rate, to reduce the error/loss and provide the most accurate results possible.
Loss function	Mean Square Error (MSE)	During the optimization, the error/loss for the current model state is repeatedly estimated using a loss function, so that the weights can be updated to reduce the error/loss on the next iteration.
Batch size	1	The batch size defines the number of samples the model takes before updating the internal parameters. At the end of the batch, the predictions are compared to the expected values and the loss is calculated. For the batch size of one sample, the learning algorithm is called stochastic gradient descent.
Number of epochs	100	The number of epochs defines the number of iterations the learning algorithm takes through the entire training dataset. An epoch contains one or more batches. Model training is a for-loop over the number of epochs. Within this for-loop is another nested for-loop that iterates over each batch of samples.

**Table 7.2:** Input data of the RNN, LSTM and GRU models in the real-time reforecasting scenario. They consist of reservoir outflow from the previous day ( $Q_{t-1}$ ), reservoir storage from the previous day ( $S_{t-1}$ ) and reservoir inflows between the time lags and lead times of two days ( $I_{t-2}$ ,  $I_{t-1}$ ,  $I_t$ ,  $I_{t+1}$  and  $I_{t+2}$ ). O refers to observed data, S to simulated data, C to real-time calculated data and F to real-time reforecast data. Note that in the baseline reforecasting scenario, the  $Q_{t-1}$  and  $S_{t-1}$  data for all time steps were obtained from observations. Recurrent inputs refer to previous inputs that are fed back to the network for output calculation. In this case, inputs of the previous seven days are taken into account to calculate the current output.

Input time step	Reforecast lead time	Inputs						
		$Q_{t-1}$	$S_{t-1}$	$I_{t-2}$	$I_{t-1}$	$I_t$	$I_{t+1}$	$I_{t+2}$
-7	Recurrent input	O	O	S	S	S	S	S
-6	Recurrent input	O	O	S	S	S	S	S
-5	Recurrent input	O	O	S	S	S	S	S
-4	Recurrent input	O	O	S	S	S	S	S
-3	Recurrent input	O	O	S	S	S	S	S
-2	Recurrent input	O	O	S	S	S	S	F
-1	Recurrent input	O	O	S	S	S	F	F
0	0	O	O	S	S	F	F	F
1	1	F	C	S	F	F	F	F
2	2	F	C	F	F	F	F	F
3	3	F	C	F	F	F	F	F
4	4	F	C	F	F	F	F	F
5	5	F	C	F	F	F	F	F
6	6	F	C	F	F	F	F	F
7	7	F	C	F	F	F	F	F
8	8	F	C	F	F	F	F	F
9	Future I input	F	C	F	F	F	F	F
10	Future I input	F	C	F	F	F	F	F

and simulations ( $I_{t-2}$ ,  $I_{t-1}$  and  $I_t$ ) for the  $Q$  reforecast of the current day. Therefore, the observed and simulated input data of the past seven days were used at the start of each reforecast. In addition, input data of the next two days were also used as the future inputs ( $I_{t+1}$  and  $I_{t+2}$ ). As a result, with each reforecast  $I$  input of 11 days (the current day and the next 10 days), each ML model resulted in a 9-day  $Q$  reforecast (the current day and the 8-day lead times).

Two types of  $Q$  reforecasts were obtained based on the reforecast  $I$  inputs: the deterministic (control) reforecast and the ensemble of 10 probabilistic reforecasts. Moreover, the  $Q$  reforecasts were conducted in two scenarios: baseline and real-time. In the baseline reforecasting, the operation models were run with the reforecast  $I$  data and the observed  $S$  and  $Q$  data. In the real-time reforecasting, the models were run with the reforecast  $I$  data, but instead of using the observed  $S$  and  $Q$  data, their real-time reforecast values were updated and used at each computing time step. This updating process was carried out in two steps. First, the reforecast  $Q$  value at the previous time step was fed back into the input dataset, replacing the observed  $Q$  value. Then, the  $S$  value was calculated based on the reservoir water balance (Equation (6.1)), replacing the

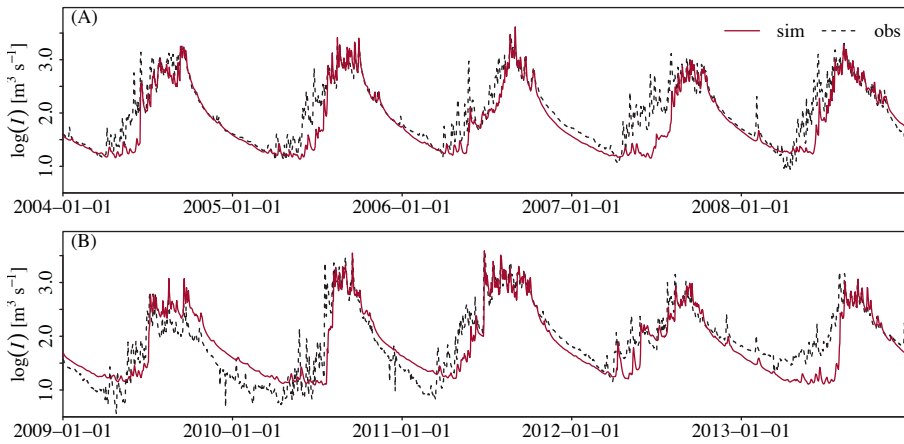


**Figure 7.3:** Simulated daily inflow ( $I$ ) of the Sirikit reservoir by the wflow\_sbm model compared to observed daily streamflow from a catchment upstream of the reservoir for the entire study period of 2004–2013. Note that reliable observed inflow data were not available for validation. For clear visualization and interpretation of both low flow and high flow simulations, the inflow result is presented on a logarithmic scale and is separated into the years 2004–2008 (Panel (A)) and 2009–2013 (panel (B)).

observed  $S$  value. These real-time  $S$  and  $Q$  updates allowed distinguishing the roles of reforecast and observed input data, and assessing the actual capability of the ML models in practice. The use of input data in the real-time reforecasting scenario is clarified in Table 7.2. Consistently with the evaluation of the reforecast  $I$  data, two criteria were applied to assess the forecast skill of the ML models: MAE for the control reforecasts and CRPS for the ensemble reforecasts.

## 7.3 Results

### 7.3.1 Simulated and reforecast daily Sirikit reservoir inflows by the wflow\_sbm model

#### *Simulated reservoir inflow*

The simulated daily inflow ( $I_{\text{sim}}$ ) of the Sirikit reservoir by the wflow\_sbm model could not be thoroughly evaluated due to the lack of reliable in-situ observations. However, visual comparison of  $I_{\text{sim}}$  to the observed daily streamflow of the catchment upstream of the Sirikit reservoir for the entire study period of 2004–2013 suggests a satisfactory result produced by the wflow\_sbm model (Figure 7.3). The daily  $I_{\text{sim}}$  hydrograph (solid red line) presents the seasonal and multi-annual variability in terms of both magnitude and timing, corresponding to the hydrograph for the upstream catchment (dashed black

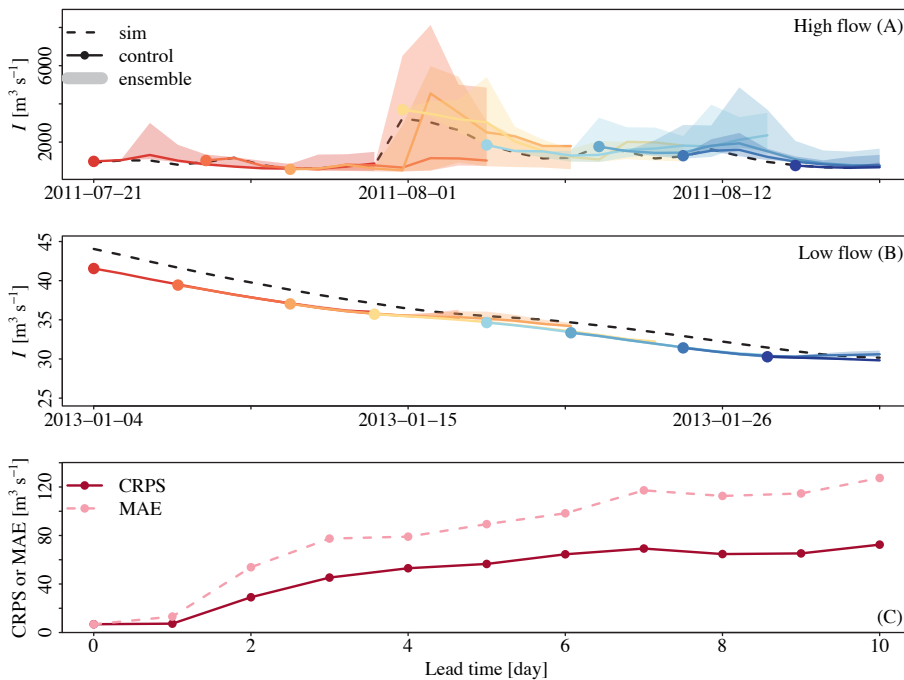


**Figure 7.4:** Reforecast daily inflow ( $I$ ) of the Sirikit reservoir by the `wflow_sbm` model compared to the simulation. The reforecasts were conducted every three and four days, of which the starting days are indicated by colored points. The reforecasts include the control reforecast (solid colored lines) and the range of ensemble reforecasts (colored bands) compared to the simulated  $I$  data (dashed black line). Panel (A) shows the high flow reforecasts during the wet season, while panel (B) shows the low flow reforecasts during the dry season. Panel (C) indicates the forecast errors for the current day up to the 10-day lead times, including the mean absolute error (MAE) of the control  $I$  reforecast and the continuous ranked probability score (CRPS) of the ensemble  $I$  reforecasts. The errors were computed over the entire study period of 2004–2013.

line). The  $I_{\text{sim}}$  hydrograph shows better correspondence to the upstream hydrograph, with more accurate recession time in normal years (e.g., 2004) than in wet years (e.g., 2006 and 2011) and dry years (e.g., 2009, 2010 and 2013). The `wflow_sbm` model simulates low flows well in normal years, but under- or overestimates them in dry years. The model estimates peak flows during August–October well, but high flows at the start of the wet season (May–July) are not captured or are somewhat underestimated. The  $I_{\text{sim}}$  values slightly lag the observations. Nonetheless, the result suggests that the `wflow_sbm` model can reconstruct the daily Sirikit reservoir inflow to some extent.

### *Reforecast reservoir inflows*

Figure 7.4 illustrates the reforecast daily inflows of the Sirikit reservoir by the wflow\_sbm model. The results include the deterministic (control) reforecast ( $I_{\text{control}}$ ) and the ensemble reforecasts ( $I_{\text{ensemble}}$ ) with 10-day lead times in comparison to the  $I_{\text{sim}}$  data. Overall, the reforecast errors per lead time (Figure 7.4(C)) indicate that both  $I_{\text{control}}$  and  $I_{\text{ensemble}}$  values agree well with the  $I_{\text{sim}}$  value for the current day and the next day. The forecast skill gradually deteriorates from a lead time of 1 day (MAE =  $13 \text{ m}^3 \text{ s}^{-1}$  and CRPS =  $7 \text{ m}^3 \text{ s}^{-1}$ ) to a lead time of 10 days (MAE =  $127 \text{ m}^3 \text{ s}^{-1}$  and CRPS =  $72 \text{ m}^3 \text{ s}^{-1}$ ).

Hydrograph examples of the inflow reforecasts during the wet season (Figure 7.4(A)) and during the dry season (Figure 7.4(B)) demonstrate the difference in forecast skill between high and low flow conditions. In the wet season (May–October), the inflow is continuously high and fluctuating due to the monsoon storms. Consequently, both  $I_{\text{control}}$  and  $I_{\text{ensemble}}$  show relatively large errors with broad uncertainty ranges and simulated flows tend to be overestimated after a lead time of 2 days. In the dry season (November–April), on the other hand, the inflow remains low and steady, resulting in small errors and uncertainties in  $I_{\text{control}}$  and  $I_{\text{ensemble}}$  throughout the 10-day lead times although simulated flows tend to be underestimated.

### **7.3.2 Simulated and reforecast daily Sirikit reservoir outflows by the machine learning models**

#### *Simulated reservoir outflows*

Hydrograph examples of simulated daily outflow ( $Q_{\text{sim}}$ ) of the Sirikit reservoir by the RNN, LSTM and GRU operation models for the testing periods are displayed in Figure 7.5, including the results in the different training-testing scenarios and different input conditions (with and without the  $Q_{t-1}$  variable). Distributions and uncertainties of the simulation performance for each model in the cross-validation are indicated with the KGE, RMSE and PBIAS values in Figure 7.6. Overall, Figure 7.5 shows that the daily  $Q_{\text{sim}}$  time series produced by RNN, LSTM and GRU are good. Figure 7.6 further reveals that the simulation accuracy of the three models is higher in the training periods (plain boxes) than in the testing periods (striped boxes). The performances of the three models are similar for the same scenario and vary amongst the different scenarios. However, GRU tends to have the smallest error in model performance in both training and testing and across the cross-validation scenarios (see also Table C.1–C.3 in Appendix C).

The effect of different training-testing periods on the simulation performance of the RNN, LSTM and GRU models is evident from Figure 7.5. The testing period of scenario 3 (years 2004–2005; left panel) includes normal and dry years, while the testing period of scenario 10 (years 2011–2012; middle panel) includes exceptionally wet years, and the testing period of scenario 1 (years 2012–2013; right panel) includes wet and normal years. In scenario 3, the  $Q_{\text{sim}}$  result is satisfactory for all three models (highest KGE =

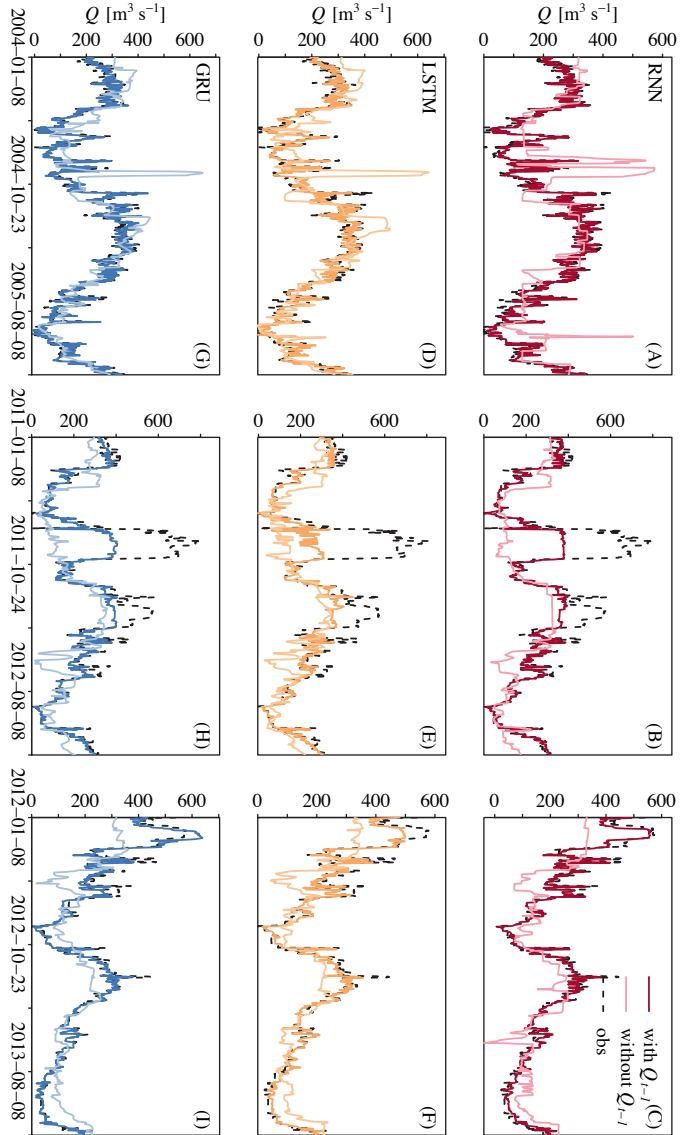


**Figure 7.5:** Simulated daily outflow ( $Q$ ) for the testing periods of the Shikot reservoir by RNN (first row), LSTM (middle row) and GRU (last row) compared to observations. The  $Q$  simulations are compared between three scenarios with different outflow conditions: scenario 3 (left panel) in the years 2004–2005, which are normal and dry years; scenario 10 (middle panel) in the years 2011–2012, which are extremely wet years and scenario 1 (right panel) in the years 2012–2013, which are wet and normal years. The  $Q$  simulations with the  $Q_{t-1}$  input (solid dark-colored line) are compared to the  $Q$  simulations without the  $Q_{t-1}$  input (solid light-colored line) and observations (dashed black lines).

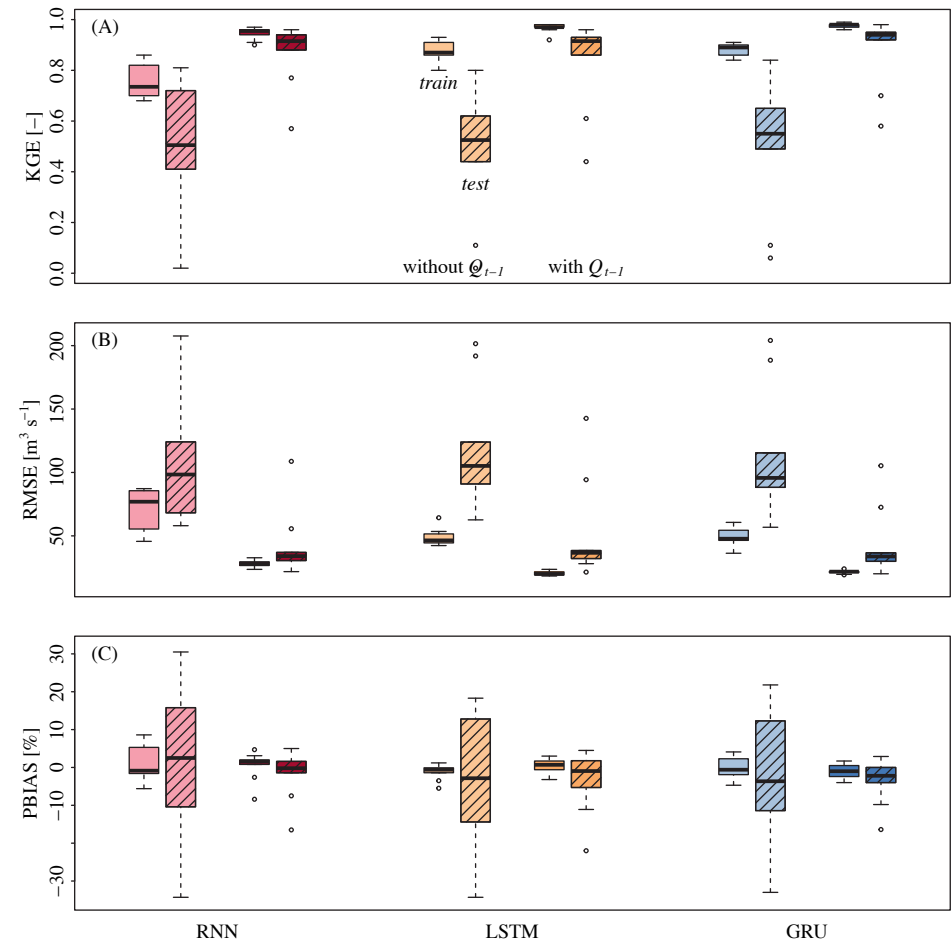


**Figure 7.6:** Performance of RNN, LSTM and GRU with regards to simulating the Sirikit reservoir outflow in the cross-validation. The criteria include KGE (panel (A)), RMSE (panel (B)) and PBIAS (panel (C)). Each box presents the performance distribution over the 10 training or testing periods (thus 10 criteria values). The performance during the training periods is indicated in plain boxes and during the testing periods in striped boxes. For each model, the performance of the simulations without  $Q_{t-1}$  as input is shown in light color, while the performance of the simulations with  $Q_{t-1}$  is shown in dark color. The actual KGE, RMSE and PBIAS values are provided in Table C.1–C.3 in Appendix C.

0.94 for GRU with  $Q_{t-1}$  input), with some overestimation (highest PBIAS = 16 for RNN without  $Q_{t-1}$  input). Meanwhile, in scenario 10, the unusual  $Q_{\text{sim}}$  peaks in both 2011 and 2012 are notably underestimated (highest PBIAS = -34 for RNN and LSTM without  $Q_{t-1}$  input). This is because such high outflow events were not present in the training data of scenario 10, and thus the models could not learn and reproduce the emergency operations that occurred in the testing period. In scenario 1, the  $Q_{\text{sim}}$  peaks in 2012 show significant improvement compared to those in scenario 10. This is due to the presence of the extreme year 2011 in the training data, leading to the models' ability to recognize and compute similar emergency operations during the year 2012 in the testing period. Consequently, the model results in scenario 1 (highest KGE = 0.96 for GRU with  $Q_{t-1}$  input) are more accurate than in scenario 10 (highest KGE = 0.58 for GRU with  $Q_{t-1}$  input).

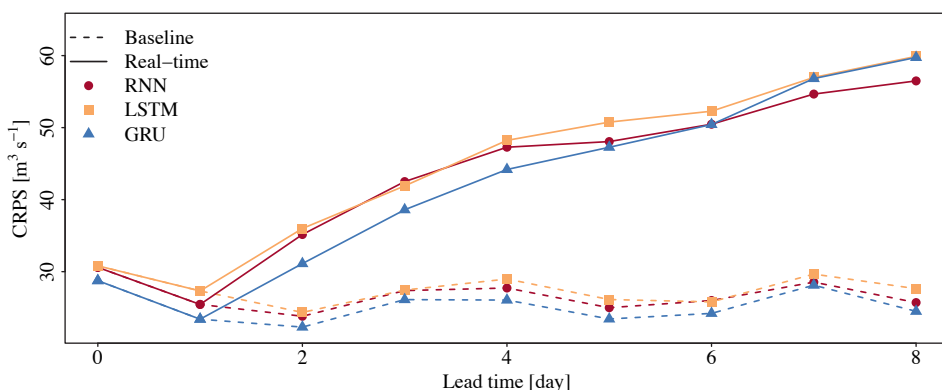
The effect of the  $Q_{t-1}$  variable as one of the inputs on the simulation performance of the RNN, LSTM and GRU models is also clearly visible in Figure 7.5. Without the  $Q_{t-1}$  input,  $Q_{\text{sim}}$  (solid light-colored lines) shows both inferior overestimations in normal and dry years (e.g. in October 2004 in scenario 3; left panel) and underestimation in wet years (e.g. in October 2011 in scenario 10; middle panel). The addition of  $Q_{t-1}$  improves the accuracy of  $Q_{\text{sim}}$  (solid dark-colored lines). This is especially the case for normal and dry years (e.g., scenario 3). The unusual peak releases in wet years are better captured, but still not accurate (e.g., scenario 10). With both the proper training data (covering all outflow conditions) and the  $Q_{t-1}$  input, the  $Q_{\text{sim}}$  results are remarkably improved (e.g., solid dark colored lines in scenario 1; right panel).

Figure 7.6 demonstrates that adding  $Q_{t-1}$  benefits the simulations in both training and testing periods, in all 10 training-testing scenarios and for all three models. During the testing periods, the KGE values for  $Q_{\text{sim}}$  with  $Q_{t-1}$  as an input improve with 0.13 to 0.75, RMSE with 32 to 133  $\text{m}^3 \text{s}^{-1}$  and PBIAS with 0.4 to 23%. RNN shows the largest improvement, followed by GRU and LSTM. The model performance tends to improve more in the scenarios where very wet years (i.e., 2006 or 2011) are present in the testing periods (i.e., scenarios 5, 9 and 10). The simulation results suggest that the RNN, LSTM and GRU operation models with the  $Q_{t-1}$  input in scenario 1 provide the most accurate results and the most robust performance for both regular and extreme outflows, and thus they were further applied in the reforecasting phase. The suitability of using the  $Q_{t-1}$  input in the model application in practice is discussed in Section 7.4.2.

#### *Reforecast reservoir outflows*

To test and evaluate the RNN, LSTM and GRU models in the reforecasting phase, the derived operation models (with the  $Q_{t-1}$  input in scenario 1) were run with the reforecast input data for the test period of 2012–2013. The reforecast daily outflow results include the control forecast ( $Q_{\text{control}}$ ) and the ensemble forecasts ( $Q_{\text{ensemble}}$ ) every three and four days (according to the reforecast  $I$  input data). Figure 7.7 presents the ensemble reforecast skills of the RNN, LSTM and GRU models, indicated by the CRPS values,





**Figure 7.7:** Overall performance of RNN, LSTM and GRU with respect to reforecasting the Sirikit reservoir outflow with lead time. The forecast skill is indicated with the continuous ranked probability score (CRPS) of the ensemble reforecasts from the current day to the next 8 days. The results from the baseline reforecasting scenario (dashed lines) and the real-time reforecasting scenario (solid lines) are compared. The mean absolute error (MAE) values of the control reforecast are almost identical to the CRPS values, and thus they are not shown.

with respect to the 8-day lead times. Since the MAE values of the control reforecasts are almost identical to the CRPS values, they are not presented here. The model results are compared between the baseline reforecasting scenario, which uses the  $Q_{t-1}$  and  $S_{t-1}$  input data obtained from observations, and the real-time reforecasting scenario, which comprises real-time calculation and updating of the  $Q_{t-1}$  and  $S_{t-1}$  input data for each time step of the  $Q_t$  reforecast (see Section 7.2.3). Although the baseline scenario is considered to be unrealistic in practice (because the observed input data are not available for multi-day forecasting), it can be used to identify the effect of the  $I_{\text{control}}$  and  $I_{\text{ensemble}}$  input data on the  $Q_{\text{control}}$  and  $Q_{\text{ensemble}}$  results.

Overall, RNN, LSTM and GRU deliver similar  $Q_{\text{ensemble}}$  results at each lead time. The differences between the model results occur mainly during extreme outflow periods (see also hydrographs of the years 2012–2013 per lead time in Figures C.1 and C.2 in Appendix C). Figure 7.7 indicates that the CRPS values of the three models in the baseline scenario (dashed lines) remain within a small range ( $22\text{--}31 \text{ m}^3 \text{ s}^{-1}$ ) over the 8-day lead times. The CRPS values are higher in the real-time scenarios (solid lines) as the real-time calculation and updating of the  $Q_{t-1}$  and  $S_{t-1}$  introduce error and uncertainty in the input data, and thus in the  $Q_{\text{ensemble}}$  results. In this scenario, the three models show a comparable increasing trend in errors with lead time. The models deliver the best performance on the current day and the next day, and their forecast skills gradually decrease with longer lead times. The errors gradually increase from the 2-day lead time ( $\sim 35 \text{ m}^3 \text{ s}^{-1}$ ) to the 8-day lead time ( $\sim 60 \text{ m}^3 \text{ s}^{-1}$ ). Note that for the reforecasts on the current day and the 1-day lead time, the  $Q_{t-1}$  and  $S_{t-1}$  values are

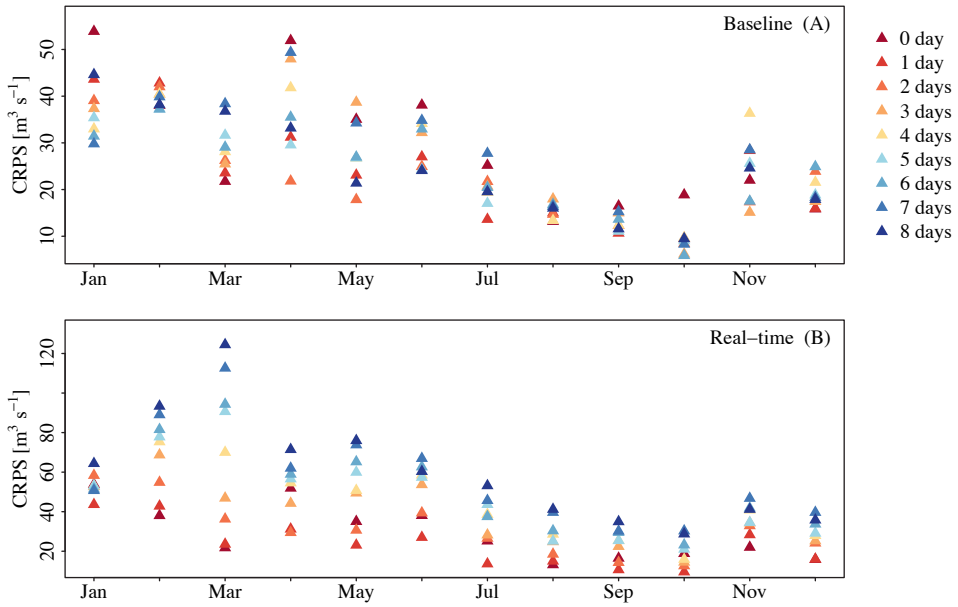


**Figure 7.8:** Performance of GRU with respect to reforecasting the Sirikit reservoir outflow with lead time as a function of the month of the year. The average values per month of the continuous ranked probability score (CRPS) of the ensemble reforecasts are shown in different colors for each lead time. The results are compared between the baseline reforecasting scenario (panel (A)) and the real-time reforecasting scenario (panel (B)). The CRPS values of RNN and LSTM are similar to the CRPS values of GRU, and thus they are excluded.

available from observations and were used as inputs, and thus the CRPS values on these two days are identical between the real-time and baseline scenarios. In both scenarios, GRU (indicated in blue triangles) tends to have the smallest errors, while LSTM (orange squares) shows the largest errors for all lead times. Although GRU is outperformed by RNN (red circles) from lead times of 7 days, the results indicate that GRU is likely the most accurate and robust reforecasting model, especially in the real-time scenario.

Figure 7.8 shows the variation in the  $Q_{\text{ensemble}}$  reforecast skill of GRU as a function of the month of the year. As can be seen, the pattern of the performance variation is more apparent in the real-time scenario (panel (B)) than in the baseline scenario (panel (C)). This indicates the clear role of the real-time  $Q_{t-1}$  and  $S_{t-1}$  input updates on the  $Q_{\text{ensemble}}$  results. Overall, the reforecast errors at all lead times tend to be larger in the dry season (November–April) than in the wet season (May–October). The decrease in forecast skill between lead times is also more rapid in the dry season, especially for February and March in the real-time scenario. The most accurate  $Q_{\text{ensemble}}$  reforecasts are likely to be in October, while the least accurate tend to take place in March.

To take a closer look at the  $Q_{\text{control}}$  and  $Q_{\text{ensemble}}$  results produced by the RNN, LSTM and

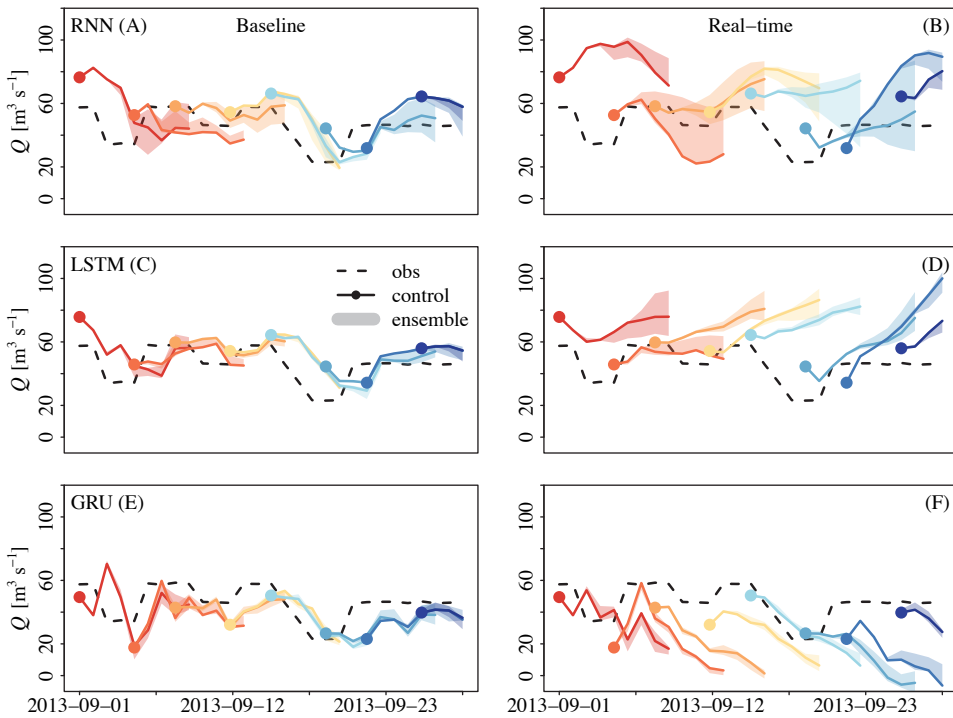


**Figure 7.9:** Reforecast daily outflow ( $Q$ ) of the Sirikit reservoir by RNN (first row), LSTM (middle row) and GRU (last row) during the wet season. The reforecasts were conducted every three and four days, of which the starting days are indicated by colored points. The reforecasts include the control reforecast (solid colored lines) and the range of ensemble reforecasts (colored bands) in comparison to the observations (dashed black line). The left panels show the results in the baseline reforecasting scenario, while the right panels show the results in the real-time reforecasting scenario.

GRU models, the daily hydrographs are shown with examples for the wet season (Figure 7.9), the dry season (Figure 7.10) and the flood period (Figure 7.11). In principle, the magnitude of the reservoir outflow is opposite to the inflow. In the wet season, the outflow generally remains low to store rain and flood water. Figure 7.9 shows that the performance of the three models with respect to reforecasting the low outflow during the wet season is relatively poor, consistent with Figure 7.8. Both the  $Q_{\text{control}}$  and  $Q_{\text{ensemble}}$  from all models show a delay of 2–3 days in the baseline scenario compared to the observations. The model performance significantly deteriorates in the real-time scenario, with increasing uncertainty from lead times of 3 to 4 days. While RNN and LSTM tend to overestimate  $Q_{\text{control}}$  and  $Q_{\text{ensemble}}$  for longer lead times, GRU tends to underestimate them and produces a few unrealistic negative values for longer lead times (Figure 7.9(F)).

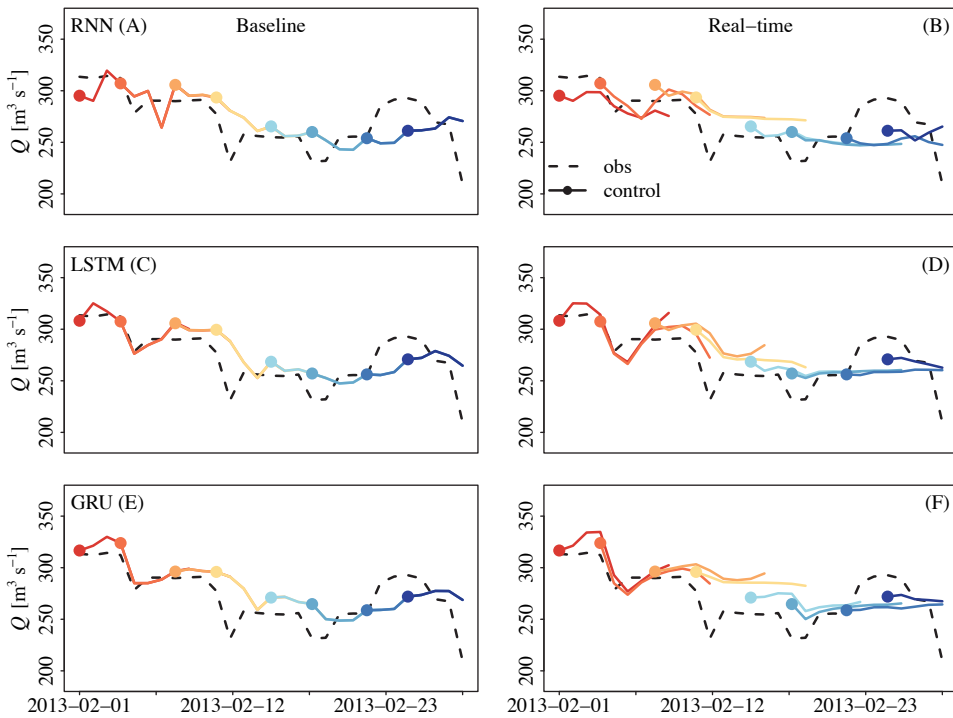


**Figure 7.10:** Reforecast daily outflow ( $Q$ ) of the Sirikit reservoir by RNN (first row), LSTM (middle row) and GRU (last row) during the dry season. The figure set-up is the same as explained in Figure 7.9. Since the 10 probabilistic  $Q$  reforecasts are almost identical, the ensemble reforecast bands are not visible.

Figure 7.10 confirms that the three models perform better in the dry season when the reservoir outflow is typically high due to the high demands for irrigation supply and downstream consumption. Since the 10 probabilistic forecast values are almost identical during high outflow periods, the ranges of  $Q_{\text{ensemble}}$  are not visible in the figure. The model performance for the baseline and real-time scenarios is comparable, implying the small role of real-time calculation and updating of the  $Q_{t-1}$  and  $S_{t-1}$  input data on the reforecasting result during high outflow periods (as also evident in Figure 7.8). The performance of the RNN, LSTM and GRU models remains stable until lead times of 6 to 7 days.

While Figure 7.10 indicates that the reservoir outflow in the dry season is generally high and stable, exceptions were found in some years. An example is January and February 2012, which was the end of the historical 2011 flood event. During that period, the Sirikit reservoir had to release the excess water that was over-stored during the recent floods, resulting in an uncommonly high outflow (see also Figures C.1 and C.2). Figure 7.11 shows the performance of the three models in reforecasting such an unusual oper-

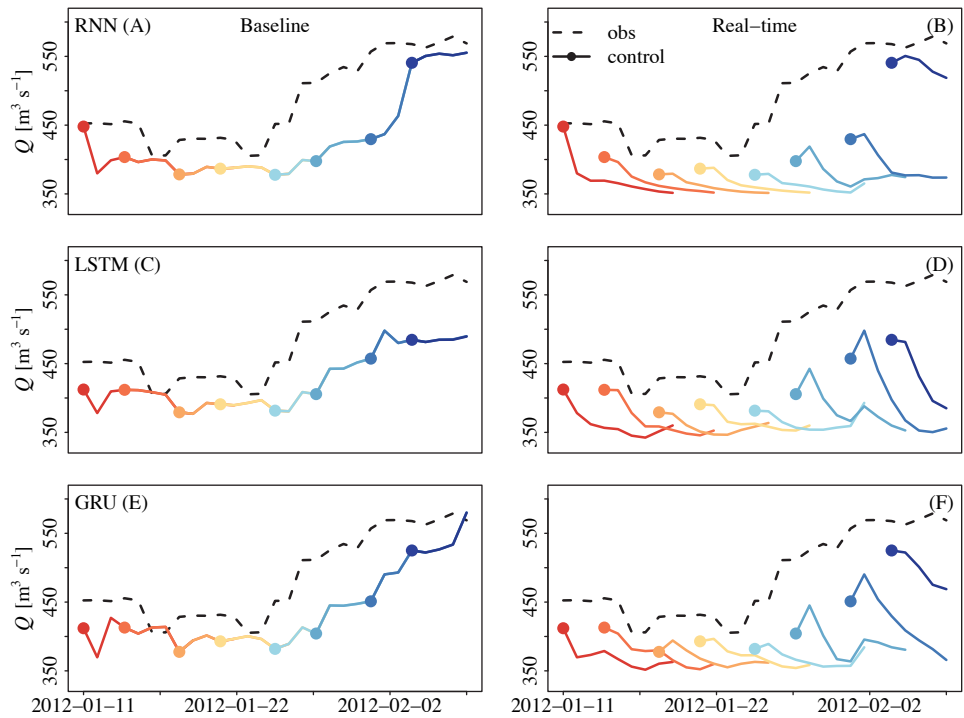


**Figure 7.11:** Reforecast daily outflow ( $Q$ ) of the Sirikit reservoir by RNN (first row), LSTM (middle row) and GRU (last row) during the flood period. The figure set-up is the same as explained in Figure 7.9. Since the 10 probabilistic  $Q$  reforecasts are almost identical, the ensemble reforecast bands are not visible.

ation and outflow in January 2012. It is clear that the models underestimate the  $Q_{\text{control}}$  at all lead times in both the baseline and the real-time scenario. Similar to the reforecast results of the high outflow in the dry season (Figure 7.10), the  $Q_{\text{ensemble}}$  values are almost identical. In the real-time scenario, the errors notably increase from a lead time of 2 days. GRU provides the best performance, followed by LSTM and RNN.

## 7.4 Discussion

### 7.4.1 Daily reservoir inflow modelling with the wflow\_sbm model

#### *Reservoir inflow simulation*

Overall, the wflow\_sbm model can reconstruct the historical inflow of the Sirikit reservoir at the daily timescale. Absences of some peak flows at the start of the wet seasons in the simulated inflow (Figure 7.3) can be caused by the use of global historical (MSWEP)

precipitation data, which neglect some local storm events (as previously discussed in Chapter 4, Section 4.4.1). The too fast or too slow falling limbs of hydrographs in some extreme years can be due to the model setup using global parameterization instead of calibration (Section 4.2.1). We acknowledge that using in-situ meteorological observations and calibrating model parameters may improve the simulated inflow accuracy, although this is not guaranteed. Previous studies of Jamrussri & Toda (2017) and Yang et al. (2019) showed that the Sirikit inflow simulations with calibrated SWAT and GBHM models forced with in-situ observed meteorological data could not capture the early-season peak flows either.

#### *Reservoir inflow reforecasts*

The wflow\_sbm model with the global forecast (ECMWF) precipitation data can also provide daily inflow reforecasts of the Sirikit reservoir, despite the tendency to overestimate high flows in the wet season and underestimate low flows in the dry season as compared to the simulation result (Figure 7.4). Both the deterministic (control) reforecast and ensemble reforecasts correspond to simulated inflows more in the dry season than in the wet season. In the dry season, the inflow reforecasts correspond to simulated inflows well at all 10-day lead times (Figure 7.4(B)). In the wet season, the error of the inflow reforecasts noticeably increases with lead time (Figure 7.4(A)). Considering the purpose of using inflow data as input of the ML models, we conclude that inflow forecasts are most accurate on the current day and the next day (with overall CRPS values lower than  $7 \text{ m}^3 \text{ s}^{-1}$ ) and are acceptable until a lead time of 5 days (with CRPS lower than  $50 \text{ m}^3 \text{ s}^{-1}$ ; Figure 7.4(C)).

Although the capability of the wflow\_sbm model for real-time reservoir inflow reforecasting in this study is limited by global data and parameterization, we suggest that the reservoir inflow reforecasts can still be improved in the future with (i) precipitation correction and (ii) inflow correction. The study of Nanda et al. (2019) suggested that the ECMWF precipitation forecasts are associated with some biases, and thus their errors should be systematically updated when used in any hydrological model for real-time operation and forecasting. Moreover, errors in the tropics may be significant since processes like convection are parameterized and not resolved (Jung et al., 2010). Therefore, correcting the precipitation ensembles before using them to run the wflow\_sbm model can reduce the model forcing biases and thus their propagation to the streamflow ensembles. Precipitation biases that are unconditional in nature can be easily corrected, while resolving conditional biases is more challenging and varies with forecast lead time, data amount, and temporal and spatial scales (Verkade et al., 2013; Schauwecker et al., 2021). Since precipitation correction is inherently intensive and difficult, it is advised to consider streamflow correction instead (Verkade et al., 2013). In principle, the reservoir inflow ensembles can be corrected or better fit with several methods, such as bias correction (Hashino et al., 2007), multi-model combination (Chen et al., 2015) and data assimilation (Liu et al., 2012). However, additional measurements would be

required, which were not available in this study.

#### 7.4.2 Daily reservoir operation and outflow modelling with the machine learning models

##### *Effects of selected input variables on model performance*

This study reveals the effects of certain input variables, including reservoir outflow at the previous time step ( $Q_{t-1}$ ), storage at the previous time step ( $S_{t-1}$ ), and inflow between the time lags and lead times of two days ( $I_{(t-2)}-I_{(t+2)}$ ), for the ML models to estimate the Sirikit reservoir outflow, especially for the multi-day reforecasts. Overall, the results indicate that (i) including  $Q_{t-1}$  can effectively improve model performance, (ii) the  $Q_{t-1}$  and  $S_{t-1}$  inputs have a stronger effect on the model performance for the low outflow estimation in the wet season than the  $I$  inputs and (iii) the  $Q_{t-1}$  and  $S_{t-1}$  inputs have a weaker effect for the high outflow estimation in the dry season and during flood events.

Including  $Q_{t-1}$  as input of ML models to compute the outflow at the current time step ( $Q_t$ ) significantly increases the resulting accuracy (Figures 7.5 and 7.6), but it can be controversial. On the one hand, it can be claimed that the actual ability of the ML models cannot be clearly specified when using the  $Q_{t-1}$  as an input, since the input and output values of the models are highly correlated. On the other hand, it can be argued that the addition of  $Q_{t-1}$  can essentially account for the operators' decisions on a daily basis, which have been the main issue in real-time reservoir operation modelling for a long time. Several studies have applied the  $Q_{t-1}$  input and achieved excellent ML model performance (e.g., Chen et al., 2018; Zhang et al., 2018a, 2019; He et al., 2021; Hong et al., 2021). In reality, however, using the  $Q_{t-1}$  input is only logical and useful when the  $Q_{t-1}$  data are obtained from prediction instead of observations, considering that the observed  $Q_{t-1}$  data are not available in the case of multi-day outflow forecasting. A realistic application was conducted in this study. In the real-time reforecasting scenario, we fed the reforecast  $Q_{t-1}$  value back into the input dataset and calculated the  $S_{t-1}$  value (based on the reservoir water balance) at each computing step to update the inputs in real-time and reforecast the  $Q_t$  value. Based on this finding, we suggest to implement the real-time calculation and updating of the  $Q_{t-1}$  and  $S_{t-1}$  input data to maximize the applicability of the ML models for real-time and multi-day outflow reforecasting.

Together, the  $Q_{t-1}$  and  $S_{t-1}$  inputs significantly affect the model performance for low outflow estimation in the wet season (May–October). This is deduced from the significant difference in the outflow results (Figures 7.9) and reforecast skills (Figures 7.8) between the baseline and real-time reforecasting scenarios. The decreasing model performance when the  $Q_{t-1}$  and  $S_{t-1}$  input data are calculated and updated in real-time instead of being taken from observations suggests that larger errors in the  $Q_{t-1}$  and  $S_{t-1}$  values lead to larger errors and higher uncertainty in the outflow reforecasts, especially at longer lead times. This indicates that, while the outflow in the wet season tends to

remain low, real-time reservoir operation is strongly influenced by the amount of water stored in the reservoir. This is because the reservoir operators must continuously and carefully consider the reservoir water level throughout the wet season in order to ensure that the outflow does not cause or magnify downstream flooding, while the storage capacity is not exceeded by rainwater. In contrast, the  $Q_{t-1}$  and  $S_{t-1}$  inputs have less influence on the high outflow estimation in the dry season (November–April) and during flood events, as inferred by the small difference in the outflow results (Figures 7.10 and 7.11) and reforecast skills (Figures 7.8) between the baseline and real-time reforecasting scenarios. This indicates that the high outflow operation is more subject to the reservoir operating rules than to the abrupt real-time decisions.

#### *Machine learning model setup*

For a fair comparison and the viability and convenience of the ML model applications in practice, the RNN, LSTM and GRU operation models were built with their simplest structures and parameterization. This means the models contained three layers (an input layer, a processing layer and an output layer) with 64 neurons and their hyperparameters were set at default (Table 7.1). The models were trained with 100 training iterations. Although increasing the number of processing layers increases the depth, and thus the complexity, of the models, this does not necessarily improve model performance. Therefore, one processing layer is the most common choice (Park & Sandberg, 1991). In streamflow modelling particularly, Zhang et al. (2019) found that the number of iterations has more effect than the number of neurons. Hence, for model applications in reality, we recommend training models with more iterations. However, one should carefully take into account the computational time, which in turn may reduce model viability and convenience, especially the real-time and continuous application.

#### *Daily reservoir outflow reforecasts with different models*

Although the exact operation mechanism that was learned by RNN, LSTM and GRU remains unknown due to their black-box nature, the three models can reconstruct the real-time operation of the Sirikit reservoir with the selected input data. As a result, the simulated outflow is highly accurate (Figures 7.5 and Figures 7.7). Despite similar performances amongst the three models, we conclude that GRU provides the best operation model in this study. GRU is not only the most accurate model, but also the most effective model in practice. This is due to its structure, which is less complex than RNN and LSTM and comes with fewer parameters. Hence, it is less at risk of overparameterization and more robust to new data, while requiring less modelling time. The result of this study is consistent with the study of Guo et al. (2021), which also proposed GRU over LSTM for reservoir inflow reforecasting. However, GRU has the drawback of producing unrealistic negative values at times (Figures 7.8). This issue is expected to be resolved with more training data, as indicated by the study of Zhang et al. (2019).



*Daily reservoir outflow reforecasts with different lead times*

Based on the findings of this study (Figures 7.7–7.11), we conclude that RNN, LSTM and GRU are capable of multi-day reforecasting the daily outflow of the Sirikit reservoir. The delay in the reforecast results increases with lead time, which is mainly caused by (i) the 1–2 day delayed reservoir inflow and (ii) errors introduced by the real-time calculation and updating of the  $Q_{t-1}$  and  $S_{t-1}$  inputs, which also occurred in the study of Yang et al. (2019). The forecast skill is subject to seasonality, given the most useful reforecast on the current day up to 2-day lead times for low flows (wet season) and up to 6–7 days for high flows (dry season and flood periods).

*Opportunities for model improvement*

There are opportunities to improve the operation models apart from a more complex model setup (as previously explained). The improvement can be done via input data, model training and model post-processing.

1. In reality, real-time operation, especially for multi-purpose reservoirs, may not only depend on historical data, experience and short-term forecast data, but also longer-term forecasts, such as seasonal and multi-annual inflow forecasts. In many cases, reservoir operators use these long-term forecast data to plan and manage the outflow, considering the water availability predicted for the coming season, the next year or the longer term (Long et al., 2019; Kompor et al., 2020). Therefore, to further improve the performance of the operation models, future studies may assess the use of such long-term data as additional inputs for the models.
2. The cross-validation addresses the model sensitivity to the input dataset (Figures 7.5 and Figures 7.7). It highlights the importance of the inclusion and frequency of the data in both regular and extreme conditions during model training as they significantly affect the accuracy and robustness of the models. Therefore, to apply the operation models in practice, we strongly suggest to re-train the models with the addition of recent data annually.
3. Applying operation models with an ensemble modelling approach, which takes into account several trained ML models and weighs the output, can provide a more practical, robust and reliable model (e.g., Khalaf et al., 2020; Zuo et al., 2020; Li et al., 2021). However, this approach is considered state-of-the-art in hydrological modelling, and its advantages and disadvantages in real-time reservoir operation modelling should still be further explored.
4. Data assimilation is highly recommended for the application of reservoir operation models in real-time. It is expected to improve the forecast skill in terms of both magnitude and timing, especially the reforecast delay, which currently increases with lead time.

## 7.5 Conclusion and outlook

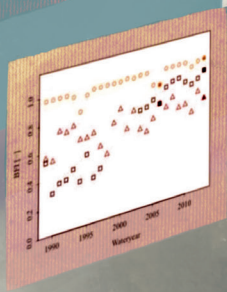
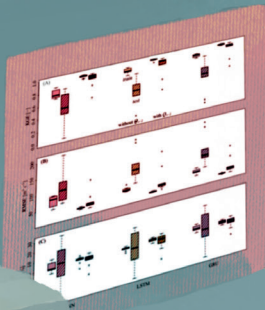
Reservoirs are essential infrastructures for water resources management; yet modelling real-time reservoir operation and outflow remains a challenge due to real-time decisions made by the reservoir operators. This chapter reveals that data-driven models can overcome the limitations typically encountered in process-based models to some extent. Machine learning models in particular can provide accurate simulation and reforecasts of real-time (daily) reservoir operation and outflow. The main findings are as follows:

1. Daily inflow modelling of the Sirikit reservoir with the process-based wflow.sbm model with global data and parameterization is found to be satisfactory for both simulation (with MSWEP precipitation data) and reforecasting (with ECMWF precipitation data), despite flaws in some peak flows and falling limbs of hydrographs.
2. RNN, LSTM and GRU can reconstruct the real-time operation and outflow of the Sirikit reservoir with the selected input data, including reservoir outflow from the previous day, reservoir storage from the previous day and inflows between the time lags and lead times of two days.
3. The performance of RNN, LSTM and GRU for multi-day outflow reforecasts is higher with smaller uncertainty in the dry season (high flows) and flood periods than in the wet season (low flows).
4. The performance of the three models is acceptable on the current day up to 2-day lead times for low flows and up to 6–7 days for high flows.
5. GRU is the most accurate, robust and convenient model in practice, considering its structure with fewer parameters and less computational time compared to LSTM and RNN.

With the effective and applicable real-time operation models, this study offers an alternative to real-time reservoir modelling, especially for areas with data scarcity often encountered in Southeast Asia. Further improvements via input data, model training and model post-processing, particularly with data assimilation, are expected to enhance model accuracy and robustness for real-time application in practice.

“So the problem is not the algorithms, or the big datasets.  
The problem is a lack of scrutiny, transparency, and debate.”

—Tim Harford, *The Data Detective: Ten Easy Rules to Make Sense of Statistics*, (2020)



# **Chapter 8**

## **Synthesis**

This final chapter synthesizes the research outcomes of this thesis in their scientific and practical contexts. It contains main findings in light of research objectives and questions (Section 8.1), implications on continuing challenges and opportunities in reservoir operation modelling (Section 8.2), discussions on reservoir abundance as a contributor and a threat to the world's development (Section 8.3) and recommendations for both future research and operational water resources management (Section 8.4).

## 8.1 Main findings

### 8.1.1 To gain insight into the physical representation and parameterization of hydrological processes with reservoir operation in a process-based model (research objective 1).

The `wflow_sbm` model can adequately represent the main hydrological processes in the upper region of the Greater Chao Phraya River (GCPR) basin with minimized calibration and maximum utilization of globally available data (Chapter 4). The represented processes cover (i) the precipitation routine (using global precipitation and potential evapotranspiration datasets); (ii) the rainfall interception routine (using land cover-related parameter maps obtained from global databases and literature review); (iii) the soil water routine (using soil-related parameter maps based on pedotransfer functions; PTFs) and (iv) the flow generation routine (using river networks and Manning's roughness coefficients obtained from global databases and literature review). As a result, the model sufficiently simulates daily streamflows for natural catchments (i.e., without reservoirs) in terms of magnitude, timing and duration. However, it fails to simulate daily streamflows for reservoir-dominated catchments since the target storage-and-release-based reservoir operation module (ROM) structure with the currently available data is not detailed enough to capture the actual operation mechanisms with the operators' decisions. The soil-related parameters with different PTFs lead to similar streamflow results. Likewise, the effect of different values of the only calibrated parameter on the simulated streamflow is not very large. These small resulting uncertainties suggest that running the model with prior estimated parameters is possible, facilitating its application in data-scarce and ungauged basins. However, other sources of model uncertainty (e.g., global meteorological data) can affect the model performance and should be further examined.

This thesis emphasizes the added value of global datasets for process-based models in (i) circumventing the poor availability of in-situ observations, (ii) preventing overparameterization and equifinality and (iii) reducing the computation time when simulating such a large basin at high spatial and temporal resolutions. Meanwhile, this thesis points out the remaining limitations of process-based models, particularly for modelling reservoir operation processes and outflow. It is clear that the model performance regarding actual reservoir operation highly depends on reservoir-related data, which are still insufficiently available. Since these reservoir-related data are required in detail (e.g.,

water release strategies for irrigation and hydropower generation), they are not available from global databases and must be obtained from in-situ observations and local reports. Nevertheless, the ability of process-based models in representing hydrological processes and reservoir operation mechanisms in the transparent and interpretable form of mathematical expressions remains their major strong point. Therefore, they are still favored for operational applications.

### **8.1.2 To gain insight into hydrological effects of reservoir operation (research objective 2).**

The Sirikit and Bhumibol reservoir operations affect the water balance, daily streamflow regime and extreme flows (Chapter 5). They alter several water balance terms (i.e., inflow, outflow, evaporation loss and change in storage), regarding both the total (summed) water for each term and variation over the year. Focusing on the Sirikit reservoir operation, it inverts the natural seasonality of the daily streamflow regime, with higher flows in the dry season (to supply irrigation and downstream water demands) and lower flows in the rainy season (to fill the reservoir storage and moderate downstream floods). It smooths flow variability, with a greater baseflow contribution and lower flashiness (to persistently support hydropower generation and assist navigation). It has mitigated many floods and extremely low flows, in particular when the operation improved over time (indicating that the experience of reservoir operators enhances operation effectiveness). Nonetheless, the magnitude and timing of the real-time-operated flow are more erratic and difficult to predict compared to the naturalized flow (without reservoirs) during extreme events. Annual flood peaks and minimum flows are more influenced by real-time reservoir operation than by extreme weather, although extreme weather does amplify the events' severity. However, since it is difficult to completely separate the roles of extreme weather and reservoir operation, this should be further investigated. In addition, the hydrological regime of the real-time-operated flow (observations) is considerably different from the regime of the baseline-operated flow (ROM simulation), indicating the important role of operators' decisions. At last, these hydrological effects highlight the importance of effective reservoir operation modelling, including reservoir inflow and outflow forecasting, particularly in real-time. This justifies the development and application of data-driven models for reservoir operation modelling in Chapters 6 and 7.

### **8.1.3 To gain insight into the capability of data-driven models in reconstructing actual reservoir operation and outflow (research objective 3).**

This thesis focused on advanced data-driven models, based on machine learning (ML). Two aspects of ML modelling for reservoir operation were investigated: input data and model algorithms (Chapter 6). Reservoir-related data that are typically available were considered, including the Sirikit outflow, inflow, storage, Bhumibol outflow, downstream river discharge, month of the year and day of the week. Most daily time series

data are available from observations, except for inflow data, which were obtained from the `wflow_sbm` simulation. The data analyses included time series decomposition and correlation to indicate potential input variables. Although more detailed data (e.g., water release strategies for irrigation and hydropower generation) have been shown to increase ML model performance (e.g., Yang et al., 2016; Zhang et al., 2019), they are not available to the public or researchers for most reservoirs (including for the Sirikit and Bhumibol reservoirs), and thus were not considered in this thesis. Widely-used ML algorithms in reservoir modelling were compared, namely Multiple Linear Regression, Support Vector Machine, K-Nearest Neighbor, Classification and Regression Tree, Random Forest, Multi-Layer Perceptron and Recurrent Neural Network. From the 17 input combination scenarios taken into account, the most suitable input dataset for the considered ML models consists of (i) observed reservoir storage from the previous day, (ii) simulated inflow (by `wflow_sbm`) from two days ago to two days ahead and (iii) month of the year, in order to simulate the Sirikit reservoir outflow on the current day. Including the Bhumibol outflow and downstream river discharge variable as input improves ML model performance. However, their in-situ data are not readily available in real-time applications and would need to be modelled, which would lead to more input uncertainty and more computational time. When focusing on real-time outflow simulations, the Recurrent Neural Network offers a high potential for further improvements.

This thesis underlines several aspects of ML modelling for reservoir operation. First, input dataset selection and pre-processing are crucial for ML models as the quality and quantity of data directly affect ML model performance. Since selecting and pre-processing data is a time-consuming process, they are often neglected with the assumption that ML models need the same input data as process-based models. However, ML model input data need to be attentively selected and scaled. Data scaling (e.g., by normalization or standardization) largely depends on data characteristics, which should be thoroughly investigated. Second, input data selection should take into account not only simulation accuracy, but also data availability and computational time in practice. Also, suitable input data sets vary per ML algorithm, reservoir and study area, and thus should be considered individually. Third, each considered ML model has different benefits and drawbacks and is preferred for a different purpose. For instance, classification and regression trees can indicate the importance index for each input variable while recurrent neural networks can take into account input sequences. In conclusion, ML models with carefully chosen and scaled input datasets can sufficiently and robustly simulate real-time reservoir operation and outflow.

#### **8.1.4 To improve multi-day forecasting of daily reservoir operation and outflow by combining a process-based model and data-driven models (research objective 4).**

The `wflow_sbm` model with global datasets (including historical and forecast precipitation data) can provide simulated and reforecast Sirikit reservoir inflow, which is an



important input variable for the ML models (Chapter 7). The accuracy of deterministic and ensemble inflow reforecasts is acceptable until a lead time of five days, although they tend to be overestimated in the wet season and underestimated in the dry season. With the modelled inflow and other input data (as stated in Section 8.1.3), the capabilities of three advanced ML models, including Recurrent Neural Networks, Long Short-Term Memory and Gated Recurring Unit in simulating and forecasting the daily Sirikit reservoir outflow were assessed. They can capture the real-time operation of the Sirikit reservoir well and provide accurate daily outflow. The models' performance is particularly high when training data cover both regular and extreme conditions. The inclusion of outflow at the previous time step as input also significantly increases the resulting accuracy since it can essentially account for the operators' decisions on a daily basis. However, this inclusion is only applicable for multi-day forecasting when the outflow is obtained from calculation instead of from observations. The models can reforecast the Sirikit outflow up to two days ahead for low outflows and up to one week for high outflows, and perform better for high outflows (during the dry season) than low outflows (during the wet season). Given the current setup of the experiment, Gated Recurring Unit is a more accurate, robust and convenient model to be used in practice than the other two models.

### 8.1.5 General conclusions

The main goal of this PhD thesis was to improve understanding of reservoir operation, its hydrological effects and its modelling. The core Chapters 4–7 presented the development, examination and application of a process-based model (fully-distributed `wflow_sbm`) and several data-driven models (machine learning) in the upper GCPR basin in Thailand, focusing on the Sirikit and Bhumibol reservoirs.

In this thesis, the development of the `wflow_sbm` model for representing hydrological processes and simulating daily streamflow fully relies on globally available datasets. The global soil- and land cover-related parameter maps were initially applied to the Rhine basin and then were regionalized to the global scale (Imhoff et al., 2020b; Van Verseveld et al., 2022b). The satisfactory daily streamflow results in natural catchments (i.e., without reservoirs) in the upper GCPR basin suggest that inter-basin characteristics and consistency exist to some extent. However, the global parameterization should be applied in other basins with different climate, hydrological and geological conditions to further investigate their transferability and scalability. Ultimately, I advocate that the `wflow_sbm` model is worth improving and has the potential to serve as a hydrological tool for the upper GCPR basin and other data-scarce or ungauged basins in SEA. It also provides opportunities to study hydrological responses in different aspects, such as under changes in streamflow under new reservoir construction and/or climate change. However, in basins where in-situ observations are sufficiently available, in-situ data should be prioritized in modelling.

Meanwhile, the ROM fully relies on local reservoir-related data in representing ac-

tual reservoir operation and simulating daily outflow. Its unsatisfactory performance is linked to limitations in detailed data and model complexity. The ROM can be further improved by adding more operational parameters and complex functions into the storage and outflow determination process (e.g., release coefficients to account for the inter-annual release variability; Hanasaki et al., 2006). However, even if reservoir operation modules become more complex with more data becoming available, in my opinion, they will not sufficiently represent the actual operation for many major multi-purpose reservoirs. This is because capturing operators' decisions is beyond explicit mathematical expressions of the ROM (and other process-based operation models). In addition, more model parameters mean more uncertainty sources and optimization efforts, and thus added values of new parameters should be carefully assessed (Yassin et al., 2019).

The performance of ML models in simulating and forecasting daily reservoir outflow relies on both in-situ reservoir-related data and modelled inflow data by the `wflow_sbm` model. Therefore, when more data become available, ML model performance can be further improved. The considered ML models outperformed the `wflow_sbm` model with the ROM in capturing the real-time reservoir operation and simulating the daily Sirikit reservoir outflow. Altogether, this thesis highlights that the combination of considered ML models and forecast inflows from the `wflow_sbm` model can serve as an effective and applicable forecasting modelling system to support operational water management in real-time. However, some further improvements are required to maximize model accuracy and robustness, including (i) the inclusion of seasonal and multi-annual inflow forecasts as input, (ii) an ensemble ML modelling approach, which weighs the output from several trained ML models, and (iii) data assimilation.

While this thesis has focused on the upper GCPR basin, the research outcomes and understanding are applicable from a broader perspective. The basin represents highly regulated areas in Southeast Asia (SEA) that are experiencing reservoir expansion and are vulnerable to climate change. Therefore, the unraveled hydrological effects also apply to major multi-purpose reservoirs located in monsoon-dominated basins. However, effects for each reservoir are unique to a certain extent, and thus they should also be quantified individually. Nevertheless, the findings can assist the planning and management of existing, newly constructed and planned reservoirs. It can be especially applicable to new reservoirs in the Mekong River basin, which are operated for the same purposes (hydropower generation and irrigation).

## **8.2 Reservoir operation modelling: continuing challenges and opportunities**

It is clear from all core chapters in this thesis that hydrological and reservoir operation modelling requires further development and will remain challenging, especially for real-time reservoir outflow forecasting. Although modelling is complex, it has only two

ingredients: data and models. Improving hydrological and reservoir operation modelling, therefore, requires fundamentally improving data and models. With continuing advancements in data, modelling techniques and computer technology, together with past and present research that provides promising directions, we are gradually taking on the modelling challenges. Here, I integrate the main findings of this thesis and other relevant research outcomes to state where we are now and how we go on.

### 8.2.1 More reservoir-related data are needed: from global to in-situ

Inadequate data availability has hindered the development of new and rigorous hydrological and reservoir operation modelling studies (Lehner et al., 2011). Although it will remain an obstacle, especially in real-time modelling, more hydrometeorological databases have become available in the past few years. Newly available reservoir-related data in global public domains are mostly based on remote sensing and global data analysis techniques. They are available with relatively high spatial and temporal resolutions. One of the most promising databases is the Global Reservoir and Lakes Database (GREALD; Birkett et al., 2022), which is the recent upgrade and combination of several global water body records, including the Global Reservoir and Dam Database (GRanD; Lehner et al., 2011). GREALD currently includes physical data (e.g., surface area and location) and water level data of reservoirs with surface areas larger than 10 km<sup>2</sup>. The data are also available for the Sirikit and Bhumibol reservoirs (and the other nine major reservoirs in Thailand). GREALD utilizes historical and current radar altimeter missions with short-repeat orbits (i.e., the reservoir re-visit time based on a single overpass). Soon, data in GREALD will be obtained mainly from the Surface-Water Ocean Topography satellite mission (SWOT; Biancamaria et al., 2016), which is scheduled to launch in December 2022. As SWOT will have a one-day repeat orbit, it will consistently monitor reservoir water levels and areas, and thus provide daily records of reservoir water storage variability for the first time in history. It will also monitor other relevant data, such as human water withdrawals. Another potential data source in GREALD is the Small Altimetry Satellites for Hydrology (SMASH; Blumstein et al., 2019) with a 10-day repeat orbit. The combination of GREALD, SWOT, SMASH and reservoir-related data from other remote sensing data sources is expected to revolutionize our knowledge and data on the world's rivers and surface waters. Their ability to have archival and near real-time measurements can be useful for improving reservoir operation models. Therefore, once these databases become available, their competency should be explored for both process-based and data-driven operation models.

Despite innovations in global databases, the ultimate source of reservoir-related data will continue to be in-situ observations as they provide direct insights into actual reservoir operation processes. Although global databases are becoming more accessible and wide-ranging, they are currently neither all-inclusive nor detailed enough for real-time reservoir operation modelling. Several global datasets, meteorological data in particular, are reanalysis-based, which is a blend of in-situ observations and model estimates,

and thus still depend on quantity and quality of in-situ data (Trenberth et al., 2008). Also, some qualitative data (e.g., water allocation policy) need to be gathered from local institutions managing water and field measurements. Hence, in-situ observations remain crucial for reservoir operation modelling, while global data serve as valuable reinforcements. Unfortunately, the designs of measurement networks are mostly for operational purposes and less ideal for scientific purposes. Streamflow gauges, for example, are typically located downstream of reservoirs. It is startling that while modelling techniques and computer technology become more advanced for the development of reservoir operation modelling, data concerning reservoirs and their operation are still not sufficiently available.

As the quantity and quality of in-situ data highly depend on local institutions, initiatives for systematic data monitoring, updates and quality control are required for both existing and planned reservoirs. Based on reservoir operation modelling (both process-based and data-driven) in this thesis, ideal in-situ reservoir-related databases and information should cover reservoir properties (e.g., water body, dam height and outlet characteristics), hydrometeorological data (i.e.; reservoir outflow, inflow, storage, precipitation and evaporation), basic operation policies (i.e., purposes, reservoir zoning and operating rule curves), basic and minimum water demands (e.g., amounts of water allocated for irrigation, hydropower generation and environmental flow) and real-time decision-making (e.g., operation strategy during emergencies, such as for flood and drought moderation and downstream water quality control). Reservoir properties and hydrometeorological data can be obtained from global databases. Opportunistic sensing of precipitation using microwave links from cellular communication networks (Overeem et al., 2021) can also serve as a potential source of hydrometeorological data for real-time reservoir operation modelling. Data on operation policies, water demands and real-time decision-making are only available locally for most reservoirs. Subsequently, active contribution and sharing of in-situ data are required, ideally with federated data repositories. Recently, the Global Dam Watch (GDW; Mulligan et al., 2021) has been initiated ([www.globaldamwatch.org](http://www.globaldamwatch.org)). It aims to collect, curate and update available reservoir-related databases from local, regional to global scales to assist reservoir management and decision-making. In-situ data from a few reservoirs around the world have been shared in GDW. Nonetheless, achieving GDW's aim requires a breakthrough in political and economic relations and cooperation at an international level.

### 8.2.2 Process-based models: from struggles to opportunities

Previous studies and this thesis have indicated the grand challenge in developing process-based models to adequately represent actual reservoir operation mechanisms with operators' decisions. As described in Chapter 1; Section 1.3.1, a large number of existing process-based hydrological models and land-surface models contain reservoir operation schemes, including the `wflow_sbm` model used in this thesis. Although these models generally share similar theoretical concepts of reservoir operation (as ex-

plained in Section 1.2.1), they are also unique in their internal structures and with different operational parameters. To effectively improve reservoir operation modelling, we first need to comprehensively and systematically review existing reservoir operation schemes and their mathematical descriptions representing operation processes. A few studies have provided brief overviews of the past development of reservoir operation models (e.g., Coerver et al., 2018; Yassin et al., 2019; Hughes et al., 2021). However, there is a lack of a systematic review and categorization of operation schemes, including (i) their mathematical descriptions and parameterization and (ii) their strengths and limitations. Such an overview can provide a much-needed guideline for improving and tailoring reservoir operation schemes for each reservoir. Therefore, this should be an urgent research topic in reservoir modelling studies.

Since reservoir operation processes include hydrological, land-surface and water resources management processes, an ideal reservoir operation model should integrate all of these key interdependent processes (Zhao et al., 2016b). These processes are typically represented by three related, yet distinct, models: (i) hydrological models, (ii) hydraulic models and (iii) water resources management models (Hughes et al., 2021). Hydrological models (including the `wflow_sbm` model in this thesis) represent the spatial-temporal distribution and fluxes of water within a river basin, including the generation of surface and subsurface reservoir inflows and outflows. Hydraulic models represent fluid mechanics of water, including backwaters, flow attenuation and tail waters at outflow control structures of reservoirs. Water resources management models represent the water storage, distribution, supply and demand linked by complex networks, including reservoir operation policies. Most existing reservoir operation models are based on hydrological models. These reservoir operation schemes focus on inflows, storage and outflows, but can not fully integrate other important operational components, such as outflow control structures and water supply and demand networks.

A few modelling frameworks offer hydrological-hydraulic-water resource model integration. A popular integrated modelling system is MIKE, in which users can include MIKE SHE (for simulating runoff; DHI, 2017c), MIKE HYDRO River (for simulating outflow control structures with user-defined control curves; DHI, 2017b) and MIKE HYDRO Basin (for simulating reservoir operation and abstraction; DHI, 2017a). As the `wflow_sbm` model is built within a flexible and transparent modelling platform (more details in Section 3.3.3), it also provides an integration opportunity. Recent studies have shown the potential of the SOBEK hydraulic model (San et al., 2020) and the RIBASIM water resources management model (Ahmadzadeh et al., 2022) when coupling with hydrological models for reservoir operation modelling. In addition, Delft3D, an integrated modelling suite for simulating flows, morphology, waves, water quality and ecology, can take into account hydrodynamic processes, including sedimentation, for river and reservoir systems (Mool et al., 2017). `wflow_sbm`, SOBEK and RIBASIM are developed by Deltares. Therefore, I suggest that the next step of the model development from this thesis is coupling the `wflow_sbm` model with (i) the SOBEK and

RIBASIM models and (ii) Delft3D. The integrated wflow\_sbm-SOBEK-RIBASIM reservoir modelling system is expected to improve accuracy in simulating and forecasting daily reservoir outflow compared to the wflow\_sbm model with the ROM alone (in Chapter 4). It would also support reservoir operation studies under climate change, land use change (e.g., deforestation and urbanization) and different water resources management scenarios. The integrated wflow\_sbm-Delft3D system would further provide an opportunity to study reservoir operation from a wider range of views, including operations concerning sedimentation, water quality and ecology.

### 8.2.3 Data-driven models: from opportunities to risks behind the hype

Several studies in hydrological and reservoir operation modelling have explored and proven ML model capability in various perspectives (as also applied and discussed in Chapters 6 and 7). In the next step of development, it is important to know how to utilize ML models to their full potential. In a broader sense of hydrological modelling, Nearing et al. (2021) suggested two innovative and ambitious directions: (i) extracting hydrological insights from ML models and (ii) injecting hydrological insights into ML models. The most challenging phase to overcome is figuring out how to access, understand and translate their complex and multilayered information into mathematical equations (or other interpretable languages). In a similar way as process-based models have been perceived with their complexity limits, ML models are generally viewed as black boxes. However, it has been claimed that it is rather the limit of human ability to translate ML models than the limit of ML model transparency (Nearing et al., 2021). With this realization, a few recent studies have focused on this aspect. Kratzert et al. (2019a,b) conducted pioneering work on extracting encoded features representing how LSTM transformed observed basin characteristics into a matrix of similarity and diversity of rainfall-runoff relationships. The opposite attempt to add hydrological insights into ML models (besides typically using numerical and classified data) has not yet been attempted. One of the empirical studies closest to this idea was a novel family of hydrological models named HydroNets, initiated by Moshe et al. (2020), which leverages river network structure based on ML models and may be seen as the start of ‘distributed hydrological ML’ models.

To my knowledge, no study has focused on extracting reservoir operation insights from or injecting reservoir operation into ML models. However, this can be an important step toward overcoming limitations in both process-based and data-driven reservoir operation models. If, for instance, we can extract patterns of operators’ decisions, which can be learned and reconstructed by ML models (see Chapters 6 and 7) in the form of equations (e.g., by neural network models) or decision diagrams (e.g., by decision tree models), we can better understand real-time operation mechanisms of each reservoir. Subsequently, we can improve operation functions in process-based models.

ML models have overwhelmed hydrological research and have offered high hopes for a long-standing desire in hydrological and reservoir operation modelling: high accuracy

in real-time. We can use them to our advantage, but should not overlook their gaps and potential risks. First of all, ML models perform well as long as there are sufficient training data, but often there is no required reservoir-related data, especially in real-time modelling. Secondly, ML models are trained with historical data, indicating that they can effectively predict the ‘future that has already occurred in the past’ (see also Chapter 7). Therefore, we still need to investigate ML model performance to predict reservoir operation and outflow under changing operating policies, climate change and land use change (e.g., deforestation and urbanization). The impacts of such changes on ML model training and testing, and thus the model robustness, need to be explored. Thirdly, ML models often, but not consistently, prevail over process-based models, especially when input data are limited. Hence, further studies still need to verify their reliability, transferability and scalability (Kim et al., 2021). As we do not understand ML models thoroughly and do not know how to constructively maximize their capability, we have to use them with caution in a similar manner to our use of process-based models.

Finally, both process-based models and data-driven models have their own merits and they are worthy of joint development. The future development of hydrological modelling lies in the combination of process-based models and data-driven models to take advantage of their pros while overcoming their cons.

## 8.3 Reservoirs: double-edged sword

Chapter 1 introduced the controversy of major reservoirs and their pros and cons shown in the past. Chapter 5 further unraveled the hydrological effects of major multi-purpose reservoirs in the upper GCPR basin. As massive reservoir construction continues worldwide, here I speculate on their future roles both as a contributor and a threat to the world’s socio-economic development.

### 8.3.1 Reservoirs as a contributor to the world’s development

The world’s development in terms of both population and economic growth is driven by three key factors: water, food and energy. The United Nations project that the global population will increase from around 8 billion in 2022 to 10.4 billion by the end of the century (Roser & Rods-Guirao, 2013). The rising demand for water, food and energy generates stress on land and water resources worldwide. Countries with emerging economies are also countries with expected large population growth, which, from here onward, are referred to as low and middle-income countries (LMICs). As major multi-purpose reservoirs can contribute to rapidly increasing water supply, irrigation and hydropower generation, they are considered a solution, particularly in LMICs, including in SEA.

The increase in global food demand is projected to be sizable, particularly in LMICs

(Molden, 2007). Part of the additional food will be produced in irrigated areas, which has been estimated to require at least 11% more water (Bruinsma, 2009). Interestingly, despite increasing irrigated areas, more than half of the food production in LMICs is still expected to come from rain-fed areas as they have high remaining potential (Valipour, 2013). Similarly, global energy consumption is projected to increase nearly linearly in the next decades (Chen et al., 2016). The additional hydropower capacity in some LMICs, however, is not mainly for domestic use, but for industrial production and power export (Zarfl et al., 2015). Nonetheless, the dramatic expansion in hydropower reservoirs will not sufficiently compensate for the outpaced increase in global electricity demand. Even if the entire technically feasible hydropower potential would be operated (which is five times more than currently used), hydropower would still contribute less than half to the global electricity demand (Zarfl et al., 2015), and thus other energy sources would still be required. Therefore, although part of the world's development depends on major reservoirs and their partial contribution to water, food and energy security, the question of whether major reservoirs are an effective, sustainable and long-term solution remains critical.

### 8.3.2 Reservoirs as a threat to the world's development

Apart from the hydrological effects of major reservoirs (with examples of the Bhumibol and Sirikit reservoirs shown in Chapter 5) and their well-known impacts on the environment and society, such as changes in ecosystems and sediment budgets (as elaborated in Section 1.1.3), there are other threats as well. The fact that the world's major reservoirs store a large volume of water inland at once should receive more attention. The additional water loss from reservoir surfaces through evaporation exceeds industrial and domestic water consumption combined, raising the question of whether impounding water is an efficient way for water resources management, especially under climate change (Shiklomanov, 2000). As most new reservoirs will be located in temperate and tropical regions, more direct evaporation is expected. A large volume of stored water may also influence the Earth's gravity field on sub-seasonal to inter-annual timescales (Wang et al., 2019) and is collectively responsible for a measurable delay in sea-level rise (Chao et al., 2008). Therefore, under climate change, it is not enough to investigate hydrological and typical environmental and societal effects of new reservoirs, but these less direct ramifications must also be seriously taken into account.

Hydropower is often promoted as 'green' energy. However, in reality, the world's major reservoirs are responsible for at least 4% of human-induced global warming in the form of greenhouse-gas emissions, especially in the tropics and particularly in the first years after construction (Lima et al., 2008; Barros et al., 2011). Therefore, despite being renewable energy, hydropower is not a climate-neutral electricity source (Wehrli, 2011). The maximum emissions by reservoirs may even exceed the emission avoided by refraining from fossil fuel usage, although life-cycle emissions of hydropower are 30 times lower than that of coal (Schlömer et al., 2014). This underlines the need of weigh-



ing the emissions against the damage to water resources and the environment before constructing a new reservoir in order to contribute to a more sustainable world.

Reservoirs and dams will inevitably deteriorate with time and eventually require decommissioning. Aging reservoirs coupled with a growing interest in river restoration have led to many dam removals. The removal of relatively small dams has started in both the United States and Europe, with over 1200 dams removed in the US (Bellmore et al., 2017). Records of dam removal worldwide and their scientific information are difficult to find, especially for major reservoirs. To be properly prepared for tremendous river basin reforms, we need to know (i) whether and how to remove dams, (ii) what are the hydrological, environmental and societal consequences and (iii) how long it would take for impacted areas to recover. Considering the ongoing reservoir expansion, it is likely that in the future, several major reservoirs need to be deconstructed simultaneously. Since more than 400 million people around the world are living near (closer than 10 km) the rivers downstream of major reservoirs (Richter et al., 2010), there is an urgent need for long-term, multidisciplinary studies in order to anticipate the unavoidable effects of dam removal and inform future decision-making. Comprehensive studies of reservoirs and impacted areas from before construction, during construction (which takes an average of 8.6 years per reservoir according to Ansar et al., 2014), during their lifetime of operation, after decommissioning and during restoration are urgently needed.

Finally, I assert that when a major reservoir is planned, especially in LMICs that are vulnerable to both economic change and climate change, disparate views on its lifetime benefit and negative impacts should be carefully considered. The basic question that needs to be asked when considering new reservoirs is whether they are needed or not. Despite the vigorous debate on ‘dam or no dam’, a world without reservoirs and dams seems unrealistic. Therefore, it is time that we think more systematically about how to better operate and maintain existing reservoirs and how to better construct new reservoirs in order to balance their actual advantages and disadvantages.

## 8.4 Recommendations for the future

The previous sections have discussed expectations and recommendations for reservoir operation, its effects and its modelling from a general perspective. Recommendations specifically on how to improve the wflow\_sbm model have been provided in Chapter 4 (Sections 4.4.1 and 4.4.2) and for the considered ML models in Chapter 7 (Section 7.4.2). In this section, I discuss expectations and recommendations, for both future research and operational purposes, with a focus on the upper region of the Greater Chao Phraya River (GCPR) basin in Thailand, in the light of sustainable reservoir resource planning and management under the 20-year National Water Resource Management Master Plan recently launched for the 2018–2037 period. These recommendations are also applicable at the national level and to neighboring countries in SEA.

### 8.4.1 Research

1. Comprehensive studies on the Sirikit and Bhumibol reservoirs and their impacted areas after decommissioning are needed in order to predict hydrological, environmental and societal impacts, as well as river basin responses and reforms. The Sirikit and Bhumibol reservoir operations cause significant changes in the water balance and streamflow regimes (Chapter 5). This implies that when the two major reservoirs have to be deconstructed, significant changes are also expected in reverse, and thus should be thoroughly investigated for effective preparation.
2. Small- and medium-sized reservoirs should receive more attention in reservoir operation modelling as their cumulative effects may be considerable. There are seven medium-sized reservoirs (Figure 2.1) and hundreds of small-sized reservoirs located in the GCPR basin. These reservoirs account for a much smaller part of the total reservoir storage in the basin compared to the Sirikit and Bhumibol reservoirs (see Section 2.3), and thus have been under-emphasized and unexamined. However, previous research (e.g., Komori et al., 2012) indicated that they play an important role in flood and drought mitigation, especially for medium-sized reservoirs. More insight into their contributions at the basin scale will improve both reservoir operation modelling and management.
3. Studies focusing on the development and application of multi-reservoir system modelling with multi-objective simulation-optimization approaches and decision-support tools for optimal water reservoir operation are urgently required. Reservoirs in the upper GCPR basin are located in series and parallel (Figure 2.1) and are operated simultaneously (as demonstrated for the Sirikit and Bhumibol reservoirs in Chapter 6). Therefore, in order to model and manage the Sirikit and Bhumibol reservoirs effectively, they should be considered as one operational system. Only a few studies (e.g., Thechamani et al., 2017) have initiated this step in the basin so far. Later, small- and medium-sized reservoirs should also be included in the system.

### 8.4.2 Reservoir operation and water management

1. The recent 2022 floods in the GCPR basin suggest the need for evaluating and updating the current water resources management and reservoir operation system, regarding both long-term operation policies and emergency strategy (which, subsequently, would encourage more research on multi-reservoir system modelling).
2. New reservoir construction should be carefully considered from past experiences (including mistakes) with previous reservoirs. If unavoidable, a new reservoir should first be considered in rivers that are already dammed while free-flowing rivers should be conserved. This is especially the case for the Kaeng Suea Ten reservoir (Kirchherr et al., 2018), whose implementation has been uncertain for 36 years on the free-flowing Yom river in the upper GCPR basin.

3. Two main obstacles to effective water resources management with reservoir operation in Thailand are (i) unclear policies and (ii) lack of coordination between governmental organizations. This is because Thailand counts 48 water-related governmental agencies across eight ministries with different proprieties and visions, of which policies often overlap or conflict. In 2017, the office of National Water Resources was established as an executive center, responsible for supporting the nation's water resources management through cooperation with all other water agencies. It is still unclear how this recent establishment has influenced water resources management with reservoir operation in the upper GCPR basin. They are encouraged to share more data and information that benefit both research and operation.
4. There is also an urgent need for constructive collaboration between governmental agencies and water-related research institutes in Thailand, particularly for data monitoring (considering data quantity and quality) and data sharing (considering in-situ field data and model forecasting results). A joint data repository that is also accessible for research and academic purposes is highly recommended.

Reservoir operation, its effects and its modelling will continue to be challenging research topics in hydrological sciences as well as a challenging task for reservoir operators and water managers. Researchers will continue to focus on improving understanding and modelling of real-time reservoir operation, while operational sectors focus on gaining first-hand knowledge and experience. Therefore, we must communicate and exchange knowledge with each other. This way, we can ensure that research reaches its ultimate aim, that is, to be useful in practice.



# Appendices

The appendices represent the supplementary results of the studies in this thesis. Appendix A, B and C belong to Chapters 4, 6 and 7, respectively.

## Appendix A

This appendix represents the additional results of Chapter 4.

**Table A.1:** KGE and its components indicating wflow\_sbm performance in simulating monthly streamflow for the four study catchments and monthly storage for the two reservoirs in the upper Greater Chao Phraya River (GCPR) basin. The model was tested with two pedotransfer parameter sets: Brakensiek (PTF-B) and Cosy (PTF-C), during the water-years 1989–2013.

		PTF-B				PTF-C			
		KGE	$r$	$\alpha$	$\beta$	KGE	$r$	$\alpha$	$\beta$
Catchment (streamflow)	Nan_natural	<b>0.69</b>	0.95	0.91	0.71	<b>0.68</b>	0.95	0.86	0.72
	Yom_natural	<b>0.84</b>	0.90	1.12	0.94	<b>0.89</b>	0.90	1.01	0.95
	Sirikit	<b>0.63</b>	0.63	0.98	0.95	<b>0.64</b>	0.65	0.96	0.97
	Bhumibol	<b>-0.22</b>	0.11	1.73	1.41	<b>-0.16</b>	0.12	1.63	1.42
Reservoir (storage)	Sirikit	<b>0.81</b>	0.89	1.06	0.86	<b>0.82</b>	0.88	1.06	0.89
	Bhumibol	<b>0.57</b>	0.66	1.06	1.26	<b>0.57</b>	0.68	1.01	1.30

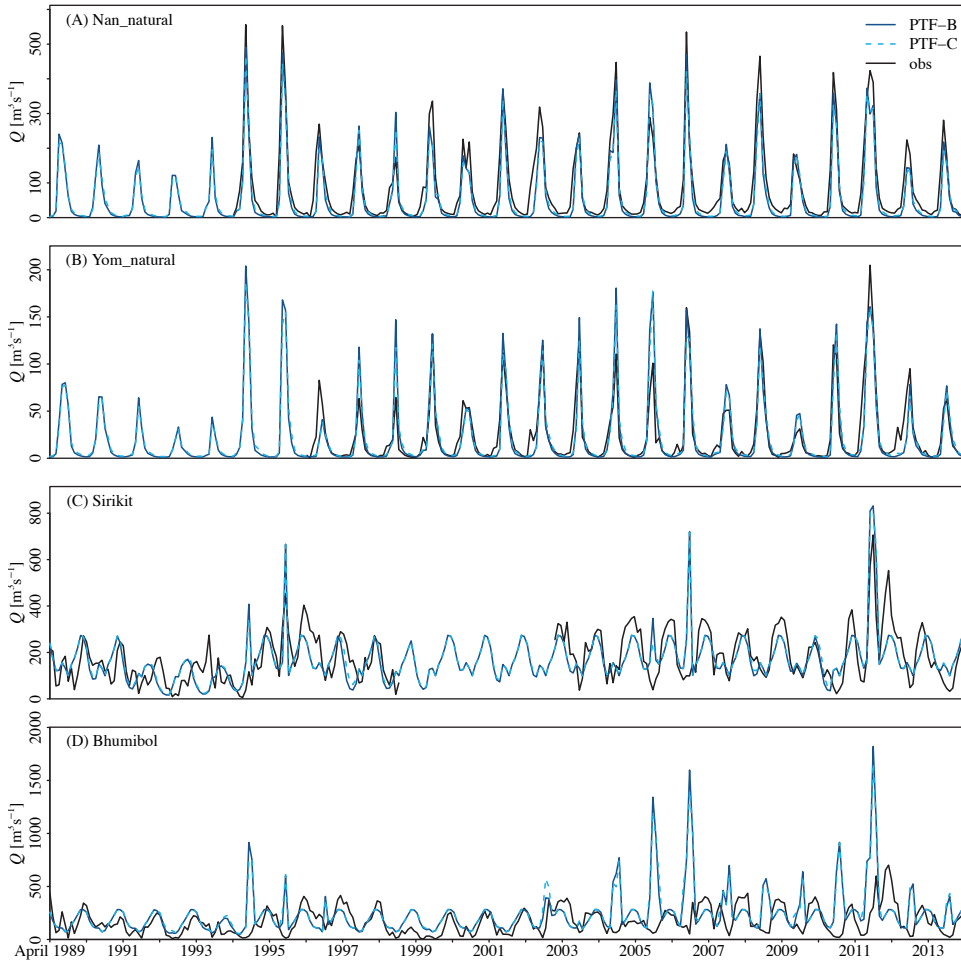


**Figure A.1:** Simulated and observed monthly mean streamflows in the water-years 1989–2013 for the Nan\_natural (first row), Yom\_natural (second row), Sirikit (third row) and Bhumibol (bottom row) catchments. The simulated streamflow with the optimized PTF-B parameter set is shown in solid dark blue lines, the simulated streamflow with the optimized PTF-C parameter set in dash light blue lines and the observations (obs) in solid black lines.

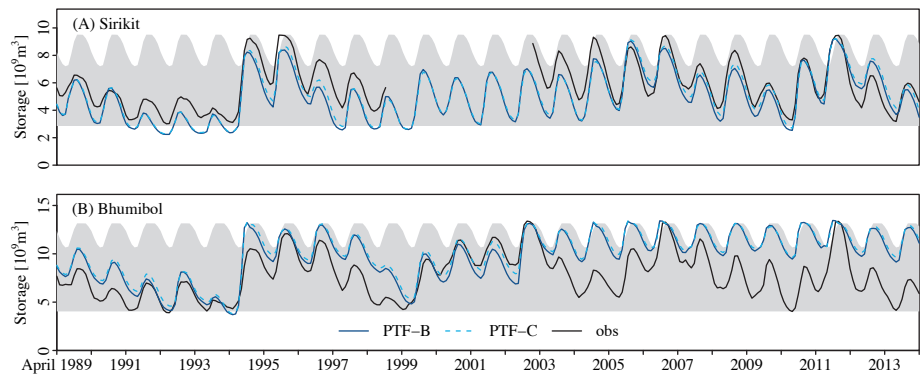


**Figure A.2:** Simulated and observed monthly storages of the Sirikit reservoir (A) and the Bhumibol reservoir (B) in the water-years 1989–2013. The grey bands represent the ranges between the monthly target maximum storage (obtained from RID) and the target minimum storage (fixed as 30% of the reservoir capacity). The simulated storage with the optimized PTF-B parameter set is shown in solid dark blue lines, the simulated storage with the optimized PTF-C parameter set in dash light blue lines and the observations (obs) in solid black lines.



## Appendix B

This appendix represents the additional results of Chapter 6.

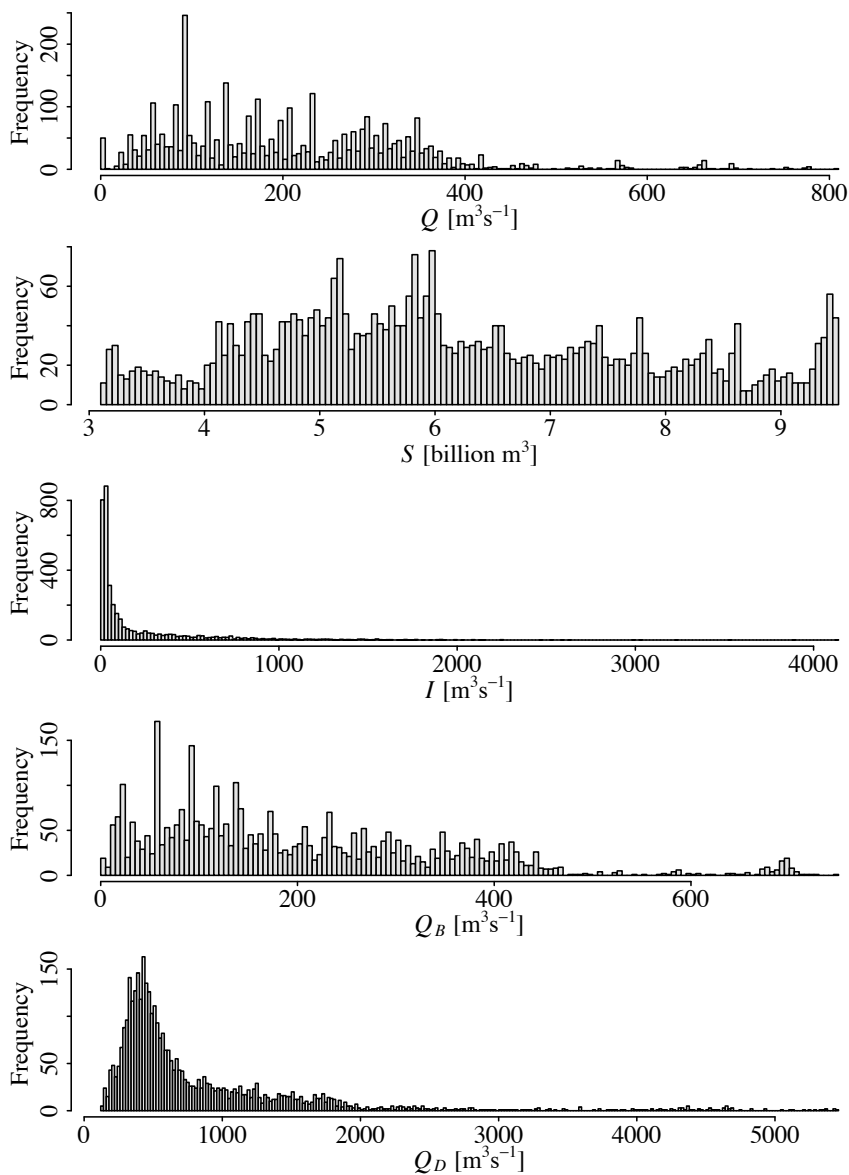


**Figure B.1:** Distribution of the daily Sirikit reservoir outflow ( $Q$ ), the Sirikit reservoir storage ( $S$ ), the Sirikit reservoir inflow ( $I$ ), the Bhumibol reservoir outflow ( $Q_B$ ) and the downstream discharge ( $Q_D$ ) during the years 2004–2013. Each dataset is distributed in 200 classes.

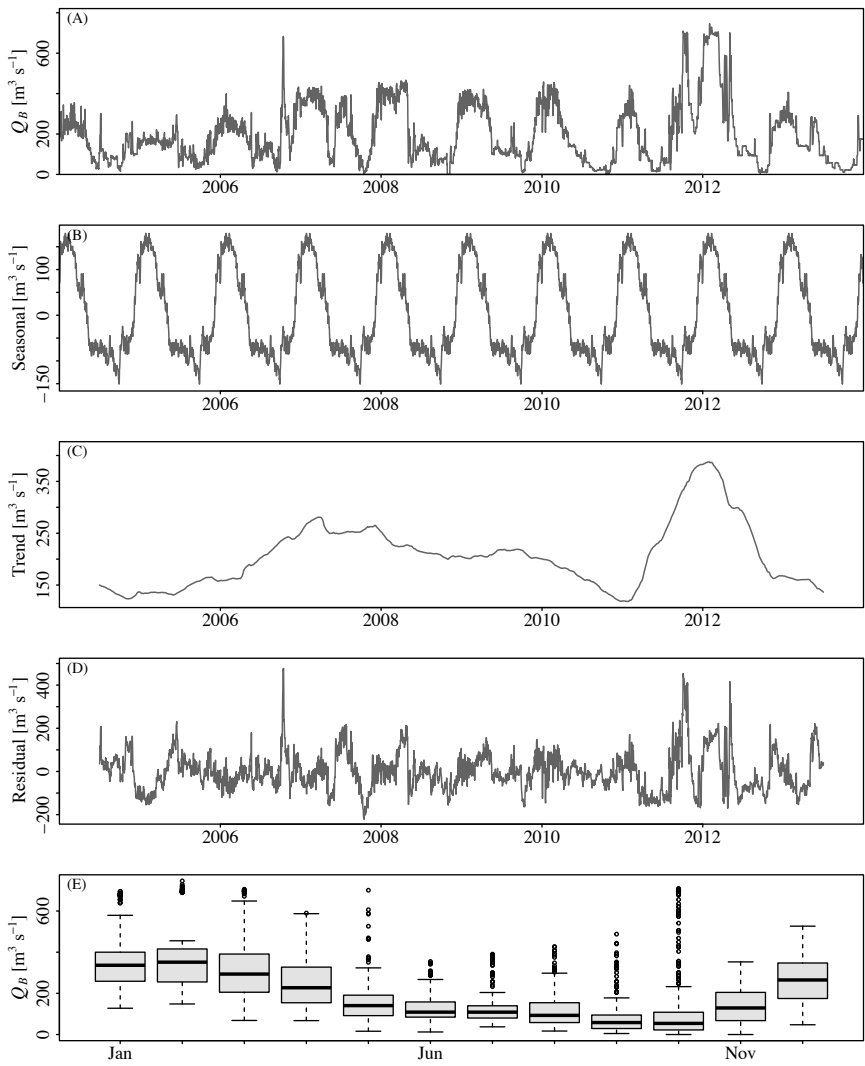


**Figure B.2:** Decomposition of the observed daily Bhumibol reservoir outflow ( $Q_B$ ) data. The original time series (A) is decomposed into the seasonal (B), trend (C) and residual (D) components. Panel (E) shows the distribution of the daily  $Q_B$  per month.

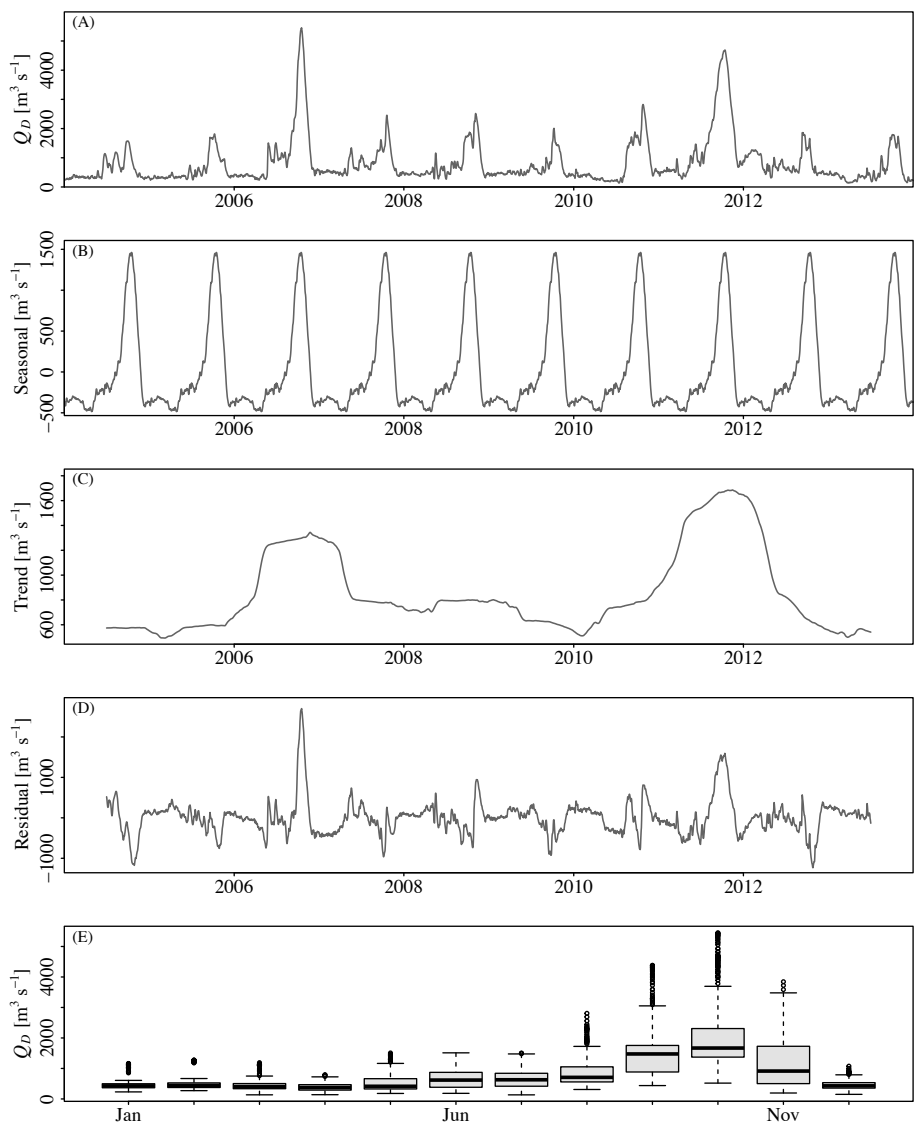


**Figure B.3:** Decomposition of the observed daily downstream discharge ( $Q_D$ ) data at Nakhon Sawan. The original time series (A) is decomposed into the seasonal (B), trend (C) and residual (D) components. Panel (E) shows the distribution of the daily  $Q_D$  per month.

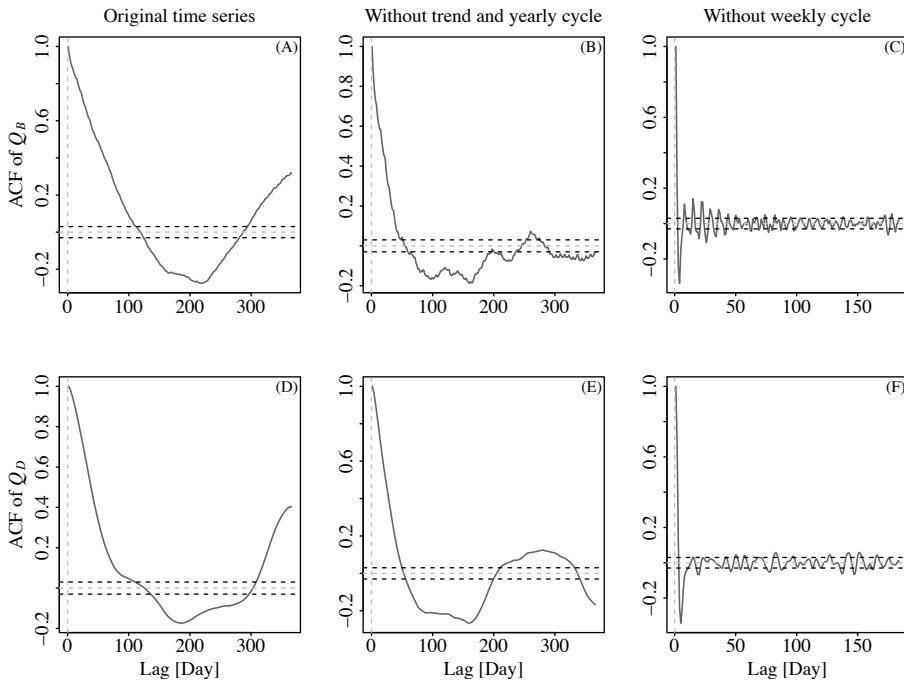


**Figure B.4:** Auto-correlation function (ACF) of the daily Bhumibol reservoir outflow ( $Q_B$ ) and the downstream discharge ( $Q_D$ ) data. The left panels show the ACFs of the original time series. The middle panels show the ACFs of the 1<sup>st</sup> residual time series (as shown in Figures B.2(D) and B.3(D)), representing the data without the long-term trend and annual cycle. The right panels show the ACFs of the 2<sup>nd</sup> residual time series (results not shown here), representing the data without the long-term trend, annual cycle and weekly cycle. Dashed black lines indicate where the correlation is significant to the 95% level.

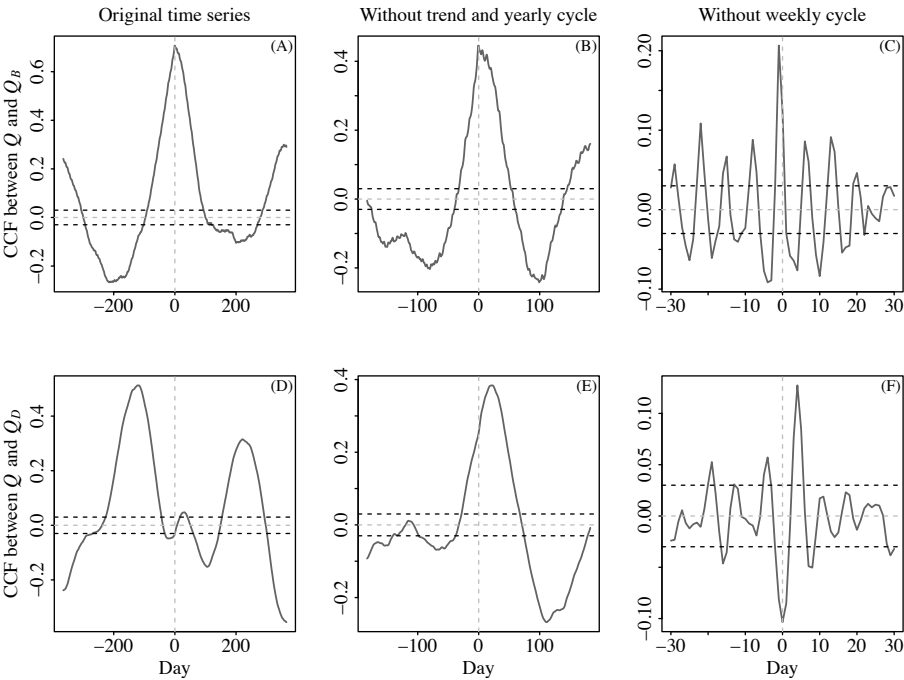


**Figure B.5:** Cross-correlation function (CCF) between the daily Sirikit reservoir outflow ( $Q$ ) and Bhumbol reservoir outflow ( $Q_B$ ) (Top panels) and downstream discharge ( $Q_D$ ) (bottom panels). The left panels show the CCFs of the original time series. The middle panels show the CCFs of the 1<sup>st</sup> residual time series. The right panels show the CCFs of the 2<sup>nd</sup> residual time series. Dashed black lines indicate where the correlation is significant to the 95% level.

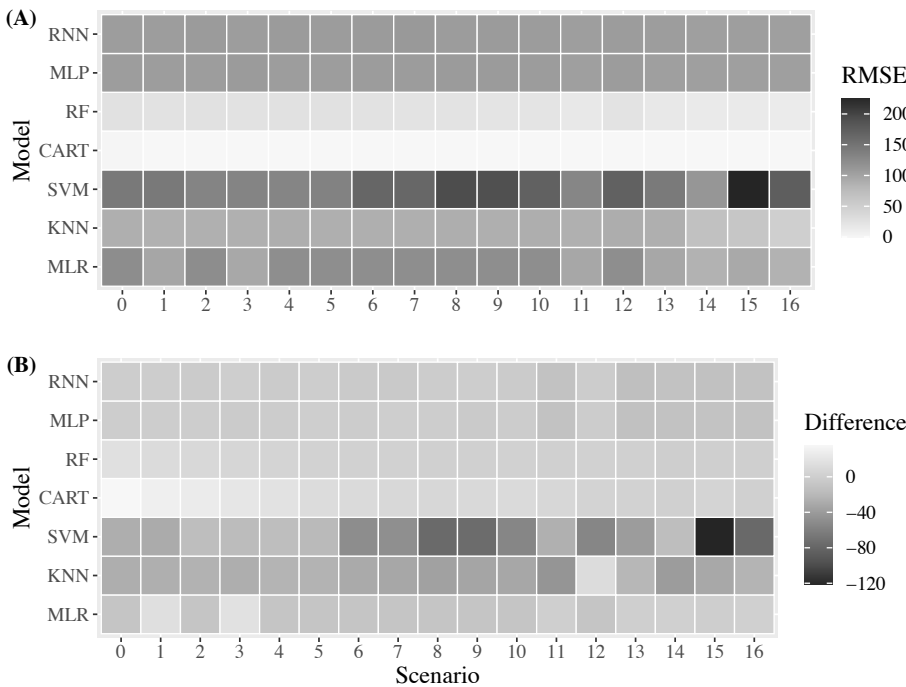


**Figure B.6:** Performance of the seven ML models on the Sirikit reservoir outflow simulations in the 17 input combination scenarios during the training period (years 2004–2011), using RMSE as the criterion. Panel (A) shows the RMSE of the model simulations with the raw input data, while Panel (B) shows the difference in RMSE between the model simulations with the raw input data and with the normalized input data, reflecting the effect of input data scaling on the model performance. The ML models consist of Multiple Linear Regression (MLR), K-Nearest Neighbors (KNN), Support Vector Machine (SVM), Classification and Regression Tree (CART), Random Forest (RF), Multi-Layer Perceptron (MLP) and Recurrent Neural Network (RNN). Differences between the input scenarios are explained in Table 6.1. In Panel (A), a lower RMSE value presented in a lighter color indicates a better model performance. In Panel (B), a higher difference presented in a darker color indicates an improvement in the model performance with the scaled input data. Lighter to white color indicates that the model performance did not improve or even decrease.

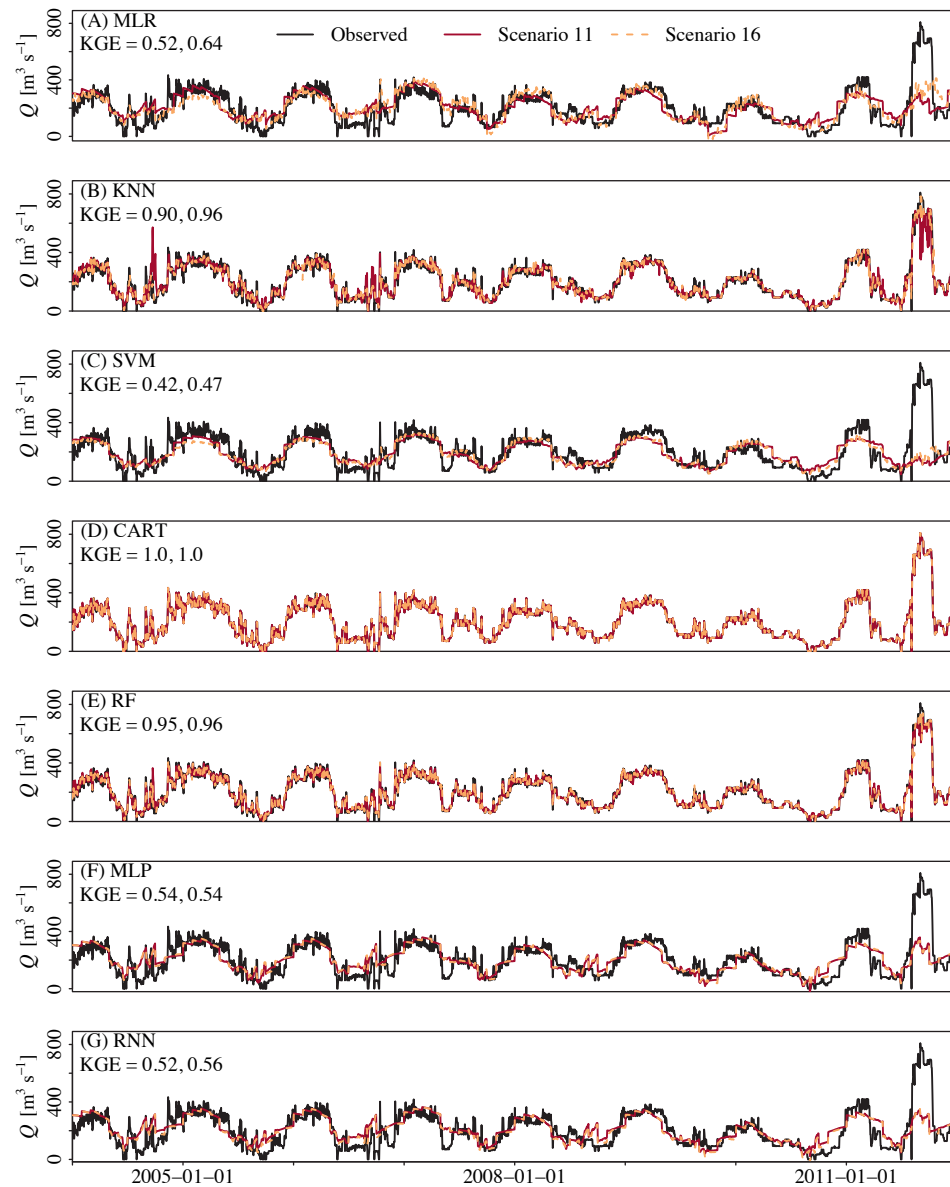


**Figure B.7:** Simulated daily outflow of the Sirikit reservoir by the seven ML models compared to the observations in the training period (years 2004–2011). The ML models consist of Multiple Linear Regression (MLR), K-Nearest Neighbors (KNN), Support Vector Machine (SVM), Classification and Regression Tree (CART), Random Forest (RF), Feed-Forward Neural Network/Multi-Layer Perceptron (MLP) and Recurrent Neural Network (RNN). The simulation results of two selected and scaled input scenarios are compared: scenario 11 (in solid red color) and scenario 16 (in dashed orange color), of which the details of each scenario can be found in Table 6.1. The KGE values are also indicated for scenarios 11 and 16, respectively.



## Appendix C

This appendix represents the additional results of Chapter 7.

**Table C.1:** KGE, RMSE and PBIAS indicating the performance of RNN in simulating daily Sirikit reservoir outflows in two cases: with and without  $Q_{t-1}$  as an input. The model was cross-validated with 10 different scenarios of training-testing periods, as indicated in Figure 7.2.

Scenario	RNN without $Q_{t-1}$ as an input						RNN with $Q_{t-1}$ as an input					
	RMSE		KGE		PBIAS		RMSE		KGE		PBIAS	
	Train	Test	Train	Test	Train	Test	Train	Test	Train	Test	Train	Test
1	76	94	0.75	0.53	6	-10	26	32	0.96	0.88	2	-1
2	55	103	0.82	0.48	-0.3	18	28	32	0.95	0.94	1	0.1
3	86	119	0.72	0.41	0.4	16	27	37	0.94	0.88	2	2
4	78	68	0.70	0.76	-3	8	27	36	0.97	0.95	2	2
5	76	124	0.71	0.42	9	31	33	37	0.91	0.90	-8	-8
6	87	83	0.68	0.59	-6	-3	28	31	0.96	0.93	-3	-1
7	86	68	0.68	0.72	-2	-10	28	23	0.96	0.96	1	1
8	79	58	0.77	0.81	5	12	30	22	0.95	0.94	3	5
9	55	188	0.83	0.02	-1	-18	30	56	0.90	0.77	5	-1
10	46	208	0.86	0.09	-2	-34	24	109	0.97	0.57	2	-17
Average	72	111	0.75	0.48	0.7	0.8	28	41	0.95	0.87	6	-2

**Table C.2:** KGE, RMSE and PBIAS indicating the performance of LSTM in simulating daily Sirikit reservoir outflows in two cases: with and without  $Q_{t-1}$  as an input. The model was cross-validated with 10 different scenarios of training-testing periods, as indicated in Figure 7.2.

Scenario	LSTM without $Q_{t-1}$ as an input						LSTM with $Q_{t-1}$ as an input					
	RMSE			KGE			RMSE			KGE		
	Train	Test	Train	Test	Train	Test	Train	Test	Train	Test	Train	Test
1	64	92	0.80	0.54	-4	-13	24	34	0.97	0.86	2	-2
2	44	109	0.92	0.47	-0.1	18	18	37	0.98	0.91	1	2
3	43	108	0.93	0.57	-1	13	21	38	0.98	0.91	-1	-0.1
4	46	102	0.91	0.62	1	18	20	36	0.97	0.94	-2	-2
5	47	124	0.89	0.44	-1	8.	20	38	0.97	0.93	3	5
6	51	91	0.87	0.51	-1	-6	19	32	0.98	0.93	1	1
7	53	75	0.84	0.68	-6	-14	23	28	0.92	0.92	-3	-5
8	52	63	0.87	0.80	-1	0	22	21	0.98	0.96	1	3
9	45	192	0.87	0.02	1	-16	19	94	0.97	0.61	2	-11
10	42	202	0.86	0.11	-0.1	-34	19	143	0.96	0.4	-0.60	-22
Average	49	116	0.88	0.48	-1	-3	21	50	0.97	1	0.26	-3

**Table C.3:** KGE, RMSE and PBIAS indicating the performance of GRU in simulating daily Sirikit reservoir outflows in two cases: with and without  $Q_{t-1}$  as an input. The model was cross-validated with 10 different scenarios of training-testing periods, as indicated in Figure 7.2.

Scenario	GRU without $Q_{t-1}$ as an input						GRU with $Q_{t-1}$ as an input					
	RMSE		KGE		PBIAS		RMSE		KGE		PBIAS	
	Train	Test	Train	Test	Train	Test	Train	Test	Train	Test	Train	Test
1	47	94	0.86	0.50	-1	-11	24	32	0.96	0.96	-2	-3
2	48	89	0.91	0.60	1	16	22	32	0.97	0.92	2	3
3	46	97	0.90	0.64	-1	12	19	37	0.98	0.94	-1	-1
4	52	98	0.85	0.65	-5	12	22	37	0.96	0.93	-4	-4
5	46	115	0.90	0.50	2	22	22	35	0.97	0.94	-3	-2
6	57	88	0.84	0.49	-2	-7	21	30	0.98	0.94	2	2
7	61	68	0.88	0.70	4	-9	22	24	0.98	0.95	-1	-3
8	54	57	0.90	0.84	-1	-0.4	22	20	0.99	0.98	-0.4	0
9	47	188	0.86	0.06	-5	-21	22	73	0.98	0.70	-1	-10
10	36	204	0.91	0.11	3	-33	20	105	0.98	0.58	1	-16
Average	49	110	0.88	0.51	-0.3	-2	22	42	0.98	0.88	-1	-3

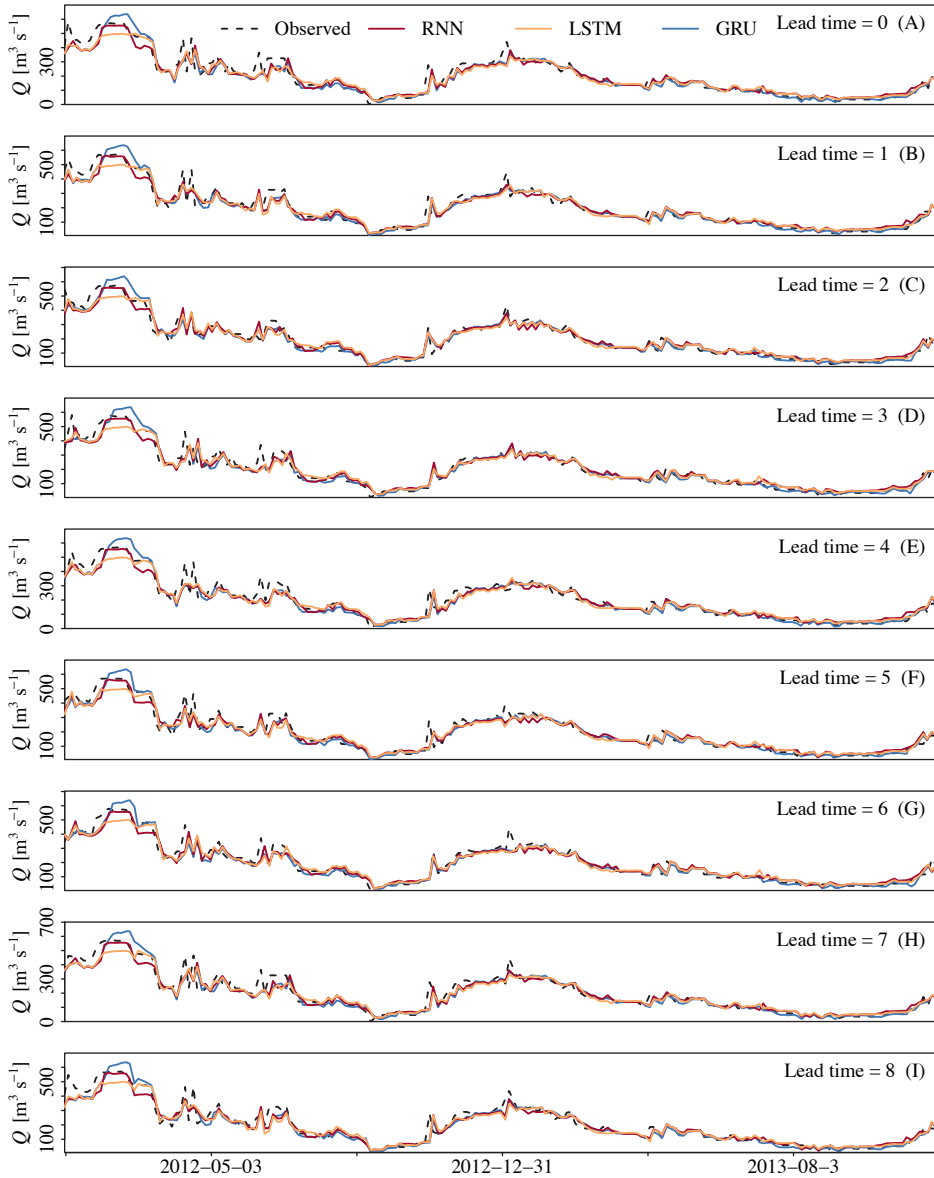


**Figure C.1:** Control reforecasts of the Sirikit reservoir outflow ( $Q$ ) by RNN (solid red lines), LSTM (solid orange lines) and GRU (solid blue lines) compared to the observations (dashed black lines) from the current day to 8-day lead times. The reforecasts were issued every three and four days. The results are from the baseline reforecasting scenario, in which the previous reservoir outflow and storage input data were obtained from in-situ observations.

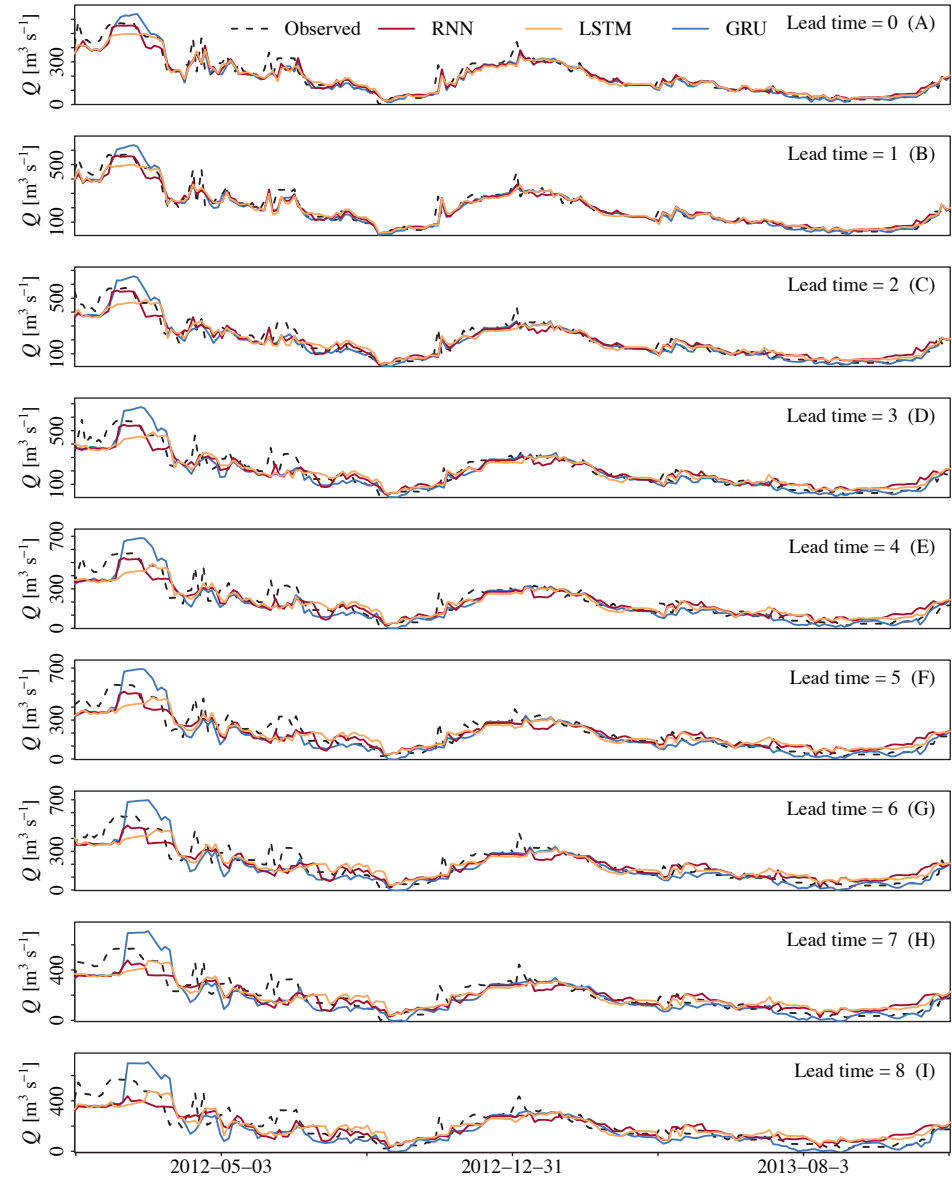


**Figure C.2:** Control reforecasts of the Sirikit reservoir outflow ( $Q$ ) by RNN (solid red lines), LSTM (solid orange lines) and GRU (solid blue lines) compared to the observations (dashed black lines) from the current day to 8-day lead times. The reforecasts were issued every three and four days. The results are from the real-time reforecasting scenario, in which the previous reservoir outflow and storage input data were calculated and updated in real-time.

# References

- Abadi, M. et al. (2016). TensorFlow: a system for large-scale machine learning. In *12th USENIX Symposium on Operating Systems Design and Implementation (OSDI 16)* (pp. 265–283). Savannah, GA, United States of America: USENIX Association.
- Abbott, M. B., Bathurst, J. C., Cunge, J. A., O'Connell, P. E., & Rasmussen, J. (1986). An introduction to the European Hydrological System Systeme Hydrologique Europeen, SHE, 1: history and philosophy of a physically-based, distributed modelling system. *Journal of Hydrology*, 87, 45–59. doi:10.1016/0022-1694(86)90114-9.
- Abell, R., Lehner, B., Thieme, M., & Linke, S. (2017). Looking beyond the fenceline: assessing protection gaps for the world's rivers. *Conservation Letters*, 10, 384–394. doi:10.1111/conl.12312.
- Aerts, J. P., Hut, R. W., van de Giesen, N. C., Drost, N., van Verseveld, W. J., Weerts, A. H., & Hazenberg, P. (2022). Large-sample assessment of varying spatial resolution on the streamflow estimates of the wflow\_sbm hydrological model. *Hydrology and Earth System Sciences*, 26, 4407–4430. doi:10.5194/hess-26-4407-2022.
- Ahmadi, A., Karamouz, M., & Moridi, A. (2010). Robust methods for identifying optimal reservoir operation strategies using deterministic and stochastic formulations. *Water Resources Management*, 24, 2527–2552. doi:10.1007/s11269-009-9566-3.
- Ahmadzadeh, H., Mansouri, B., Fathian, F., & Vaheddoost, B. (2022). Assessment of water demand reliability using SWAT and RIBASIM models with respect to climate change and operational water projects. *Agricultural Water Management*, 261, 107377. doi:10.1016/j.agwat.2021.107377.
- Ahsan, M. M., Mahmud, M. P., Saha, P. K., Gupta, K. D., & Siddique, Z. (2021). Effect of data scaling methods on machine learning algorithms and model performance. *Technologies*, 9, 52. doi:10.3390/technologies9030052.
- Ajami, N. K., Hornberger, G. M., & Sunding, D. L. (2008). Sustainable water resource management under hydrological uncertainty. *Water Resources Research*, 44, W11406. doi:10.1029/2007WR006736.
- Allen, R. G., Pereira, L. S., Raes, D., Smith, M. et al. (1998). Crop evapotranspiration-guidelines for computing crop water requirements-FAO irrigation and drainage paper 56. *FAO, Rome*, 300, D05109.
- Althoff, D., & Rodrigues, L. N. (2021). Goodness-of-fit criteria for hydrological models: model calibration and performance assessment. *Journal of Hydrology*, 600, 126674. doi:10.1016/j.jhydrol.2021.126674.
- Altinbilek, D. (2002). The role of dams in development. *Water Science and Technology*, 45, 169–180. doi:10.2166/wst.2002.0172.
- Aminyavari, S., & Saghafian, B. (2019). Probabilistic streamflow forecast based on spatial post-processing of TIGGE precipitation forecasts. *Stochastic Environmental Research and Risk Assessment*, 33, 1939–1950. doi:10.1007/s00477-019-01737-4.
- Angelini, P. (1997). Correlation and spectral analysis of two hydrogeological systems in Central Italy. *Hydrological Sciences Journal*, 42, 425–438. doi:10.1080/02626669709492038.

- Ansar, A., Flyvbjerg, B., Budzier, A., & Lunn, D. (2014). Should we build more large dams? The actual costs of hydropower megaproject development. *Energy Policy*, 69, 43–56. doi:10.1016/j.enpol.2013.10.069.
- Aobpaet, A., Cuenca, M. C., Hooper, A., & Trisirisatayawong, I. (2013). InSAR time-series analysis of land subsidence in Bangkok, Thailand. *International Journal of Remote Sensing*, 34, 2969–2982. doi:10.1080/01431161.2012.756596.
- Apaydin, H., Feizi, H., Sattari, M. T., Colak, M. S., Shamshirband, S., & Chau, K.-W. (2020). Comparative analysis of recurrent neural network architectures for reservoir inflow forecasting. *Water*, 12, 1500. doi:10.3390/w12051500.
- Apichitchat, S., & Jung, K. (2015). Hydrological simulation for impact assessment of Kaeng Sue Ten dam in Thailand. *KSCE Journal of Civil Engineering*, 19, 2325–2332. doi:10.1007/s12205-015-0322-3.
- Arnell, N. W., & Gosling, S. N. (2016). The impacts of climate change on river flood risk at the global scale. *Climatic Change*, 134, 387–401. doi:10.1007/s10584-014-1084-5.
- Arnold, J. G., Srinivasan, R., Muttiah, R. S., & Williams, J. R. (1998). Large area hydrologic modeling and assessment Part I: model development 1. *Journal of the American Water Resources Association*, 34, 73–89. doi:10.1111/j.1752-1688.1998.tb05961.x.
- Arroyo, J., & Maté, C. (2009). Forecasting histogram time series with k-nearest neighbours methods. *International Journal of Forecasting*, 25, 192–207. doi:10.1016/j.ijforecast.2008.07.003.
- Atkeson, C. G., Moore, A. W., & Schaal, S. (1997). Locally weighted learning. In D. W. Aha (Ed.), *Lazy Learning* (pp. 11–73). Dordrecht: Springer Netherlands. doi:10.1007/978-94-017-2053-3\_2.
- Bachelet, D., Brown, D., Böhm, M., & Russell, P. (1992). Climate change in Thailand and its potential impact on rice yield. *Climatic Change*, 21, 347–366. doi:10.1007/BF00141376.
- Bagley, J. E., Desai, A. R., Harding, K. J., Snyder, P. K., & Foley, J. A. (2014). Drought and deforestation: has land cover change influenced recent precipitation extremes in the Amazon? *Journal of Climate*, 27, 345–361. doi:10.1175/JCLI-D-12-00369.1.
- Baker, D. B., Richards, R. P., Loftus, T. T., & Kramer, J. W. (2004). A new flashiness index: characteristics and applications to Midwestern rivers and streams. *Journal of the American Water Resources Association*, 40, 503–522. doi:10.1111/j.1752-1688.2004.tb01046.x.
- Barros, N., Cole, J. J., Tranvik, L. J., Prairie, Y. T., Bastviken, D., Huszar, V. L., Del Giorgio, P., & Roland, F. (2011). Carbon emission from hydroelectric reservoirs linked to reservoir age and latitude. *Nature Geoscience*, 4, 593–596. doi:10.1038/ngeo1211.
- Batalla, R. J., Gomez, C. M., & Kondolf, G. M. (2004). Reservoir-induced hydrological changes in the Ebro River basin (NE Spain). *Journal of Hydrology*, 290, 117–136. doi:10.1016/j.jhydrol.2003.12.002.
- Baxter, R. (1977). Environmental effects of dams and impoundments. *Annual Review of Ecology and Systematics*, 8, 255–283.
- Beard, L. R. (1967). *Functional Evaluation of a Water Resources System*. Department of Defense, Department of the Army, Corps of Engineers, Hydrologic Engineering Center, United States of America.
- Beck, H. E., Vergopolan, N., Pan, M., Levizzani, V., Van Dijk, A. I., Weedon, G. P., Brocca, L., Pappenberger, F., Huffman, G. J., & Wood, E. F. (2017). Global-scale evaluation of 22 precipitation datasets using gauge observations and hydrological modeling. *Hydrology and Earth System Sciences*, 21, 6201–6217. doi:10.1007/978-3-030-35798-6\_9.
- Beck, H. E., Wood, E. F., McVicar, T. R., ZambranoBigiarini, M., AlvarezGarretton, C., BaezVillanueva, O. M., Sheffield, J., & Karger, D. N. (2020). Bias correction of global high-resolution precipitation climatologies using streamflow observations from 9372 catchments. *Journal of Climate*, 33, 1299–1315. doi:10.1175/JCLI-D-19-0332.1.



- Beck, H. E., Wood, E. F., Pan, M., Fisher, C. K., Miralles, D. G., Van Dijk, A. I., McVicar, T. R., & Adler, R. F. (2019). MSWEP V2 global 3-hourly 0.1° precipitation: methodology and quantitative assessment. *Bulletin of the American Meteorological Society*, 100, 473–500. doi:10.1175/BAMS-D-17-0138.1.
- Bell, V., Kay, A., Jones, R., & Moore, R. (2007). Development of a high resolution grid-based river flow model for use with regional climate model output. *Hydrology and Earth System Sciences*, 11, 532–549. doi:10.5194/hess-11-532-2007.
- Bellmore, R. J., Duda, J. J., Craig, L. S., Greene, S. L., Torgersen, C. E., Collins, M. J., & Vittum, K. (2017). Status and trends of dam removal research in the United States. *Wiley Interdisciplinary Reviews: Water*, 4, e1164. doi:10.1002/wat2.1164.
- Beltran-Peña, A., Rosa, L., & DODorico, P. (2020). Global food self-sufficiency in the 21st century under sustainable intensification of agriculture. *Environmental Research Letters*, 15, 095004. doi:10.1088/1748-9326/ab9388.
- Benchimol, M., & Peres, C. A. (2015). Widespread forest vertebrate extinctions induced by a mega hydroelectric dam in lowland Amazonia. *PloS one*, 10, e0129818. doi:10.1371/journal.pone.0129818.
- Bengio, Y., Simard, P., & Frasconi, P. (1994). Learning long-term dependencies with gradient descent is difficult. *IEEE Transactions on Neural Networks*, 5, 157–166. doi:10.1109/72.279181.
- Bergström, S. (1992). *The HBV Model—Its Structure and Applications*, SMHI Reports RH 4. Technical Report, Swedish Meteorological & Hydrological Institute (SMHI), Norrköping, Sweden.
- Bessler, F. T., Savic, D. A., & Walters, G. A. (2003). Water reservoir control with data mining. *Journal of Water Resources Planning and Management*, 129, 26–34. doi:10.1061/(ASCE)0733-9496(2003)129:1(26).
- Best, J. (2019). Anthropogenic stresses on the worlds big rivers. *Nature Geoscience*, 12, 7–21. doi:10.1038/s41561-018-0262-x.
- Beven, K. (2006). A manifesto for the equifinality thesis. *Journal of Hydrology*, 320, 18–36. doi:10.1016/j.jhydrol.2005.07.007.
- Beven, K. J. (2000). Uniqueness of place and process representations in hydrological modelling. *Hydrology and Earth System Sciences*, 4, 203–213. doi:10.5194/hess-4-203-2000.
- Beven, K. J., & Kirkby, M. J. (1979). A physically based, variable contributing area model of basin hydrology. *Hydrological Sciences Journal*, 24, 43–69. doi:10.1080/02626667909491834.
- Bezanson, J., Karpinski, S., Shah, V. B., & Edelman, A. (2012). *Julia: a fast dynamic language for technical computing*. Technical Report, MIT. doi:10.48550/arXiv.1209.5145.
- Bhagabati, S. S., & Kawasaki, A. (2017). Consideration of the rainfall-runoff-inundation (RRI) model for flood mapping in a deltaic area of Myanmar. *Hydrological Research Letters*, 11, 155–160. doi:10.3178/hrl.11.155.
- Biancamaria, S., Lettenmaier, D. P., & Pavelsky, T. M. (2016). The SWOT mission and its capabilities for land hydrology. In *Remote Sensing and Water Resources* (pp. 117–147). Cham, Switzerland: Springer. doi:10.1007/978-3-319-32449-4.
- Bianchi, T. S. (2016). *Deltas and Humans: A Long Relationship Now Threatened by Global Change*. Oxford University Press, Oxford, United Kingdom. doi:10.1093/oso/9780199764174.001.0001.
- Birkett, C. M., O'Brien, K., Kinsey, S., Ricko, M., & Li, Y. (2022). Enhancement of a global lake and reservoir database to aid climate studies and resource monitoring utilizing satellite radar altimetry. *Journal of Great Lakes Research*, 48, 37–51. doi:10.1016/j.jglr.2021.11.013.
- Blumstein, D., Biancamaria, S., Guérin, A., & Maisongrande, P. (2019). A potential constellation of small altimetry satellites dedicated to continental surface waters (SMASH mission). In *AGU Fall Meeting*

- Abstracts* (pp. H43N–2257). San Francisco, CA, United States of America.
- Bontemps, S., Defourny, P., Van Bogaert, E., Arino, O., Kalogirou, V., & Perez, J. R. (2011). GLOBCOVER 2009–Products description and validation report. URL: <http://due.esrin.esa.int/page-globcover.php>, last accessed on 15/07/2020.
- Box, G. E., Jenkins, G. M., Reinsel, G. C., & Ljung, G. M. (2015). *Time Series Analysis: Forecasting and Control*. John Wiley & Sons, NJ, United States of America.
- Bozorg-Haddad, O., Aboutaleb, M., Ashofteh, P.-S., & Loáiciga, H. A. (2018). Real-time reservoir operation using data mining techniques. *Environmental Monitoring and Assessment*, 190, 1–22. doi:10.1007/s10661-018-6970-2.
- Brakensiek, D., Rawls, W., & Stephenson, G. (1984). Modifying SCS hydrologic soil groups and curve numbers for rangeland soils. In *ASAE Paper No. PNR-84-203* (pp. 84–203). St. Joseph, MI, United States of America: American Society of Agricultural Engineers.
- Breck, E., Polyzotis, N., Roy, S., Whang, S., & Zinkevich, M. (2019). Data validation for machine learning. In *Proceedings of Machine Learning and Systems 1 (MLSys 2019)*. Palo Alto, CA, United States of America.
- Breiman, L. (2001). Random forests. *Machine learning*, 45, 5–32. doi:10.1023/A:1010933404324.
- Breiman, L., Friedman, J., Olshen, R., & Stone, C. (1984). *Classification and Regression Trees*. Wadsworth International Group, Belmont, CA, United States of America. doi:10.1201/9781315139470.
- Brijain, M., Patel, R., Kushik, M., & Rana, K. (2014). A survey on decision tree algorithm for classification. *International Journal of Engineering Development and Research*, 2, 1–5.
- Brooks, E. S., Boll, J., & McDaniel, P. A. (2004). A hillslope-scale experiment to measure lateral saturated hydraulic conductivity. *Water Resources Research*, 40, W04208. doi:10.1029/2003WR002858.
- Brooks, R. H., & Corey, A. T. (1964). *Hydraulic Properties of Porous Media*. Colorado State University Libraries, CO, United States of America.
- Bruinsma, J. (2009). The resource outlook to 2050: by how much do land, water and crop yields need to increase by 2050? In *How to Feed the World in 2050. Proceedings of a Technical Meeting of Experts* (pp. 1–33). Rome, Italy: Food and Agriculture Organization of the United Nations (FAO).
- Bunn, S. E., & Arthington, A. H. (2002). Basic principles and ecological consequences of altered flow regimes for aquatic biodiversity. *Environmental Management*, 30, 492–507. doi:10.1007/s00267-002-2737-0.
- Calver, A., & Cammeraat, L. (1993). Testing a physically-based runoff model against field observations on a Luxembourg hillslope. *Catena*, 20, 273–288. doi:10.1016/0341-8162(93)90005-A.
- Camargo, J. A., & de Jalon, D. G. (1990). The downstream impacts of the Burgomillodo reservoir, Spain. *Regulated Rivers: Research & Management*, 5, 305–317. doi:10.1002/rrr.3450050403.
- Canuto, N., Ramos, T. B., Oliveira, A. R., Simionesei, L., Basso, M., & Neves, R. (2019). Influence of reservoir management on Guadiana streamflow regime. *Journal of Hydrology: Regional Studies*, 25, 100628. doi:10.1016/j.ejrh.2019.100628.
- Ceola, S., Laio, F., & Montanari, A. (2014). Satellite nighttime lights reveal increasing human exposure to floods worldwide. *Geophysical Research Letters*, 41, 7184–7190. doi:10.1002/2014GL061859.
- Chang, H., & Franczyk, J. (2008). Climate change, land-use change, and floods: toward an integrated assessment. *Geography Compass*, 2, 1549–1579. doi:10.1111/j.1749-8198.2008.00136.x.
- Chang, L.-C., & Chang, F.-J. (2001). Intelligent control for modelling of real-time reservoir operation. *Hydrological Processes*, 15, 1621–1634. doi:10.1002/hyp.226.
- Chao, B. F., Wu, Y.-H., & Li, Y. (2008). Impact of artificial reservoir water impoundment on global sea

- level. *Science*, 320, 212–214. doi:10.1126/science.1154580.
- Chaves, P., & Chang, F.-J. (2008). Intelligent reservoir operation system based on evolving artificial neural networks. *Advances in Water Resources*, 31, 926–936. doi:10.1016/j.advwatres.2008.03.002.
- Chen, J., Shi, H., Sivakumar, B., & Peart, M. R. (2016). Population, water, food, energy and dams. *Renewable and Sustainable Energy Reviews*, 56, 18–28. doi:10.1016/j.rser.2015.11.043.
- Chen, K., Guo, S., He, S., Xu, T., Zhong, Y., & Sun, S. (2018). The value of hydrologic information in reservoir outflow decision-making. *Water*, 10, 1372. doi:10.3390/w10101372.
- Chen, L., Zhang, Y., Zhou, J., Singh, V. P., Guo, S., & Zhang, J. (2015). Real-time error correction method combined with combination flood forecasting technique for improving the accuracy of flood forecasting. *Journal of Hydrology*, 521, 157–169. doi:10.1016/j.jhydrol.2014.11.053.
- Chen, X.-w., & Jeong, J. C. (2007). Enhanced recursive feature elimination. In *Sixth International Conference on Machine Learning and Applications (ICMLA 2007)* (pp. 429–435). Cincinnati, OH, United States of America: IEEE. doi:10.1109/ICMLA.2007.35.
- Chen, Y., Li, D., Zhao, Q., & Cai, X. (2022). Developing a generic data-driven reservoir operation model. *Advances in Water Resources*, 167, 104274. doi:10.1016/j.advwatres.2022.104274.
- Cho, K., van Merriënboer, B., Bahdanau, D., & Bengio, Y. (2014). On the properties of neural machine translation: Encoder–decoder approaches. In *Proceedings of SSST-8, Eighth Workshop on Syntax, Semantics and Structure in Statistical Translation* (pp. 103–111). Doha, Qatar: Association for Computational Linguistics. doi:10.3115/v1/W14-4012.
- Cloke, H., & Pappenberger, F. (2009). Ensemble flood forecasting: a review. *Journal of Hydrology*, 375, 613–626. doi:10.1016/j.jhydrol.2009.06.005.
- Coerver, H. M., Rutten, M. M., & Van De Giesen, N. C. (2018). Deduction of reservoir operating rules for application in global hydrological models. *Hydrology and Earth System Sciences*, 22, 831–851. doi:10.5194/hess-22-831-2018.
- Cook, E. R., Anchukaitis, K. J., Buckley, B. M., D'Arrigo, R. D., Jacoby, G. C., & Wright, W. E. (2010). Asian monsoon failure and megadrought during the last millennium. *Science*, 328, 486–489. doi:10.1126/science.1185188.
- Cosby, B., Hornberger, G., Clapp, R., & Ginn, T. (1984). A statistical exploration of the relationships of soil moisture characteristics to the physical properties of soils. *Water Resources Research*, 20, 682–690. doi:10.1029/WR020i006p00682.
- Crawford, N. H. (1966). *Digital simulation in hydrology: stanford watershed model IV*. Technical Report, Department of Civil Engineering, Stanford University, CA, United States of America.
- Dai, A. (2011). Drought under global warming: a review. *Wiley Interdisciplinary Reviews: Climate Change*, 2, 45–65. doi:10.1002/wcc.81.
- Dai, A. (2013). Increasing drought under global warming in observations and models. *Nature Climate Change*, 3, 52. doi:10.1038/nclimate1633.
- De Stefano, L., Petersen-Perlman, J. D., Sproles, E. A., Eynard, J., & Wolf, A. T. (2017). Assessment of transboundary river basins for potential hydro-political tensions. *Global Environmental Change*, 45, 35–46. doi:10.1016/j.gloenvcha.2017.04.008.
- DHI (2017a). *MIKE HYDRO Basin User Guide*. Technical Report, Danish Hydrological Institute, Denmark. URL: [https://manuals.mikepoweredbydhi.help/latest/Water\\_Resources/MIKEHydro\\_basin\\_UserGuide.pdf](https://manuals.mikepoweredbydhi.help/latest/Water_Resources/MIKEHydro_basin_UserGuide.pdf), last accessed on 03/11/2022.
- DHI (2017b). *MIKE HYDRO River User Guide*. Technical Report, Danish Hydrological Institute, Denmark. URL: [https://manuals.mikepoweredbydhi.help/2017/Water\\_Resources/MIKEHydro\\_River\\_UserGuide.pdf](https://manuals.mikepoweredbydhi.help/2017/Water_Resources/MIKEHydro_River_UserGuide.pdf),

last accessed on 03/11/2022.

- DHI (2017c). *MIKE SHE Volume 1: User Guide*. Technical Report, Danish Hydrological Institute, Denmark. URL: [https://manuals.mikepoweredbydhi.help/2017/Water\\_Resources/MIKE\\_SHE\\_Printed.V1.pdf](https://manuals.mikepoweredbydhi.help/2017/Water_Resources/MIKE_SHE_Printed.V1.pdf), last accessed on 03/11/2022.
- Di Baldassarre, G., Wanders, N., AghaKouchak, A., Kuil, L., Rangelcroft, S., Veldkamp, T. I., Garcia, M., van Oel, P. R., Breinl, K., & Van Loon, A. F. (2018). Water shortages worsened by reservoir effects. *Nature Sustainability*, 1, 617–622. doi:10.1038/s41893-018-0159-0.
- Döll, P., Fiedler, K., & Zhang, J. (2009). Global-scale analysis of river flow alterations due to water withdrawals and reservoirs. *Hydrology and Earth System Sciences*, 13, 2413–2432. doi:10.5194/hess-13-2413-2009.
- Draper, A. J., Munévar, A., Arora, S. K., Reyes, E., Parker, N. L., Chung, F. I., & Peterson, L. E. (2004). CalSim: generalized model for reservoir system analysis. *Journal of Water Resources Planning and Management*, 130, 480–489. doi:10.1061/(ASCE)0733-9496(2004)130:6(480).
- Durrans, S. R. (1988). Total probability methods for problems in flood frequency estimation. In *Statistical and Bayesian Methods in Hydrological Sciences*. UNESCO Technical Documents in Hydrology (pp. 299–326). Paris, France.
- ECMWF (2022). Operational archive: Meteorological Archival and Retrieval System (MARS). URL: <https://www.ecmwf.int/en/forecasts/dataset/operational-archive>, last accessed on 26/09/2022.
- EGAT (2013). Exploring EGAT power plants and dams: Electricity Generating Authority of Thailand. URL: <https://www.egat.co.th/home/en/powerplants-and-dams/>, last accessed on 24/07/2022.
- Engman, E. T. (1986). Roughness coefficients for routing surface runoff. *Journal of Irrigation and Drainage Engineering*, 112, 39–53. doi:10.1061/(ASCE)0733-9437(1986)112:1(39).
- Fix, E., & Hodges, J. L. (1989). Discriminatory analysis. Nonparametric discrimination: consistency properties. *International Statistical Review*, 57, 238–247. doi:10.2307/1403797.
- Fortin, J. P., Turcotte, R., Massicotte, S., Moussa, R., Fitzback, J., & Villeneuve, J. P. (2001). Distributed watershed model compatible with remote sensing and GIS data. I: description of model. *Journal of Hydrologic Engineering*, 6, 91–99. doi:10.1061/(ASCE)1084-0699(2001)6:2(91).
- Fowe, T., Karambiri, H., Paturel, J.-E., Poussin, J.-C., & Cecchi, P. (2015). Water balance of small reservoirs in the Volta basin: a case study of Boura reservoir in Burkina Faso. *Agricultural Water Management*, 152, 99–109. doi:10.1016/j.agwat.2015.01.006.
- Gai, L., Nunes, J. P., Baartman, J. E., Zhang, H., Wang, F., de Roo, A., Ritsema, C. J., & Geissen, V. (2019). Assessing the impact of human interventions on floods and low flows in the Wei River basin in China using the LISFLOOD model. *Science of the Total Environment*, 653, 1077–1094. doi:10.1016/j.scitotenv.2018.10.379.
- Gale, E. L., & Saunders, M. A. (2013). The 2011 Thailand flood: climate causes and return periods. *Weather*, 68, 233–237. doi:10.1002/wea.2133.
- Gangrade, S., Lu, D., Kao, S.-C., & Painter, S. L. (2022). Machine learning assisted reservoir operation model for long-term water management simulation. *Journal of the American Water Resources Association*, JAWR-22-0009-P. doi:10.1111/1752-1688.13060.
- Gash, J. (1979). An analytical model of rainfall interception by forests. *Quarterly Journal of the Royal Meteorological Society*, 105, 43–55. doi:10.1002/qj.49710544304.
- Gauch, M., Mai, J., & Lin, J. (2021). The proper care and feeding of CAMELS: how limited training data affects streamflow prediction. *Environmental Modelling & Software*, 135, 104926. doi:10.1016/j.envsoft.2020.104926.

- Gauthier, M. J., Camporese, M., Rivard, C., Paniconi, C., & Larocque, M. (2009). A modeling study of heterogeneity and surface water-groundwater interactions in the Thomas Brook catchment, Annapolis Valley (Nova Scotia, Canada). *Hydrology and Earth System Sciences*, 13, 1583–1596. doi:10.5194/hess-13-1583-2009.
- Gebremicael, T., Mohamed, Y., & Van der Zaag, P. (2019). Attributing the hydrological impact of different land use types and their long-term dynamics through combining parsimonious hydrological modelling, alteration analysis and PLSR analysis. *Science of the Total Environment*, 660, 1155–1167. doi:10.1016/j.scitotenv.2019.01.085.
- Gers, F. A., Schmidhuber, J., & Cummins, F. (2000). Learning to forget: continual prediction with LSTM. *Neural Computation*, 12, 2451–2471. doi:10.1162/089976600300015015.
- Giardino, A., Schrijvershof, R., Nederhoff, C., De Vroeg, H., Brière, C., Tonnon, P. K., Caires, S., Walstra, D., Sosa, J., Van Verseveld, W. et al. (2018). A quantitative assessment of human interventions and climate change on the West African sediment budget. *Ocean & Coastal Management*, 156, 249–265. doi:10.1016/j.ocecoaman.2017.11.008.
- Gneiting, T., & Raftery, A. E. (2007). Strictly proper scoring rules, prediction, and estimation. *Journal of the American statistical Association*, 102, 359–378. doi:10.1198/016214506000001437.
- Gourley, J. J., & Vieux, B. E. (2006). A method for identifying sources of model uncertainty in rainfall-runoff simulations. *Journal of Hydrology*, 327, 68–80. doi:10.1016/j.jhydrol.2005.11.036.
- Graf, W. L. (2006). Downstream hydrologic and geomorphic effects of large dams on American rivers. *Geomorphology*, 79, 336–360. doi:10.1016/j.geomorph.2006.06.022.
- Grayson, R., & Blöschl, G. (2001). *Spatial Modelling of Catchment Dynamics*. Cambridge University Press, Cambridge, United Kingdom.
- Grill, G., Lehner, B., Lumsdon, A. E., MacDonald, G. K., Zarfl, C., & Liermann, C. R. (2015). An index-based framework for assessing patterns and trends in river fragmentation and flow regulation by global dams at multiple scales. *Environmental Research Letters*, 10, 015001. doi:10.1088/1748-9326/10/1/015001.
- Grill, G., Lehner, B., Thieme, M., Geenen, B., Tickner, D., Antonelli, F., Babu, S., Borrelli, P., Cheng, L., Crochetiere, H. et al. (2019). Mapping the worlds free-flowing rivers. *Nature*, 569, 215–221. doi:10.1038/s41586-019-1111-9.
- Guo, Y., Yu, X., Xu, Y.-P., Chen, H., Gu, H., & Xie, J. (2021). AI-based techniques for multi-step stream-flow forecasts: application for multi-objective reservoir operation optimization and performance assessment. *Hydrology and Earth System Sciences*, 25, 5951–5979. doi:10.5194/hess-25-5951-2021.
- Gupta, H. V., Kling, H., Yilmaz, K. K., & Martinez, G. F. (2009). Decomposition of the mean squared error and NSE performance criteria: implications for improving hydrological modelling. *Journal of Hydrology*, 377, 80–91. doi:10.1016/j.jhydrol.2009.08.003.
- Gupta, H. V., Sorooshian, S., & Yapo, P. O. (1999). Status of automatic calibration for hydrologic models: comparison with multilevel expert calibration. *Journal of Hydrologic Engineering*, 4, 135–143. doi:10.1061/(ASCE)1084-0699(1999)4:2(135).
- Gustard, A., Bullock, A., & Dixon, J. (1992). *Low Flow Estimation in the United Kingdom*. Institute of Hydrology, Oxford, United Kingdom.
- Hamed, K. H., & Rao, A. R. (1998). A modified Mann-Kendall trend test for autocorrelated data. *Journal of Hydrology*, 204, 182–196. doi:10.1016/S0022-1694(97)00125-X.
- Han, D., Chan, L., & Zhu, N. (2007). Flood forecasting using support vector machines. *Journal of Hydroinformatics*, 9, 267–276. doi:10.2166/hydro.2007.027.
- Hanasaki, N., Kanae, S., & Oki, T. (2006). A reservoir operation scheme for global river routing models.

- Journal of Hydrology*, 327, 22–41. doi:10.1016/j.jhydrol.2005.11.011.
- Hanasaki, N., Saito, Y., Chaiyasaen, C., Champathong, A., Ekkawatpanit, C., Saphaokham, S., Sukhappunnaphan, T., Sumdin, S., & Thongduang, J. (2014). A quasi-real-time hydrological simulation of the Chao Phraya River using meteorological data from the Thai Meteorological Department Automatic Weather Stations. *Hydrological Research Letters*, 8, 9–14. doi:10.3178/hrl.8.9.
- Hashino, T., Bradley, A., & Schwartz, S. (2007). Evaluation of bias-correction methods for ensemble streamflow volume forecasts. *Hydrology and Earth System Sciences*, 11, 939–950. doi:10.5194/hess-11-939-2007.
- Hassaballah, K., Mohamed, Y., Uhlenbrook, S., & Biro, K. (2017). Analysis of streamflow response to land use and land cover changes using satellite data and hydrological modelling: case study of Dinder and Rahad tributaries of the Blue Nile (Ethiopia–Sudan). *Hydrology and Earth System Sciences*, 21, 5217. doi:10.5194/hess-21-5217-2017.
- Hastie, T., Tibshirani, R., Friedman, J. H., & Friedman, J. H. (2009). *The Elements of Statistical Learning: Data Mining, Inference, and Prediction*. Springer New York, NY, United States of America. doi:10.1007/978-0-387-84858-7.
- He, S., Gu, L., Tian, J., Deng, L., Yin, J., Liao, Z., Zeng, Z., Shen, Y., & Hui, Y. (2021). Machine learning improvement of streamflow simulation by utilizing remote sensing data and potential application in guiding reservoir operation. *Sustainability*, 13, 3645. doi:10.3390/su13073645.
- He, S., Guo, S., Zhang, J., Liu, Z., Cui, Z., Zhang, Y., & Zheng, Y. (2022). Multi-objective operation of cascade reservoirs based on short-term ensemble streamflow prediction. *Journal of Hydrology*, 610, 127936. doi:10.1016/j.jhydrol.2022.127936.
- He, X., Wada, Y., Wanders, N., & Sheffield, J. (2017). Intensification of hydrological drought in California by human water management. *Geophysical Research Letters*, 44, 1777–1785. doi:10.1002/2016GL071665.
- Hecht, J. S., Lacombe, G., Arias, M. E., Dang, T. D., & Piman, T. (2019). Hydropower dams of the Mekong River basin: a review of their hydrological impacts. *Journal of Hydrology*, 568, 285–300. doi:10.1016/j.jhydrol.2018.10.045.
- Hengl, T., de Jesus, J. M., Heuvelink, G. B., Gonzalez, M. R., Kilibarda, M., Blagotić, A., Shangguan, W., Wright, M. N., Geng, X., Bauer-Marschallinger, B. et al. (2017). SoilGrids250m: global gridded soil information based on machine learning. *PLoS one*, 12, e0169748. doi:10.1371/journal.pone.0169748.
- Hennig, T., & Magee, D. (2017). Comment on An index-based framework for assessing patterns and trends in river fragmentation and flow regulation by global dams at multiple scales. *Environmental Research Letters*, 12, 038001. doi:10.1088/1748-9326/aa5dc6.
- Hersbach, H. (2000). Decomposition of the continuous ranked probability score for ensemble prediction systems. *Weather and Forecasting*, 15, 559–570. doi:10.1175/1520-0434(2000)015%3C0559:DOTCRP%3E2.0.CO;2.
- Hirabayashi, Y., Mahendran, R., Koirala, S., Konoshima, L., Yamazaki, D., Watanabe, S., Kim, H., & Kanae, S. (2013). Global flood risk under climate change. *Nature Climate Change*, 3, 816. doi:10.1038/nclimate1911.
- Hisdal, H., Tallaksen, L. M., Clausen, B., Peters, E., Gustard, A., & Van Lanen, H. (2004). Hydrological drought characteristics. *Developments in Water Science*, 48, 139–198.
- Hochreiter, S., & Schmidhuber, J. (1997). Long short-term memory. *Neural Computation*, 9, 1735–1780. doi:10.1162/neco.1997.9.8.1735.
- Hogeboom, R. J., Knook, L., & Hoekstra, A. Y. (2018). The blue water footprint of the world's artificial reservoirs for hydroelectricity, irrigation, residential and industrial water supply, flood protection, fish-

- ing and recreation. *Advances in Water Resources*, 113, 285–294. doi:10.1016/j.advwatres.2018.01.028.
- Hong, J., Lee, S., Lee, G., Yang, D., Bae Hyun, J., Kim, J., Kim, K., & Lim Jae, K. (2021). Comparison of machine learning algorithms for discharge prediction of multipurpose dam. *Water*, 13, 3369. doi:10.3390/w13233369.
- Houshmand Kouchi, D., Esmaili, K., Faridhosseini, A., Sanaeinejad, S. H., Khalili, D., & Abbaspour, K. C. (2017). Sensitivity of calibrated parameters and water resource estimates on different objective functions and optimization algorithms. *Water*, 9, 384. doi:https://doi.org/10.3390/w9060384.
- Hsu, N.-S., Huang, C.-L., & Wei, C.-C. (2015). Multi-phase intelligent decision model for reservoir real-time flood control during typhoons. *Journal of Hydrology*, 522, 11–34. doi:10.1016/j.jhydrol.2014.12.013.
- Hughes, D., Birkinshaw, S., & Parkin, G. (2021). A method to include reservoir operations in catchment hydrological models using SHETRAN. *Environmental Modelling & Software*, 138, 104980. doi:10.1016/j.envsoft.2021.104980.
- Ibrahim, K. S. M. H., Huang, Y. F., Ahmed, A. N., Koo, C. H., & El-Shafie, A. (2022). A review of the hybrid artificial intelligence and optimization modelling of hydrological streamflow forecasting. *Alexandria Engineering Journal*, 61, 279–303. doi:10.1016/j.aej.2021.04.100.
- Imandoust, S. B., Bolandraftar, M. et al. (2013). Application of k-nearest neighbor (KNN) approach for predicting economic events: theoretical background. *International Journal of Engineering Research and Applications*, 3, 605–610.
- Imhoff, R., Brauer, C., Overeem, A., Weerts, A., & Uijlenhoet, R. (2020a). Spatial and temporal evaluation of radar rainfall nowcasting techniques on 1,533 events. *Water Resources Research*, 56, e2019WR026723. doi:10.1029/2019WR026723.
- Imhoff, R., van Verseveld, W., van Osnabrugge, B., & Weerts, A. (2020b). Scaling point-scale (pedo) transfer functions to seamless large-domain parameter estimates for high-resolution distributed hydrologic modeling: an example for the Rhine River. *Water Resources Research*, 56, e2019WR026807. doi:10.1029/2019WR026807.
- International Hydropower Association (2022). *Hydropower Status Report 2022*. Technical Report, IHA, London, UK.
- Jain, A., Patel, H., Nagalapatti, L., Gupta, N., Mehta, S., Guttula, S., Mujumdar, S., Afzal, S., Sharma Mittal, R., & Munigala, V. (2020). Overview and importance of data quality for machine learning tasks. In *Proceedings of the 26th ACM SIGKDD International Conference on Knowledge Discovery & Data Mining* (pp. 3561–3562). NY, United States of America. doi:10.1145/3394486.3406477.
- Jain, S., Das, A., & Srivastava, D. (1999). Application of ANN for reservoir inflow prediction and operation. *Journal of Water Resources Planning and Management*, 125, 263–271. doi:10.1061/(ASCE)0733-9496(1999)125:5(263).
- Jain, S. K., & Singh, V. P. (2003). *Water Resources Systems Planning and Management*. Elsevier Science B.V., Amsterdam, the Netherlands.
- Jaiswal, A. (2022). Tutorial on RNN, LSTM and GRU with implementation. URL: <https://www.analyticsvidhya.com/blog/2022/01/tutorial-on-rnn-lstm-gru-with-implementation/>, last accessed on 08/11/2022.
- Jamrussri, S., & Toda, Y. (2017). Simulating past severe flood events to evaluate the effectiveness of nonstructural flood countermeasures in the upper Chao Phraya River basin, Thailand. *Journal of Hydrology: Regional Studies*, 10, 82–94. doi:10.1016/j.ejrh.2017.02.001.
- Jarvis, A., Reuter, H. I., Nelson, A., & Guevara, E. (2008). Hole-filled seamless SRTM data V4. URL: <http://srtm.csi.cgiar.org>, last accessed on 15/07/2020.

- Jenkins, G. M. (1968). *Spectral Analysis and Its Applications*. Holden-Day, Inc., San Francisco, CA, United States of America.
- Johnson, S. A., Stedinger, J. R., & Staschus, K. (1991). Heuristic operating policies for reservoir system simulation. *Water Resources Research*, 27, 673–685. doi:10.1029/91WR00320.
- Jung, T., Balsamo, G., Bechtold, P., Beljaars, A., Koehler, M., Miller, M., Morcrette, J.-J., Orr, A., Rodwell, M., & Tompkins, A. M. (2010). The ECMWF model climate: recent progress through improved physical parametrizations. *Quarterly Journal of the Royal Meteorological Society*, 136, 1145–1160. doi:10.1002/qj.634.
- Kampf, S. K., & Burges, S. J. (2010). Quantifying the water balance in a planar hillslope plot: effects of measurement errors on flow prediction. *Journal of Hydrology*, 380, 191–202. doi:10.1016/j.jhydrol.2009.10.036.
- Karamouz, M., Ahmadi, A., & Moridi, A. (2009). Probabilistic reservoir operation using Bayesian stochastic model and support vector machine. *Advances in Water Resources*, 32, 1588–1600. doi:10.1016/j.advwatres.2009.08.003.
- Karssenbergh, D., Schmitz, O., Salamon, P., De Jong, K., & Bierkens, M. F. (2010). A software framework for construction of process-based stochastic spatio-temporal models and data assimilation. *Environmental Modelling & Software*, 25, 489–502. doi:10.1016/j.envsoft.2009.10.004.
- Kendall, M. G. (1946). *The Advanced Theory of Statistics*. 2nd Ed. Charles Griffin and Co., Ltd., London, United Kingdom.
- Ketkar, N. (2017). Introduction to Keras. In *Deep Learning with Python: A Hands-on Introduction* (pp. 97–111). Berkeley, CA, United States of America: Apress. doi:10.1007/978-1-4842-2766-4-7.
- Khalaf, M., Alaskar, H., Hussain, A. J., Baker, T., Maamar, Z., Buyya, R., Liatsis, P., Khan, W., Tawfik, H., & Al-Jumeily, D. (2020). IoT-enabled flood severity prediction via ensemble machine learning models. *IEEE Access*, 8, 70375–70386. doi:10.1109/ACCESS.2020.2986090.
- Kilgore, J. L. (1997). *Development and Evaluation of a GIS-Based Spatially Distributed Unit Hydrograph Model*. Virginia Tech, VA, United States of America.
- Kim, M., Kim, Y., Kim, H., Piao, W., & Kim, C. (2016). Evaluation of the k-nearest neighbor method for forecasting the influent characteristics of wastewater treatment plant. *Frontiers of Environmental Science & Engineering*, 10, 299–310. doi:10.1007/s11783-015-0825-7.
- Kim, T., Yang, T., Gao, S., Zhang, L., Ding, Z., Wen, X., Gourley, J. J., & Hong, Y. (2021). Can artificial intelligence and data-driven machine learning models match or even replace process-driven hydrologic models for streamflow simulation?: a case study of four watersheds with different hydro-climatic regions across the CONUS. *Journal of Hydrology*, 598, 126423. doi:10.1016/j.jhydrol.2021.126423.
- Kingma, D. P., & Ba, J. (2014). Adam: a method for stochastic optimization. In *2017 International Conference on Industrial Engineering, Management Science and Application (ICIMSA)*. San Diego, CA, United States of America. doi:10.48550/arXiv.1412.6980.
- Kinouchi, T., Yamamoto, G., Komsai, A., & Liengcharernsit, W. (2018). Quantification of seasonal precipitation over the upper Chao Phraya River basin in the past fifty years based on monsoon and El Niño/Southern Oscillation Related Climate Indices. *Water*, 10, 800. doi:10.3390/w10060800.
- Kirchherr, J., Pomun, T., & Walton, M. J. (2018). Mapping the social impacts of Damocles projects: the case of Thailand's (as yet Unbuilt) Kaeng Suea Ten dam. *Journal of International Development*, 30, 474–492. doi:10.1002/jid.3246.
- Kirchner, J. W. (2006). Getting the right answers for the right reasons: linking measurements, analyses, and models to advance the science of hydrology. *Water Resources Research*, 42, W03S04. doi:10.1029/2005WR004362.



- Kite, G. (2000). *Developing a Hydrological Model for the Mekong Basin: Impacts of Basin Development on Fisheries Productivity*. International Water Management Institute, Colombo, Sri Lanka. doi:10.3910/2009.137.
- Kite, G. (2001). Modelling the Mekong: hydrological simulation for environmental impact studies. *Journal of Hydrology*, 253, 1–13. doi:10.1016/S0022-1694(01)00396-1.
- Klemeš, V. (1986). Operational testing of hydrological simulation models. *Hydrological Sciences Journal*, 31, 13–24. doi:10.1080/02626668609491024.
- Klipsch, J. D., & Evans, T. A. (2006). Reservoir operations modeling with HEC-ResSim. In *Proceedings of the 3rd Federal Interagency Hydrologic Modeling Conference*. NV, United States of America.
- Knoben, W. J., Freer, J. E., & Woods, R. A. (2019). Inherent benchmark or not? Comparing Nash–Sutcliffe and Kling–Gupta efficiency scores. *Hydrology and Earth System Sciences*, 23, 4323–4331. doi:10.5194/hess-23-4323-2019.
- Komori, D., Mateo, C. M., Saya, A., Nakamura, S., Kiguchi, M., Klinkhachorn, P., Sukhaphunnaphan, T., Champathong, A., Takeya, K. et al. (2013). Application of the probability evaluation for the seasonal reservoir operation on flood mitigation and water supply in the Chao Phraya River watershed, Thailand. *Journal of Disaster Research*, 8, 432–446. doi:10.20965/jdr.2013.p0432.
- Komori, D., Nakamura, S., Kiguchi, M., Nishijima, A., Yamazaki, D., Suzuki, S., Kawasaki, A., Oki, K., & Oki, T. (2012). Characteristics of the 2011 Chao Phraya River flood in central Thailand. *Hydrological Research Letters*, 6, 41–46. doi:10.3178/hrl.6.41.
- Kompot, W., Yoshikawa, S., & Kanae, S. (2020). Use of seasonal streamflow forecasts for flood mitigation with adaptive reservoir operation: a case study of the Chao Phraya River basin, Thailand, in 2011. *Water*, 12, 3210. doi:10.3390/w12113210.
- Kratzert, F., Klotz, D., Herrnegger, M., Sampson, A. K., Hochreiter, S., & Nearing, G. S. (2019a). Toward improved predictions in ungauged basins: exploiting the power of machine learning. *Water Resources Research*, 55, 11344–11354. doi:10.1029/2019WR026065.
- Kratzert, F., Klotz, D., Shalev, G., Klambauer, G., Hochreiter, S., & Nearing, G. (2019b). Towards learning universal, regional, and local hydrological behaviors via machine learning applied to large-sample datasets. *Hydrology and Earth System Sciences*, 23, 5089–5110. doi:10.5194/hess-23-5089-2019.
- Kripalani, R., Singh, S., Panchawagh, N., & Briksavana, M. (1995). Variability of the summer monsoon rainfall over Thailand and comparison with features over India. *International Journal of Climatology*, 15, 657–672. doi:10.1002/joc.3370150606.
- Krzywinski, M., & Altman, N. (2017). Classification and regression trees. *Nature Methods*, 14, 757–758. doi:10.1038/nmeth.4370.
- Kubat, M. (1999). Neural networks: a comprehensive foundation by Simon Haykin, Macmillan, 1994. *Knowledge Engineering Review*, 13, 409–412.
- Kumar, D. N., & Reddy, M. J. (2007). Multipurpose reservoir operation using particle swarm optimization. *Journal of Water Resources Planning and Management, ASCE*, 133, 192–201. doi:10.1061/(ASCE)0733-9496(2007)133:3(192).
- Kure, S., & Tebakari, T. (2012). Hydrological impact of regional climate change in the Chao Phraya River basin, Thailand. *Hydrological Research Letters*, 6, 53–58. doi:10.3178/hrl.6.53.
- Langat, P. K., Kumar, L., & Koech, R. (2019). Identification of the most suitable probability distribution models for maximum, minimum, and mean streamflow. *Water*, 11, 734. doi:10.3390/w11040734.
- Lauri, H., de Moel, H., Ward, P. J., Räsänen, T. A., Keskinen, M., & Kummu, M. (2012). Future changes in Mekong River hydrology: impact of climate change and reservoir operation on discharge. *Hydrology and Earth System Sciences*, 16, 4603–4619. doi:10.5194/hess-16-4603-2012.

- Lee, J., Heo, J.-H., Lee, J., & Kim, N. (2017). Assessment of flood frequency alteration by dam construction via SWAT simulation. *Water*, 9, 264. doi:10.3390/w9040264.
- Lehner, B., & Grill, G. (2013). Global river hydrography and network routing: baseline data and new approaches to study the world's large river systems. *Hydrological Processes*, 27, 2171–2186. doi:10.1002/hyp.9740.
- Lehner, B., Liermann, C. R., Revenga, C., Vörösmarty, C., Fekete, B., Crouzet, P., Döll, P., Endejan, M., Frenken, K., Magome, J. et al. (2011). High-resolution mapping of the world's reservoirs and dams for sustainable river-flow management. *Frontiers in Ecology and the Environment*, 9, 494–502. doi:10.1890/100125.
- Li, D., Long, D., Zhao, J., Lu, H., & Hong, Y. (2017). Observed changes in flow regimes in the Mekong River basin. *Journal of Hydrology*, 551, 217–232. doi:10.1016/j.jhydrol.2017.05.061.
- Li, F., Ma, G., Chen, S., & Huang, W. (2021). An ensemble modeling approach to forecast daily reservoir inflow using bidirectional long-and short-term memory (Bi-LSTM), variational mode decomposition (VMD), and energy entropy method. *Water Resources Management*, 35, 2941–2963. doi:10.1007/s11269-021-02879-3.
- Li, J., Zhong, P.-a., Yang, M., Zhu, F., Chen, J., Liu, W., & Xu, S. (2020). Intelligent identification of effective reservoirs based on the random forest classification model. *Journal of Hydrology*, 591, 125324. doi:10.1016/j.jhydrol.2020.125324.
- Li, Q., Yu, M., Zhao, J., Cai, T., Lu, G., Xie, W., & Bai, X. (2012). Impact of the Three Gorges reservoir operation on downstream ecological water requirements. *Hydrology Research*, 43, 48–53. doi:10.2166/nh.2011.121.
- Li, R., Shi, J., Ji, D., Zhao, T., Plermkamon, V., Moukomla, S., Kuntiyawichai, K., & Kruasilp, J. (2019). Evaluation and hydrological application of TRMM and GPM precipitation products in a tropical monsoon basin of Thailand. *Water*, 11, 818. doi:10.3390/w11040818.
- Ligaray, M., Kim, H., Sthiannopkao, S., Lee, S., Cho, K. H., & Kim, J. H. (2015). Assessment on hydrologic response by climate change in the Chao Phraya River basin, Thailand. *Water*, 7, 6892–6909. doi:10.3390/w7126665.
- Lima, I. B., Ramos, F. M., Bambace, L. A., & Rosa, R. R. (2008). Methane emissions from large dams as renewable energy resources: a developing nation perspective. *Mitigation and Adaptation Strategies for Global Change*, 13, 193–206. doi:10.1007/s11027-007-9086-5.
- Lindström, G., Johansson, B., Persson, M., Gardelin, M., & Bergström, S. (1997). Development and test of the distributed HBV-96 hydrological model. *Journal of Hydrology*, 201, 272–288. doi:10.1016/S0022-1694(97)00041-3.
- Liu, C., Sun, J., Yang, X., Jin, S., & Fu, S. (2021). Evaluation of ECMWF precipitation predictions in China during 2015–18. *Weather and Forecasting*, 36, 1043–1060. doi:10.1175/WAF-D-20-0143.1.
- Liu, J., Shangquan, D., Liu, S., Ding, Y., Wang, S., & Wang, X. (2019a). Evaluation and comparison of CHIRPS and MSWEP daily-precipitation products in the Qinghai-Tibet Plateau during the period of 1981–2015. *Atmospheric Research*, 230, 104634. doi:10.1016/j.atmosres.2019.104634.
- Liu, J., Yuan, X., Zeng, J., Jiao, Y., Li, Y., Zhong, L., & Yao, L. (2022). Ensemble streamflow forecasting over a cascade reservoir catchment with integrated hydrometeorological modeling and machine learning. *Hydrology and Earth System Sciences*, 26, 265–278. doi:10.5194/hess-26-265-2022.
- Liu, S. (1998). Estimation of rainfall storage capacity in the canopies of cypress wetlands and slash pine uplands in North-Central Florida. *Journal of Hydrology*, 207, 32–41. doi:10.1016/S0022-1694(98)00115-2.
- Liu, X., Liu, F. M., Wang, X. X., Li, X. D., Fan, Y. Y., Cai, S. X., & Ao, T. Q. (2017). Combining rainfall data

- from rain gauges and TRMM in hydrological modelling of Laotian data-sparse basins. *Applied Water Science*, 7, 1487–1496. doi:10.1007/s13201-015-0330-y.
- Liu, Y., Qin, H., Zhang, Z., Yao, L., Wang, Y., Li, J., Liu, G., & Zhou, J. (2019b). Deriving reservoir operation rule based on Bayesian deep learning method considering multiple uncertainties. *Journal of Hydrology*, 579, 124207. doi:10.1016/j.jhydrol.2019.124207.
- Liu, Y., Weerts, A., Clark, M., Hendricks Franssen, H.-J., Kumar, S., Moradkhani, H., Seo, D.-J., Schwanen-berg, D., Smith, P., Van Dijk, A. et al. (2012). Advancing data assimilation in operational hydrologic forecasting: progresses, challenges, and emerging opportunities. *Hydrology and Earth System Sciences*, 16, 3863–3887. doi:10.5194/hess-16-3863-2012.
- Liu, Z., Martina, M. L., & Todini, E. (2005). Flood forecasting using a fully distributed model: application of the TOPKAPI model to the upper Xixian Catchment. *Hydrology and Earth System Sciences Discussions*, 9, 347–364. doi:10.5194/hess-9-347-2005.
- Livneh, B., Rajagopalan, B., Kasprzyk, J. et al. (2017). Hydrological model application under data scarcity for multiple watersheds, Java Island, Indonesia. *Journal of Hydrology: Regional Studies*, 9, 127–139. doi:10.1016/j.ejrh.2016.09.007.
- Lohani, A., Kumar, R., & Singh, R. (2012). Hydrological time series modeling: a comparison between adaptive neuro-fuzzy, neural network and autoregressive techniques. *Journal of Hydrology*, 442, 23–35. doi:10.1016/j.jhydrol.2012.03.031.
- Long, Y., Wang, H., Jiang, C., & Ling, S. (2019). Seasonal inflow forecasts using gridded precipitation and soil moisture information: implications for reservoir operation. *Water Resources Management*, 33, 3743–3757. doi:10.1007/s11269-019-02330-8.
- Loo, Y. Y., Billa, L., & Singh, A. (2015). Effect of climate change on seasonal monsoon in Asia and its impact on the variability of monsoon rainfall in Southeast Asia. *Geoscience Frontiers*, 6, 817–823. doi:10.1016/j.gsf.2014.02.009.
- López López, P. (2018). *Application of Global Hydrological Datasets for River Basin Modelling*. Utrecht University, Utrecht, the Netherlands.
- López López, P., Wanders, N., Schellekens, J., Renzullo, L. J., Sutanudjaja, E., & Bierkens, M. F. (2016). Improved large-scale hydrological modelling through the assimilation of streamflow and downscaled satellite soil moisture observations. *Hydrology and Earth System Sciences*, 20, 3059–3076. doi:10.5194/hess-20-3059-2016.
- Lund, J. R., & Guzman, J. (1999). Derived operating rules for reservoirs in series or in parallel. *Journal of Water Resources Planning and Management*, 125, 143–153. doi:10.1061/(ASCE)0733-9496(1999)125:3(143).
- Luu, C., Von Meding, J., & Kanjanabootra, S. (2018). Assessing flood hazard using flood marks and analytic hierarchy process approach: a case study for the 2013 flood event in Quang Nam, Vietnam. *Natural Hazards*, 90, 1031–1050. doi:10.1007/s11069-017-3083-0.
- Malekmohammadi, B., Zahraie, B., & Kerachian, R. (2010). A real-time operation optimization model for flood management in river-reservoir systems. *Natural hazards*, 53, 459–482. doi:10.1007/s11069-009-9442-8.
- Manga, M. (1999). On the timescales characterizing groundwater discharge at springs. *Journal of Hydrology*, 219, 56–69. doi:10.1016/S0022-1694(99)00044-X.
- Matalas, N. C. (1963). *Probability Distribution of Low Flows*. US Government Printing Office, DC, United States of America.
- Mateo, C. M., Hanasaki, N., Komori, D., Tanaka, K., Kiguchi, M., Champathong, A., Sukhapunnaphan, T., Yamazaki, D., & Oki, T. (2014). Assessing the impacts of reservoir operation to floodplain inunda-

- tion by combining hydrological, reservoir management, and hydrodynamic models. *Water Resources Research*, 50, 7245–7266. doi:10.1002/2013WR014845.
- McDonnell, J., Sivapalan, M., Vaché, K., Dunn, S., Grant, G., Haggerty, R., Hinz, C., Hooper, R., Kirchner, J., Roderick, M. et al. (2007). Moving beyond heterogeneity and process complexity: a new vision for watershed hydrology. *Water Resources Research*, 43, W07301. doi:10.1029/2006WR005467.
- Mei, X., Dai, Z., Darby, S. E., Gao, S., Wang, J., & Jiang, W. (2018). Modulation of extreme flood levels by impoundment significantly offset by floodplain loss downstream of the Three Gorges Dam. *Geophysical Research Letters*, 45, 3147–3155. doi:10.1002/2017GL076935.
- Mitchell, T. M., & Mitchell, T. M. (1997). *Machine Learning*. McGraw-hill New York, NY, United States of America.
- Mittal, N., Bhave, A. G., Mishra, A., & Singh, R. (2016). Impact of human intervention and climate change on natural flow regime. *Water Resources Management*, 30, 685–699. doi:10.1007/s11269-015-1185-6.
- Molden, D. (2007). *Water for Food Water for Life: A Comprehensive Assessment of Water Management in Agriculture*. Routledge, London, United Kingdom. doi:10.4324/9781849773799.
- Mool, P., Popescu, I., Giri, S., Omer, A., Sloff, K., Kitamura, Y., & Solomatine, D. (2017). Delft3D morphological modelling of sediment management in daily peaking run-of-the-river hydropower (PROR) reservoirs in Nepal. In *Proceedings of the 85th Annual Meeting of International Commission on Large Dams*. Prague, Czech Republic.
- Moriasi, D. N., Gitau, M. W., Pai, N., & Daggupati, P. (2015). Hydrologic and water quality models: performance measures and evaluation criteria. *Transactions of the ASABE*, 58, 1763–1785. doi:10.13031/trans.58.10715.
- Mosavi, A., Sajedi Hosseini, F., Choubin, B., Goodarzi, M., Dineva, A. A., & Rafiei Sardooi, E. (2021). Ensemble boosting and bagging based machine learning models for groundwater potential prediction. *Water Resources Management*, 35, 23–37. doi:10.1007/s11269-020-02704-3.
- Moshe, Z., Metzger, A., Elidan, G., Kratzert, F., Nevo, S., & El-Yaniv, R. (2020). HydroNets: Leveraging river structure for hydrologic modeling. In *the 1st AI for Earth Sciences workshop, ICLR2020*. Virtual. doi:10.48550/arXiv.2007.00595.
- Mulligan, M., Lehner, B., Zarfl, C., Thieme, M., Beames, P., van Soesbergen, A., Higgins, J., Januchowski-Hartley, S. R., Brauman, K. A., De Felice, L. et al. (2021). Global Dam Watch: curated data and tools for management and decision making. *Environmental Research: Infrastructure and Sustainability*, 1, 033003. doi:10.1088/2634-4505/ac333a.
- Murphree, D. H., Arabmakki, E., Ngufor, C., Storlie, C. B., & McCoy, R. G. (2018). Stacked classifiers for individualized prediction of glycemic control following initiation of metformin therapy in type 2 diabetes. *Computers in Biology and Medicine*, 103, 109–115. doi:10.1016/j.compbiomed.2018.10.017.
- Myneni, R., Knyazikhin, Y., & Park, T. (2015). MOD15A2H MODIS/terra leaf area index/FPAR 8-day L4 global 500 m SIN grid V006 by NASA EOSDIS Land Processes DAAC. doi:10.5067/MODIS/MOD15A2H.006.
- Myo Lin, N., Rutten, M., & Tian, X. (2018). Flood mitigation through optimal operation of a multi-reservoir system by using model predictive control: a case study in Myanmar. *Water*, 10, 1371. doi:10.3390/w10101371.
- Mysiak, J., Giupponi, C., & Rosato, P. (2005). Towards the development of a decision support system for water resource management. *Environmental Modelling & Software*, 20, 203–214. doi:10.1016/j.envsoft.2003.12.019.
- Nagesh Kumar, D., Srinivasa Raju, K., & Sathish, T. (2004). River flow forecasting using recurrent neural networks. *Water Resources Management*, 18, 143–161. doi:10.1023/B:WARM.0000024727.94701.12.

- Nanda, T., Sahoo, B., & Chatterjee, C. (2019). Enhancing real-time streamflow forecasts with wavelet-neural network based error-updating schemes and ECMWF meteorological predictions in Variable Infiltration Capacity model. *Journal of Hydrology*, 575, 890–910. doi:10.1016/j.jhydrol.2019.05.051.
- Nash, J. E., & Sutcliffe, J. V. (1970). River flow forecasting through conceptual models Part Ia discussion of principles. *Journal of Hydrology*, 10, 282–290. doi:10.1016/0022-1694(70)90255-6.
- Nayak, M. A., Herman, J. D., & Steinschneider, S. (2018). Balancing flood risk and water supply in California: policy search integrating short-term forecast ensembles with conjunctive use. *Water Resources Research*, 54, 7557–7576. doi:10.1029/2018WR023177.
- Nazemi, A., & Wheeler, H. S. (2015a). On inclusion of water resource management in Earth system models—Part 1: problem definition and representation of water demand. *Hydrology and Earth System Sciences*, 19, 33–61. doi:10.1029/WR012i002p00263.
- Nazemi, A., & Wheeler, H. S. (2015b). On inclusion of water resource management in Earth system models—Part 2: Representation of water supply and allocation and opportunities for improved modeling. *Hydrology and Earth System Sciences*, 19, 63–90. doi:10.5194/hess-19-63-2015.
- Nearing, G. S., Kratzert, F., Sampson, A. K., Pelissier, C. S., Klotz, D., Frame, J. M., Prieto, C., & Gupta, H. V. (2021). What role does hydrological science play in the age of machine learning? *Water Resources Research*, 57, e2020WR028091. doi:10.1029/2020WR028091.
- Neitsch, S., Arnold, J., Kiniry, J., Williams, J., & King, K. (2005). *Soil and water assessment tool theoretical documentation version 2005. Grassland*. Technical Report, Soil and Water Research Laboratory, Agricultural Research Service, Blackland Research Center, Texas Agricultural Experiment Station, TX, United States of America.
- Nilsson, C., & Berggren, K. (2000). Alterations of riparian ecosystems caused by river regulation: dam operations have caused global-scale ecological changes in riparian ecosystems. How to protect river environments and human needs of rivers remains one of the most important questions of our time. *BioScience*, 50, 783–792. doi:10.1641/0006-3568(2000)050[0783:AORECB]2.0.CO;2.
- Nilsson, C., Reidy, C. A., Dynesius, M., & Revenga, C. (2005). Fragmentation and flow regulation of the world's large river systems. *Science*, 308, 405–408. doi:10.1126/science.1107887.
- Niu, W.-J., Feng, Z.-K., Feng, B.-F., Min, Y.-W., Cheng, C.-T., & Zhou, J.-Z. (2019). Comparison of multiple linear regression, artificial neural network, extreme learning machine, and support vector machine in deriving operation rule of hydropower reservoir. *Water*, 11, 88. doi:10.3390/w11010088.
- Nourani, V., Baghanam, A. H., Adamowski, J., & Kisi, O. (2014). Applications of hybrid wavelet-artificial intelligence models in hydrology: a review. *Journal of Hydrology*, 514, 358–377. doi:10.1016/j.jhydrol.2014.03.057.
- O'Connor, J. E., Duda, J. J., & Grant, G. E. (2015). 1000 dams down and counting. *Science*, 348, 496–497. doi:10.1126/science.aaa9204.
- Ogilvie, A., Riaux, J., Massuel, S., Mulligan, M., Belaud, G., Le Goulven, P., & Calvez, R. (2019). Socio-hydrological drivers of agricultural water use in small reservoirs. *Agricultural Water Management*, 218, 17–29. doi:10.1016/j.agwat.2019.03.001.
- Oliveira, R., & Loucks, D. P. (1997). Operating rules for multireservoir systems. *Water Resources Research*, 33, 839–852. doi:10.1029/96WR03745.
- Ouyang, W., Lawson, K., Feng, D., Ye, L., Zhang, C., & Shen, C. (2021). Continental-scale streamflow modeling of basins with reservoirs: towards a coherent deep-learning-based strategy. *Journal of Hydrology*, 599, 126455. doi:10.1016/j.jhydrol.2021.126455.
- Overeem, A., Leijnse, H., van Leth, T. C., Bogerd, L., Priebe, J., Tricarico, D., Droste, A., & Uijlenhoet, R. (2021). Tropical rainfall monitoring with commercial microwave links in Sri Lanka. *Environmental*

- Research Letters*, 16, 074058.
- Page, A., Turner, J., Mohsenin, T., & Oates, T. (2014). Comparing raw data and feature extraction for seizure detection with deep learning methods. In *The Twenty-Seventh International Flairs Conference* (pp. 284–287).
- Park, J., & Sandberg, I. W. (1991). Universal approximation using radial-basis-function networks. *Neural Computation*, 3, 246–257. doi:10.1162/neco.1991.3.2.246.
- Pedregosa, F., Varoquaux, G., Gramfort, A., Michel, V., Thirion, B., Grisel, O., Blondel, M., Prettenhofer, P., Weiss, R., Dubourg, V. et al. (2011). Scikit-learn: machine learning in Python. *Journal of Machine Learning Research*, 12, 2825–2830. doi:10.48550/arXiv.1201.0490.
- Pham, L. T., Luo, L., & Finley, A. (2021). Evaluation of random forests for short-term daily streamflow forecasting in rainfall-and snowmelt-driven watersheds. *Hydrology and Earth System Sciences*, 25, 2997–3015. doi:10.5194/hess-25-2997-2021.
- Pitman, J. I. (1989). Rainfall interception by bracken in open habitats—Relations between leaf area, canopy storage and drainage rate. *Journal of Hydrology*, 105, 317–334. doi:10.1016/0022-1694(89)90111-X.
- Poff, N. L., Allan, J. D., Bain, M. B., Karr, J. R., Prestegard, K. L., Richter, B. D., Sparks, R. E., & Stromberg, J. C. (1997). The natural flow regime. *BioScience*, 47, 769–784. doi:10.2307/1313099.
- Pokhrel, Y. N., Hanasaki, N., Wada, Y., & Kim, H. (2016). Recent progresses in incorporating human land–water management into global land surface models toward their integration into Earth system models. *Wiley Interdisciplinary Reviews: Water*, 3, 548–574. doi:10.1002/wat2.1150.
- Ponomarenko, A., Avrelín, N., Naidan, B., & Boytsov, L. (2014). Comparative analysis of data structures for approximate nearest neighbor search. In *DATA ANALYTICS 2014, the Third International Conference on Data Analytics* (pp. 125–130). Pittsburgh, PA, United States of America.
- Qie, G., Zhang, Z., Getahun, E., & Mamer, E. A. (2022). Comparison of machine learning models performance on simulating reservoir outflow: a case study of two reservoirs in Illinois, USA. *Journal of the American Water Resources Association*, (pp. JAWR–21–0019–P). doi:10.1111/1752-1688.13040.
- Räsänen, T. A., Varis, O., Scherer, L., & Kummu, M. (2018). Greenhouse gas emissions of hydropower in the Mekong River basin. *Environmental Research Letters*, 13, 034030. doi:10.1088/1748-9326/aaa817.
- Rathor, S. (2018). Simple RNN vs GRU vs LSTM : difference lies in more flexible control. URL: <https://medium.com/@saurabh.rathor092/simple-rnn-vs-gru-vs-lstm-difference-lies-in-more-flexible-control-5f33e07b1e57>, last accessed on 08/11/2022.
- Rawls, W., & Brakensiek, D. (1989). Estimation of soil water retention and hydraulic properties. In *Unsaturated Flow in Hydrologic Modeling* (pp. 275–300). Dordrecht, the Netherlands: Springer.
- Refsgaard, J. C. (1997). Parameterisation, calibration and validation of distributed hydrological models. *Journal of Hydrology*, 198, 69–97. doi:10.1016/S0022-1694(96)03329-X.
- Refsgaard, J. C., & Knudsen, J. (1996). Operational validation and intercomparison of different types of hydrological models. *Water Resources Research*, 32, 2189–2202. doi:10.1029/96WR00896.
- Revenga, C., Brunner, J., Henninger, N., Kassem, K., & Payne, R. (2000). *Freshwater Systems*. World Resources Institute Washington, DC, United States of America.
- Richter, B. D., Postel, S., Revenga, C., Scudder, T., Lehner, B., Churchill, A., & Chow, M. (2010). Lost in development's shadow: the downstream human consequences of dams. *Water Alternatives*, 3, 14.
- Rippl, W. (2003). Water: the bloodstream of the biosphere. *Philosophical Transactions of the Royal Society of London. Series B: Biological Sciences*, 358, 1921–1934. doi:10.1098/rstb.2003.1378.
- Rippl, W. (1883). The capacity of storage-reservoirs for water-supply. In *Minutes of the Proceed-*

- ings of the Institution of Civil Engineers 1883 (pp. 270–278). Thomas Telford-ICE Virtual Library. doi:10.1680/imotp.1883.21797.
- Rittima, A. (2018). *Reservoir Systems and Operation Planning (in Thai language)*. Mahidol University, Thailand.
- Roser, M., & Rods-Guirao, L. (2013). Our world in data: future population growth. URL: <https://ourworldindata.org/future-population-growth>, last accessed on 03/11/2022.
- Rusli, S., Weerts, A., Taufiq, A., & Bense, V. (2021). Estimating water balance components and their uncertainty bounds in highly groundwater-dependent and data-scarce area: an example for the Upper Citarum basin. *Journal of Hydrology: Regional Studies*, 37, 100911. doi:10.1016/j.ejrh.2021.100911.
- Rutter, A., Kershaw, K., Robins, P., & Morton, A. (1971). A predictive model of rainfall interception in forests, 1. Derivation of the model from observations in a plantation of Corsican pine. *Agricultural Meteorology*, 9, 367–384. doi:10.1016/0002-1571(71)90034-3.
- Rutter, A., Morton, A., & Robins, P. (1975). A predictive model of rainfall interception in forests. II. Generalization of the model and comparison with observations in some coniferous and hardwood stands. *Journal of Applied Ecology*, 12, 367–380. doi:10.2307/2401739.
- Sachindra, D., Huang, F., Barton, A., & Perera, B. (2013). Least square support vector and multi-linear regression for statistically downscaling general circulation model outputs to catchment streamflows. *International Journal of Climatology*, 33, 1087–1106. doi:10.1002/joc.3493.
- Samaniego, L., Kumar, R., & Attinger, S. (2010). Multiscale parameter regionalization of a grid-based hydrologic model at the mesoscale. *Water Resources Research*, 46, W05523. doi:10.1029/2008WR007327.
- San, Z. M. L. T., Zin, W. W., Kawasaki, A., Acierto, R. A., & Oo, T. Z. (2020). Developing flood inundation map using RRI and SOBEK models: a case study of the Bago River basin, Myanmar. *Journal of Disaster Research*, 15, 277–287. doi:10.20965/jdr.2020.p0277.
- Savenije, H. H. (2010). HESS opinions “Topography driven conceptual modelling (FLEX-Topo)”. *Hydrology and Earth System Sciences*, 14, 2681–2692. doi:10.5194/hess-14-2681-2010.
- Sawicz, K., Wagener, T., Sivapalan, M., Troch, P. A., & Carrillo, G. (2011). Catchment classification: empirical analysis of hydrologic similarity based on catchment function in the eastern USA. *Hydrology and Earth System Sciences*, 15, 2895–2911. doi:10.5194/hess-15-2895-2011.
- Sayama, T., Tatebe, Y., Iwami, Y., & Tanaka, S. (2015). Hydrologic sensitivity of flood runoff and inundation: 2011 Thailand floods in the Chao Phraya River basin. *Natural Hazards and Earth System Sciences*, 15, 1617–1630. doi:10.5194/nhess-15-1617-2015.
- Schauwecker, S., Schwarb, M., Rohrer, M., & Stoffel, M. (2021). Heavy precipitation forecasts over Switzerland—An evaluation of bias-corrected ECMWF predictions. *Weather and Climate Extremes*, 34, 100372. doi:10.1016/j.wace.2021.100372.
- Schellekens, J., Dutra, E., la Torre, A. M. d., Balsamo, G., van Dijk, A., Weiland, F. S., Minvielle, M., Calvet, J. C., Decharme, B., Eisner, S. et al. (2017). A global water resources ensemble of hydrological models: the earth2Observe Tier-1 dataset. *Earth System Science Data*, 9, 389–413. doi:10.5194/essd-2016-55.
- Schellekens, J. et al. (2020). openstreams/wflow: bug fixes and updates for release 2020.1.2. URL: <https://github.com/openstreams/wflow>, last accessed on 29/09/2022.
- Schellekens, J., Verseveld van, W., Euser, T., Winsemius, H., Thiange, C., Bouaziz, L., & et al. (2019). Openstreams/wflow. URL: <https://github.com/openstreams/wflow>, last accessed on 28/10/2022.
- Schlömer, S., Bruckner, T., Fulton, L., Hertwich, E., McKinnon, A., Perczyk, D., Roy, J., Schaeffer, R., Sims, R., Smith, P. et al. (2014). Annex III: technology-specific cost and performance parameters. In *Climate Change 2014: Mitigation of Climate Change: Contribution of Working Group Iii to the Fifth*

- Assessment Report of the Intergovernmental Panel on Climate Change* (pp. 1329–1356). Cambridge, United Kingdom: Cambridge University Press.
- Schoups, G., Van de Giesen, N., & Savenije, H. (2008). Model complexity control for hydrologic prediction. *Water Resources Research*, 44, W00B03. doi:10.1029/2008WR006836.
- Scudder, T. T. (2012). *The Future of Large Dams: Dealing With Social, Environmental, Institutional and Political Costs*. Routledge, London, United Kingdom. doi:10.4324/9781849773904.
- Shen, C. (2018). A transdisciplinary review of deep learning research and its relevance for water resources scientists. *Water Resources Research*, 54, 8558–8593. doi:10.1029/2018WR022643.
- Shiklomanov, I. A. (2000). Appraisal and assessment of world water resources. *Water International*, 25, 11–32. doi:10.1080/02508060008686794.
- Shumway, R. H., & Stoffer, D. S. (2000). Spectral analysis and filtering. In *Time Series Analysis and Its Applications* (pp. 213–300). Cham, Switzerland: Springer. doi:10.1007/978-1-4757-3261-0\_3.
- Siciliano, G., Urban, F., Kim, S., & Lonn, P. D. (2015). Hydropower, social priorities and the rural–urban development divide: the case of large dams in Cambodia. *Energy Policy*, 86, 273–285. doi:10.1016/j.enpol.2015.07.009.
- Siebert, S., Henrich, V., Frenken, K., & Burke, J. (2013). *Update of the digital global map of irrigation areas to version 5*. Technical Report, Rheinische Friedrich-Wilhelms-Universität, Bonn, Germany and Food and Agriculture Organization of the United Nations, Rome, Italy. doi:10.13140/2.1.2660.6728.
- Sigvaldson, O. (1976). A simulation model for operating a multipurpose multireservoir system. *Water Resources Research*, 12, 263–278. doi:10.1029/WR012i002p00263.
- Singh, V. P., & Woolhiser, D. A. (2002). Mathematical modeling of watershed hydrology. *Journal of Hydrologic Engineering*, 7, 270–292. doi:10.1061/(ASCE)1084-0699(2002)7:4(270).
- Singhrattana, N., Rajagopalan, B., Kumar, K. K., & Clark, M. (2005). Interannual and interdecadal variability of Thailand summer monsoon season. *Journal of Climate*, 18, 1697–1708. doi:10.1175/JCLI3364.1.
- Skidmore, A. (2017). *Environmental Modelling With GIS And Remote Sensing*. CRC Press, London, United Kingdom. doi:10.4324/9780203302217.
- Solomatine, D. P., & Ostfeld, A. (2008). Data-driven modelling: some past experiences and new approaches. *Journal of Hydroinformatics*, 10, 3–22. doi:10.2166/hydro.2008.015.
- Spurna Weiland, F., Lopez Lopez, P., Van Dijk, A., Schellekens, J. et al. (2015). Global high-resolution reference potential evaporation. In *MODSIM2015, 21st International Congress on Modelling and Simulation. Modelling and Simulation Society of Australia and New Zealand*. Gold Coast, Australia.
- Sun, N., Zhang, S., Peng, T., Zhang, N., Zhou, J., & Zhang, H. (2022). Multi-variables-driven model based on random forest and gaussian process regression for monthly streamflow forecasting. *Water*, 14, 1828. doi:10.3390/w14111828.
- Takeda, M., Laphimsing, A., & Putthividhya, A. (2016). Dry season water allocation in the Chao Phraya River basin, Thailand. *International Journal of Water Resources Development*, 32, 321–338. doi:10.1080/07900627.2015.1055856.
- Tanty, R., Desmukh, T. S., & Bhopal, M. (2015). Application of artificial neural network in hydrologyA review. *International Journal of Engineering and Technical Research*, 4, 184–188. doi:10.17577/IJERTV4IS060247.
- Tarnavsky, E., Chavez, E., & Boogaard, H. (2018). Agro-meteorological risks to maize production in Tanzania: sensitivity of an adapted Water Requirements Satisfaction Index (WRSI) model to rainfall. *International Journal of Applied Earth Observation and Geoinformation*, 73, 77–87. doi:10.1016/j.jag.2018.04.008.



- Tebakari, T., Yoshitani, J., & Suvanpimol, P. (2012). Impact of large-scale reservoir operation on flow regime in the Chao Phraya River basin, Thailand. *Hydrological Processes*, 26, 2411–2420. doi:10.1002/hyp.9345.
- Thanapakpawin, P., Richey, J., Thomas, D., Rodda, S., Campbell, B., & Logsdon, M. (2007). Effects of landuse change on the hydrologic regime of the Mae Chaem River basin, NW Thailand. *Journal of Hydrology*, 334, 215–230. doi:10.1016/j.jhydrol.2006.10.012.
- Thechamani, I., Visessri, S., & Jarumaneeroj, P. (2017). Modeling of multi-reservoir systems operation in the Chao Phraya River basin. In *2017 International Conference on Industrial Engineering, Management Science and Application (ICIMSA)* (pp. 1–5). Seoul, South Korea: IEEE. doi:10.1109/ICIMSA.2017.7985595.
- Todini, E., & Ciarapica, L. (2002). The TOPKAPI model. Mathematical models of large watershed hydrology. *Water Resources Publications Edition*, (pp. 471–506).
- Tongal, H. (2013). Nonlinear forecasting of stream flows using a chaotic approach and artificial neural networks. *Earth Sciences Research Journal*, 17, 119–126.
- Tóth, B., Weynants, M., Nemes, A., Makó, A., Bilas, G., & Tóth, G. (2015). New generation of hydraulic pedotransfer functions for Europe. *European Journal of Soil Science*, 66, 226–238. doi:10.1111/ejss.12192.
- Trenberth, K. E., Dai, A., Van Der Schrier, G., Jones, P. D., Barichivich, J., Briffa, K. R., & Sheffield, J. (2014). Global warming and changes in drought. *Nature Climate Change*, 4, 17–22. doi:10.1038/nclimate2067.
- Trenberth, K. E., Koike, T., & Onogi, K. (2008). Progress and prospects for reanalysis for weather and climate. *EOS, Transactions American Geophysical Union*, 89, 234–235. doi:10.1029/2008EO260002.
- Urban, F., Siciliano, G., & Nordensvard, J. (2018). Chinas dam-builders: their role in transboundary river management in South-East Asia. *International Journal of Water Resources Development*, 34, 747–770. doi:10.1080/07900627.2017.1329138.
- Valipour, M. (2013). Necessity of irrigated and rainfed agriculture in the world. *Irrigation Drainage Systems Engineering*, 9, e001. doi:10.4172/2168-9768.S9-e001.
- Van Dijk, A., & Bruijnzeel, L. (2001). Modelling rainfall interception by vegetation of variable density using an adapted analytical model. Part 2. Model validation for a tropical upland mixed cropping system. *Journal of Hydrology*, 247, 239–262. doi:10.1016/S0022-1694(01)00393-6.
- Van Looy, K., Bouma, J., Herbst, M., Koestel, J., Minasny, B., Mishra, U., Montzka, C., Nemes, A., Pachepsky, Y. A., Padarian, J. et al. (2017). Pedotransfer functions in Earth system science: challenges and perspectives. *Reviews of Geophysics*, 55, 1199–1256. doi:10.1002/2017RG000581.
- Van Oldenborgh, G. J., Urk, A., & Allen, M. (2012). The absence of a role of climate change in the 2011 Thailand floods. *Bulletin of the American Meteorological Society*, 93, 1047–1049. doi:10.1175/BAMS-D-12-00021.1.
- Van Osnabrugge, B., Uijlenhoet, R., & Weerts, A. (2019). Contribution of potential evaporation forecasts to 10-day streamflow forecast skill for the Rhine River. *Hydrology and Earth System Sciences*, 23, 1453–1467. doi:10.5194/hess-23-1453-2019.
- Van Verseveld, W., Visser, M., Boisgontier, H., Bootsma, H., Bouaziz, L., Buitink, J., Eilander, D., & Hegnauer, M. (2022a). wflow.jl (v0.6.1). URL: <https://github.com/Deltares/Wflow.jl>, last accessed on 26/09/2022.
- Van Verseveld, W. J., Weerts, A. H., Visser, M., Buitink, J., Imhoff, R. O., Boisgontier, H., Bouaziz, L., Eilander, D., Hegnauer, M., ten Velden, C. et al. (2022b). Wflow\_sbm v0. 6.1, a spatially distributed hydrologic model: from global data to local applications. *Geoscientific Model Development Discussions*,

- (pp. 1–52). doi:10.5194/gmd-2022-182.
- Vapnik, V. (2000). *The Nature of Statistical Learning Theory*. Springer Science & Business Media, NY, United States of America. doi:10.1007/978-1-4757-3264-1.1.
- Veldkamp, T., Wada, Y., Aerts, J., Döll, P., Gosling, S. N., Liu, J., Masaki, Y., Oki, T., Ostberg, S., Pokhrel, Y. et al. (2017). Water scarcity hotspots travel downstream due to human interventions in the 20th and 21st century. *Nature Communications*, 8, 1–12. doi:10.1038/ncomms15697.
- Verkade, J., Brown, J., Reggiani, P., & Weerts, A. (2013). Post-processing ECMWF precipitation and temperature ensemble reforecasts for operational hydrologic forecasting at various spatial scales. *Journal of Hydrology*, 501, 73–91. doi:10.1016/j.jhydrol.2013.07.039.
- Vertessy, R. A., & Elsenbeer, H. (1999). Distributed modeling of storm flow generation in an Amazonian rain forest catchment: effects of model parameterization. *Water Resources Research*, 35, 2173–2187. doi:10.1029/1999WR900051.
- Vo, N. D., & Gourbesville, P. (2016). Application of deterministic distributed hydrological model for large catchment: a case study at Vu Gia Thu Bon catchment, Vietnam. *Journal of Hydroinformatics*, 18, 885–904. doi:10.2166/hydro.2016.138.
- Vörösmarty, C. J., Meybeck, M., Fekete, B., Sharma, K., Green, P., & Syvitski, J. P. (2003). Anthropogenic sediment retention: major global impact from registered river impoundments. *Global and Planetary Change*, 39, 169–190. doi:10.1016/S0921-8181(03)00023-7.
- Vuorinen, H. S., Juuti, P. S., & Katko, T. S. (2007). History of water and health from ancient civilizations to modern times. *Water Science and Technology: Water Supply*, 7, 49–57. doi:10.2166/ws.2007.006.
- Wada, Y., Bierkens, M. F., De Roo, A., Dirmeyer, P. A., Famiglietti, J. S., Hanasaki, N., Konar, M., Liu, J., Müller Schmied, H., Oki, T. et al. (2017). Human–water interface in hydrological modelling: current status and future directions. *Hydrology and Earth System Sciences*, 21, 4169–4193. doi:10.5194/hess-21-4169-2017.
- Wagener, T., Sivapalan, M., Troch, P., & Woods, R. (2007). Catchment classification and hydrologic similarity. *Geography Compass*, 1, 901–931. doi:10.1111/j.1749-8198.2007.00039.x.
- Wang, L., Kaban, M. K., Thomas, M., Chen, C., & Ma, X. (2019). The challenge of spatial resolutions for GRACE-based estimates volume changes of larger man-made lake: the case of Chinas Three Gorges reservoir in the Yangtze River. *Remote Sensing*, 11, 99. doi:10.3390/rs11010099.
- Wang, Q., Du, Y., Su, Y., & Chen, K. (2012). Environmental impact post-assessment of dam and reservoir projects: a review. *Procedia Environmental Sciences*, 13, 1439–1443. doi:10.1016/j.proenv.2012.01.135.
- Wang, W., Lu, H., Yang, D., Sothea, K., Jiao, Y., Gao, B., Peng, X., & Pang, Z. (2016). Modelling hydrologic processes in the Mekong River basin using a distributed model driven by satellite precipitation and rain gauge observations. *PLoS one*, 11, e0152229. doi:10.1371/journal.pone.0152229.
- Wannasin, C., Brauer, C. C., Uijlenhoet, R., Van Verseveld, W. J., & Weerts, A. H. (2021a). Daily flow simulation in Thailand Part II: unraveling effects of reservoir operation. *Journal of Hydrology: Regional Studies*, 34, 100792. doi:10.1016/j.ejrh.2021.100792.
- Wannasin, C., Brauer, C. C., Uijlenhoet, R., van Verseveld, W. J., & Weerts, A. H. (2021b). Daily flow simulation in Thailand Part I: testing a distributed hydrological model with seamless parameter maps based on global data. *Journal of Hydrology: Regional Studies*, 34, 100794. doi:10.1016/j.ejrh.2021.100794.
- Ward, J. (1989). The four-dimensional nature of lotic ecosystems. *Journal of the North American Benthological Society*, 8, 2–8. doi:10.2307/1467397.
- Ward, P. J., Jongman, B., Weiland, F. S., Bouwman, A., van Beek, R., Bierkens, M. F., Ligotvoet, W., & Winsemius, H. C. (2013). Assessing flood risk at the global scale: model setup, results, and sensitivity.

- Environmental Research Letters*, 8, 044019. doi:10.1088/1748-9326/8/4/044019.
- Weedon, G. P., Balsamo, G., Bellouin, N., Gomes, S., Best, M. J., & Viterbo, P. (2014). The WFDEI meteorological forcing data set: WATCH Forcing Data methodology applied to ERA-Interim reanalysis data. *Water Resources Research*, 50, 7505–7514. doi:10.1002/2014WR015638.
- Wehrli, B. (2011). Renewable but not carbon-free. *Nature Geoscience*, 4, 585–586. doi:10.1038/ngeo1226.
- Weiler, M., & McDonnell, J. (2007). Conceptualizing lateral preferential flow and flow networks and simulating the effects on gauged and ungauged hillslopes. *Water Resources Research*, 43, W03403. doi:10.1029/2006WR004867.
- Werbos, P. J. (1990). Backpropagation through time: what it does and how to do it. *Proceedings of the IEEE*, 78, 1550–1560. doi:10.1109/5.58337.
- Wichakul, S., Tachikawa, Y., Shiiba, M., & Yoroza, K. (2013). Developing a regional distributed hydrological model for water resources assessment and its application to the Chao Phraya River basin. *Journal of Japan Society of Civil Engineers, Ser. B1 (Hydraulic Engineering)*, 69, I-43–I-48. doi:10.1007/978-94-009-2352-2\_10.
- Wicks, J., & Bathurst, J. (1996). SHESED: a physically based, distributed erosion and sediment yield component for the SHE hydrological modelling system. *Journal of Hydrology*, 175, 213–238. doi:10.1016/S0022-1694(96)80012-6.
- Winsemius, H. C., Aerts, J. C., van Beek, L. P., Bierkens, M. F., Bouwman, A., Jongman, B., Kwadijk, J. C., Ligtoet, W., Lucas, P. L., Van Vuuren, D. P. et al. (2016). Global drivers of future river flood risk. *Nature Climate Change*, 6, 381. doi:10.1038/nclimate2893.
- Wisser, D., Fekete, B. M., Vörösmarty, C., & Schumann, A. (2010). Reconstructing 20th century global hydrography: a contribution to the Global Terrestrial Network-Hydrology (GTN-H). *Hydrology and Earth System Sciences*, 14, 1–24. doi:10.5194/hess-14-1-2010.
- Witten, I. H., & Frank, E. (2002). Data mining: practical machine learning tools and techniques with Java implementations. *Acm Sigmod Record*, 31, 76–77. doi:10.1145/507338.507355.
- World Commission on Dams (2000). *Dams and Development: A New Framework for Decision-Making: The Report of the World Commission on Dams*. Earthscan, London, United Kingdom.
- Wu, J., Liu, Z., Yao, H., Chen, X., Chen, X., Zheng, Y., & He, Y. (2018). Impacts of reservoir operations on multi-scale correlations between hydrological drought and meteorological drought. *Journal of Hydrology*, 563, 726–736. doi:10.1016/j.jhydrol.2018.06.053.
- Wu, Y., & Chen, J. (2012). An operation-based scheme for a multiyear and multipurpose reservoir to enhance macroscale hydrologic models. *Journal of Hydrometeorology*, 13, 270–283. doi:10.1175/JHM-D-10-05028.1.
- Xu, M., Watanachaturaporn, P., Varshney, P. K., & Arora, M. K. (2005). Decision tree regression for soft classification of remote sensing data. *Remote Sensing of Environment*, 97, 322–336. doi:10.1016/j.rse.2005.05.008.
- Xu, T., & Liang, F. (2021). Machine learning for hydrologic sciences: an introductory overview. *Wiley Interdisciplinary Reviews: Water*, 8, e1533. doi:10.1002/wat2.1533.
- Xu, Z., Wu, Z., He, H., Wu, X., Zhou, J., Zhang, Y., & Guo, X. (2019). Evaluating the accuracy of MSWEP V2. 1 and its performance for drought monitoring over mainland China. *Atmospheric Research*, 226, 17–31. doi:10.1016/j.atmosres.2019.04.008.
- Yang, S., Yang, D., Chen, J., & Zhao, B. (2019). Real-time reservoir operation using recurrent neural networks and inflow forecast from a distributed hydrological model. *Journal of Hydrology*, 579, 124229. doi:10.1016/j.jhydrol.2019.124229.

- Yang, T., Asanjan, A. A., Faridzad, M., Hayatbini, N., Gao, X., & Sorooshian, S. (2017). An enhanced artificial neural network with a shuffled complex evolutionary global optimization with principal component analysis. *Information Sciences*, 418, 302–316. doi:10.1016/j.ins.2017.08.003.
- Yang, T., Gao, X., Sorooshian, S., & Li, X. (2016). Simulating California reservoir operation using the classification and regression-tree algorithm combined with a shuffled cross-validation scheme. *Water Resources Research*, 52, 1626–1651. doi:10.1002/2015WR017394.
- Yang, T., Zhang, L., Kim, T., Hong, Y., Zhang, D., & Peng, Q. (2021). A large-scale comparison of artificial intelligence and data mining (AI&DM) techniques in simulating reservoir releases over the Upper Colorado Region. *Journal of Hydrology*, 602, 126723. doi:10.1016/j.jhydrol.2021.126723.
- Yassin, F., Razavi, S., Elshamy, M., Davison, B., Sapriza-Azuri, G., & Wheeler, H. (2019). Representation and improved parameterization of reservoir operation in hydrological and land-surface models. *Hydrology and Earth System Sciences*, 23, 3735–3764. doi:10.5194/hess-23-3735-2019.
- Yates, D., Sieber, J., Purkey, D., & Huber-Lee, A. (2005). WEAP21A demand-, priority-, and preference-driven water planning model: Part 1: model characteristics. *Water International*, 30, 487–500. doi:10.1080/02508060508691893.
- Ye, F., Zhang, Z., Chakrabarty, K., & Gu, X. (2016). *Knowledge-Driven Board-Level Functional Fault Diagnosis*. Springer International Publishing, Switzerland. doi:10.1007/978-3-319-40210-9.
- Ylla Arbós, C., Blom, A., Viparelli, E., Reneerkens, M., Frings, R., & Schielen, R. (2021). River response to anthropogenic modification: channel steepening and gravel front fading in an incising river. *Geophysical Research Letters*, 48, e2020GL091338. doi:10.1029/2020GL091338.
- Yu, H., & Kim, S. (2012). SVM tutorial—classification, regression and ranking. *Handbook of Natural computing*, 1, 479–506. doi:10.1007/978-3-540-92910-9\_15.
- Yuan, F., Zhang, L., Soe, K. M. W., Ren, L., Zhao, C., Zhu, Y., Jiang, S., & Liu, Y. (2019). Applications of TRMM-and GPM-era multiple-satellite precipitation products for flood simulations at sub-daily scales in a sparsely gauged watershed in Myanmar. *Remote Sensing*, 11, 140. doi:10.3390/rs11020140.
- Yun, X., Tang, Q., Wang, J., Liu, X., Zhang, Y., Lu, H., Wang, Y., Zhang, L., & Chen, D. (2020). Impacts of climate change and reservoir operation on streamflow and flood characteristics in the Lancang-Mekong River basin. *Journal of Hydrology*, 590, 125472. doi:10.1016/j.jhydrol.2020.125472.
- Yusuf, A. A., & Francisco, H. (2009). Climate change vulnerability mapping for Southeast Asia. In *Workshop on Mapping Vulnerability to Climate Change in Southeast Asia*. Singapore: EEPSEA, IDRC Regional Office for Southeast and East Asia.
- Zajac, Z., Revilla-Romero, B., Salamon, P., Burek, P., Hirpa, F. A., & Beck, H. (2017). The impact of lake and reservoir parameterization on global streamflow simulation. *Journal of Hydrology*, 548, 552–568. doi:10.1016/j.jhydrol.2017.03.022.
- Zarei, M., Bozorg-Haddad, O., Baghban, S., Delpasand, M., Goharian, E., & Loáiciga, H. A. (2021). Machine-learning algorithms for forecast-informed reservoir operation (FIRO) to reduce flood damages. *Scientific Reports*, 11, 1–21. doi:10.1038/s41598-021-03699-6.
- Zarfl, C., Lumsdon, A. E., Berlekamp, J., Tydecks, L., & Tockner, K. (2015). A global boom in hydropower dam construction. *Aquatic Sciences*, 77, 161–170. doi:10.1007/s00027-014-0377-0.
- Zeng, X. (2001). Global vegetation root distribution for land modeling. *Journal of Hydrometeorology*, 2, 525–530. doi:10.1175/1525-7541(2001)002i0525:GVRDFL2.0.CO;2.
- Zenkoji, S., Tebakari, T., & Dotani, K. (2019). Rainfall and reservoirs situation under the worst drought recorded in the Upper Chao Phraya River basin, Thailand. *Journal of Japan Society of Civil Engineers, Ser. G (Environmental Research)*, 75, I.115–I.124. doi:10.2208/jscejer.75.I.115.
- Zhang, D., Lin, J., Peng, Q., Wang, D., Yang, T., Sorooshian, S., Liu, X., & Zhuang, J. (2018a). Modeling

- and simulating of reservoir operation using the artificial neural network, support vector regression, deep learning algorithm. *Journal of Hydrology*, 565, 720–736. doi:10.1016/j.jhydrol.2018.08.050.
- Zhang, D., Peng, Q., Lin, J., Wang, D., Liu, X., & Zhuang, J. (2019). Simulating reservoir operation using a recurrent neural network algorithm. *Water*, 11, 865. doi:10.3390/w11040865.
- Zhang, Z., Zhang, Q., & Singh, V. P. (2018b). Univariate streamflow forecasting using commonly used data-driven models: literature review and case study. *Hydrological Sciences Journal*, 63, 1091–1111. doi:10.1080/02626667.2018.1469756.
- Zhao, C., Shao, M., Jia, X., Nasir, M., & Zhang, C. (2016a). Using pedotransfer functions to estimate soil hydraulic conductivity in the Loess Plateau of China. *Catena*, 143, 1–6. doi:10.1016/j.catena.2016.03.037.
- Zhao, G., Gao, H., Naz, B. S., Kao, S. C., & Voisin, N. (2016b). Integrating a reservoir regulation scheme into a spatially distributed hydrological model. *Advances in Water Resources*, 98, 16–31. doi:10.1016/j.advwatres.2016.10.014.
- Zheng, Y., Liu, P., Cheng, L., Xie, K., Lou, W., Li, X., Luo, X., Cheng, Q., Han, D., & Zhang, W. (2022). Extracting operation behaviors of cascade reservoirs using physics-guided long-short term memory networks. *Journal of Hydrology: Regional Studies*, 40, 101034. doi:10.1016/j.ejrh.2022.101034.
- Zhou, T., Nijssen, B., Gao, H., & Lettenmaier, D. P. (2016). The contribution of reservoirs to global land surface water storage variations. *Journal of Hydrometeorology*, 17, 309–325. doi:10.1175/JHM-D-15-0002.1.
- Zuo, G., Luo, J., Wang, N., Lian, Y., & He, X. (2020). Decomposition ensemble model based on variational mode decomposition and long short-term memory for streamflow forecasting. *Journal of Hydrology*, 585, 124776. doi:10.1016/j.jhydrol.2020.124776.

# Statement of authorship contribution

The general research ideas of this thesis were proposed by Chanoknun Wannasin. The research scope and direction were shaped by her promotors and co-promotor. Chanoknun wrote the introduction (Chapter 1) and synthesis (Chapter 8), with minor suggestions from her (co-)promotors. Chapter 2 combines the information on the study area from the core Chapters 4–7. Likewise, Chapter 3 combines the data, models and performance criteria from the core chapters. Therefore, Chapters 2–3 have the same contributions as the listed contributions to Chapters 4–7 below.

Names have been abbreviated:

CW = Chanoknun Wannasin (WUR)

AW = Albrecht Weerts (Deltares/WUR)

CB = Claudia Brauer (WUR)

RU = Remko Uijlenhoet (TUD)

WV = Willem van Verseveld (Deltares)

PT = Paul Torfs (WUR)

## Chapters 4–5

Conceptualization: CW, AH, CB and RU

Data collection: CW

Modelling: CW in consultation with AH, CB, RU and WV

Data analysis and interpretation: CW in consultation with AH, CB and RU

Writing: CW

Revision & validation: AH, CB and RU

## Chapters 6–7

Conceptualization: CW, AH, CB and RU

Data collection: CW in consultation with AH

Modelling: CW in consultation with AH, CB and RU

Data analysis and interpretation: CW in consultation with AH, CB, RU and PT

Writing: CW

Revision & validation: AH, CB and RU

# Acknowledgements

My PhD (and MSc) journey was not only about learning and doing research, but also living abroad, discovering my authentic self and growing from my 20s to my 30s. It was one of the most important periods in my life, which has shaped me into the person I am today. I dedicate this space to acknowledge everyone who has contributed to this beautiful experience. To have known you, learned from you and shared quality times with you have made the years memorable. And for that, I am genuinely grateful.

I would like to express my gratitude to my supervisors, Claudia, Albrecht and Remko. Thank you for giving me the opportunity to start this PhD project based on my own research ideas, for guiding me through this endeavour, for trusting my capability, and for being understanding and patient with my progress. There is a saying in Thai that educators are like sailors; they steer the boat and make sure students cross the ocean successfully in the right direction. You steered my boat with me through the PhD ocean.

Claudia, I am still not entirely sure what you saw in me while supervising my MSc thesis. I was rather new to both hydrology and programming. When you agreed to brainstorm and write the PhD proposal with me, it lifted my self-confidence and motivation in this new path. Your scientific engagement (especially in result analyses and visualization) and your emotional support throughout my PhD time were crucially helpful. Your friendly reminder that 'it doesn't have to be perfect before you send it to us' always came when I needed to hear it the most. You should know that you are not an ordinary supervisor, even through the eyes of many others that you didn't supervise.

Albrecht, thank you for giving me the opportunity to do the MSc internship at Deltares and explore the hydrological modelling world there. Those four months of learning among the experts certainly prepared and inspired me to pursue this PhD. This thesis would not have been possible without your wisdom and ability to see things from a bird's eye view. Your inputs and advice on my research were always substantial and on point. I appreciate how you always listened to my perspectives first even when you had completely different opinions. It was a great pleasure to learn from you.

Remko, I value your consistent involvement in this PhD project. The thoughts you shared during our discussions were always alternative, creative and critical, which have left a strong impression on me. Thank you very much for all the detailed feedback and comments on my work (for the record, you gave me 2,509 comments for all papers

and chapters combined, excluding conference abstracts and other documents). It is a mystery how you managed to find time to join the meetings and thoroughly read my work, despite your very tight schedules. I sincerely appreciate it.

Apart from my supervision team, the contributions of my co-authors and other scientific supporters in this PhD project were much obliged. Willem, I am thankful for your continuous assistance on the `wflow_sbm` model setup and improvement. Paul, your enthusiastic suggestions and statistical point of view on the machine learning models were of great help. I extend appreciation to Kanjanawan, Thattanaporn and Pintip (and other people that I may not be aware of) for collecting the national and local data and reports used in this thesis for me. Ruben, thanks for the `wflow` maps you created and the codes you shared with me. Wasin, thanks for being my programming guru. Many thanks to my MSc and BSc thesis students who joined parts of this PhD: Reinout, Simone, Yisu, Maarten and Ties. Special thanks to Jan, who mentored me during the MSc internship at Deltares and has shaped the way I conduct modelling work since then—check, double-check, and recheck! Needless to say, I have learned a lot from all of you, which is invaluable for the rest of my research career.

Shout-out to my paranympths, Judith and Rose. Judith, *bedankt* for being such a kind and considerate office mate. When two introvert PhD'ers work in the same office or stay in the same hotel room, they do not talk a lot. Instead, they naturally enjoy their own things in each other's company. The comfortable quietness we had while working were priceless and the social times (which often came with your dry humours) we had outside the office hours were joyful. Rose, *medaase* for pouring the liveliness and colorfulness into my PhD time and for awakening the half-crazy side of me (and of Judith and many others). Your optimistic and cheerful personality has changed the dynamic of the chair group in the way I thought impossible. Ladies, both of you were amazing colleagues and friends in your own ways, and it was an honour to have you as my paranympths.

A lot of my PhD time was spent with my HWM colleagues, especially the 'Young and Hot' ones. My Lovely Linda, thanks a lot for sharing personal perspectives, comfort, support, endless hugs and unique laughs across the rooms. Steven, thanks for being my Asian buddy at work and such a caring friend, who always attentively listened to anything I needed advice for (extending thanks to Litha for delicious food and warm welcome at your place). Janneke, thanks for the fun lady nights we shared, which were always with food (and wine). Femke, thanks for brightening many of my typical office days (you received million 'points' from me for that). Anne, thanks for our afternoon coffee walks and the *gezellig* Christmas Eve dinner with your family (I have listened to the Top 2000 since then). Sony, thanks for staying beside me since when both of us were only the non-Dutch in the chair group. Tamara, thanks for all your help, which had made my PhD administration smooth since day one. The Asian Squad, thanks for the Asian food, Asian dances and Asian jokes. Thanks to all other HWM colleagues. I enjoyed the *borrels* and social events we had, particularly De Veluweloop, writing weeks, geocaching and Science Cafe. I am happy to see how HWM has grown in the past years and how



internationally friendly it has become. Cheers to all of you for contributing to making it a more and more welcoming and comfortable space for everyone.

Many other WUR colleagues had nothing to do with my PhD project, but with my PhD life. One of them is the WIMEK PhD Council. Especially, Kim, Meng and Anne, thanks for sharing your efforts and time to try to make the PhD conditions better. Meng, I am proud of our WIMEK PhD guideline. I also thank the PhD'ers whom I was a PhD buddy for. The idea was that I supported and guided them to start their PhD life smoothly when they moved to Wageningen. It was initially to give, but turned out I also received a lot from them. Ara, I am glad that our buddy time has turned us into good friends. You all considerably fulfilled my non-scientific time with joy and it meant a lot to me.

My journey would not have been this mirthful without friends and special people in my life. Thanks to the Thai students' community in Wageningen for goodwill. Exclusively, thanks to P'Gahn, P'Tarn, P'Mai, Tuck and Keaw for our good times, trips, personal talks and empathy we exchanged in Thai. Thanks to P'Waew and Kees for your kindness and welcome. Thanks to my international friends, especially Julissa, Lien and Felix, for the relaxing gatherings and river picnics after intensive working days. Cisca, Klaas and Roald, thanks for the ultimate experience of Dutch culture. Carlos and Edwin, thanks for the bike-packing trip that effectively cured the stress. Cycling Ladies, thanks for the jolly weekend and summer rides with cakes. Korya, Teaw, Som, Mick, P'Jum, AJ'Pupe, N'Frame, and others, thanks for the virtual support and magnet-like reunions whenever I visited Thailand. Bart, *khob khun kha* for all the hikes, road trip, bubble tea, deep conversations and for gently introducing the whole world outside academia to me. It has always been impressive and exciting to see things through your eyes. I have been lightheartedly learning and taking on new adventures when I am around you.

An important acknowledgement also goes to the Royal Thai Government Scholarship that sponsored my MSc and PhD programs. I thank P'Nice, K'Nareenut and K'Somchai, as well as the Royal Thai Embassy in the Netherlands and in France, for supporting me (and other Thai students) with a lot of efforts throughout the part years.

Dear Mom, Dad and Little An-an, to say thank you is not enough. I would not have become the person I am today without your incredible support. Seeing your daughter/big sister keeps moving further away and living thousands of miles apart must have not been easy. I am sorry that I have missed so much of our time together. Despite everything, you have never said no to my dreams. You back me up with all your strengths and keep believing in me even in the moments when I could not believe in myself. Thank you from the bottom of my heart for letting me flourish in my own way.

Last, I dedicate this thesis to the best botanist I have known, James Franklin Maxwell. Teacher James, Wageningen is a nice place like you said and the Arboretum is exactly how you described it. I have tried to live my expat life as best as you suggested and it has been delightful so far. As much as I missed our adventurous jungle work, I have found a new path I love—in water. Are you watching me graduate from up there?

# About the author

Chanoknun Wannasin, known by family and friends as Tang-Mo, was born on 5 November 1991 in Southern Thailand. Mo grew up in the backcountry in Surat Thani. Her childhood was full of reading by candlelight and exploring the surrounding wildernesses with her father. It has shaped her interest in the Earth and nature. At the age of 12, Mo went to a Catholic school in the city, despite being raised in Buddhism. She enjoyed the multicultural and multi-religious time there, started to wonder about other cultures and countries, and slowly picked up English. Since then, her life decisions, driven by a curiosity about the world, have gradually led her further away from home.

Mo started the BSc program in Environmental Science and Technology at Mahidol University in 2010. She chose to specialize in Natural Resources Conservation and dived into relevant subjects: geology, limnology, oceanography, forestry, ecology and meteorology. As part of the Youth-Exchange Project with Asia-Oceania & North America in 2013, she went to Fukushima, Japan to learn about the 2011 earthquake and tsunami. During her undergraduate internships, she explored her interests with a variety of work experiences, including at National Parks (forestry), an elephants' hospital (wildlife) and an NGO delving into deforestation concerning ethnic minorities (human ecology). Afterward, she worked as a research assistant in environmental projects (e.g., community-based adaptation to climate change). On one of her field trips into the jungle in Northern Thailand, she got infected by a lethal disease. Despite the desire to continue her adventurous career, she decided to deviate from her path to give her family relief.

In 2015, Mo moved to the Netherlands and started her new journey. With a scholarship from the Thai Government, she joined the MSc program in Earth and Environment at Wageningen University & Research. As water has held a fascination for her (apart from the jungle), she went for the specialization in Hydrology and Water Resources. Her thesis in 2016 focused on the structure comparison of two Wageningen-based hydrological models, WALRUS and SWAP, which allowed her to foretaste her interest in modelling. During her research internship at Deltares in 2017, she applied the wflow.HBV model for flood simulation in the Suir catchment in Ireland. Two years after leaving the jungle work behind, she stared at her model as it was implemented for real-time forecasting by the Irish authority and realized that she had found another type of joy and challenge in computer modelling.

Inspired by the successful modelling work from her MSc internship, Mo continued her challenges with a PhD research project in hydrological modelling in 2017. She focused on applying the wflow\_sbm model and machine learning models for reservoir operation modelling in a river basin in her home country (where those jungles she used to trek through are located, of course). From WALRUS and SWAP to wflow and machine learning, She has had a lot of fun exploring different perspectives of hydrological modelling; from lumped to distributed, from process-based to data-driven, from soil moisture to streamflow, from field scale to regional scale, from in-situ observations to global data, from calibration to transfer functions, and from highly accurate to terribly flawed.

After her PhD, Mo sets her sight on combining her interests in both hydrology and human ecology, and thus socio-hydrology. She is walking down her career path toward interdisciplinarity, seeking for opportunities to actually turn research into practice. She looks forwards to expanding her expertise and enriching her perspectives in water management with human interactions. Outside scientific hours, she is merrily putting her experience of slow living in Wageningen together with the local Thai wisdom in the hope of building a self-sufficient homestead and farm garden in her Thai hometown.

## Peer-reviewed journal publications

**Wannasin, C.**, Brauer, C. C., Uijlenhoet, R., Van Verseveld, W. J., & Weerts, A. H. (2021). Daily flow simulation in Thailand Part I: Daily flow simulation in Thailand Part I: Testing a distributed hydrological model with seamless parameter maps based on global data. *Journal of Hydrology: Regional Studies*, 34, 100794, doi:10.1016/j.ejrh.2021.100794

**Wannasin, C.**, Brauer, C.C., Uijlenhoet, R., Van Verseveld, W.J., & Weerts, A.H. (2021). Daily flow simulation in Thailand Part II: Unraveling effects of reservoir operation. *Journal of Hydrology: Regional Studies*, 34, 100792, doi:10.1016/j.ejrh.2021.100792

**Wannasin, C.**, Brauer, C.C., Uijlenhoet, R., Torfs, J. J. F., & Weerts, A.H. (2023). Machine learning for real-time reservoir operation simulation: insights into algorithms and input variables. *Submitted to Journal of Hydroinformatics*.

**Wannasin, C.**, Brauer, C.C., Uijlenhoet, R., & Weerts, A.H. (2023). Simulating and reforecasting real-time reservoir operation using combined neural networks and a distributed hydrological model. *Submitted to Hydrology and Earth System Sciences*.

van Hateren, T. C., Jongen, H. J., Al-Zawaidaha, H., Beemster, J. G. W., Boekee, J., Bogerd, L., Gao, S., Kannen, C., van Meerveld, I., de Lange, S., Linke, F., Pinto, R. B., Remmers, J., Ruijsch, J., Rusli, S. R., van de Vijzel, R. C., Aerts, J., Agoungbome, S. M. D., Anys, M., van Emmerik, T., Gallitelli, L., Gesualdo, G., Hanus, S., Hea, Z., Hoffmesiter, S., Imhoff, R. O. Imhoff, R. O., Meshram, S., Meyer, J., Oliveira, A. M., Mller, A. C. T., Nijzink, R., Schellerberg, M., Schreyers, L., Schymanski, S., Sehgal, D., Tasserion, P., Teuling, A. J., Trevisson, M., Waldschlger, K., Walraven, B., **Wannasin, C.**, Wienhfer, J., Zander, M., Zhanga, S., Zhoua, J., Zomer, J. Y., and Zwartendijk, B. W. (2022). Where should hydrology go? An early-career perspective on the next IAHS Scientific Decade, *Hydrological Sciences Journal*, accepted.



*Netherlands Research School for the  
Socio-Economic and Natural Sciences of the Environment*

# D I P L O M A

*for specialised PhD training*

The Netherlands research school for the  
Socio-Economic and Natural Sciences of the Environment  
(SENSE) declares that

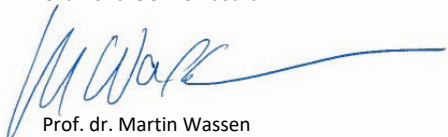
***Chanoknun Wannasin***

born on 5<sup>th</sup> November 1991 in Nakhon Si Thammarat, Thailand

has successfully fulfilled all requirements of the  
educational PhD programme of SENSE.

Wageningen, 21<sup>st</sup> February 2023

Chair of the SENSE board



Prof. dr. Martin Wassen

The SENSE Director



Prof. Philipp Pattberg

*The SENSE Research School has been accredited by the Royal Netherlands Academy of Arts and Sciences (KNAW)*



K O N I N K L I J K E N E D E R L A N D S E  
A K A D E M I E V A N W E T E N S C H A P P E N



The SENSE Research School declares that **Chanoknun Wannasin** has successfully fulfilled all requirements of the educational PhD programme of SENSE with a work load of 45.4 EC, including the following activities:

#### SENSE PhD Courses

- o Environmental research in context (2018)
- o Research in context activity: 'HWM Science Café: a friendly platform for research sharing and networking in hydrology and water sciences' (2021-2022)

#### Selection of Other PhD and Advanced MSc Courses

- o Summer School on Sensitivity Analysis of Model Output, Joint Research Centre (2018)
- o Training Introduction to RTC-Tools 2, Deltares (2018)
- o Crash Course High Performance Computer (2018)
- o Crash Course Machine Learning for Beginners, Wageningen University (2020)
- o PGR Catchment Science Summer School, University of Birmingham (2019)
- o Essentials of Scientific Writing and Presenting, Wageningen Graduate Schools (2017)
- o Research data management Part 1 and 2, Wageningen Graduate Schools (2018)
- o Project and time management, Wageningen Graduate Schools (2018)
- o Brain training, Wageningen Graduate Schools (2019)
- o Effective Behaviour in your professional surroundings (2019) & Working on your PhD research in times of crisis, Wageningen Graduate Schools (2020)
- o Supervising BSc & MSc thesis students, Wageningen Graduate Schools (2019)
- o Scientific Writing, Wageningen Graduate Schools (2021)

#### Management and Didactic Skills Training

- o Organizing presentations and discussion sessions with scientists and governmental experts in the study area in Thailand (2019)
- o Member of WIMEK PhD council (2020-2022)
- o Supervising three MSc students (2018-2020) and two BSc students (2019) with thesis
- o Assisting practicals of the MSc courses 'Catchment Hydrology' (2018-2021), Research Master Cluster (2019), and the BSc courses 'Integration course on Soil, Water and Atmosphere' (2019-2021) and 'Water Quantity and Quality' (2019-2020)

#### Oral Presentations

- o *Daily flow simulation in Thailand*. Asia Oceania Geosciences Society, 1-6 August 2021, Virtual conference based in Singapore
- o *Simulating and multi-step reforecasting real-time reservoir operation using combined neural network and distributed hydrological model*. General Assembly of the European Geosciences Union, 23-27 May 2022, Vienna, Austria

SENSE coordinator PhD education

Dr. ir. Peter Vermeulen

The research described in this thesis was financially supported by the Royal Thai Government Scholarship offered by the Office of the Civil Service Commission, Thailand. The research was carried out at the Hydrology and Quantitative Water Management Group, Department of Environmental Sciences, Wageningen University & Research, The Netherlands.

Financial support from Wageningen University for printing this thesis is gratefully acknowledged.

Cover design by Chanoknun Wannasin and Gonthicha Puttaraksa

Layout design by Chanoknun Wannasin, using  $\text{\LaTeX}$

Printed by ProefschriftMaken



